The University Of Sheffield.

Variation in scale structure, structural colour and its genetic basis in two co-mimic species of *Heliconius* butterflies

Juan Enciso-Romero

A thesis submitted in partial fulfillment of the requirements
for the degree of Doctor of Philosophy

The University of Sheffield
Faculty of Science
School of Biosciences

Submission Date
January 2022

Declaration of Authorship

I, Juan Enciso-Romero, declare that this thesis titled, "Variation in scale structure, structural colour and its genetic basis in two co-mimic species of *Heliconius* butterflies" and the work presented in it are my own. I confirm that:

- This work was done wholly or mainly while in candidature for a research degree at the University of Sheffield.
- Where any part of this thesis has previously been submitted for a degree or any other qualification at this University or any other institution, this has been clearly stated.
- Where I have consulted the published work of others, this is always clearly attributed.
- Where I have quoted from the work of others, the source is always given. With the exception of such quotations, this thesis is entirely my own work.
- I have acknowledged all main sources of help.
- Where the thesis is based on work done by myself jointly with others, I have made clear exactly what was done by others and what I have contributed myself.

"*Your assumptions are your windows to the world. Scrub them off every once in a while, or the light won't come in.*" Possibly something many people realise while writing their PhD.

Isaac Asimov

Abstract

Butterfly wings are adorned with colours that allow them to adapt to their environment in different ways. *Heliconius erato* and *Heliconius melpomene* are two species that display a striking variety of colours that in most cases converge due to Müllerian mimicry. The genetic basis of these patterns is well characterised. It shows simple Mendelian inheritance in most cases and it is parallel in the two species; homologous loci of large effect have been targeted by evolution during adaptation. In certain geographical regions these species also show convergence in blue wing iridescence; an angle dependent colour produced using nano-structures present in their scales. In contrast to pigmented patterns, little is known about the genetic basis of structural colour in *Heliconius* and other butterflies. In this thesis I characterise nano-structure variation relevant for structural colour production and explore its genetic basis. I describe its variation in natural and artificial populations, find loci controlling its variation and describe its putative genetic architecture. The genetic architecture of scale nano-structure and structural colour appears to be highly polygenic and divergent genetic mechanisms are used between species, unlike the case of pigmented wing patterns.

Acknowledgements

First and foremost I would like to thank my supervisors Nicola Nadeau and Andrew Parnell for their guidance, encouragement and support, especially during uncertain times due to the pandemic. I also would like to thank past and current members of the Nadeau group at Sheffield, in particular to Emma Curran, Mel Brien, Vicky Lloyd and Angel Nguyen. I am grateful for all the feedback, help, guidance in the lab and around Sheffield, stimulating conversations academic or otherwise, and for your friendship. I also want to thank my friends and former housemates in Sheffield for making my time enjoyable and for your support when I needed it, especially to Tessa Dawson-Pell, Nat Phon-or, Favour Felix and Andrei Bota. I am grateful to Universidad del Rosario for partly sponsoring my PhD in Sheffield, and for giving me the opportunity to come back to apply my newly gained experience as a researcher. In particular I want to thank Carolina Pardo and Camilo Salazar for their assistance with samples, ideas and feedback. Finally I would like to thank my family, especially my wife Catalina, for supporting me during the whole of my PhD and to my friends Javier, Diego, Fran, Andrés, Ana, Sasha, Cata Cruz and Salda for always being there for me.

Contents

List of Figures

List of Tables

This thesis is dedicated to Mariela Méndez, Gilma Romero and Marcela Enciso, whom I lost during the pandemic and with whom I would have loved to share the joy of finishing my PhD

Chapter 1

General introduction

1.1 Structural colour

Animals display a broad range of visual cues that fulfill diverse roles, allowing them to adapt to the conditions of their environment. One of the most noticeable features that many organisms possess is structural colour, which results from the interaction of light and sub-micron-scale arrangements present in the surface of many living systems, without the need for pigments (Ingram et al., 2008; Kinoshita et al., 2008). The described interaction produces diverse observable phenomena; from wide-angle intense light, to total cancellation of light reflection (Kinoshita et al., 2008).

Structural colour has long been of interest, perhaps due to the striking visual effects that it produces and its potential applications to materials design and manufacturing. The evolution in sophistication of ideas and techniques used in the fields of optics and photonics has yielded increasingly detailed descriptions of spatial organisation and an exhaustive survey of the diverse mechanisms by which this mode of colour is produced. In the earliest works known to address the topic, Robert Hooke, using observations in the microscope, and Isaac Newton, as part of his treatise in optics, described and explained how light passing through thin layers present in feathers produced luminous colours (Kinoshita et al., 2008; Parker, 2000). By mid 1920's studies involving chemical tests and manipulation of optical properties of animal coloured tissue permitted the differentiation between structural colour and pigmentation (Mason, 1925), and a series of experimental studies were instrumental in establishing the relationship between different microscopical arrangements and macroscopic visuals on certain animals (Kinoshita et al., 2008). The invention of the electron microscope in the decade of 1930's helped reveal key features of the complex mechanisms that were present in bird feathers and butterfly wings, it enabled the first accurate descriptions of the anatomy of reflectors: structures made of transparent materials, in which the interaction of light with microscopical features causes the structural coloration (Kinoshita et al., 2008; Parker, 1998). After the second half of the 20^{th} century, the understanding of structural colour developed at a fast pace in the light of the theories

proposed in early 1900's and with the availability of more sophisticated instrumentation. The study of this type of coloration became widespread; its physical aspects are now well understood in a large number of species.

In spite of the important discoveries made in the field of optics, biological aspects of structural colour such as its evolution, genetic basis and ecological role have only recently begun to be unveiled. This is in contrast to the extensive research on biology of colour produced by pigmentation, which in comparison has yielded a large body knowledge of about its function, perception, mechanisms of evolution and the relationship of genetic architecture and diverse pigmentation patterns. Although the published research in the field of optics contains sensible biological assertions about the evolution and genetics of structural colour, there still remains an extensive gap of knowledge.

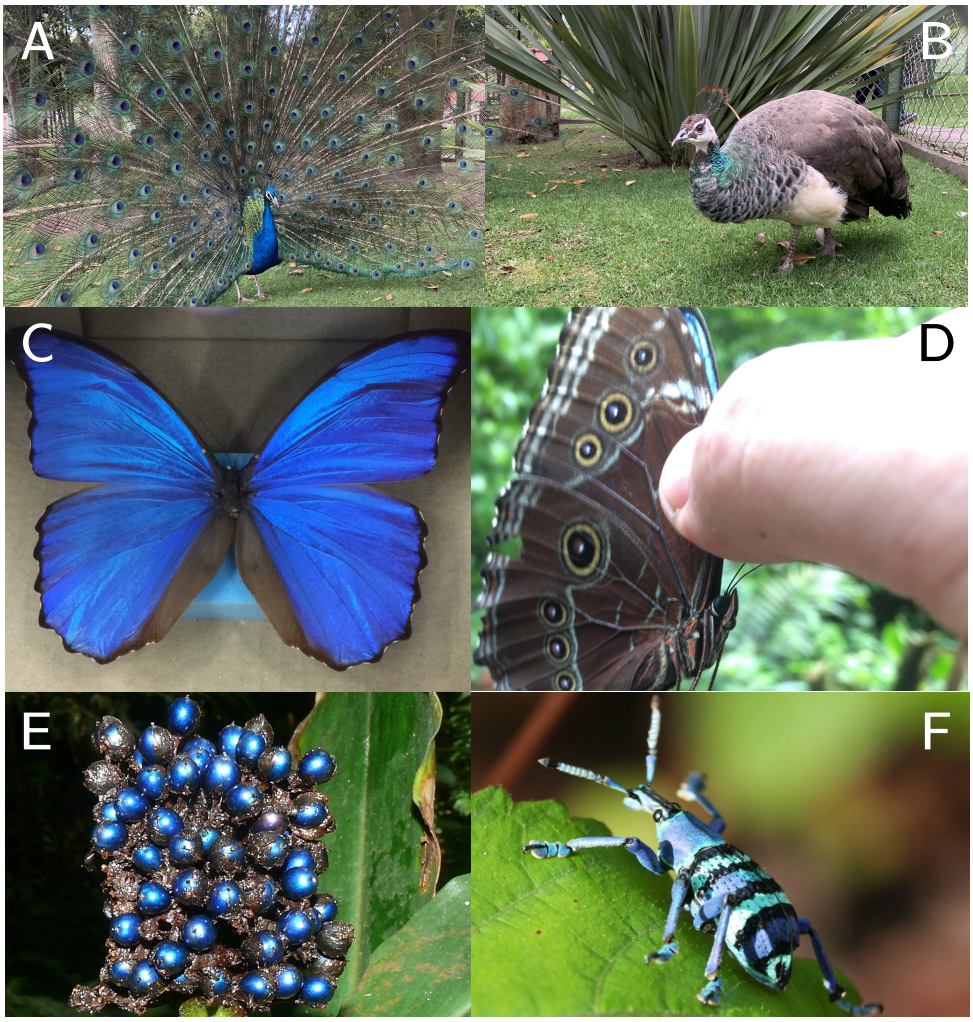

FIGURE 1.1: Structural colour is a widespread trait in nature. The marked sexual dimorphism between males and females of the indian peafowl (*Pavo cristatus*) is displayed using structural colour. A) The peacock is widely covered in blue and green feathers, whilst the peahen B) only has green feathers around the neck. C) Dorsal and D) ventral sides of *Morpho menelaus*. E) Structural colour can be found in plants such as the marble berry (*Pollia condensata*) (credit: Juliano Costa). F) The *Eupholus magnificus* weevil displays a spectacular variety of structural green and blue (credit: Dr. Jaroslav Bacovsky).

1.2 The lepidopteran scale: Morphology and development

1.2.1 General morphology of the lepidopteran scale

Although structural colour is present in many groups of animals, butterflies and moths are the taxon in which this trait has been most extensively studied (Ingram et al., 2008). The reason for this may be the diversity of visual effects that these insects display; there exist around 15 000 species and almost as many different wing designs and colour arrangements (Sekimura et al., 2017). Lepidopteran wings are covered by a mosaic of chitin scales, each of which is produced from a single cell (Ghiradella, 1989). Scales are normally arranged in two layers on the dorsal and the ventral side of the

wing; the scales on the top layer are refered to as cover scales, which partially overlap the scales in the bottom layer, referred to as ground scales. This overlap combines the optical effects of individual scales and determines the macroscopic visual properties of the wing (Stavenga et al., 2014; Yoshioka et al., 2004). Scales can get their colour from pigments and micro-structures made of chitin that reflect and diffract light selectively (Nijhout, 1990).

The morphology of the lepidopteran scale is generally conserved, with small variations across different taxa (Ghiradella, 1991). The scale is divided in two parts; a lower section and upper section. The lower section is commonly a flat layer of chitin that faces the wing surface. The upper section of the scale is more elaborate in morphology than the lower section; it is composed of ridges that run in parallel, longitudinally across the scale. The ridges are interconnected by cross-ribs that run perpendicular to the ridges, forming small windows in the upper surface. The ridges are formed by a stack of lamellae that have a slight inclination with respect to the lower surface of the scale. The upper and lower sections are connected by trabeculae and the hollow part between upper and lower sections normally contains pigment granules (Ghiradella, 1989). In general, the structure of the scale changes depending on the visual appearance that the scale has, regardless of getting its colour from pigments or from structural colour (Gilbert et al., 1988). Structural colour can be produced in diverse ways by tuning structures of either the lower or the upper section of the scale (Ghiradella, 1989). The morphology of the lepidopteran scale is shown in figure 1.2.

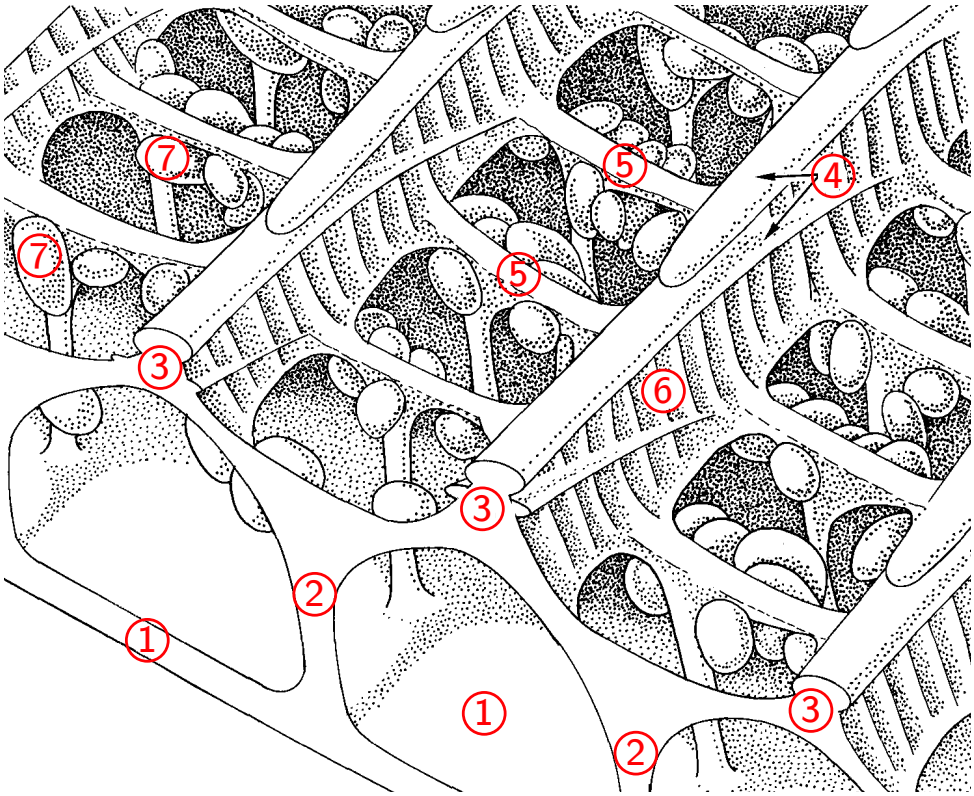

FIGURE 1.2: Diagram of the lepidopteran scale. The lower section (1, bottom) is formed by a chitin layer and is joined to the upper section of the scale by trabeculae (2). Parallel ridges (3) are found on top of the trabeculae and are formed by lamellae (4) and supported by micro-ribs (6). The rows of ridges are interconnected between them by cross-ribs (5). Pigment granules (7) can be found between the upper and lower sections. Modified from (Ghiradella, 1989).

Reflector structures of butterfly and moth scales have been extensively studied, yielding a good understanding on the physical mechanisms that produce structural colour in these organisms. Using optical microscopy (Mason, 1926) it was shown that iridescent colour was a product of interference produced by thin film arrangements. Electron microscopy was extensively used throughout most of the 20th century to retrieve detailed images of scale ultrastructure, and to describe more precisely the distinctive morphological features of structurally coloured scales. In particular, studies of iridescent blue scales of *Morpho* butterflies revealed that the ridges of these were taller than those of non-iridescent scales, and that the distances between some elements of the scale anatomy were reduced compared to scales lacking structural colour (Anderson et al., 1942). Studies complementary to those focused on scale anatomy aimed their attention at intrinsic properties of reflective materials of biological origin. These provided the first calculations of the refractive index of chitin and finer aspects of scale morphology relevant to structural colour production. From this exploration of the microscopic aspects of the scale researchers were able to describe how an 'optimal' visual signal could be tuned by the variation on the number and dimensions of layers, as well as by the alternation of materials with different refractive indexes in a

multi-layer reflective system (Land, 1972). Examples of butterfly structural colours and the nano-structures that produce them can be found in figure 1.3.

For many years the examination of wing sections using electron microscopy also helped to build a classification of the different reflector structures and their individual components from a morphological perspective (Ghiradella, 1985; Ghiradella, 1991). Later, research efforts began to focus on single scale properties, allowing the quantification of reflectivity and transmission of light in scale micro-structures as well as a more precise estimation of refractive indexes of scale cuticle (Vukusic et al., 1999). Analyses of single scales were also useful to conclude that the angle of tilting of the scale with respect to the wing base membrane can also affect the production and perception of structural colour (Berthier et al., 2003).

The variety and complexity of reflector structures found in butterflies is a consequence of the plasticity of arthropod cuticle (Ghiradella, 1991) combined with finely tuned cellular processes that likely differ across butterfly lineages. Although it has been argued that self assembly is the cause of different cuticular configurations (Ingram et al., 2008) and there is evidence showing that environmental changes affect iridescent phenotypes (Kemp et al., 2006; Kértesz et al., 2017), structural colour is probably governed by genetics, which in turn is affected by the biological processes inherent to natural butterfly populations. Taking these biological processes into account will offer a different way to think about the variation in structural colour found in nature, and an opportunity to study this variation in a controlled fashion.

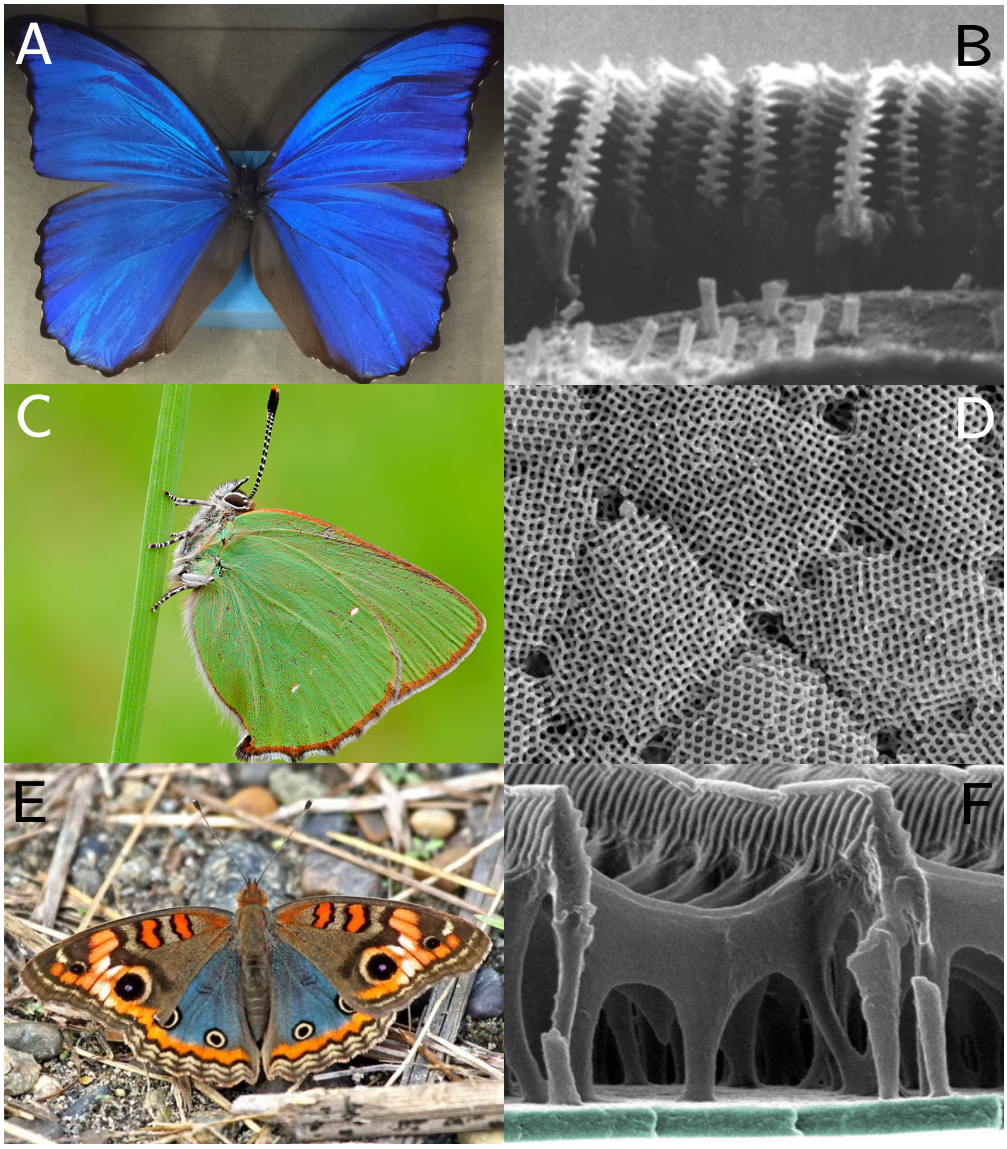

FIGURE 1.3: Colour produced from different scale nano-structures. Lamellae in the ridges of the *Morpho* scale form a multi-layer structure that produces colour by constructive interference (A, B credit: Kinoshita et al. 2008). C) *Callophrus rubi* (credit: Francesco Cassulo) and other butterflies with vivid green colouration have scales bearing gyroid crystals (D, credit: Wilts, Zubiri, et al. 2017) that produce colour by diffraction. E) *Junonia evarete* (credit: Roger Ahlman) produces the blue colour of the hindwing and the eyespots by adjusting the thickness of the lower lamina (F credit: Thayer et al. 2020).

Despite the sound discoveries on the physical basis of structural colour, there is still place for further description of the complexity of reflector structures (Vukusic et al., 2003). In particular, no studies have documented within-species variation in scale structure in the wild or attempted to link this to colour variation on a large scale.

1.2.2 Development of the lepidopteran scale and nano-structures that produce structural colour

The development of the lepidopteran scale is a process that has been the focus of attention of researchers for decades, but only recently has begun to be studied from a molecular perspective. Understanding the cellular components and processes involved may help identifying developmental pathways and key gene products that control the production of structural colour.

During the development of scales two types of cells are involved: socket cells, which are located on the wing surface and form the structure to which scales attach; and the cells that develop into the scale proper, which are wrapped by the socket cells. The scale forming cells have three distinctive regions, each of which seems to be associated with different cellular processes during scale development: there is a basal region on the inner side of the wing, a neck region wrapped around by the socket and a protruding region on the outer side of the wing which will transform into the scale. A schematic of the developing scale and its main parts is shown in figure 1.4.

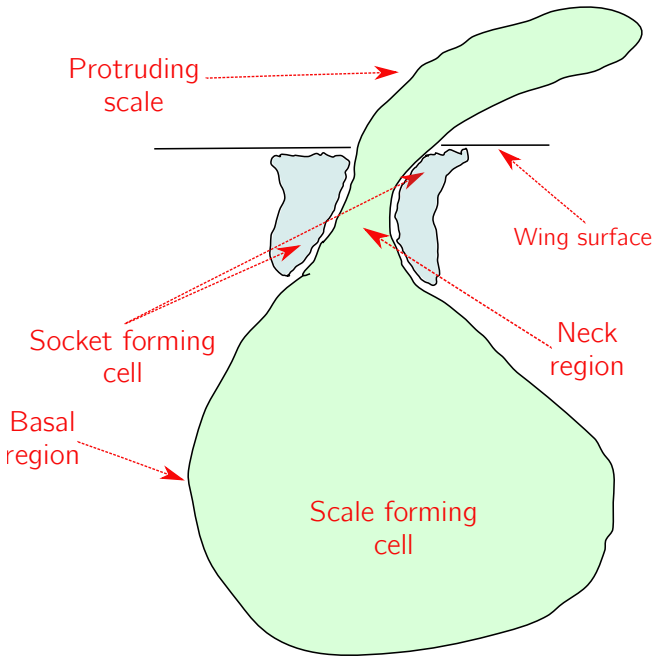

FIGURE 1.4: Scheme of a developing scale. Cells that give rise to scales (green) are enlarged compared to other epidermal cells and project to the outer side of the wing through socket forming cells (teal). During development, different processes take place in the basal, neck and budding scale regions shown in the figure. Adapted from Greenstein 1972a.

Patterns of scale formation are presumed to be conserved across lepidoptera. The scale starts its development as a flask shaped structure that will gradually become flattened. The scale forming cell undergoes several endomitotic divisions and becomes polyploid and enlarged compared to a regular epidermal cell (Cho et al., 2013; Greenstein, 1972a). Chromatin is densely staining and largely visible, which indicates possibly

only a small fraction of the genome is active (Greenstein, 1972a) and involved in transcription. Organelles such as the rugose endoplasmic reticulum, Golgi complexes and protracted mitochondria are present in the basal region during the process of scale formation, which is interpreted as this region being largely involved in bio-synthetic processes (Greenstein, 1972a). The neck and the protruding part of the developing scale start to accumulate longitudinally arranged micro-tubules and bundles of actin, which are involved in movement of the cytoplasm and ridge formation (Overton, 1966), and in shaping the scale in its final form (Greenstein, 1972a).

One of the key parts of the developing scale for structural colour production is the cuticulin layer, which is the outermost layer of cuticle in insects, and is invovled in the formation of surface patterns (Locke, 1966). These surface patterns will produce some of the variety of structural colour observed in butterflies and moths; they are often molded into multiple layers of thin films, lattices and other nano-structure arrangements that produce colour by interaction with light (Ghiradella, 1994). The actin bundles and microtubules found in the neck region and the budding scale have been proposed to play a key role in shaping the cuticulin layer. Specifically, since they are laid before the cuticulin layer is secreted, their periodic arrangement is thought to determine periodic layout of the ridges seen on a typical lepidopteran scale (Ghiradella, 1974; Greenstein, 1972a). It has been proposed that contraction within the actin bundles may create tension that results in buckling of the cuticle and the posterior formation of the scale ridges, and that a similar mechanism may give rise to the lamellae that make up the ridges (Ghiradella, 1974).

Since the arrangement of actin bundles appears highly correlated with the organisation of structures in the adult scale, in recent years their role has been studied in further detail using confocal microscopy and functional validation of molecular activity. This allowed the confirmation that actin bundles are a crucial factor in the positioning of chitin ridges, and are also essential for growth of finger-like projections at the distal end of scales and for initial elongation of budding scales (Day et al., 2019; Dinwiddie et al., 2014). The same patterns of actin dynamics were observed across several butterfly and moth species, which indicates these mechanisms are fairly conserved across lepidoptera. More importantly for the case of structural colour, cells destined to become structurally coloured have higher amounts of actin and a tighter bundle distribution compared to those that develop into pigmented scales (Dinwiddie et al., 2014). Thus, a next step in researching the development of structural colour could be to try to target molecules that interact with actin bundles and determine candidates that produce differences in amount of actin and spacing of bundles. It has been proposed that the Fascin protein and dynamics of microtubules may have an effect on the distribution of the actin network (Day et al., 2019).

1.3 Genetics and evolution of structural colour

Colour is fundamental for adaptation in butterflies and other animals, and understanding the evolution and genetic basis of coloured traits remains a major goal in biology. The study of colour has played an important role in the areas of genetics and evolution (Hoekstra, 2006). Various genes and developmental pathways involved in adaptive colouration are fairly well known in several taxa such as birds (Mundy et al., 2016; Nadeau et al., 2006), mammals (Jackson, 1997), fishes (Henning et al., 2013; Kottler et al., 2013), butterflies and moths (Hof et al., 2016; Kronforst et al., 2015; Kunte et al., 2014), and other insects (Comeault et al., 2016; Dembeck et al., 2015). The functional basis of pigment colouration, albeit still limited, has been increasingly explored in recent years with the help of high throughput sequencing methods and validation assays (San-Jose et al., 2017) . In contrast, basic biological aspects related to genetics and evolution of iridescence or other forms of structural colour remain largely unexplored in butterflies and other organisms.

Structural colour plays diverse roles in butterfly biology; it has been shown that iridescence modulates intra-specific communication as a long range signal used for mate recognition in habitats with reduced illumination (Sweeney et al., 2003), that it is part of bright and colourful male ornamentation (Kemp, 2007) used in courtship, and that it is used in agonistic interactions between males of a single species (reviewed in Doucet, 2009), probably involved in territoriality and individual range delimitation (Vukusic et al., 1999). Bright reflective colours are also important for inter-specific interactions as a key component of aposematic coloration; they are used to convey unpalatability to predators in the butterfly species *Eumaeus atala* (Bowers et al., 1989). Other studies have suggested functions of structural colour other than communication; some authors have suggested that reflective structures in the wing are an important part of butterfly physiology as thermal regulators (Doucet et al., 2009). More specifically, nano-structures found in scales with structural colouration may aid thermal regulation by balancing solar absorption and infrared emission (Krishna et al., 2020).

The phenotypic variation observed within species or populations may give an idea about the genetic basis of structural colour in different groups of butterflies. In some species structural colour appears as a discrete trait, being different between males and females, for example. This is the case in several species of *Morpho* butterflies for which differences in flight patterns and dispersal rates between males and females may be driving sexual dimorphism that involves structural colour and wing shape differences (Chazot et al., 2016). In some pierid butterflies like the orange suplhur *Colias eurytheme* and the southern dogface *Zerene cesonia* there is sexual dimorphism; males display UV iridescence that is absent in females (Fenner et al., 2019; Ghiradella et al., 1972). This suggests that in these species the trait may be subject to Mendelian inheritance that controls a simple switch between structurally coloured males and with pigment coloured females.

Other butterflies show quantitative variation in structural colour. In species *Bicyclus anynana* and *Junonia coenia* it has been shown that individuals with structural colouration can evolve from ancestors in which the trait is absent in a short number of generations, each generation showing a gradual change towards the trait. In these species a change in the thickness of the lower lamina results in the appearance of structural blue colour (Thayer et al., 2020; Wasik et al., 2014). In *Heliconius* butterflies quantitative variation is observed within and among natural populations, and individuals reared in selection experiments (Emsley, 1965) and controlled crosses (Brien et al., 2018; Emsley, 1965). This suggests that structural colour variation in these species is a quantitative trait that is likely under polygenic control.

The identity of the loci that control structural colour and their effect on phenotypic variation has begun to be unveiled recently both for quantitative and discrete phenotypes in several butterfly species. Zhang et al., (2017) showed that *optix*, a transcription factor that coordinates wing element pigmentation (Reed et al., 2011) and the development of wing coupling scales in nymphalid butterflies (A. Martin et al., 2014; Reed et al., 2011), has an effect on structural colour in the species *Junonia coenia* when knocked out. The effect of *optix* knockouts on the visual appearance of *Junonia coenia* was later confirmed and dissected more finely; *optix* jointly controls pigment deposition and lamina thickness, creating a wide range of colour variation in *Junonia* butterflies (Thayer et al., 2020). In the sister genera *Colias* and *Zerene* two different genes control the production of UV reflectance in males. A paralog of *doublesex* is responsible for the presence/absence of this phenotype in *Zerene cesonia*, putatively suppressing UV scale differentiation in females (Rodriguez-Caro et al., 2021). In *Colias eurytheme cis*-regulatory variation around the *bric-a-brac* gene underlies UV iridescence (Ficarrotta et al., 2021). Finally, in *Bicyclus anynana* a putative network including the genes *apterous A*, *Antennapedia*, *Ultrabithorax*, *doublesex* and *optix* mediates the appearance of silver scales (Prakash et al., 2021). These results indicate that evolution has targeted a variety of genes to produce structural colour in butterflies and moths. In only a handful of species studied, the catalogue of genes that potentially have an effect on structural colour is not modest. Thus, it is possible that in other lineages more and different genes to the ones listed above are targeted by selection to promote, inhibit or regulate structural colour production.

1.4 *Heliconius* butterflies: Pigmented wing patterns and structural colour

Heliconius is a genus of neo-tropical butterflies that has served as a study system in several areas in biology; the diversity of their wing patterns and the tight link between this diversity and ecological, behavioural, genetic and developmental processes has been studied for more than 150 years, yielding substantial insights into their biology. This rich body of knowledge has resulted in the development of theories in ecology,

speciation, adaptation and genome evolution that have been influential for formulating and addressing various biological questions in other organisms (Merrill et al., 2015).

Mimicry and aposematic colouration are the most prominent traits of *Heliconius* butterflies. As larvae, these insects feed on fresh shoots of plants of the genus *Passiflora*, from which they sequestrate chemical defences for their own use to avoid predation as adults, while at the same time defusing the host plant's anti-hervibore mechanisms (Engler et al., 2000). Conspicuous, colourful patterns in the wings convey distastefulness to predators as they rapidly learn the association between visual appearance and the unpalatable condition of adults. *Heliconius* are the classic example of Müllerian mimicry; geographical races of distantly related species, all of them unpalatable, resemble each others' wing patterns locally (Fig. 1.5), thus sharing the cost of predator learning (Kapan, 2001). A natural consequence of Müllerian mimicry is that divergent natural selection maintains stability of local visual signals and penalises hybridisation. This in turn has an effect on mate choice dynamics and introduces an additional function for wing patterns as nuptial signals (Merrill et al., 2011).

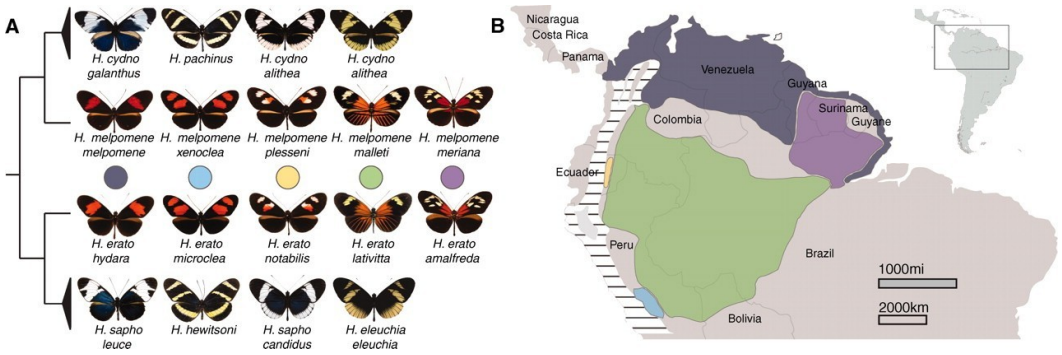

FIGURE 1.5: Convergence in wing patterns across several mimicry rings (Reed et al., 2011). A) Closely related *Heliconius* species show striking phenotypic differences and distantly related lineages form mimicry rings when converging geographically. B) Geographical distribution of the showcased lineages.

What is the genetic architecture underlying the large assortment of *Heliconius* wing patterns? The diversity in *Heliconius* wing patterns can be mapped to a surprisingly small number of loci of large effect; it is said that *Heliconius* uses a 'tool-kit' of unlinked Mendelian loci (Nadeau, 2016) to control their wing patterns. Multiple studies involving controlled crosses, association mapping, expression analyses and functional validation have allowed a highly precise dissection of these loci and the identification of individual genes and regulatory regions that control wing pattern variation (Jiggins et al., 2017; Kronforst et al., 2015; Nadeau, 2016). Examples of particular traits and their underlying loci/genes are shown in Figure 1.6. *Cis*-regulatory activity around these genes is a key factor in the evolution of mimicry adaptations (Concha et al., 2019; Livraghi et al., 2021; Van Belleghem et al., 2017; Wallbank et al., 2016).

How can this striking variety of wing patterns evolve in a relatively short time frame?

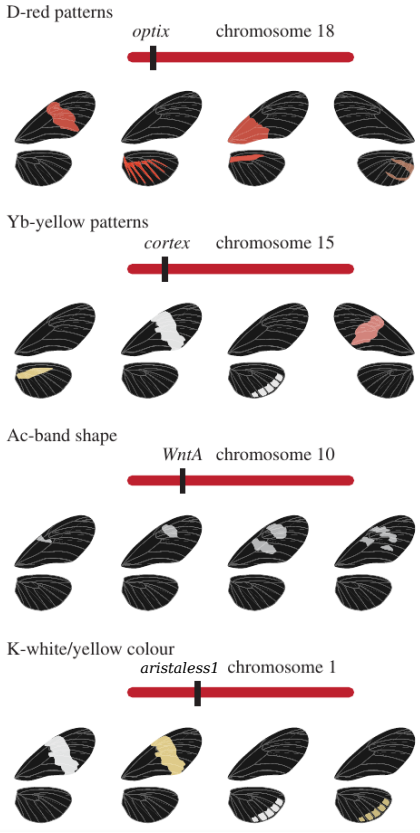

FIGURE 1.6: Schematic showing the main colour pattern loci and their genomic localisation (chromosomes), the names of genes controlling the phenotypic variation and examples of their phenotypic effects. Figure adapted from Jiggins et al. (2017).

Recent studies have shown that there is more than one way in which such complexity may have arisen. On the one hand, evidence suggests that although the loci of adaptation are the same in distantly related species (Supple et al., 2013), convergent phenotypes evolve following independent trajectories (Hines et al., 2011; Quek et al., 2010; Supple et al., 2013), reinforcing the assertion that evolution is predictable to some extent, and that it targets and re-uses a few genetic mechanisms to produce adaptive traits (A. Martin et al., 2013; Stern et al., 2009). On the other hand, closely related species with a history of hybridisation and compatible genomic backgrounds can share variants of adaptive loci across the species boundary (Consortium, 2012; Pardo-Diaz et al., 2012) leading to rapid processes of adaptation.

Apart from the warning colouration produced using pigmented wing patterns, several *Heliconius* lineages have evolved wings with structural colour (fig. 1.7 A). Structurally coloured species use different physical mechanisms and variations of scale morphology to this end. On the one hand, some species use the lamellae in the ridges of the scale as multi-layer reflectors to produce blue colour (Parnell et al., 2018), a similar optical mechanism to that of the *Morpho* butterflies (fig. 1.7 B-D). On the other hand, in the species *H. doris* it has been observed that the lower lamina of their cover scales acts as a thin film reflector to produce blue colour, and this can be further

combined with yellow pigment to achieve a green hue (Wilts, Vey, et al., 2017). This indicates that different species have likely followed different evolutionary trajectories to produce structural colour, and possibly different genes and developmental pathways are involved in each case.

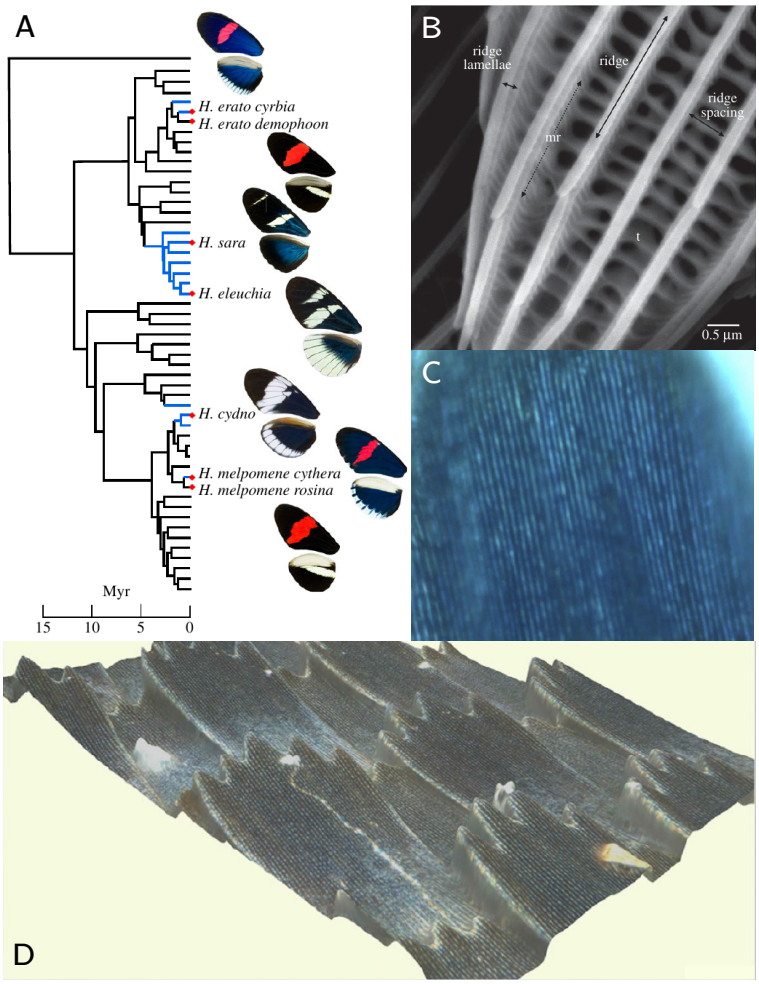

FIGURE 1.7: Structural colour in *Heliconius* butterflies. A) The trait has evolved independently several times in the *Heliconius* adaptive radiation (blue branches denote presence of trait). B) General structure of the *Heliconius* scale labelling the nano-structures involved in structural colour production in certain lineages. C, D) Several structurally coloured *Heliconius* use multi-layer ridges to produce blue colour, as seen using optical microscopy (*H. erato cyrbia* shown). The figure is adapted from Parnell et al. (2018).

In contrast to the extensive knowledge on adaptations controlled by major loci, the knowledge about complex quantitative traits such as structural colour is limited. We are yet to discover whether similar conclusions about the evolutionary aspects of these traits hold and how their genetic architecture compares to that of major loci and to that of structural colour in other butterfly species. I hypothesise that micro and macro-evolutionary aspects of *Heliconius* structural colour partly depend on the ecological role of this trait, but this has not been studied to a large extent. We know that structural colour is important for long-distance mate recognition in the forest (Sweeney et al., 2003), and it is presumably involved in mimicry as suggested

by selection patterns being coupled to those of some pigmented wing patterns in co-mimetic species (Curran et al., 2020), and by vision models of butterflies and potential predators (birds) (Parnell et al., 2018). It is also possible that structural colour in *Heliconius* is involved in mate choice, as it is condition dependent and could be an honest signal of developmental quality to potential mates (Brien, 2019).

Interestingly, while in some *Heliconius* species iridescence is ubiquitous (for example *H. sara*), it is possible to find populations of blue iridescent individuals in species that normally lack reflective features. This is the case of *Heliconius erato* and *Heliconius melpomene*; these species have co-evolved mimetic forms in nearly all of their geographic races, and local forms of both species found along the western coast of Panama, Colombia and Ecuador display a shift from non-reflective to iridescent phenotype that varies with latitude. Additionaly, evidence from crosses shows that hybrids between iridescent and matt-black parentals have phenotypes of intermediate reflectance and blue chromaticity (Brien et al., 2018; Emsley, 1965). This suggests that iridescence is a trait that has continuous variation, possibly underpinned by a polygenic architecture in *H. erato* and *H. melpomene*, and makes these butterfly species suitable to study the genetics of complex adaptive traits. In this thesis I use wild populations and F2 offspring individuals of the co-mimics *H. erato* and *H. melpomene* to analyse quantitative variation in structural colour and the scale structures associated with it. I assess and compare the genetic architecture of scale structure variation between the two co-mimic species and attempt to find SNP variants associated with variation in structural colour.

1.5 Outline of thesis

Chapter 2 explores the variation in scale structure related to structural colour in wild caught individuals and individuals derived from controlled crosses in the co-mimic species *H. erato* and *H. melpomene*. I do this by examining electron microscopy data, small angle X-ray scattering data, and colour data from wing photographs. I also explore the degree of correlation between scale nano-structure variation and structural colour variation in both wild caught and offspring individuals, and determine whether there are associations between sex and phenotypic variation related to structural colour.

Chapter 3 builds on the phenotypic analysis done in Chapter 2 for F2 individuals, and aims to find loci explaining this phenotypic variation using a QTL analysis. For this, RAD-sequencing data is used to build linkage maps for both species and then using variation in scale structure and colour as phenotypes. Besides finding loci that explain variation in structural colour, by doing the QTL analysis I aimed to establish whether the same loci are reused for evolution of structural colour between *H. erato* and *H. melpomene*.

Chapter 4 aims to find sites significantly associated with structural colour variation in *H. erato* and *H. melpomene* using a GWAS approach. My predictions were that this analysis would reveal SNPs within the QTL confidence intervals reported on Chapter 3 and possibly additional SNPs in other parts of the genome. I use whole genome sequencing for individuals sampled along a natural structural colour gradient going from Panama to Ecuador. I use optical spectroscopy to phenotype individuals; a different phenotyping approach to those used on Chapters 2 and 3, so that I can obtain several measurements of colour variability. I complement the GWAS results with analyses of population structure and admixture between populations.

Chapter 5 provides a discussion of the findings of this thesis and enumerates further research questions about the biology of structural colour in *Heliconius*, in particular about its evolutionary and ecological aspects.

Chapter 2

Understanding within-species variation in scale structure and colour in two iridescent *Heliconius* co-mimics

2.1 Abstract

The optical underpinnings of the production of structural colour from nano-structures in the scales of butterflies are well known yet fundamental biological aspects like its evolution and genetics are still poorly understood. Using a combination of data from digital photographs, scanning electron microscopy and USAXS we studied the variation in scale morphology associated with structural colour in wild populations and F2 cohorts of two butterfly species that show convergent evolution of structural colour. We found that scale ridge spacing and cross-rib spacing vary in a correlated manner with iridescent structural colour along a latitudinal gradient in natural populations of both species. There are subtle differences in associations between structure and colour in nature and further differences are revealed when comparing samples from controlled crosses pointing towards a complex genetic architecture that possibly is not shared between the co-mimics *H. erato* and *H. melpomene* unlike other aspects of their visual appearance.

2.2 Introduction

Structural colour decorates the surface of countless organisms in many taxa. It is produced by the interaction of light and nano-structures present in the external organs of living specimens, the most outstanding of which are perhaps butterflies and moths. The diversity of structural colour production mechanisms of these insects has been well studied and documented mostly during the last century (Kinoshita et al., 2008).

It has been established that there are diverse ways in which butterflies and moths have evolved their scale morphology to produce finely tuned complex visuals (Ghiradella, 1991, 1994). A large part of the studies on the structural colour of butterflies and moths has relied on morphological descriptions of the scale structure and theoretical analyses of the interaction of scale morphology with light to produce colour (Vukusic et al., 1999), while other aspects of structural colour such as its evolution and genetics have received less attention.

In recent years these less studied aspects of structural colour have increasingly come into the scope of the research community, but most details about the evolution of structural colour, specifically the micro-evolutionary aspects, remain largely unknown. For the most part the recent characterisations of biological mechanisms underlying structural colour have been done in individuals of a single species (Dinwiddie et al., 2014; Matsuoka et al., 2018) or in several species across large phylogenetic scales (Fenner et al., 2020; Parnell et al., 2018). Recent studies have begun to address the micro-evolutionary aspects of structural colour (Brien et al., 2018; Thayer et al., 2020; Wasik et al., 2014), but the great diversity of mechanisms by which structural colour is produced in butterflies and moths (Ghiradella, 1991; Stavenga et al., 2014) warrants a more extensive exploration of the micro-evolution of these various mechanisms and scale architectures; we still lack detailed characterisations of phenotypic variation at short phylogenetic scales in most species. Additionally, comparing evolutionary aspects of structural colour between species and establishing the existence of parallels, or lack thereof, at a broader evolutionary scope can help us to understand whether the same genetic mechanisms are used by different groups of butterflies to produce structural colour.

One group of butterflies of particular interest for the study of structural colour is the *Heliconius* genus. *Heliconius* butterflies have evolved structural colour using different modifications of the morphology of the scale. On the one hand *Heliconius* species that show iridescent structural colouration have scales with ridges more densely distributed than non iridescent *Heliconius* butterflies (Parnell et al., 2018). They also show a ridge morphology different to non iridescent *Heliconius*. The reduced ridge spacing and specialised ridge morphology are features that iridescent *Heliconius* share with other butterflies and moths that produce structural colour by constructive interference using the lamellae in the ridges of the scale (Ghiradella, 1974; Vukusic et al., 1999). On the other hand species like *H. doris*, which has variants showing blue and green patterns on the hind-wing, has a basal lamina with modified thickness that produces blue colour (Wilts, Vey, et al., 2017). When this structural modification is combined with the yellow pigment 3-OH Kynurenine, a bright green colour is produced (Wilts, Vey, et al., 2017). These studies show that across the *Heliconius* adaptive radiation evolution has targeted both the formation and distribution of the ridges and the thickness of the lower lamina and pigment deposition. Moreover they show that like in other groups of organisms, *Heliconius* structural colour is a complex trait in which

several aspects of the scale architecture interplay to produce the phenotypic variation we observe. Our understanding of phenotypic variation related to structural colour in *Heliconius* is limited to discrete groups of organisms both for scale structure and colour; species or races that produce blue structural colour have had their spectral properties and scale morphology compared to races which lack structural colouration. Often these discrete groups are geographically isolated or distant in the evolutionary sense, making the attribution of cause and effect difficult because of the large number of genetic differences that has accumulated between them.

One approach that allows the exploration of micro-evolutionary aspects of phenotypic evolution is the study of trait variation in hybrid populations. Hybrid individuals can be either collected from natural hybrid zones or produced from controlled crosses and reared in a common environment. Natural hybrids are useful because they offer the possibility of examining natural occurrences of intermediate phenotypes, giving information about how selection may be shaping a trait like structural colour in the wild. Controlled crosses complement this by allowing the examination of how phenotypic variation segregates after a few generations, revealing more specific aspects about the possible genetic architecture of the trait. The *Heliconius* adaptive radiation is one of the better known organism groups in which extensive hybridisation is present at almost all evolutionary scales (Mallet et al., 2007), allowing the collection and examination of both natural hybrids and hybrids from controlled crosses between different races.

The co-mimic species *H. erato* and *H. melpomene* are one of the most notable examples of convergent evolution in which local forms or geographic races evolve highly similar pigmented wing patterns to warn about their unpalatable condition and to share the cost of predator learning. Some sympatric local forms of both species not only show phenotypic convergence in wing pigmentation patterns, but they also show some degree of convergence in structural colour, which is observed only on their dorsal side (Curran et al., 2020; Parnell et al., 2018). This convergence allows us to explore the question of whether both species have followed the exact same scale structure modifications for producing iridescent blue colour. In addition, there exists natural variation in structural colour among populations within each species and it is possible to cross and breed individuals with different phenotypes in the insectary. This creates an opportunity to tease apart more detailed relationships between scale structure and colour variation, and constitutes a first step to the study of genetic architecture of these traits. We aim to explore in more detail the relationships between variation in scale architecture and variation in structural colour. Our objectives are: i) to assess the variation in scale structure that can be found in natural populations of pure and mixed ancestry and among F2 offspring of controlled crosses between sub-species that differ in structural colour; ii) to describe the relationship between variation in scale structure with the variation in visual properties of wings; iii) to examine the similarities and differences in scale structure evolution that have arisen in the convergent evolution of

structural colour in the co-mimic *H. erato* and *H. melpomene*.

There are technical challenges for analysing phenotypic variation in structural colour which are a consequence of the nature of this trait. In many cases structural colour is angle dependent or iridescent, and will vary highly depending on both the angle of incidence of light and the angle of observation. This makes measuring colour variation difficult because slight changes in the setup or sample positioning may introduce noise that is difficult to account for. In addition, factors such as the age of the samples and the level of damage and wearing will affect their visual appearance. Thus, if an approach like digital photography is chosen as the method for phenotyping, it is possible that there is unwanted variation in the data and biased phenotypic measurements (Kertész et al., 2021). Approaches such as optical spectroscopy may help to control some of the technical error that can be introduced using photography, but may also be sensitive to age and wearing of the samples.

Directly measuring variation in scale structure is an alternative that offers more precision since it bypasses some of the difficult aspects of quantifying colour variation. Electron microscopy has been perhaps the most important tool for studying scale structure ever since its invention allowing the first studies of structural colour in animals in the decade of 1940 (Anderson et al., 1942; Frank et al., 1939). Despite being highly useful and important, electron microscopy has some drawbacks, albeit not major. For practical reasons it is often important to preserve the analysed tissue in the best condition possible. Electron microscopy does not allow this, as samples must undergo an irreversible transformation during the preparation steps, which renders them unusable for future experiments. In addition, the process of sample preparation may induce changes in the structure of samples introducing measurement bias that is difficult to account for. Finally, electron microscopy produces detailed local images of a particular region, and getting representative measurements apt for quantitative analyses can be cumbersome (yet achievable, see Day et al. 2019).

Other experimental techniques allow for the interrogation of scale ultra-structure without the shortcomings of electron microscopy. Scattering techniques rely on exposing the region of interest to focused radiation; the interaction of the radiation with the structure of the material produces deviations of the radiation from its original trajectory that can be captured by a detector. The pattern captured in the detector contains information of the size and orientation of the structures in the material and therefore the structure can be analysed qualitatively and quantitatively. Scattering experiments require little or no preparation in most cases and samples can be reused in future experiments. Since there is no preparation the samples remain unmodified thus producing unbiased estimates. Scattering experiments can be done on a relatively large scale over a short period of time. Hence, scattering experiments typically result in robust data that is representative of the sample and is apt for statistical analyses. There is however one obstacle for the analysis of scattering data: The captured pattern does not contain the fully resolved structure, resulting in ambiguous data (Pauw,

2013). This ambiguity needs to be resolved using previous knowledge of the structure or complementing the scattering experiment with data from microscopy experiments (Pauw, 2013). Techniques relying on scattering radiation have been used to describe in detail the nano-structural changes required for producing structural colour in a wide range of taxa (Brien et al., 2018; Gur et al., 2020; Parnell et al., 2015, 2018; Saranathan et al., 2010).

Here we present a phenotypic analysis of a subset of structural changes between iridescent and non-iridescent scales. We use a combination of data from Ultra Small Angle X-ray Scattering experiments (USAXS) and colour variation from wild populations and insectary crosses to show that two major components of scale structure of *H. erato* and *H. melpomene* vary continuously between matt-black and iridescent blue races, revealing parallel evolution of scale morphology in two co-mimic butterfly species. In addition, we analyse the distribution of these traits in controlled crosses as an initial exploration of the possible genetic architecture in scale structure variation between matt-black and structurally coloured phenotypes. We suggest a mode of phenotypic change and development of ridges by expanding the interpretations made on evidence presented in previous studies and our own data. We expect that a phenotypic analysis using both colour and scale structure variation data will allow us to determine functional relationships between scale structure and colour variation.

2.3 Methods

We followed two approaches to study scale structure variation directly. We first analysed scales using SEM to have an idea of how scale structure compares between blue and black butterflies, and between the dorsal and ventral sides of the wing. We then analysed samples in a synchrotron beamline to have high-throughput measurements of scale structure that would have been prohibitive to obtain with SEM since we are interested in keeping the wings in the best shape possible for other analyses and measuring these samples in the electron microscope would be prohibitively long. Finally, we incorporate colour measurements in our analysis to get an idea of the role that scale structure plays in blue colour production in *Heliconius* butterflies.

2.3.1 Butterfly samples

We analysed three sets of samples: We analysed cover and ground scales of insectary-reared individuals of pure *H. e. cyrbia* and *H. e. petiverana* using SEM; this analysis was done with the purpose of confirming that cover and ground scales have different distributions of ridge spacing variation. We analysed wild caught individuals of different races of *H. erato* and *H. melpomene* spanning a geographical range from Panama to Ecuador along the western side of the Andes and the Pacific coast of Colombia. This geographical range comprises a gradient of phenotypes from matt-black to iridescent blue in both species. Finally, we analysed families of crosses between matt-black and

TABLE 2.1: Details of crosses and offspring used for phenotyping colour and scale structure. *demophoon* and *rosina* are the Panamanian matt-black races and *cyrbia* and *cythera* are the blue, Ecuadorian races.

Cross ID	Cross Type	Father ID	Mother ID	No. Samples
H. erato				
EC01F1	*demophoon* ♂ × *cyrbia* ♀	14N012	14N011	
EC10F1	*cyrbia* ♂ × *demophoon* ♀	14N065	14N064	
EC17F2	*cyrbia* maternal grandfather	14N112 (EC01F1)	14N111 (EC10F1)	56
H. melpomene				
EC48F1	*rosina* ♂ × *cythera* ♀	14N366	14N365	
EC49F1	*cythera* ♂ × *rosina* ♀	14N368	14N367	
EC70	Unknown	15N614 (EC49F1)	Unknown	73

iridescent blue races of *H. erato* and *H. melpomene* to study the segregation of structural colour related traits. The last two sets of individuals (wild caught and families from crosses) were phenotyped for scale morphology using X-ray scattering (USAXS) as well as chromatic and achromatic estimates of structural colour variation. Only the largest family from each species was phenotyped because beamline access is restricted to 24h. Details of the crosses for both species are specified in table 2.1. There was a mix-up in the insectary with the crosses of *H. melpomene* and as a consequence its only family phenotyped for scale structure is the result of the cross of an F1 father and a mother of unknown ancestry. This means the phenotyped family is not a true F2 in terms of parentage. For the remainder of the text we refer to this family by its name (EC70).

2.3.2 Scanning Electron Microscopy on dorsal and ventral scales

We used individuals of two races of *H. erato* and *H. melpomene* that differ in structural colour: *H. erato cyrbia* (blue, n=4), *H. erato demophoon* (black, n=8), *H. melpomene cythera* (blue, n=3), and *H. melpomene rosina* (black, n=3) for a comparative analysis of scale structure. Due to availability of samples that were suitable for imaging using SEM we had to use different individuals for dorsal and ventral sides comparison in *H. e. demophoon*. For the rest of the races, dorsal and ventral sides from single individuals were measured. We did two comparisons:

1. Ridge spacing of blue individuals vs. ridge spacing of black individuals on the dorsal side. This comparison allows us to gauge the expected range of scale structure variation in blue and black coloured scales.

2. Ridge spacing of dorsal side scales vs. ridge spacing of ventral side scales within each race. This comparison reveals differences in scale structure variation expected when comparing the dorsal vs. ventral side, allowing us to separate convoluted signals coming from overlapping scales in a USAXS experiment.

We cut portions of the wing of approximate square shape $\approx$ (8mm $\times$ 8mm) from the region of interest shown in figure 2.1. We mounted the wing samples on aluminium SEM stubs using 9 mm adhesive carbon tabs and coated them with a thin layer of gold using vacuum evaporation. We imaged the samples on a JEOL JSM-6010LA

microscope and used the InTouchScope software to take images of the regions of interest at magnification ranging from 750X to 1400X. Images included both cover and ground scales and from each sample we measured 5 cover scales and 5 ground scales. Cover and ground scales are not expected to show significant differences in scale structure other than the shape and length of the scales themselves.

At the midpoint of scale length, we drew a transect perpendicular to the orientation of the ridges; the most salient and accessible structure to measure on butterfly scales (supplementary figure S2.1, top). We calculated ridge spacing using the PeakFinder tool (Vischer, 2013); a plugin for the Fiji (v 1.52p) (Schindelin et al., 2012) image analysis package, using a tolerance level of 60 and a minimum distance of 10 pixels between peaks. PeakFinder detects spikes of intensity above the set threshold along the linear transect, each peak corresponding to one ridge. It then yields the distances between subsequent peaks in pixels (supplementary figure S2.1, bottom). Using the scale bar of SEM pictures we determined the variable rate of conversion from pixels to nm to be $25 \times 10^3/M$, where M is the level of magnification and estimated the distances between ridges in nm using this rate. Finally, we averaged over all the distances between ridges to get an estimate of average ridge spacing per scale.

2.3.3 Ultra Small Angle X-ray Scattering experiments

We carried out two USAXS experiments at the ID02 beamline at the ESRF (Grenoble, France) on two butterfly sample sets: Wild caught individuals and broods from controlled crosses. We probed the wings with an X-ray beam on several points along a linear segment in the proximal section of the fore-wing, as shown in figure 2.1. The X-ray beam wavelength was $\lambda = 0.0995$ nm and it had 12.45 keV energy. The beam was collimated to a section of 20 µm × 20 µm so that a small area within a single scale could be probed. The scattered radiation was recorded with a high-sensitivity FReLon 16M Kodak CCD detector with an effective area of 2048×2048 pixels and a 24 µm pixel size. Each measurement was stored as an image with a metadata header in plain text; a format called edf. We refer to a single edf file and to the data it contains as a frame. The frames were corrected for dark current and spatial distortion.

We first examined wings of wild caught individuals; 24 *H. erato* and 23 *H. melpomene* comprising geographical races that inhabit the forests of Panama, Colombia and Ecuador, West of the Andes mountain range (Fig. 2.6, table S2.1). We took between 14 and 108 measurements per individual. The accessible range of measurements for this experiment was between 1903 nm and 87 nm at a sample to detector distance of 30.98 m. However, upon preliminary data observation, we found that a sensible interpretation of our results could only be done for ranges above 160 nm.

We also examined wings of individuals obtained from crosses between matt-black and iridescent blue parental races; 56 *H. erato* and 73 *H. melpomene* individuals. The experimental setup was similar to that used for the wild caught individuals; there were

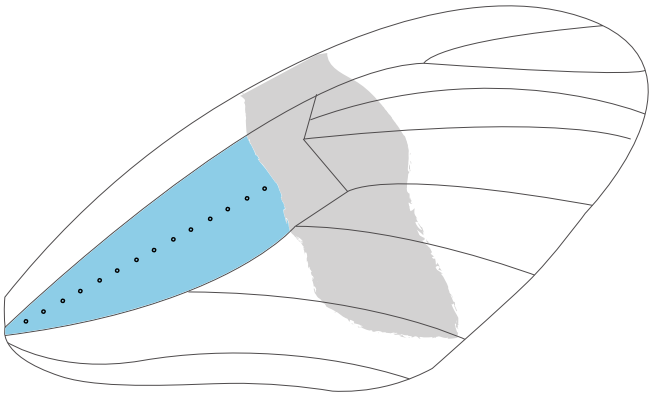

FIGURE 2.1: Area of the wing and linear segment along which measurements were taken in the USAXS experiment. The number of measurements varied per individual. The dots in the figure are a representation of the linear path that was sampled. No measurements were taken in any of the fore-wing patches (grey). The blue shading indicates the region used for colour analysis (together with a proximal region of the hind-wing).

between 33 and 113 points measured per wing and the sample to detector distance was slightly shorter (30.69 m). For this experiment we had an accessible range of measurements from 3696 nm to 83 nm, again limited to values above 160 nm for sensible data interpretation. Although there were slight differences in the experimental setup and in the processing of the raw data, the results from the two experiments are comparable for the purpose of phenotyping butterflies for scale structure variation.

We did a qualitative joint assessment of our USAXS and SEM data to get an idea of what scale structures could be resolved in our experiment and how to best extract the relevant information. For this, we mainly took into account the orientation that structures have in the scale and related these to the orientation of scattering patterns; structures that have a perpendicular arrangement in the sample should produce perpendicular scattering patterns and nano-structures organised in parallel arrays on the scale should leave a signature scattering pattern known as Bragg scattering, whereby scattered intensity shows a diffraction pattern of several equally spaced spots of scattered radiation along a straight line (Fig. 2.2).

We used the observations from our qualitative assessment to implement a script that extracts relevant information of scale structure from the USAXS data. The script scans the 2D scattering pattern in non-overlapping regions of 5°, scanning only along 180° because of the radial symmetry of the scattering patterns. If a section contains periodic scattering, it is assumed to correspond to the ridges of the scale (Fig. 2.2), and it is kept for comparison with other sections that also show periodic scattering. Among these, the one section that has the highest magnitude of the scattering vector $\overrightarrow{q}$ is considered to come from the dorsal side of the wing based on the observation that dorsal scales have narrower ridge spacing than ventral scales. The scattering vector $\overrightarrow{q}$ carries information of the length and orientation of scale structures. It is expressed as

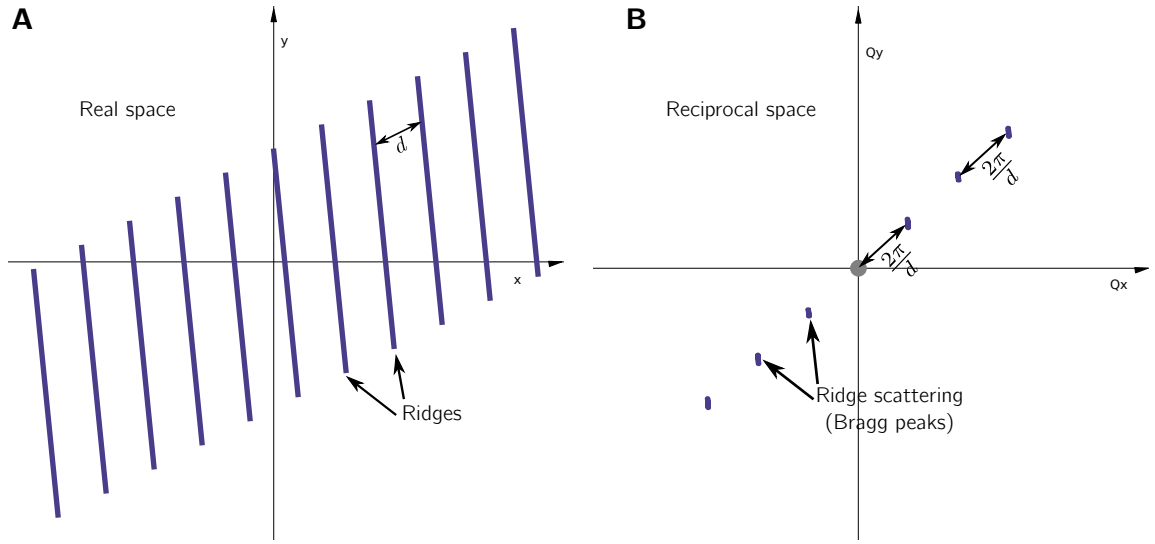

FIGURE 2.2: Parallel array of nano-structures (A) and its expected periodic scattering pattern (B). Notice that if the average distance between structures in real space is d, then the expected distance between the centre of the detector (grey circle), and between scattered spots in reciprocal space is $\frac{2\pi}{d}$. Scattered spots with this particular layout are known as Bragg peaks. Figure adapted from Sivia (2011), chapter 7.

$$\overrightarrow{q} = \frac{4\pi \sin\theta}{\lambda}$$

where 2θ is the scattering angle.

After identification of ridge scattering, the script rotates the angular section 85° anticlockwise to get the scattering due to the cross-ribs, which have an orientation perpendicular to that of ridge scattering. Azimuthal integration is then performed on the ridge and the cross-rib sections, reducing them to a one-dimensional representation of scattered intensity I as a function of the scattering vector $\overrightarrow{q}$. We normalised the data by transmitted flux and masked the pixels corresponding to the beam stop. The script uses the fabio (Knudsen et al., 2013) and pyFAI (Kieffer et al., 2013) libraries to read and write USAXS scattering data and to perform the azimuthal integration.

Despite dividing the scattering pattern in small regions to pick apart the signals due to different structures and scales, some frames still contained information from more than one scale, producing ambiguous peaks of intensity (Figure S2.2). Other frames didn't show the characteristic pattern expected for scale structures. These two phenomena introduce the possibility of erroneous measurements in the downstream analysis. 1D frames containing ambiguous peaks of intensity can be the result of overlapping scales with identical orientations that were probed by the beam in their area of overlap. Frames containing patterns significantly different from the expectation of a butterfly scale may be the result of the beam probing a region of the wing devoid of scales,

which is common for wings of old butterflies, or wings damaged by predators or careless manipulation. Our automatic procedure rejected frames possibly affected by either of these two phenomena flagging them as invalid. A frame was considered valid only if it contained at least two Bragg peaks, its highest measured intensity was above the stated threshold (1000 arbitrary units of scattered intensity for our experiments) and the error between predicted and estimated Bragg peaks was smaller than 1×10^{-4}. In a small number of cases the program was not able to flag invalid frames appropriately so we did a subsequent round of manual inspection to ensure all frames used downstream did not contain ambiguous or erroneous information.

Some of the frames contain a low-to-moderate amount of noise that can affect the estimation of nano-structure measurements. To reduce the level of noise and get more robust estimates we did a standard PCA using the scikit-learn package (Pedregosa et al., 2011). We retained the first 10 principal components, which explain over 90% of variation in the data. We projected the data onto the retained PCs, thus reducing the level of noise. The 90% explained variance threshold is arbitrary, but we find it is a good balance between noise reduction and retained information for our data.

The peaks of scattered intensity were fit to a Lorentzian curve (Fig. S2.3) using the `FitManager` module of the silx package (Vincent et al., 2020). The `center` parameter of the fitting procedure gives the magnitude of the vector $\overrightarrow{q}$. This magnitude contains information on the distance between peaks of intensity in reciprocal space; its units of measurement are inverse nano-metres (nm^{-1}). To get estimates of structure sizes in real space, we use the expression

$$d = \frac{2\pi}{\overrightarrow{q}}$$

where d is the corresponding quantity in real space, with units of measurement in real distance (nm).

2.3.4 Colour measurements

To investigate the relationship between colour and scale structure variation, we quantified changes in chromatic and achromatic components of digital photographs from wild caught and insectary reared and crossed individuals. Specifically, we measured the variation in blue colour and the total brightness or luminance of the discal cell of the wing.

The photographs were taken from fore and hind wings of butterflies lying on a flat surface under standard lightning conditions using a mounted Nikon D7000 DSLR camera with a 40mm f/2.8 lens with aperture set to f/10, shutter speed set to 1/60 and ISO set to 100. Lights were mounted at a 45° of incidence so that the observed blue reflection was maximised. An X-rite Colour Checker standard was included in all the images and subsequent step of standardisation was done using the `levels`

tool in Adobe Photoshop CS2 v9.0 software. RGB values were then recorded from standardised pictures using the ImageJ (Schneider et al., 2012) `Color histogram` plugin. The RGB values were averaged from the discal cell, the same wing area that USAXS measurements were taken from, as shown in Figure 2.1. We used the expression

$$BR = \frac{B - R}{B + R}$$

to quantify variation in blue colour. Here B and R are the blue and red components of the average `(R, G, B)` values obtained from the discal cell. This measurement gives us variation in blue-red value ranging from -1 to 1 where 1 is blue and -1 is red. Similar measurements have been used in other studies to quantify colour variation in a way that allows comparison between different species (Comeault et al., 2016). We also quantified luminance as

$$Luminance = R + G + B$$

2.3.5 Statistical analysis

Correlations between traits were estimated and tested using the Spearman's rank correlation coefficient ρ. Differences in trait estimates between races were assessed using one-way ANOVA and post-hoc Tukey tests. For ANOVA we wanted to evaluate differences in trait estimates between 'pure' races. We thus excluded individuals sampled in Fondiadero, Rio Chado and Rio Jaque (Jaque, table S2.1), since these locations harbour a high number of recombinant phenotypes and individuals of mixed ancestry (Nicola Nadeau, personal communication, and Curran et al., 2020) that may confound the analysis. We also assessed the presence of sexual dimorphism in a subset of the wild caught samples where sample availability allowed it, and in the individuals coming from crosses. For the wild caught samples we were only able to analyse *H. erato* races *H. e. cyrbia* and *H. e. venus*. Sex and race were jointly assessed using a two-way ANOVA to account for the possibility of sexual dimorphism depending on race. Sexual dimorphism in the crosses was assessed using a Welch's t-test. These analyses were done in the R statistical package (v3.6.1) (R Core Team, 2019).

2.4 Results

2.4.1 Dorsal and ventral sides differ in scale structure

We observed qualitative differences in scale structure between dorsal and ventral sides of the wing: comparisons within a single race reveal that scales on the dorsal side have ridges that are arranged more densely than those of the ventral side of the wing (Fig. 2.3 left vs. right). When comparing between iridescent and matt-black races of the same species (Fig. 2.3 row 1 vs. row 2, row 3 vs. row 4) it can be seen that the scale

architecture on the ventral side shows no apparent differences, whereas the dorsal side of iridescent races (Fig. 2.3, rows 2 and 4) shows smaller spacing between the ridges than that of the matt-black races (Fig. 2.3, rows 1 and 3). The non iridescent races *H. e. demophoon* and *H. m. rosina* show little to no differences between dorsal and ventral scales. In the iridescent races, apart from narrower ridge spacing, we observe that ridges appear wider, presumably accumulating larger quantities of chitin compared to those of matt-black individuals. Cover and ground scales from the same side of wings show no apparent differences between them in SEM images.

The observed differences in scale architecture between dorsal and ventral sides were quantified by measuring ridge spacing in SEM micrographs. We found that the ridge spacing of the dorsal side of the wing tends to be smaller than that of the ventral side of the wing in both *H. erato* and *H. melpomene*. This is regardless of butterflies being matt-black or iridescent blue (Fig. 2.4, table 2.2). We found differences in scale structure between races of the same species regardless of the side being compared. Apart from having slightly larger ridge spacing, *H. melpomene* shows more variation between individual scales than *H. erato* in both iridescent and matt-black individuals (Fig. 2.4, table 2.2).

TABLE 2.2: Summary statistics of ridge spacing variation in matt black and a blue iridescent races of *H. erato* and *H. melpomene*, as estimated from SEM. Measurements for single scales by race are plotted in figure 2.4.

Race	Ridge spacing (nm)			
	Dorsal scales		Ventral scales	
	Mean	Std. dev.	Mean	Std. dev.
H. erato				
demophoon	943	70.1	1147	70.5
cyrbia	782	82.2	1041	62.3
H. melpomene				
rosina	1068	123	1191	146
cythera	815	91.4	1153	172

2.4.2 Qualitative analysis of USAXS data reveals variation in main scale structures

We first inspected visually the frames resulting from the USAXS experiment. We could identify scattering patterns corresponding to a parallel array of structures, which in the case of the butterfly scales corresponds to scattering due to the ridges; notice the similarity between distributions of structures in real space and their scattering patterns in reciprocal space in both expected (Fig. 2.2) and observed (Fig. 2.5) results. When compared to cross-ribs in SEM images, ridges are clearly the more salient structures; they have higher amounts of chitin compared to cross-ribs (Fig. 2.5, right). Higher contrasts between chitin structures and air produce higher scattered intensities in the USAXS pattern. Since ridges contain more chitin than cross-ribs,

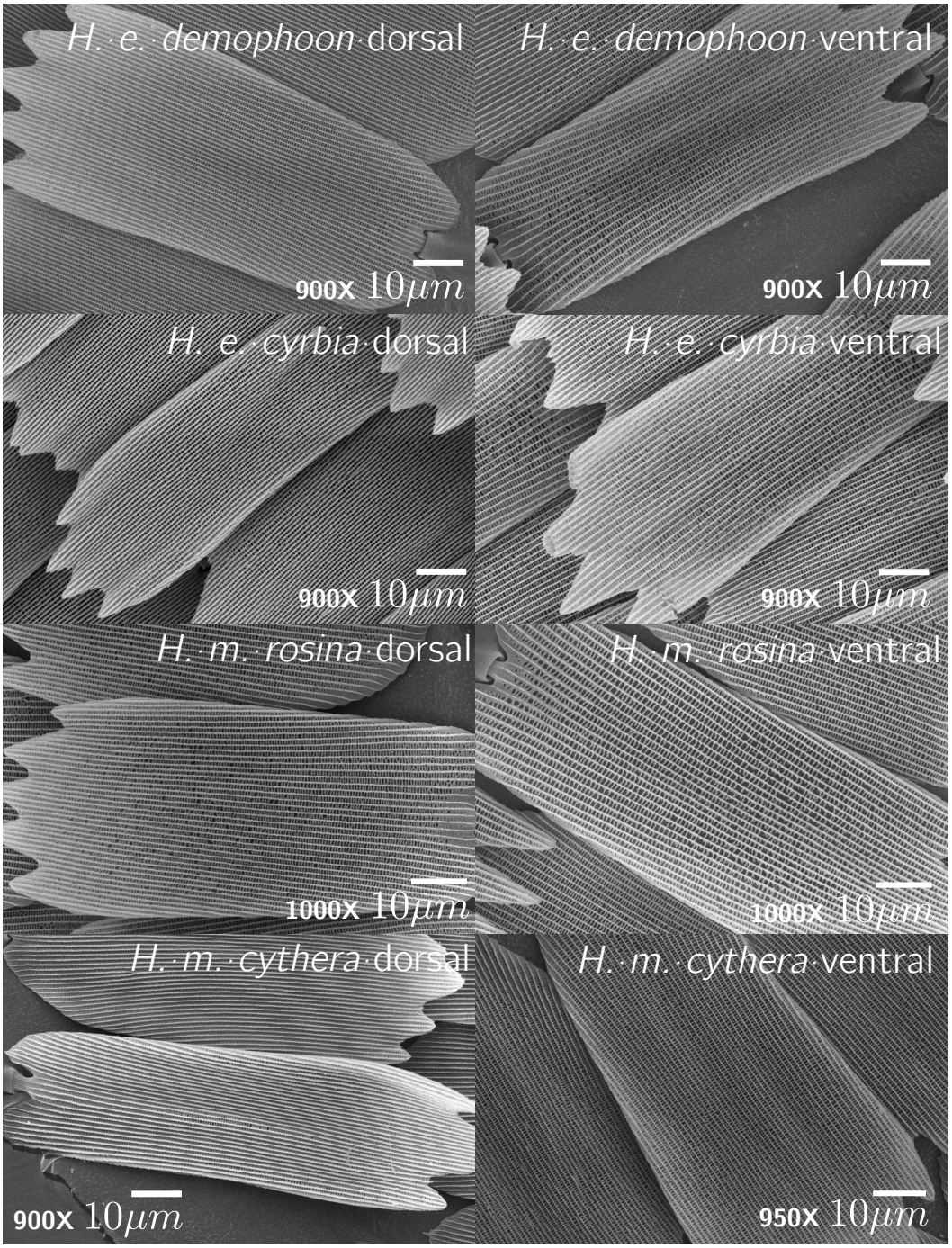

FIGURE 2.3: SEM images of dorsal (left) and ventral (right) non iridescent (rows 1, 3) and iridescent (rows 2, 4) individuals of *H. erato* and *H. melpomene*.

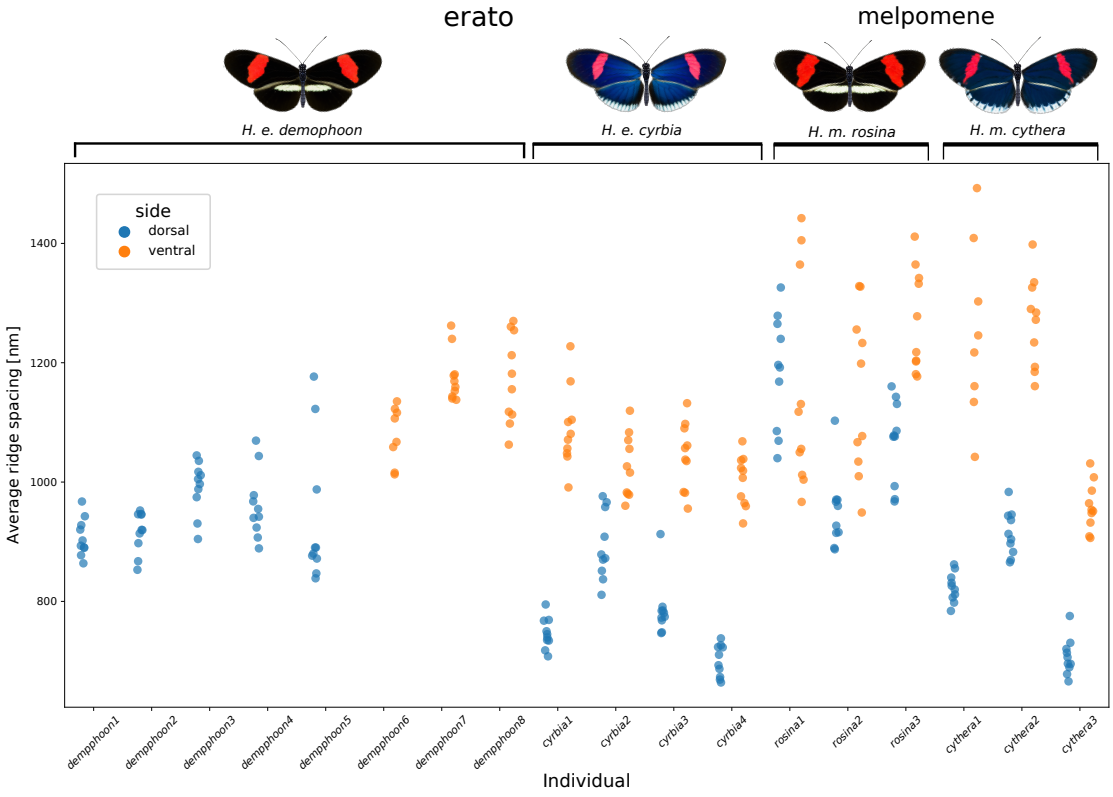

FIGURE 2.4: Comparison of ridge spacing between dorsal and ventral scales of insectary reared matt black and iridescent blue *H. erato* and *H. melpomene* estimated from SEM slides. Ventral scales show higher average spacing between ridges regardless of presence or absence of iridescence in the wing.

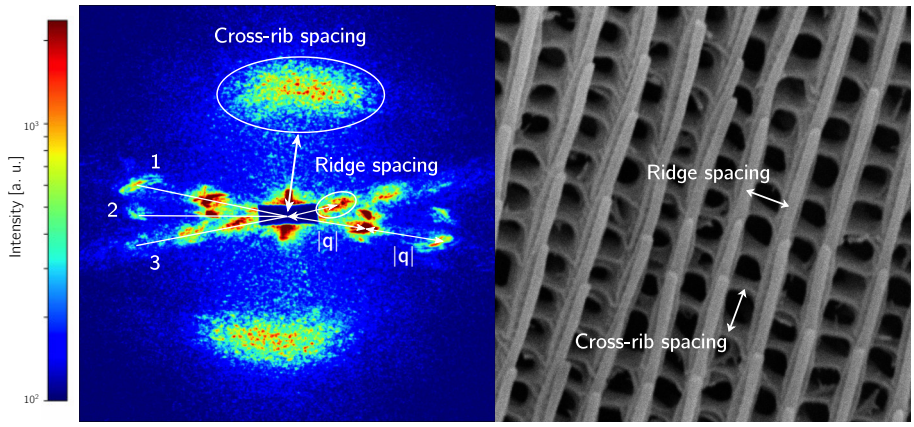

FIGURE 2.5: Representative scattering pattern captured in the USAXS experiment on *Heliconius* wings (left) and SEM slide of a *Heliconius* butterfly scale (right). Scattered intensities reveal oriented structures; these correspond to spacing between ridges and spacing between cross-ribs, which have a perpendicular orientation in the scale. For the ridges, it can be observed that blobs of scattered intensity appear with a regular spacing $|q|$ along a linear path; this is due to their organisation as a parallel array in the surface of the scale. Scattering of at least 3 different scales is observed, as indicated by the enumeration on the left hand side of the image.

their scattering pattern is higher in intensity (Fig. 2.5, left). We also observe that the scattering patterns with higher intensities are highly oriented; they follow straight lines stemming from the centre of the picture. Blobs appear along these straight lines with regular spacing; this is due to the interaction of the x-ray beam with a parallel array of structures as shown in figure 2.2. Thus, scattering patterns annotated with segments and numbers in figure 2.5 (left) correspond to scattering due to ridges. Perpendicular to these we find blobs of scattered intensity which are more disperse along the 2D layout than those produced by the ridges: these correspond to scattering due to cross-ribs, which are reduced compared to the ridges and have a less conserved orientation.

We noticed that scattering patterns of most individuals contained more than a single signature pattern of a butterfly scale. Figure 2.5 shows a frame with scattering from 3 different scales with slightly different orientations. This is because in our experimental setup the x-ray beam goes through the dorsal and ventral sides of the wing, projecting onto the detector the scattering due to structures of as many as four scales per sample: cover and ground scales on both dorsal and ventral sides of the wing. Our SEM analysis reveals that the dorsal side of the wing is covered in scales with smaller ridge spacing than the ventral side regardless of the visual appearance of the individual. These differences in ridge spacing between dorsal and ventral scales are discernible in the USAXS data (fig. 2.5, left). As we were only interested in the dorsal side of the wing, which has the iridescent colour, we selected the scattering patterns corresponding to the ridges with the smallest spacing.

2.4.3 Selective azimuthal integration

After selecting the scattering patterns with the smallest ridge spacing, some were left out because they did not meet the quality thresholds mentioned earlier. We retained 385 good quality 2D USAXS patterns out of 795 total (48%) for wild caught *H. erato*. For wild caught *H. melpomene* 315 good quality USAXS patterns out of a total 539 were retained (58%). For crossed individuals we retained 2901 good quality patterns out of a total 14 457 (20%) for *H. erato* and 3664 out of 18 733 (19.5%) for *H. melpomene*. The number of frames used per individual for wild caught samples ranged from 5 to 120 for *H. erato* and from 3 to 73 frames per individual for *H. melpomene*. For F1 and F2 offspring the number of frames used per individual ranged from 17 to 73 for *H. erato* and from 20 to 86 for *H. melpomene*. Full details of the number of frames used per individual can be found in supplementary tables S2.1 and S2.2.

2.4.4 Quantitative variation of scale morphology in wild caught individuals

We found that scale structure and colour vary quantitatively along the transects from Panama to Ecuador in both species. It can be observed that as latitude decreases, the spacing between ridges is gradually reduced (Fig. 2.6 A, B). The variation among locations and across latitudinal transects is different for both species. For *H. erato* the ridge spacing decreases along the transect, having a maximum in Panama and a minimum in *H. e. venus* in West Colombia (Fig. 2.6, left). Interestingly, as the transect continues further south into Ecuador, the iridescent race *H. e. cyrbia*, which has wings that are brighter and of a more vivid blue colour than than those of *H. e. venus*, shows a slight increase in ridge spacing. For *H. melpomene* a similar behaviour can be observed in which ridge spacing decreases as the transect extends down south. In this species the lowest estimates of ridge spacing can be found in the Ecuadorian iridescent *H. m. cythera*, which is the race of *H. melpomene* that shows the most conspicuous iridescent blue colour.

Cross-rib spacing shows a pattern opposite to that of ridge spacing in *H. erato*: Individuals from the Panamanian populations (north) show a slight increase as latitude decreases (Fig. 2.6 C). In *H. melpomene* cross-rib estimates show a decreasing trend as latitude decreases albeit the change is not substantial (Fig. 2.6 D). Overall cross-rib spacing shows the largest variation of all phenotype estimates, possibly suggesting that it may be under weaker selection.

BR value, the estimate used to measure variation between black and blue, increases in both species as latitude decreases, which is expected as iridescent races are found in West Colombia (Purple) and in Ecuador (Orange) (Fig. 2.6 E, F). BR value shows more variability in *H. melpomene* than in *H. erato* across all localities except in Ecuador, where individuals of both species show the most vivid structural colour.

Luminance behaves similarly to BR value, with *H. erato* individuals from northern latitudes showing the lowest values and individuals from West Colombia (Purple) and Ecuador (Orange) showing an increase in luminance (Fig. 2.6 G). In *H. melpomene* similar levels of luminance are observed across several localities except for those corresponding to admixed individuals where luminance values are the lowest (Fig. 2.6 H).

It is noteworthy that individuals that have previously been reported as of mixed ancestry between Panamanian and Colombian populations (Curran et al., 2020) show intermediate levels of variation in scale structure and structural colour (Fig. 2.6, pink fringes) except for cross-rib spacing in *H. erato* and luminance in *H. melpomene*. We also find that variation in scale morphology and structural colour is quantitative within populations that show otherwise no obvious variations in pigmented wing patterns (i.e. are described as a single geographical race, Figs. 2.6). This suggests that there is considerable quantitative variation in scale structure and structural colour within populations defined both as collections of individuals from a singular location (Fig. 2.6) and as individuals that share membership to defined geographical races (Figs. 2.4, 2.7).

If selection pressure on a particular trait is not very strong in hybrid populations we would expect to find greater variation of that trait in hybrids than in parental populations. This is because intermediate phenotypes are viable and thus a wide range of phenotypic variation can be observed. The variation in hybrids is greater for some trait estimates in hybrid populations compared to parental populations. In particular, ridge spacing and luminance in *H. erato* (Fig. 2.6 A, G) show large variation in hybrids compared to parental races *H. e. hydara* and *H. e. venus*. Interestingly, individuals from the iridescent race *H. e. venus* from the northernmost locality show greater variability in ridge spacing than other *H. e. venus* (Fig. 2.6 A). This could possibly be because of natural back-crossing of hybrids with populations of *H. e. venus* that are close to the hybrid zone.

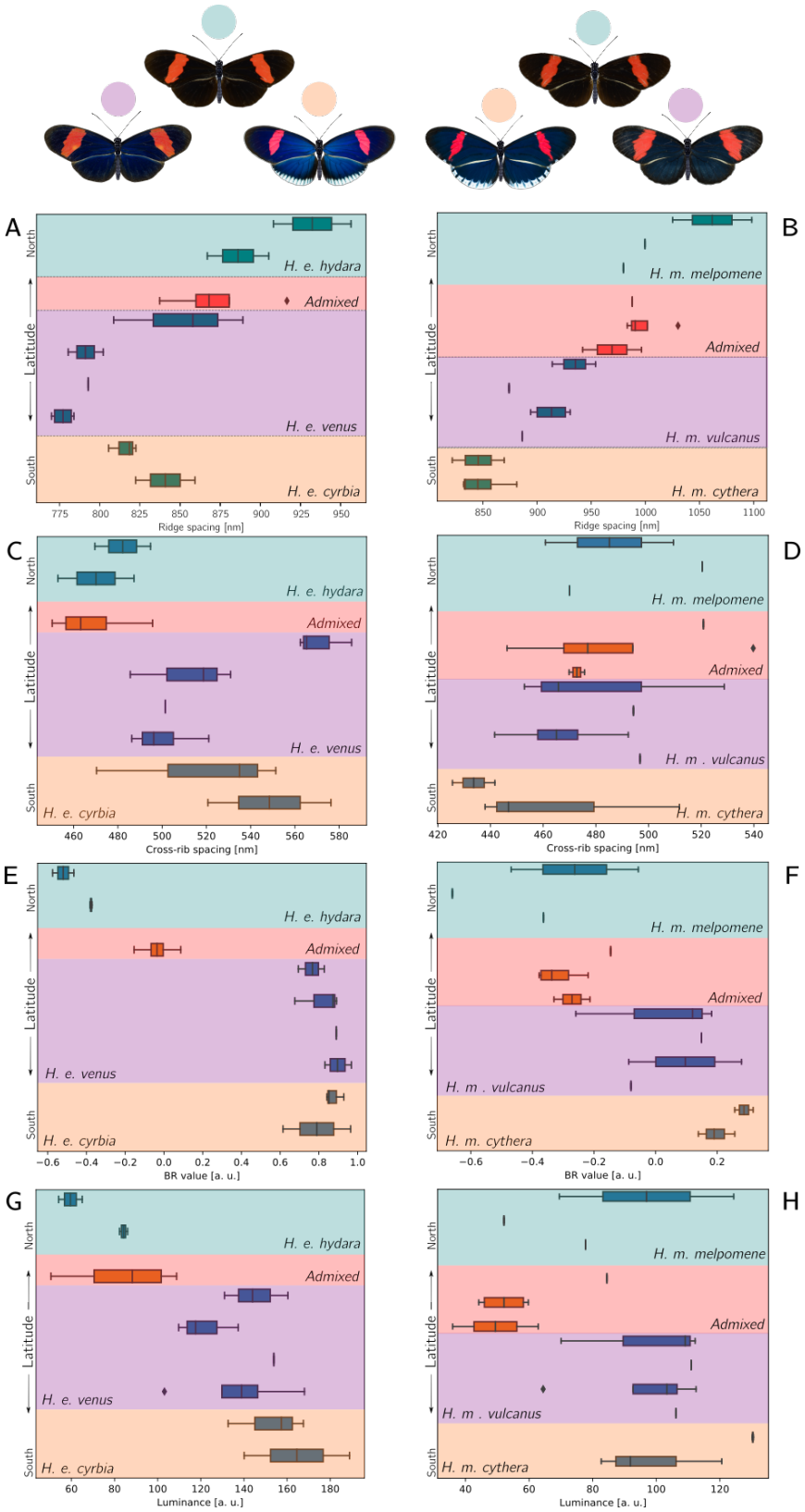

FIGURE 2.6: Phenotypic variation (scale morphology and colour) across a latitudinal gradient in *H. erato* (left) and *H. melpomene* (right). Location of wild caught samples is arranged by latitude from north (Panama) to south (Ecuador) along the vertical axis. Overlay colours indicate the geographical race to which populations belong. BR value is a measure of variation between blue and matt-black and luminance is a measure of variation in brightness of the wing. Ridge spacing (A, B); cross-rib spacing (C, D); BR-value (E, F); luminance (G, H).

2.4.5 Variation in scale morphology and structural colour between populations and between sexes

We tested whether there are differences in scale structure and structural colour among geographic races within each species. There is a significant association between race and mean ridge spacing for both species (*H. erato* F = 14.39; n = 20; d.f. = 2; $p < 0.001$. *H. melpomene* F = 34.58; n = 18; d.f. = 2; $p < 0.001$), as seen in panels A and B of figure 2.7. There is also a significant association between race and BR value estimates for both species (*H. erato* F = 243.49; n = 20; d.f. = 2; $p < 0.001$. *H. melpomene* F = 14.36; n = 18; d.f. = 2; $p < 0.001$) (panels G, H, figure 2.7). Only *H. erato* showed significant differences for luminance among races (F = 22.03; n = 20; d.f. = 2; $p < 0.001$), figure 2.7 E. We found there are no significant differences in mean cross-rib spacing between races of either species (*H. erato* F = 3.48; n = 20; d.f. = 2; p = 0.053; *H. melpomene* F = 2.79; n = 18; d.f. = 2; p = 0.09), figure 2.7 C, D. Specifically, the significant differences were found for the comparison between iridescent blue races vs. matt-black races, except for ridge spacing in *H. melpomene*, which showed significant differences in ridge spacing among the three races that were compared (Table 2.3).

TABLE 2.3: Summary statistics of variation of four traits across geographical races of each species. Mean estimates followed by the same letter superscript did not differ significantly between them (Tukey test, $p > 0.05$). Mean estimates without a superscript did not show significant differences between races.

Race	Ridge spacing (nm)		Cross-rib spacing (nm)		BR value (a.u.)		Luminance (a.u.)	
	Mean	Std. dev.	Mean	Std. dev.	Mean	Std. dev.	Mean	Std. dev.
H. erato								
hydara	909^a	36.7	476	18.7	-0.45^a	0.09	71.8^a	15.0
venus	803^b	37.5	523	34.7	0.84^b	0.09	137^b	20.4
cyrbia	826^b	20.1	531	39.6	0.84^b	0.14	157^b	22.4
H. melpomene								
melpomene	1018^a	47.9	496	28.7	-0.34^a	0.24	81.6	26.8
vulcanus	913^b	25.8	478	27	0.05^b	0.16	99.1	18.5
cythera	848^c	26.1	453	33.9	0.23^b	0.07	111	22.4

Furthermore, we assessed the effects of race and sex on phenotypic variation jointly to examine whether there is sexual dimorphism and whether sex differences vary among races. We did this only for *H. erato* because of lack of phenotyped females in *H. melpomene*. We used a two-way ANOVA (n = 16), accounting for an unbalanced design since the number of available individuals of each race and sex combination was unequal among different categories (Table S2.1). Here we tested *H. erato* individuals from the blue, iridescent races *H. e. cyrbia* (Ecuador) and *H. e. venus* (West Colombia) and excluded *H. e. hydara* (Panama), which had only one female available. Using this approach we found significant effects of sex on ridge spacing variation at a significance threshold of 0.05, but we found no evidence that race or the interaction between sex and race have an effect on ridge spacing (Table 2.4). Similarly, sex has a

significant effect on cross-rib spacing variation according to our data, but race or the interaction between sex and race did not show significant effects on cross-rib spacing (Table 2.4). For BR value and luminance, none of sex, race or the interaction between these factors showed significant effects (Table 2.4). These results require careful interpretation since sample sizes are small (*H. e. cyrbia*: 3F, 2M; *H. e. venus*: 3F, 8M) and they will likely change as more samples are included. In this analysis race does not have a significant effect on phenotypic variation because only iridescent races were compared, resulting in a similar outcome to that of the one-way ANOVA (Table 2.3). It is possible that we may observe a significant effect of race if iridescent and non-iridescent races of *H. erato* are included in the joint analysis of sex and race, possibly also resulting in evidence for an interaction between sex and race.

TABLE 2.4: Two-way ANOVA results for *H. erato*. Only the iridescent races *H. e. cyrbia* and *H. e. venus* were assessed. The degrees of freedom were 1 for all contrasts. The F statistic and p-value from the statistical analysis are shown for four traits. Significance levels: $p < 0.05^{*}$, $p < 0.01^{**}$

	F	p-value
Ridge spacing		
sex	5.24	0.04*
race	1.53×10^{-1}	0.70
sex:race	1.51	0.24
Cross-rib spacing		
sex	13.06	3.55×10^{-3}**
race	0.38	0.55
sex:race	0.07	0.80
BR value		
sex	2.13	0.17
race	0.46	0.83
sex:race	2.79	0.12
Luminance		
sex	0.13	0.73
race	2.12	0.17
sex:race	0.68	0.42

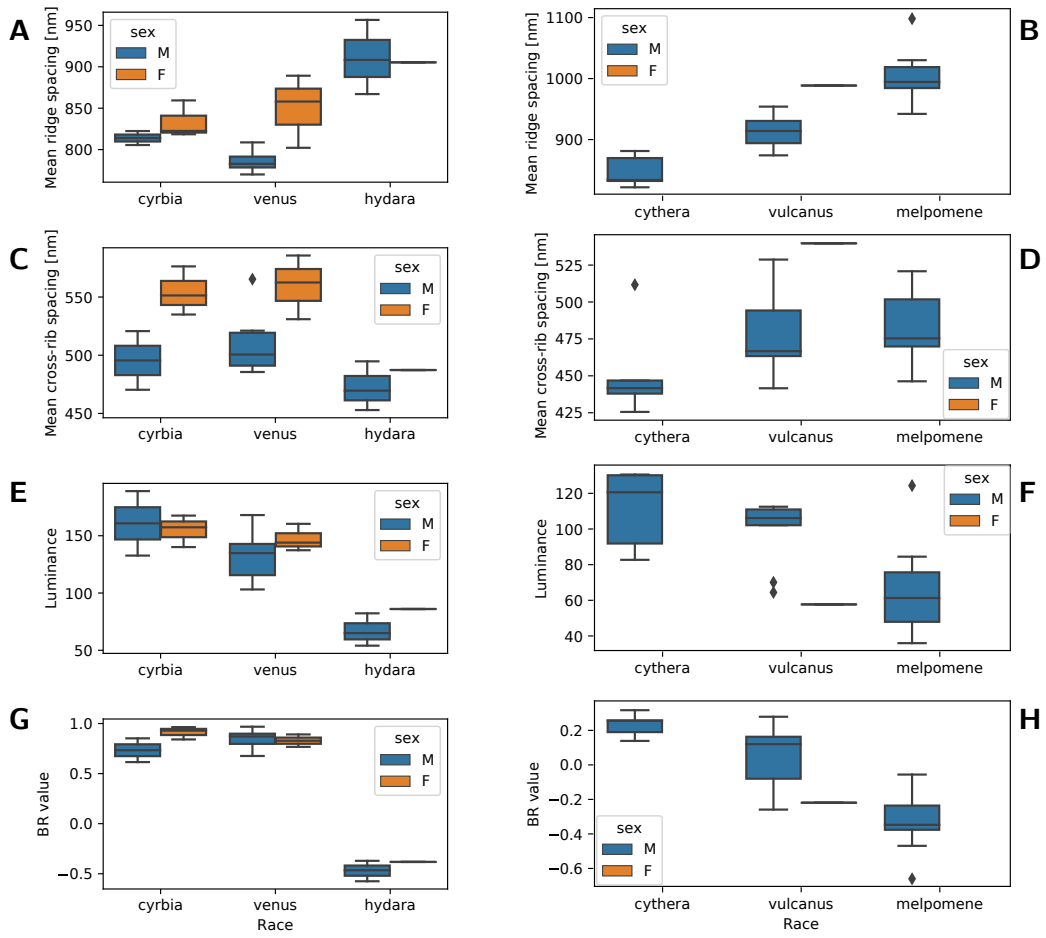

FIGURE 2.7: Distributions of phenotypic estimations for *H. erato* discriminating by sex and race (left) and *melpomene* (right). Note that for *H. erato hydara* and *H. melpomene* there are very low numbers of females, leading to narrow quantile ranges. Ridge spacing (A, B); cross-rib spacing (C, D); luminance (E, F); BR-value (G, H).

2.4.6 Scale morphology is correlated with structural colour in wild caught *Heliconius*

We expected to find a correlation between ridge spacing and luminance because it has been hypothesised that a denser arrangement of reflective structures will lead to a more reflective wing (Parnell et al., 2018). We found significant correlations between ridge spacing and estimates of colour variation in *H. erato* (luminance, $p < 0.05$, BR-value $p < 0.001$, n=24) and *H. melpomene* (luminance $p < 0.001$, BR-value $p < 0.001$, n=25) (Fig. 2.8, Table 2.5). A stronger negative correlation between ridge spacing and luminance was observed for *H. melpomene* compared to *H. erato* in terms of correlation coefficient ρ, which is probably due to the increased spacing in the iridescent race *H. e. cyrbia* compared to *H. e. venus*, which is also iridescent.

Cross-rib spacing was found to correlate positively and significantly with colour measurements only in *H. erato* (luminance $p < 0.01$, BR-value $p < 0.05$), suggesting that this species may modulate scale architecture in a different manner compared to *H. melpomene*. The positive correlation between cross-rib spacing and colour variation is unexpected because this aspect of scale architecture has not been reported to play a role in the production of iridescent structural colour, and because we do not observe significant correlations between ridge spacing and cross-rib spacing in *H. erato* (Table 2.5).

Luminance and BR-value correlate positively and strongly as expected since both estimates will depend strongly on the amount of blue reflectance, as this is expected to be the main colour channel in which reflectance varies ($p < 0.001$ for *H. erato* and *H. melpomene*).

TABLE 2.5: Spearman's ρ estimates of correlation for scale structure and colour variation in wild caught *H. erato* and *H. melpomene*. Significance levels: $p < 0.05^{*}$, $p < 0.01^{**}$, $p < 0.001^{***}$.

Race	Ridge spacing	Cross-rib spacing	BR value
H. erato			
Cross-rib spacing	-0.135		
BR value	-0.711^{***}	0.460^{*}	
Luminance	-0.504^{*}	0.586^{*}	0.641^{***}
H. melpomene			
Cross-rib spacing	0.238		
BR value	-0.818^{***}	-0.211	
Luminance	-0.674^{***}	-0.030	0.777^{***}

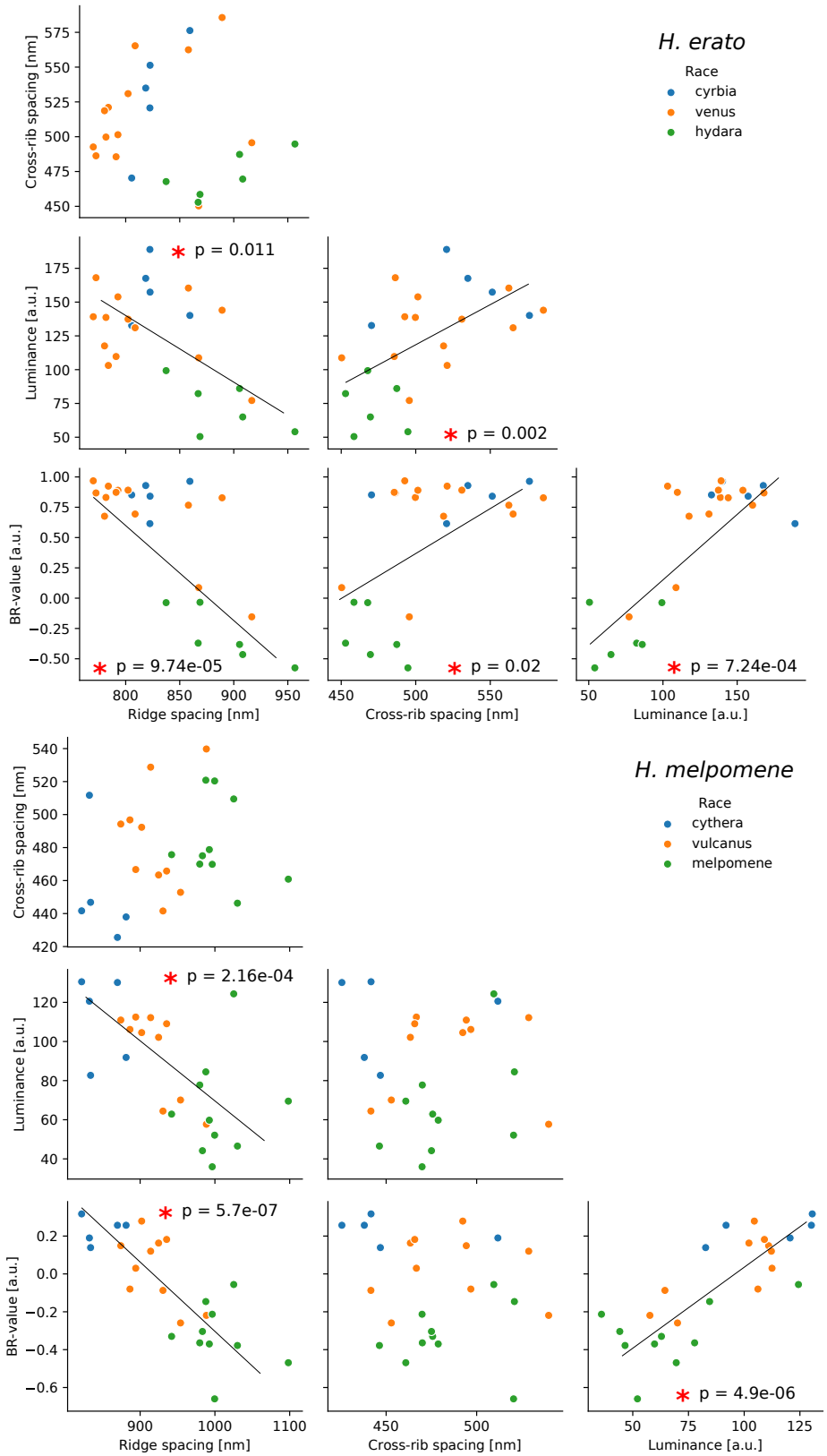

FIGURE 2.8: Scatter plots showing the relationships between estimates of colour and scale structure in wild caught *H. erato* (top) and *H. melpomene* (bottom). Colour is used to discriminate estimates by geographical race. Significant correlations are indicated with a red asterisk (*), a trend line showing the direction of the correlation, and its p-value. Correlation estimates are given in the table 2.5.

2.4.7 Quantitative variation of scale morphology in crosses

The distributions of estimates of scale structure variation in *H. erato* EC17 and *H. melpomene* EC70 families overlap the mean phenotypic values of 'pure' individuals (Fig. 2.9). No discrete phenotypic variation related to scale structure, blue colour or luminance was detected among the offspring of the crosses of *H. erato* or *H. melpomene*. This suggests that in both species multiple loci are involved in the modulation of scale architecture (ridge spacing and cross-rib spacing), and the production of structural colour. Trait distributions of F1 generations show in general less variance than those of later generations (F2 for *H. erato*, EC70 for *H. melpomene* Fig. 2.9), although we would require larger sample sizes of F1 individuals to further comment on their phenotypic variation and how it compares to that of later or parental generations.

2.4.8 Correlations between scale morphology and colour in offspring individuals

We assessed correlations between traits among insectary reared individuals (EC17 and EC70 families) to determine whether variation in scale structure and variation in structural colour could be genetically coupled. This allows us to assess where tighter genetic couplings between different traits may be and may hint about whether these couplings are conserved among different races and species. Correlations in the wild and correlations in the crosses may differ because of genetic couplings being lost after a few events of recombination among generations and also because a broader sampling in the wild caught individuals may include genetic backgrounds and specific variants associated with phenotypes that vary across the sampling range. We found significant correlations between scale structure and colour measurements for the *H. erato* EC17 family ($n = 56$). Ridge spacing shows a negative correlation with both luminance ($p < 0.001$) and BR value ($p < 0.001$). We also found significant correlations between ridge spacing and cross-rib spacing ($p < 0.01$) and between BR value and luminance ($p < 0.05$). For the *H. melpomene* EC70 family ($n=73$) we found significant correlations only between BR value and luminance ($p < 0.01$) but not for BR value and ridge spacing ($p = 0.709$), luminance and ridge spacing ($p = 0.277$), or ridge spacing and cross-rib spacing ($p = 0.25$). Note that due to the unknown ancestry of the mother of EC70 this comparison requires careful interpretation as it is likely that there are differences in power because crosses have different structures.

2.4.9 Sexual dimorphism in scale structure and structural colour

We assessed the presence of sexual dimorphism in offspring individuals. Only later generation individuals (EC70 and EC17) were assessed for sexual dimorphism. We found that only *H. erato* F2 showed significant differences between female and male estimates of variation for ridge spacing, cross-rib spacing and BR-value but not luminance. Individuals from *H. melpomene* EC70 family do not show differences between males and females in any of the four estimates analysed (Table 2.7). Again, it is likely

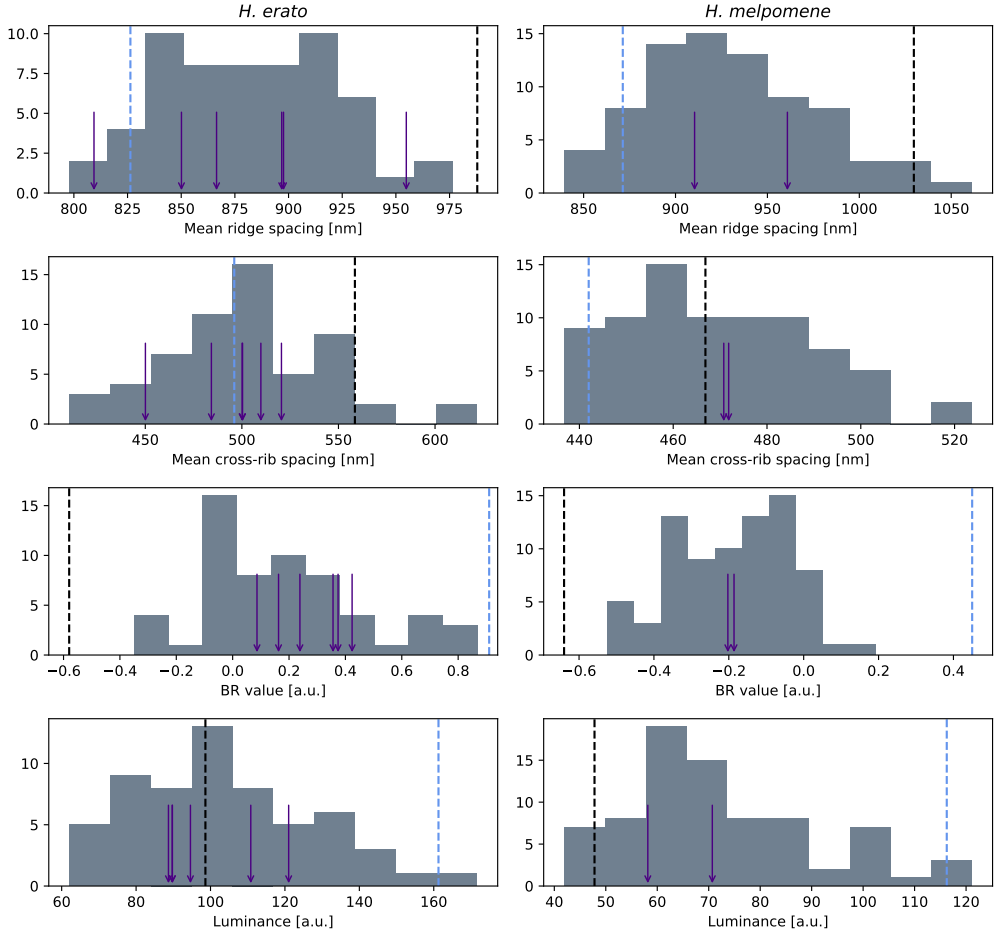

FIGURE 2.9: Histograms of trait distributions for F1 and later generations of *H. erato* (EC17) and *H. melpomene* (EC70) inter-crosses. The dashed lines correspond to the mean trait estimates of *H. e. demophoon*, *H. m. rosina* (black), *H. e. cyrbia* and *H. m. cythera* (blue). Trait estimates represented by dashed lines come from wild caught individuals of each race unrelated to the offspring individuals. Purple arrows correspond to phenotypic measurements of F1 individuals.

TABLE 2.6: Spearman's ρ estimates of correlation for scale structure and colour variation in offspring individuals of *H. erato* and *H. melpomene*. Only data from the offspring individuals (EC17 and EC70) is included in this table. Significance levels: $p < 0.05^{*}$, $p < 0.01^{**}$, $p < 0.001^{***}$.

Race	Ridge spacing	Cross-rib spacing	BR value
H. erato			
Cross-rib spacing	0.342^{**}		
BR value	-0.41^{**}	-0.325^{**}	
Luminance	-0.46^{***}	-0.18	0.341^{***}
H. melpomene			
Cross-rib spacing	-0.088		
BR value	0.001	0.056	
Luminance	-0.117	0.138	0.295^{**}

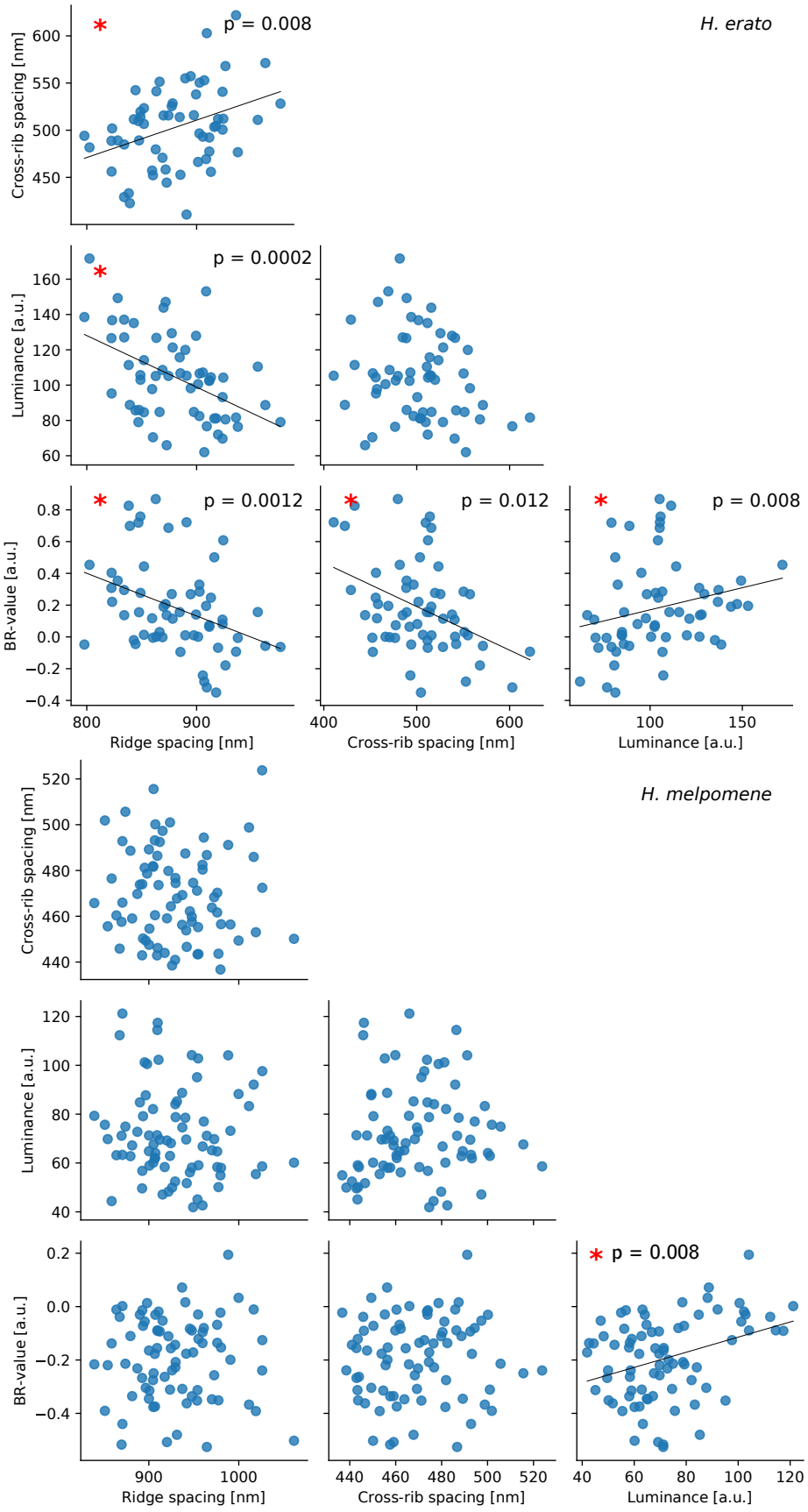

FIGURE 2.10: Trait correlations for offspring individuals of *H. erato* and *H. melpomene* inter-crosses. Only trait estimates of offspring individuals (EC17 and EC70) are included in this plot. Trend lines are included where correlations are significant to indicate the levels of correlation among traits. Significant correlations are marked with a red asterisk (*) and have their p-values included.

TABLE 2.7: Female-male comparison of scale structure and colour estimates in crosses. Welch's t-test results are shown. Numbers in parentheses next to the name of each race/generation denote the number of females and males available and used for the test. Significance levels: $p < 0.05^{*}$, $p < 0.01^{**}$, $p < 0.001^{***}$.

	Trait	Estimate (F)	Estimate (M)	t	d.f.	p-value
H. erato						
$F2_{(34,\ 25)}$	Ridge spacing	896	861	3.74	57	4.25×10^{-4}***
	Cross-rib spacing	521	479	4.28	49	8.57×10^{-5}***
	Luminance	102	108	-1.01	48.6	0.32
	BR value	0.08	0.33	-3.51	44	0.001**
H. melpomene						
$EC70_{(37,\ 41)}$	Ridge spacing	929	930	-0.03	73.6	0.97
	Cross-rib spacing	471	468	0.52	75.8	0.61
	Luminance	74.5	70	1.07	75.9	0.29
	BR value	-0.21	-0.18	-0.99	75.3	0.33

that the power to do this analysis is different between EC17 and EC70 due to the differences in cross structure, so we cannot completely discard the presence of sexual dimorphism in offspring *H. melpomene* with this analysis.

2.5 Discussion

A great variety of mechanisms of colour production in butterflies, moths and other animals; plants and micro-organisms have been well documented. The physical principles of structural colour production are well established and newer descriptions are more detailed variations of mechanisms described and explained mostly during the twentieth century (Ghiradella, 1985; Ghiradella et al., 1972; Ghiradella, 1974; Silberglied et al., 1973; Vukusic et al., 1999). We are starting to focus on the lesser known biological aspects of structural colour such as detailed descriptions of its natural variation (Araki et al., 2020; Curran et al., 2020; Parnell et al., 2018; Wilts, Vey, et al., 2017), its ecological function, genetic basis and development (Brien et al., 2018; Dinwiddie et al., 2014; Thayer et al., 2020; Zhang et al., 2017). The results presented in this chapter offer insights into the natural variation of scale structure associated with structural colour.

2.5.1 Technical considerations

In this chapter we show that USAXS complemented with electron microscopy experiments can be used to accurately quantify aspects of scale structure that differ between populations and are correlated with changes in structural colour.

Structural colour is a complex trait with various sides to it and the effort of measuring and quantifying its variation may be equally complex. Historically, researchers have relied on optical theory and electron microscopy to study structural colour, achieving highly detailed characterisations of the nano-structures behind structural colour production. These characterisations are often limited to a few samples and this is normally sufficient for the description of the production of colour from structure.

Scaling these methods can prove impractical, nevertheless some studies have successfully applied electron microscopy on large numbers of samples when specimen wings are expendable (Day et al., 2019).

In our large scale phenotyping approach we used USAXS, which offers several advantages over microscopy, including the possibility to re-use wings of particular interest for other measurements since it is a non-destructive method. It does require, however, complementary microscopy data for disambiguation of scattering signals and for identification of the features of interest. The rationale behind signal selection from our USAXS data using the SEM results as reference allowed us to separate measurements from the dorsal surface only; we showed that scales from the dorsal side show overall smaller spacing between ridges. Hence, we expect good resolution that allows us to make comparisons of scale morphology based on the dorsal surface of the individuals analysed. Despite using a technique that allows access to minute details of materials, we found a limitation in the resolution that we could achieve to analyse *Heliconius* scale structures. Future experiments should be done at closer sample to detector distances and involve single scales for full resolution of the smallest components of scale architecture. This would allow, for example, the interrogation of the lamellae layering within the ridges, which is also key in the understanding of structural colour production (Kinoshita et al., 2008; Parnell et al., 2018).

We also present estimates of colour variation derived from digital photography, which bear relationships with structural features of the scales as shown by our results. Data derived from digital pictures has advantages and limitations. Analysis of data from photographs can be done in relatively short time but prohibits the examination of interesting features of iridescent structural colour such as angle dependence. In addition, it may not allow the characterisation of true colours (Kertész et al., 2021) and it may not capture all the variation in colour. Transformations of colour values extracted from photographs are useful for characterisation of phenotypic variation but require careful interpretation, as they may introduce error or unwanted effects in some cases. For example, wings that are more reflective will have higher values of luminance. On average, it is expected that all colour channels of a more reflective wing will increase in value; in the case of blue wings, not only blue and green are expected to show high values but possibly also the red channel will have an increased value. This means that when we subtract red from blue in the BR value expression, the resulting BR value will be smaller for a wing with high luminance than for one with decreased overall luminance. For example, wings from the iridescent *H. e. chestertonii* (part of the data but not shown in the main results) are qualitatively brighter and have a more conspicuous blue hue than those of the blue *H. e. venus* and *H. e. cyrbia*. Nevertheless, the blue-red value of *H. e. chestertonii* is the lowest compared to any of the *H. e. venus* or *H. e. cyrbia* individuals of our data set (Fig. S2.4, F, H). Incidentally, the *H. e. cyrbia* and *H. e. venus* with the lowest blue-red values do not have low blue values but rather high red values and luminance estimates (Figs. S2.4 and S2.5).

2.5.2 Variation in scale morphology offers insights into the genetics and evolution of structural colour

H. erato and *H. melpomene* have a rather high degree of overlap in scale structure variation, but there are differences between them. This is unsurprising if we consider the obvious differences in visual appearance between iridescent races of both species (Fig. 2.6, top), but it becomes intriguing when we consider that matt black races of both species have different ranges of variation in ridge spacing, as seen in figure 2.6. Although clearly selection is acting on both species and causing morphological change in the scales, there seem to be physical limitations to both ends of ridge spacing distribution and our data suggests that limitations are different for different species. From both SEM and USAXS data we observe that *H. erato* possibly is restricted to having ridges with spacing between 750 nm and 980 nm approximately, whereas ridge spacing in *H. melpomene* may possibly be restricted to an approximate range between 850 nm and 1100 nm. Similar ranges of scale structure variation are observed in both wild caught and offspring individuals, which means that the inter-cross experiments captured the morphological variation for both species comprehensively and are adequate for a genetic analysis of scale structure variation.

As of yet we do not know what underlies the different limits in scale structure variation for different species independent of wing appearance: We observe that *H. melpomene* may not produce ridges as tightly packed as those of *H. erato*, but we also observe that *H. erato* cannot produce ridge spacing as sparse as *H. melpomene* does, yet it is able to produce matt black wings with no appreciable difference to those of *H. melpomene*. It is possible that a long divergence time between *H. erato* and *H. melpomene*, which is approximately 10 to 13 million years (Kozak et al., 2015), and the myriad evolutionary processes and effects of divergent selection between the two species likely have resulted in accumulation of differences in developmental processes that give rise to adult scales (Van Belleghem et al., 2021). It has been argued that the blue iridescence of *H. melpomene* is not as colourful and bright as that of *H. erato* likely because of developmental constraints (Curran et al., 2020; Parnell et al., 2018). Our results provide evidence that partly supports the explanation that developmental biases explain differences in structural colour between sympatric *H. erato* and *H. melpomene*. Nevertheless we cannot rule out the hypothesis that ecology has played a role in shaping the differences between co-mimic structurally coloured butterflies of these two species.

Comparisons of SEM measurements of dorsal and ventral scales of iridescent and black *H. erato* and *H. melpomene* revealed an interesting feature of scale structure evolution and hints about a possible genetic mechanism underlying this trait in some butterflies. The dorsal and ventral scales differ in morphology in both species. This difference is accentuated when the individuals have iridescent structural colour, which in *Heliconius* butterflies is observed on the dorsal side only as opposed, for example, to some species of Pipevine Swallowtail butterflies that display dorsal and ventral

blue iridescence (Rutowski et al., 2010). This suggests that the development of scales that produce iridescent structural colour in *Heliconius* depends on genes that will not diffuse to both sides of the wing but that rather have their expression restricted to the abwing (dorsal side). It is possible that homeotic selector genes are involved in the developmental network of structural colour, enabling different developmental cascades in the dorsal and ventral sides of the wings of matt-black and iridescent blue individuals. Homeotic selector genes have been shown to mediate differential development and patterning of dorsal and ventral sides of butterfly wings (Prakash et al., 2018).

Another aspect that could hint about the genetic architecture of structural colour in these co-mimics is the association between trait variation and sex, or lack of thereof, in wild caught and offspring individuals of both species. The associations between trait variation and sex differ between *H. erato* and *H. melpomene*. There are differences in scale structure variation between sexes when comparing these within geographical races and in F2 individuals of *H. erato*. Wild caught males of iridescent races and males in the F2 offspring tend to have more closely distributed ridges and cross-ribs. Males with higher BR-value estimates were observed in the F2 and not in the wild caught individuals, and luminance was slightly higher in F2 males albeit not significantly. Our observations on sex differences in scale structure variation and colour related traits in *H. erato* are possibly due to structural colour being sex-linked in this species (Brien et al., 2018). Sex differences could not be tested for wild caught *H. melpomene* because of the limited availability of females in our USAXS experiment, but *H. melpomene* F2 males and females did not show differences in any of the traits analysed. Thus, it is possible that there are not associations between trait variation and sex in *H. melpomene* and sex linkage may be weak or absent in this species.

Sex differences in structural colour have been observed in other butterfly species in which structural colour is used for courtship (Silberglied et al., 1978) and mate choice (Rutowski, 1985). These differences possibly arise due to the ecological role of structural colour in inter-sex interactions even when both sexes show iridescent structural colour (Rutowski et al., 2017). The presence of sex differences in structural colour in only one of the species hereby analysed could hint at different genetic architectures of structural colour for these co-mimics, because it is predicted that traits that are sexually dimorphic are controlled by genes located on the sex chromosomes (Rice, 1984). Thus, we may predict that genes controlling structural colour will be likely located on the sex chromosomes of *H. erato* and on one or several autosomes of *H. melpomene*. For completeness and appropriate comparisons between races and between species it would be useful to analyse differences in scale structure variation between sexes using sufficient and balanced sampling of wild caught individuals.

Variation in scale structure as measured by changes in ridge spacing and cross-rib spacing possibly has a complex, sparse genetic architecture. The distributions of these traits among the wild caught individuals of both species hint towards traits being

controlled by several loci. Both when examining trait distributions among individuals belonging to the same nominal race (Fig. 2.4) and when doing a finer discrimination by geographical locality for ridge spacing (Fig. 2.6) we observe a continuous distribution along the geographical variation we studied here and continuous variation within localities. The wild caught individuals we use here are a sub-set of those analysed by Emma Curran in her hybrid zone cline analysis paper (Curran et al., 2020). A few individuals of both species were collected in localities of the hybrid zone in which specimens show mixed genetic ancestry (Curran et al., 2020). These individuals show intermediate levels of variation in structural colour related traits relative to their putative parental populations. Our interpretation of this result is that there are possibly blocks of either ancestry recombining in the genome of admixed individuals and that these ancestry blocks containing the different alleles of several genes controlling these traits are producing the observed intermediate levels of variation. This is backed up by the presence of intermediate phenotypes in controlled crosses in both species. This assert requires confirmation by estimating statistical associations between local ancestry and changes in colour or scale structure in wild admixed populations. It is also possible that variation in structural colour in *Heliconius* has an important component of environmental variation coming from condition dependence (Brien, 2019) as in other butterfly species (Kemp et al., 2007). Therefore, estimating heritabilities of scale structure and colour variation could be a next step in structural colour genetics research.

Segregation of scale structure traits in the offspring of both species also points towards a complex genetic architecture of scale structure and structural colour. Trait estimates among F1 individuals of both species show high variation, especially that of ridge spacing for *H. erato* F1. This could mean that some alleles in the parental populations were interacting epistatically and that these inter-locus interactions were broken down when crossing different genetic backgrounds. However, this high variability could be due to having F1 individuals from different parental crosses, as there may have been genetic effects that are specific to each cross. Trait variation among F2 individuals apparently exceeds that of parental races for all traits except BR-value in both species, again possibly due to epistatic interactions broken down in the crosses. Careful interpretation is required here again because parental individuals phenotyped do not correspond to the grandparents of the F2 generations. Nevertheless, the majority of trait estimates are close to or within the values of parental races and their distribution reaches both ends of parental values, showing a similar behaviour to trait distributions of admixed wild caught specimens. Taken together these observations indicate that there are probably several loci of varied effect sizes that are shaping the changes that take place in the scale and that give rise to iridescent structural colour in *H. erato* and *H. melpomene*.

We found that continuous variation in scale structure, mainly variation in ridge spacing, is significantly correlated with changes in two estimates of colour variation; luminance and BR-value in wild *H. erato* and *H. melpomene*. From previous work both using microscopy and USAXS data it was known that matt-black races had larger spacing between ridges than iridescent blue races (Parnell et al., 2018), yet the relationship between scale structure variation and colour in natural and insectary reared hybrids remained unclear. Although the iridescent colour of the so called ridge reflector butterflies is well known to come primarily from the stacking lamellae of the ridges (Parnell et al., 2018), it has been shown that ridge spacing also bears an important relationship with structural colour. Iridescent UV and blue reflections from the wings of various species of butterflies have been associated with reduced ridge spacing (Ghiradella, 1974; Kinoshita, Yoshioka, Fujii, et al., 2002; Parnell et al., 2018; Silberglied et al., 1973). In particular it is brightness that has a high covariance with ridge spacing (Parnell et al., 2018) and this covariance can be maintained even when butterfly specimens grow in conditions that alter the structural colour of the wings (Kemp et al., 2006). Densely packed ridges have been hypothesised to produce brighter colours due to an increased effective area of reflection on the scale (Kemp et al., 2006; Parnell et al., 2018), and it has been suggested that closely positioned ridges may compensate inefficient multi-layer ridge reflectors in some butterfly species (Kinoshita, Yoshioka, Fujii, et al., 2002). This is yet to be precisely determined in *Heliconius* and other ridge reflector butterflies. Despite the strong correlations found, our USAXS experiment did not allow for a comprehensive examination of other elements of the scale that are relevant for the production of structural colour in these two species. As stated by Parnell et al. (2018), other aspects of scale structure are relevant for structural colour production in addition to ridge spacing. Specifically, differences in ridge architecture between matt-black and iridescent forms and between species are responsible for the rather big differences in colour in spite of the similarities in ridge spacing variation. As of yet we have only been able to associate variation in ridge spacing with variation in luminance but a more precise description of its role in the production of structural colour is required, especially for the purpose of comparative analyses between scale morphology between species.

In wild caught individuals cross-rib spacing was found to correlate positively with BR value and luminance in *H. erato*, which is unexpected as this aspect of scale structure is not known to be related to production of iridescent structural colour. A significant correlation is also found in the F2 individuals between cross-rib spacing and BR-value but in the opposite direction. The correlations in opposite directions show that there is not direct effect of cross-rib spacing on colour variation. Rather, the observed correlations must be mediated through associations with other factors. The correlation observed in the wild caught individuals suggests that cross-rib spacing could have different selective optima in different populations. In crosses the correlation between cross-rib and BR value could be the result of a correlation between ridge spacing and cross-rib spacing. We did not find a significant correlation between cross-rib spacing

and luminance. In *H. melpomene* neither wild caught nor offspring individuals show a correlation of cross-rib with any aspect of colour. In addition, cross-rib spacing varied significantly between sexes when taking population membership into account. These results suggest that in *H. erato* there might be a role for cross-rib spacing in structural colour variation, but it is not directly implicated in colour production. A more detailed analysis of cross-rib spacing variation and its association with colour production is required in *H. erato* but we speculate that it may have a role in the production of ultra black wing regions, which would optimise the contrast between coloured wing patterns and the rest of the wing (Vukusic et al., 2004).

Our results show that variation in ridge spacing related to changes in colour is tightly coupled, at least in *H. erato*. In contrast the significant correlations found for ridge spacing and colour estimates in wild caught *H. melpomene* are not found in the F2 generation and suggest that ridge spacing, cross-rib spacing and colour variation are more weakly linked in this species. Our interpretation of this observation is that in *H. erato* different alleles of genes underlying particular aspects of iridescence may be in linkage disequilibrium due to close physical linkage and not easily broken by recombination. In contrast, in *H. melpomene* recombination may more readily break associations between alleles that cause tighter ridge spacing and alleles that cause brighter, more chromatic wings. We hypothesise that this is presumably because genes are far apart in the same linkage group or on different linkage groups. Genetic explorations of these traits are required for asserting that this is a difference between *H. erato* and *H. melpomene* in terms of genetic architecture.

We observe a high level of variation in ridge spacing across geographic races and localities for both *H. erato* and *H. melpomene*. This variation can be observed in the F1 and further offspring of individuals coming from crosses as shown by our data, suggesting high heritability. However, it is also possible that some of this variation is explained by environmental factors, specifically stressful conditions of growth and development (Badyaev, 2005). It is the case that in other butterfly species stress during larval and pupal stages results in perturbations of scale structure and structural colour. Scale structure and structural colour have been shown an important dependence on factors like larval diet (Fenner et al., 2019; Kemp et al., 2006) and thermal stress during development (Brien, 2019; Kemp et al., 2006). Thus, it is possible that our observations with respect to quantitative variation in colour and scale structure may be a mixture of plasticity related to diet or other factors affecting larval growth and development and phenotypic variation due to genetics. Since variation in scale structure and colour were also observed in F2 cohorts in both species and F2 individuals were reared in similar conditions of temperature and good food availability, we may expect that the variation explained by genetics is rather large compared to that induced by the environment. As in other butterfly species (Rutowski, 1977, 1985), variation in structural colour in *Heliconius* may play a role as an indicator of mate quality and may be subject to sexual selection.

Despite having observed high levels of variation in offspring individuals, we think our offspring data has important power limitations. These limitations stem from the number of samples and families that we were able to phenotype, and to the fact that the *H. melpomene* family is not an F2. Our phenotyping experiments were limited by availability of technical resources. Firstly, the time allocated in the beamline is very tight (24h) and only a limited number of individuals can be done in one of these slots. Secondly, the beamline we used (ID02) was closed during a large part of the development of my project (part of 2018 and 2019), meaning that we could not use the same instrument to produce more data. This was further restricted by the COVID-19 pandemic in 2020. Having only one family from each species highly limits the potential to reveal the full extent of variation in scale structure and structural colour. Additionally, data from more families would have allowed for the inclusion of independent evidence, useful to verify the results that we show. This in turn may limit downstream analysis such as QTL (Slate, 2004), because it is likely that QTL effects will be overestimated, and that a very limited number of QTL can be detected.

Our results offer an interesting avenue of research on the genetics and the tempo of morphological change. Neither the genes that dictate scale architecture changes for structural colour nor the pace at which it may evolve in *Heliconius* butterflies are known. We can make predictions based on what is the case in other species. Structural colour produced by the lower lamina of the scale in other butterfly taxa has been shown to evolve at remarkable pace using human mediated selection (Thayer et al., 2020; Wasik et al., 2014). The gene underlying these rapid changes is the transcription factor *optix* (Zhang et al., 2017), which possibly has an effect on the thickening of the basal scale lamina (Thayer et al., 2020). We do not think that *optix* is having an effect on the scale structure of *Heliconius* that is related to structural colour production. Firstly, *Heliconius* has been shown to produce structural colour by means of multi-layer ridge reflection and not lower lamina thickening (Parnell et al., 2018). Secondly, other studies have shown that *optix* has been co-opted in *Heliconius* to control the variation of red elements on the wings (A. Martin et al., 2014), and although pleiotropy is a possibility, functional assays of *optix* in several species including *Heliconius* revealed structural colours only in other butterfly genera (Zhang et al., 2017). Thus, we predict that it is other genes and not *optix* that dictate the distribution of the ridges on the scale and produce iridescent phenotypes in *H. erato*, *H. melpomene* and possibly other butterfly species that produce iridescence using the ridges as multi-layered reflectors. The number of generations that *Heliconius* butterflies take to evolve changes in ridge spacing and other aspects of scale structure in the face of selection is yet to be studied and would offer an interesting opportunity to explore the evolution of quantitative traits in these butterflies.

2.6 Conclusion and next steps

We found strong correlations between scale structure variation, particularly ridge spacing, and two aspects of structural colour variation: BR-value and luminance. These correlations are in good agreement with results found in other iridescent butterfly species with similar mechanisms of structural colour production. We take this as supporting evidence of a fundamental relationship between the density of reflector ridges in the scale and an iridescent visual appearance.

The correlations between colour and scale structure behave differently depending on the species. Associations that are present in wild caught individuals are maintained in *H. erato* F2 specimens but disappear in *H. melpomene* F2 generation. This indicates that the genetic underpinnings of scale structure and iridescent structural colour and its evolution may be different between these co-mimic species, unlike other aspects of morphological evolution such as pigmented wing patterns.

Variation in natural hybrids and offspring individuals of controlled crosses suggests that ridge spacing and cross-rib spacing variation are possibly controlled by multiple genes in both species. These traits seem to be largely heritable although some of the observed variation may also be attributed to environmental conditions.

Our study has revealed interesting aspects of morphological evolution in the two co-mimics *H. erato* and *H. melpomene*. There are a couple of steps that we think can be followed in order to achieve full resolution of butterfly scales underlying iridescent blue phenotypes.

Firstly, a simulation analysis in which dimensions of different scale components can be varied across a wide range should allow the exploration of variation in reflectance. The parameters of the simulation could be drawn from our results and can be put together with other parameters of scale structure variation available from the literature to hypothesise how *Heliconius* butterflies may be varying their scale structures both in nature and in controlled crosses.

Secondly, directly investigating finer aspects of scale structure variation should allow teasing apart which structural component controls which aspect of structural colour. Although ridge spacing is important for modulating visual aspects of the scale, the ridge lamellae and how they vary are expected to have a large effect on hue and brightness. If it is possible to include hybrids from both natural populations and controlled crosses these would allow the analysis of which configurations of scale structure are more commonly found in nature and the range of variation of scale components. This can be done using TEM since this technique will allow the exploration of cross sections of ridges and ridge lamellae, as well as ridge spacing.

2.7 Contributions to this chapter

Wild caught individuals were collected by Emma Curran, Nicola Nadeau, and Melanie Brien with the assistance of various colleagues in Panama, Colombia and Ecuador between 2013 and 2016. Broods were reared and preserved by Emma Curran, Melanie Brien and Nicola Nadeau with the assistance of various colleagues in Ecuador. Colour measurements of samples analysed in this chapter were collected and processed by Emma Curran and Melanie Brien. USAXS data collection was coordinated by Andrew Parnell and data was collected by Andrew Parnell, Emma Curran, Melanie Brien and Dr. Nicola Nadeau during two visits to the ESRF facilities during 2015 and 2017. The USAXS data was collected with support from Adam Washington, Thomas Zinn and Andrew Dennison. The analysis of dorsal and ventral sides using SEM data and its use in filtering USAXS data was devised by Juan Enciso and SEM data was collected by Juan Enciso, Victoria Lloyd and Andrew Parnell. The development of the tool used for automated analysis of USAXS data was done by Juan Enciso. Qualitative and quantitative analyses of USAXS data were done by Juan Enciso with the supervision of Andrew Parnell. Qualitative and quantitative analyses of SEM data were done by Juan Enciso. All data were collated analysed and interpreted by Juan Enciso.

2.8 Supplementary material

TABLE S2.1: Information on wild caught samples used for the USAXS experiment. # Frames corresponds to the number of USAXS frames used to estimate average ridge spacing and cross-rib spacing.

Species	Race	ID	# Frames	Sex	Latitude	Longitude	Locality	Country
H. erato	*hydara*	18008	15	M	8.61	-78.14	Puerto Lara	Panama
	hydara	18009	9	M	8.61	-78.14	Puerto Lara	Panama
	hydara	18121	11	M	8.15	-77.69	Yavitza	Panama
	hydara	18125	13	F	8.15	-77.69	Yavitza	Panama
	hydara	15N320	10	F	7.49	-78.13	Fondiadero	Panama
	hydara	15N321	15	M	7.49	-78.13	Fondiadero	Panama
	venus	15N322	76	F	7.49	-78.13	Fondiadero	Panama
	venus	15N323	21	M	7.49	-78.13	Fondiadero	Panama
	venus	15N261	46	F	5.57	-77.50	Amargal	Colombia
	venus	15N241	9	F	5.57	-77.50	Amargal	Colombia
	venus	15N238	11	M	5.57	-77.50	Amargal	Colombia
	venus	15N193	16	F	3.83	-77.26	San Pedro	Colombia
	venus	15N194	9	M	3.83	-77.26	San Pedro	Colombia
	venus	15N195	8	M	3.83	-77.26	San Pedro	Colombia
	venus	15N160	8	M	3.57	-76.78	La Elsa	Colombia
	venus	15N104	5	M	3.53	-76.76	Queremal	Colombia
	venus	15N121	10	M	3.53	-76.76	Queremal	Colombia
	venus	15N112	9	M	3.53	-76.76	Queremal	Colombia
	venus	15N111	7	M	3.53	-76.76	Queremal	Colombia
	chestertonii	15N135	17	M	3.88	-76.59	Rio Bravo	Colombia
	cyrbia	14N510	14	M	0.22	-78.89	Guayllabamba	Ecuador
	cyrbia	14N514	15	F	0.22	-78.89	Guayllabamba	Ecuador
	cyrbia	14N513	7	F	0.22	-78.89	Guayllabamba	Ecuador
	cyrbia	15N016	15	M	0.17	-78.91	Mashpi Town	Ecuador
	cyrbia	15N017	9	F	0.17	-78.91	Mashpi Town	Ecuador
H. melpomene	*melpomene*	18005	15	M	8.61	-78.14	Puerto Lara	Panama
	melpomene	18014	17	M	8.61	-78.14	Puerto Lara	Panama
	melpomene	18191	13	M	8.39	-77.85	Lajas Blancas	Panama
	melpomene	18093	10	M	8.28	-77.85	Santa Librada	Panama
	melpomene	15N387	17	M	7.55	-78.15	Rio Chado	Panama
	melpomene	15N355	8	M	7.53	-78.18	Rio Jaque	Panama
	melpomene	15N421	10	M	7.53	-78.18	Rio Jaque	Panama
	melpomene	15N354	11	M	7.53	-78.18	Rio Jaque	Panama
	melpomene	15N353	10	M	7.49	-78.13	Fondiadero	Panama
	melpomene	15N338	12	M	7.49	-78.13	Fondiadero	Panama
	vulcanus	15N328	15	F	7.53	-78.18	Rio Jaque	Panama
	vulcanus	15N306	12	M	5.57	-77.50	Amargal	Colombia
	vulcanus	15N240	11	M	5.57	-77.50	Amargal	Colombia
	vulcanus	15N260	11	M	5.57	-77.50	Amargal	Colombia
	vulcanus	15N133	16	M	3.88	-76.59	Rio Bravo	Colombia
	vulcanus	15N154	16	M	3.57	-76.78	La Elsa	Colombia
	vulcanus	15N153	7	M	3.57	-76.78	La Elsa	Colombia
	vulcanus	15N151	14	M	3.57	-76.78	La Elsa	Colombia
	vulcanus	15N144	3	M	3.57	-76.78	La Elsa	Colombia
	vulcanus	15N123	19	M	3.53	-76.76	Queremal	Colombia
	cythera	14N038	9	M	0.22	-78.89	Guayllabamba	Ecuador
	cythera	14N015	13	M	0.22	-78.89	Guayllabamba	Ecuador
	cythera	14N009	20	M	0.20	-78.87	Mashpi	Ecuador
	cythera	14N004	16	M	0.20	-78.87	Mashpi	Ecuador
	cythera	14N023	10	M	0.20	-78.87	Mashpi	Ecuador

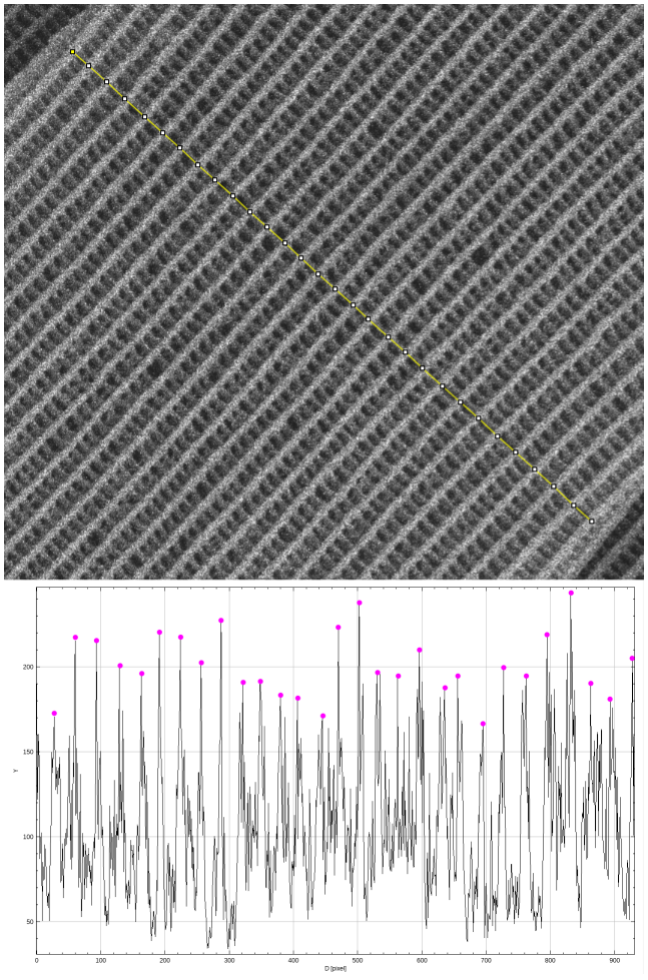

FIGURE S2.1: Illustration of the procedure used for measuring ridge spacing on scanning electron microscopy images. Top: perpendicular transect and highlighting of detected ridges across the scale. Bottom: variation in contrast across the transect and position of peaks along the transect in pixels.

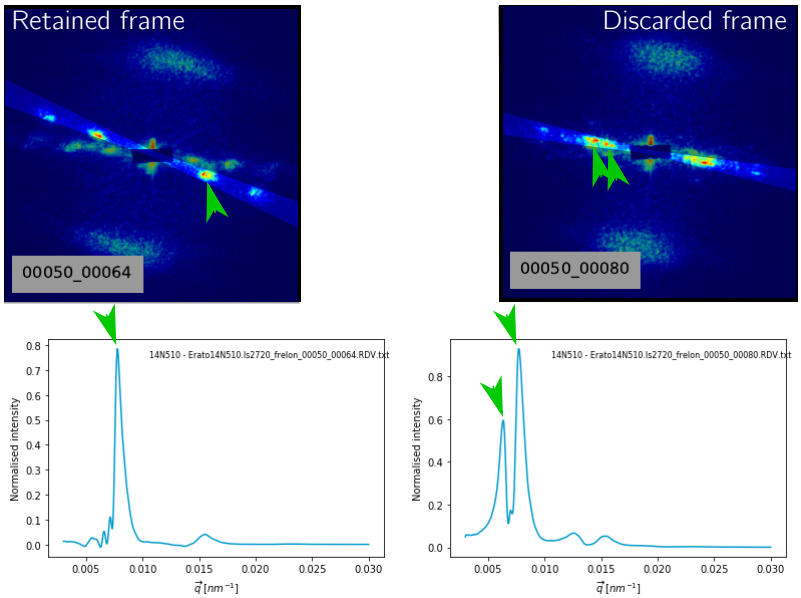

FIGURE S2.2: Example of a retained (left) vs. a manually discarded frame (right). Green arrow heads point to intensity peaks corresponding to scattering due to ridge spacing in 2D (top) and 1D (bottom) scattering frames. The retained frame shows a single peak corresponding to a single scale that is discernible to the automatic integration procedure. In the discarded frame the scales overlap too closely in orientation and their signals are not discernible and cannot be picked apart using small angles.

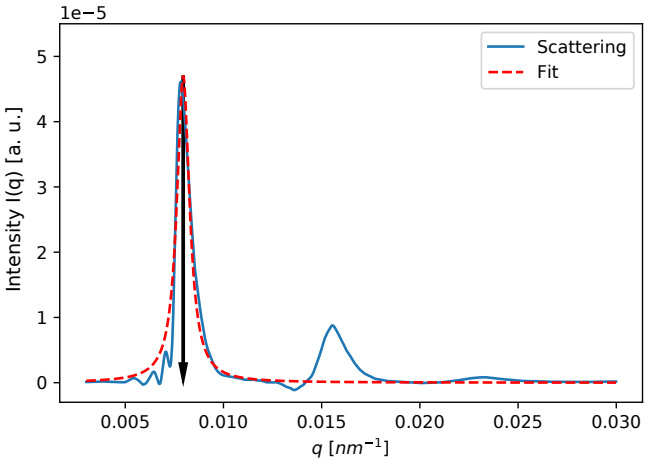

FIGURE S2.3: Peak fitting procedure used to estimate scale ultra-structure measurements from USAXS data. The 2D images are previously scanned for Bragg peaks and integrated over a small region to produce the blue curve. The main peak is observed at q $\approx$ 0.0075 (black arrow) and Bragg peaks can be observed at q $\approx$ 0.0152 and 0.023. The fitting is done on the main peak using the red curve.

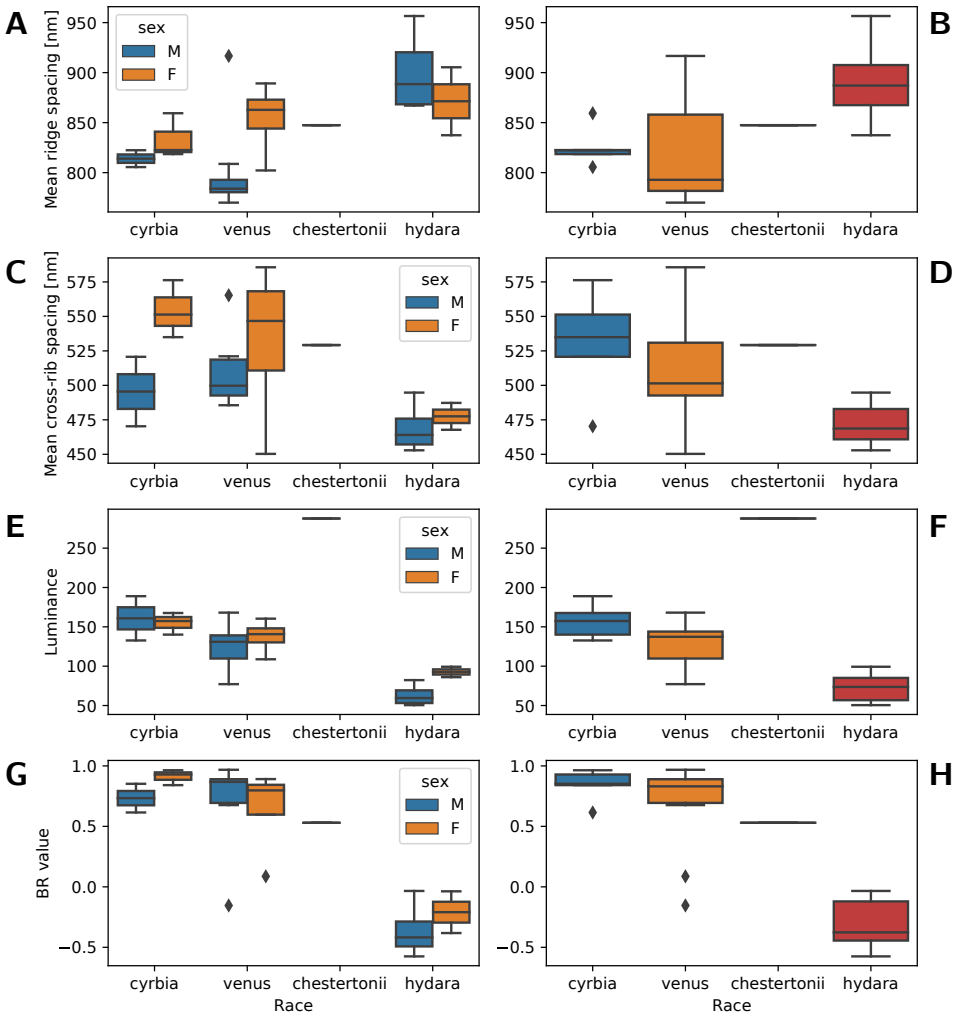

FIGURE S2.4: Distributions of phenotypic estimations for *H. erato* discriminating by sex and race (left) and only by race (right). This graph includes a single individual of *H. e. chestertonii* for comparison with other races. Notice that like the other iridescent races, *H. e. chestertonii* has narrower ridge spacing compared to the matt-black *H. e. hydara* (A, B). Despite having higher estimates of luminance (E, F), *H. e. chestertonii* has lower estimates of BR value compared to the iridescent *H. e. venus* and *H. e. cyrbia* (G, H).

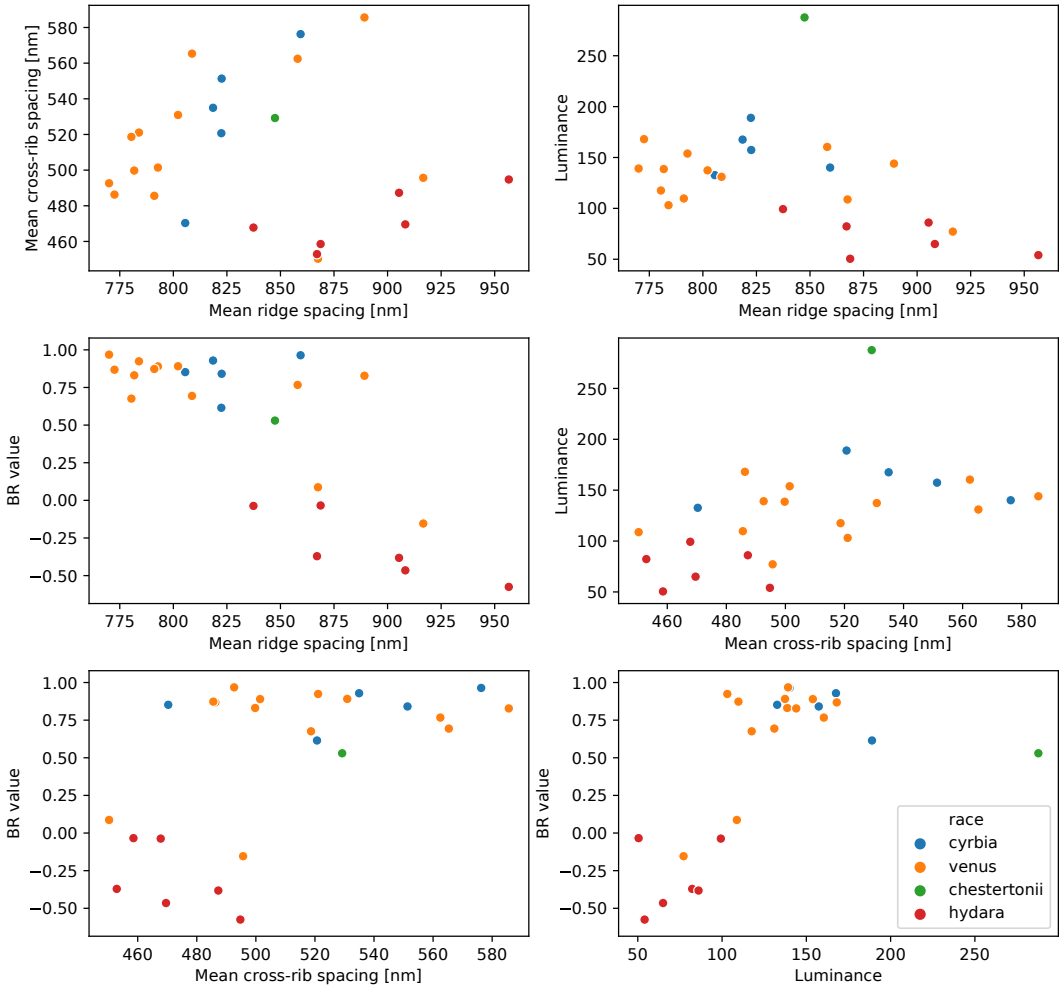

FIGURE S2.5: Correlations of scale structure variation estimates for *H. erato*. *H. e. chestertonii* has an estimate of luminance that is outstanding in the distribution of the scatter plots.

TABLE S2.2: Information on number of frames and identity of offspring individuals used in the USAXS experiment. F2 individuals correspond to a single family of both *H. erato*. The generation of individuals from the EC70 family of (*H. melpomene*) is designated as 'Unknown'. F1 individuals with an asterisk are the parents of the F2 family of *H. erato*.

Species	ID	Generation	# Frames	Sex
H. erato	14N078	F1	23	M
	14N111*	F1	32	F
	14N112*	F1	41	M
	14N113	F1	42	F
	14N114	F1	36	M
	14N348	F1	27	M
	14N195	F2	37	F
	14N196	F2	39	M
	14N201	F2	68	F
	14N206	F2	25	F
	14N207	F2	35	F
	14N212	F2	18	F
	14N224	F2	30	M
	14N227	F2	17	F
	14N229	F2	48	F
	14N230	F2	34	F
	14N235	F2	41	M
	14N240	F2	31	F
	14N241	F2	40	M
	14N242	F2	39	F
	14N243	F2	22	M
	14N244	F2	47	F
	14N247	F2	36	F
	14N250	F2	34	F
	14N251	F2	35	F
	14N255	F2	32	F
	14N256	F2	44	M
	14N257	F2	55	M
	14N260	F2	45	F
	14N262	F2	17	F
	14N264	F2	40	M
	14N265	F2	50	F
	14N273	F2	50	M
	14N276	F2	44	F
	14N277	F2	46	F
	14N278	F2	62	F
	14N279	F2	53	F
	14N282	F2	30	F
	14N283	F2	35	F
	14N284	F2	48	F
	14N285	F2	41	M
	14N287	F2	56	M
	14N288	F2	40	F
	14N289	F2	49	M
	14N291	F2	26	M
	14N293	F2	40	M
	14N294	F2	50	F
	14N297	F2	32	F
	14N298	F2	44	F
	14N299	F2	26	M
	14N306	F2	73	F
	14N307	F2	51	F
	14N308	F2	59	M
	14N310	F2	31	M

	14N326	F2	33	M
	14N328	F2	60	M
	14N330	F2	45	M
	14N331	F2	31	F
	14N333	F2	31	M
	14N334	F2	20	M
	14N335	F2	49	M
	14N341	F2	25	M
	14N343	F2	24	M
	14N344	F2	52	F
	14N351	F2	40	F
H. melpomene	14N480	F1	46	M
	15N563	F1	45	M
	15N797	Unknown	27	M
	15N798	Unknown	49	M
	15N800	Unknown	40	F
	15N801	Unknown	34	F
	15N802	Unknown	40	M
	15N803	Unknown	30	M
	15N804	Unknown	35	M
	15N805	Unknown	35	F
	15N811	Unknown	45	M
	15N818	Unknown	46	F
	15N821	Unknown	38	F
	15N826	Unknown	23	M
	15N830	Unknown	45	F
	15N831	Unknown	44	M
	15N835	Unknown	40	F
	15N836	Unknown	32	F
	15N837	Unknown	34	M
	15N846	Unknown	28	F
	15N847	Unknown	47	F
	15N848	Unknown	43	M
	15N850	Unknown	47	F
	15N851	Unknown	41	F
	15N853	Unknown	43	M
	15N859	Unknown	52	F
	15N861	Unknown	49	M
	15N862	Unknown	37	F
	15N867	Unknown	38	F
	15N868	Unknown	32	M
	15N875	Unknown	63	M
	15N878	Unknown	37	M
	15N880	Unknown	51	M
	15N886	Unknown	39	M
	15N887	Unknown	37	M
	15N888	Unknown	59	F
	15N891	Unknown	35	M
	15N894	Unknown	51	F
	15N897	Unknown	53	F
	15N899	Unknown	50	F
	15N900	Unknown	28	M
	15N901	Unknown	49	F
	15N902	Unknown	63	M
	15N905	Unknown	46	F
	15N908	Unknown	41	F
	15N912	Unknown	35	M
	15N915	Unknown	59	F
	15N920	Unknown	55	M

15N922	Unknown	35	F
15N923	Unknown	58	M
15N924	Unknown	55	M
15N925	Unknown	52	F
15N928	Unknown	51	F
15N934	Unknown	45	M
15N935	Unknown	63	F
15N936	Unknown	48	M
15N938	Unknown	47	M
15N940	Unknown	56	M
15N942	Unknown	50	M
15N948	Unknown	46	M
15N950	Unknown	46	F
15N952	Unknown	48	M
15N955	Unknown	43	M
15N958	Unknown	53	M
15N961	Unknown	44	M
15N966	Unknown	27	M
15N977	Unknown	86	F
15N978	Unknown	45	M
15N984	Unknown	29	F
15N985	Unknown	38	M
15N990	Unknown	33	M
15N992	Unknown	54	F
15N995	Unknown	47	F
15N996	Unknown	32	F
15N997	Unknown	43	M
15N1001	Unknown	20	M
15N1005	Unknown	35	F
15N1006	Unknown	33	F
15N1008	Unknown	27	F
15N1009	Unknown	39	F

Chapter 3

QTL analysis reveals lack of gene reuse in the evolution of scale ultra-structure and structural colour.

3.1 Abstract

The co-mimics *H. erato* and *H. melpomene* show phenotypic convergence in structural colour and scale structure. Analysis of variation in scale structure and structural colour revealed differences between species that could be due to differences in genetic architectures. This is in contrast to pigmented wing patterns involved in Müllerian mimicry, which are nearly identical in both species and are controlled by homologous loci. In this chapter we explore the genetic architecture of scale structure and structural colour and assess whether the same loci underlie convergent phenotypic evolution. We found evidence for divergent genetic architecture of structural colour and scale structure variation between the co-mimics *H. erato* and *H. melpomene*. Different chromosomes harbour the loci that explain the largest phenotypic variance between matt-black and blue iridescent races in the two species. As opposed to other forward and reverse genetics studies of structural colour variation and functional validation of wing patterning genes, the loci we find do not correspond to and are not linked physically to any major wing patterning gene previously reported. One QTL associated with structural colour and scale structure variation is located in the sex chromosome. We hypothesise that this QTL is probably related to an ecological function which may include mate selection or mate recognition which may evolve in the sex chromosome to bypass sexual conflict.

3.2 Introduction

Butterfly structural colour has been studied extensively, yet little is known about its genetics and evolution. In particular, we don't know what molecular changes underlie scale ultra-structure variation associated with production of structural colour in butterfly wings.

Diverse scale morphologies give rise to a wide variety of visual properties of butterfly structural colour. The various components of the scale have been studied in detail using electron microscopy and the relationship between nano-structures found in the scale and the optical properties of wings of butterflies and moths are fairly well understood (Ghiradella, 1991). Two common modifications found in scales that are related to the production of structural colour are the thickening of the basal lower lamina which acts as a thin film that reflects blue light (Stavenga et al., 2014), and the use of a multi-layer reflection mechanism in the ridge of the scales that can reflect different hues at different intensities depending on the particular arrangement of the ridges and the dimensions of the multi-layer (Ghiradella et al., 1972; Kinoshita, Yoshioka, Fujii, et al., 2002; Vukusic et al., 1999). A multitude of species of butterflies and moths make extensive use of these nano-structure modifications to produce an impressive array of different wing appearances.

One such group of butterflies is the nymphalid *Heliconius* genus. These neo-tropical butterflies have evolved various instances of iridescent blue colour that involve the aforementioned mechanisms (Parnell et al., 2018; Wilts, Vey, et al., 2017). In some species like *H. cydno*, *H. sapho*, *H. eleuchia* and *H. sara* this trait appears in most or all geographic races, whereas in other species like *H. doris* and the co-mimics *H. erato* and *H. melpomene*, only a few races display this trait. The dominant trend seems to be that ancestral forms are matt black and structural colour appears as a derived trait along the species phylogeny of *Heliconius* (Fig. 2 in Parnell et al. 2018).

The co-mimics *H. erato* and *H. melpomene* share natural histories extensively. Their range of distribution overlaps largely and wherever they coincide in a geographical region, their local forms resemble each other almost perfectly. Both species are unpalatable to predators and signal their toxicity by means of Müllerian mimicry to share the cost of educating potential attackers that rely on vision to track prey. This makes them one of the most remarkable examples of phenotypic convergence. Some of the local forms of both species have developed a blue wing colouration that is also coincident geographically: The sympatric races of West Ecuador *H. e. cyrbia* and *H. m. cythera* both have blue wings, and in West Colombia *H. e. venus* and *H. m. vulcanus* show a more subtle iridescent blue colour. Thus, we can consider structural colour in the co-mimics *H. erato* and *H. melpomene* as a case of parallel evolution.

Structural colour has an important role for mate communication in butterflies. Studies done in other butterfly species have concluded that structural colour allows males to distinguish females from other males (Rutowski, 1977), and that it is used as an honest

indicator of mate condition (Kemp et al., 2007), with individuals grown in poor or stressful conditions showing variations in structural colour that potential mates can discriminate (Kemp et al., 2006; Kemp et al., 2007). This highlights the importance of structural colour for the life history of butterflies. It is possible that this role extends into *Heliconius* butterflies under certain circumstances. It is known that structurally coloured wing regions of *Heliconius cydno* are involved in long range mate recognition in some environments with particular light conditions (Sweeney et al., 2003).

As of yet it is unclear whether structural colour in *H. erato* and *H. melpomene* has a similar role as it does in other butterflies. Although *H. erato* and *H. melpomene* are highly similar in their pigmented wing pattern, their structural colour is noticeably different, with *H. erato* showing a much brighter iridescent blue colour than *H. melpomene* (Fig. S3.4). It has been proposed that the differences in structural colour between the co-mimics *H. erato* and *H. melpomene* may be caused by developmental constraints. These constraints have been hypothesised to impede the evolution of *H. melpomene*'s phenotype towards a fitness optimum, which would be to more closely resemble *H. erato* (Parnell et al., 2018). However, it is likely that the visual cues emitted by the wings of each species are compatible with the sensory properties of their con-specifics and co-mimics and also that organisms are well suited to their environment and are at a fitness optimum or very close to it (Orr, 2005). Therefore, parallel evolution of structural colour in *H. erato* and *H. melpomene* may rather be driven by their ecology, albeit in a different way than their mimicry-related pigment patterns.

In many organisms, including *Heliconius* butterflies, it has been shown that parallel evolution is predictable to some degree: The same loci (Hines et al., 2011; Supple et al., 2013) and occasionally the same nucleotide substitutions (Wood et al., 2005), are associated with similar phenotypic changes that lead to adaptation. In some cases molecular targets for parallel evolution span large phylogenetic scales (A. Martin et al., 2013), showing that the predictability of evolution may potentially be higher and more far-reaching than it was previously thought. Nevertheless, the predictability of evolution is still a matter of debate and we are yet to develop a more complete picture of its prevalence across a broad range of organisms and traits.

Evolution often modifies the function of genes to play different roles across divergent taxa. In the case of scale structure variation, it has been shown that genes that are involved in pigment production in *Drosophila* may act as modifiers of scale structure in butterflies (Matsuoka et al., 2018). Recent studies using reverse genetics approaches have also shown that genes involved in wing pattern development may also modify the architecture of scales at a sub-micron level (Concha et al., 2019; Fenner et al., 2020; Thayer et al., 2020; Zhang et al., 2017). It is still unknown whether these results hold widely across various butterfly lineages and whether a wide array of scale architectures that produce structural colour are governed by the same genetic mechanisms and developmental pathways.

Based on all the described findings we set three predictions for the outcome of our study. Firstly, in terms of the genetics of structural colour we expect that genes that are involved in colour pattern, such as *optix*, *cortex* or *wnta* are either directly involved in the production of structural colour or linked to the genes that are directly involved in structural colour production; in other words, we expect to find QTL for structural colour in linkage groups that contain major colour pattern genes. In the second place we expect that genes involved in pigmentation pathways also play a role in modification of scale structure that results in production of structural colour. Finally, in terms of genetic architecture given the high level of synteny and genetic conservation between *H. erato* and *H. melpomene*, we predict that genes that produce morphological change related to structural colour have been targeted repeatedly by evolution. In other words, we expect a partial or total overlap of the loci underlying structural colour production and scale structure variation in these two co-mimic species.

Here we follow a forward genetics approach that leverages the natural phenotypic variation in iridescent structural colour that exists across geographic races of *H. erato* and *H. melpomene* to pin down the loci underlying this trait. Specifically, we use crosses between wild caught parental individuals of matt black and blue races of each species to perform a Quantitative Trait Locus (QTL) analysis on complex traits related to structural colour: two scale morphology measurements, and two measures of the chromatic and achromatic properties of wing colour. We discuss our findings in the context of repeatability of evolution and gene reuse in parallel phenotypic evolution, and the possible link between genes of large effect that control wing patterning and variation of scale architecture. Comparing the results of complex trait QTL with those for traits with simpler genetic architecture allows us to understand the power and limitations of our work.

3.3 Methods

3.3.1 Phenotype scoring

Scale structure and structural colour

Offspring individuals of *H. erato* and *H. melpomene* were phenotyped for scale structure variation and colour as described in the Methods section of Chapter 2. From these results we could derive two measurements of variation of scale morphology; ridge spacing and cross-rib spacing. In addition we will use two estimates related to the wing's visual appearance: BR-value and luminance, which describe chromatic and achromatic aspects of structural colour respectively.

Hind-wing margin phenotypes - *Cr* and *Yb*

We scored the offspring of crosses of both species for the locus controlling the yellow bar and the white margin. In *H. erato* this locus is denoted *Cr* and in *H. melpomene*

this locus is denoted *Yb*. The yellow bar is typical of the Panamanian races and the white margin is typical of the Ecuadorian races. In both species these two colour pattern elements are known to map to homologous loci (L. Ferguson et al., 2010; Joron et al., 2006). We categorised three different phenotypes here: yellow bar present, white margin present or neither.

3.3.2 Crosses

Individuals of matt-black races *H. erato demophoon* and *H. melpomene rosina* from Gamboa, Panama (9.12° N, 79.67° W) were mated with individuals of iridescent races *H. erato cyrbia* and *H. melpomene cythera* from Mashpi, Ecuador (0.17° N, 78.87° W) to produce F_1 hybrid offspring. F_2 offspring were then produced by crossing F_1 individuals. The details of the crossing design for both species can be found in Table 2.1 in Chapter 2. Shortly after emerging from pupal state, adults had wings removed and stored in glassine envelopes and their bodies were preserved in a solution of 20% dimethyl sulfoxide 0.25M EDTA saturated with NaCl to preserve DNA.

3.3.3 Sequencing and genetic data processing

Genomic DNA was extracted from the thorax of each butterfly using the Qiagen DNeasy Blood and Tissue kit. Restriction site Associated DNA (RAD) libraries were prepared and sequenced by the Edinburgh Genomics facility (University of Edinburgh). DNA was digested with a single restriction enzyme with estimated cut-sites separated by 10kb approximately (*PstI*). Libraries were sequenced using an Illumina HiSeq2500 sequencing system producing 125bp paired-end reads.

RAD sequences were demultiplexed using the RADpools tool from RADtools v1.2.4 (Baxter et al., 2011), allowing one mismatch per barcode. Quality control of sequence data was done using FastQC v0.11.5 (Babraham Bioinformatics). Quality checked reads of each species were mapped to the *H. erato* v1 genome (Van Belleghem et al., 2017) and to the *H. melpomene* v2.5 genome (Davey et al., 2016) respectively using Bowtie v2.3.2 (Langmead et al., 2012). PCR duplicates were removed using the `MarkDuplicates` tool (v1.102) in the picard toolkit (*The Picard Toolkit* 2019) and the resulting alignments were indexed and sorted using the `index` and `sort` tools in samtools v1.3.1 (Li, Handsaker, et al., 2009). Genotype posterior probabilities were estimated using samtools `mpileup` (Li, 2011) called using the LepMap3 pre-processing scripts (Rastas, 2017) with a minimum mapping and base qualities of 10. Variant sites with coverage $<$ 3X were discarded.

3.3.4 Linkage map construction

In total, 155 *H. erato* individuals (3 *demophoon*, 3 *cyrbia*, 10 F_1, 40 back-cross and 99 F_2) and 228 *H. melpomene* individuals (1 *rosina*, 2 *cythera*, 5 F_1 and 219 F_2) were used for linkage map construction for each species respectively. Prior to the estimation of the linkage map for each species, sex of the samples was confirmed comparing the

coverage of the mapping of the sex chromosome, which for the heterogametic sex (females) is expected to be roughly half of that of autosomes. Five individuals of *H. melpomene* were discarded from the pipeline because of a mismatch between the sex inferred from the wings and the sex inferred from sequencing data. Linkage maps were constructed using the LepMap3 suite (Rastas, 2017). After verification of the pedigree using the `IBD` program, a further 5 individuals (1 *H. erato*, 4 *H. melpomene*) were left out because ancestry could not be verified for them.

The `ParentCall2` program was run to call parental genotypes and markers on sex chromosomes more accurately using the genotype posteriors and the pedigree information as input. The `Filtering2` program was then run on genotypes to discard those with high segregation distortion using a distortion tolerance threshold 0.001. Markers were assigned to linkage groups using the `SeparateChromosomes2` program; the `distortionLOD=1` option was set to use LOD scores aware of segregation distortion and linkage groups with less than 50 markers were excluded using the option `sizeLimit=50`. `JoinSingles2All` was used to further assign single markers to the constructed linkage groups. Finally, the `OrderMarkers2` program was run 5 times to order markers within each linkage group. Here we set the male recombination rate to 0.05 (using the same setting as previous studies in *Heliconius* (Morris et al., 2019)) and the female recombination rate was set to 0 because female lepidoptera do not produce recombination during meiosis (Suomalainen et al., 2009). We used the `hyperPhaser` option to improve the phasing of markers. From the 5 separate runs we retained the output with the highest likelihood. The full set of options and scripts used for each module during the construction of linkage maps can be found in figure S3.1.

Maps were checked for errors in marker order and markers causing long gaps at the start or end of a linkage group were removed. The script `map2genotypes.awk` was used to convert phased output data from the LepMap3 main pipeline to genotypes coded as `1 1`, `1 2`, `2 1` or `2 2` depending on the parental alleles present and the gametic phase, and markers were assigned names using the script `map.awk` following the format of the reference genomes (`scaffold_position`). After naming the markers, a final verification of correct marker assignment was done. A small group of markers with a mismatch between genomic position and assigned linkage group was further removed from the data ($< 1\%$).

3.3.5 QTL mapping

We used the R/qtl R package (Broman et al., 2003) for the QTL mapping and analysis. We subset the output data from LepMap3 to include only the individuals that were phenotyped for scale structure, namely the *H. erato* EC17 family (n = 56) and the *H. melpomene* EC70 family (n = 70). The phased markers were coded as `AA`, `AB`, `BA` or `BB`, setting `BA` to `AB` since R/qtl works with un-phased genotype data. Sex assignment was inverted to have females as the hemizygous sex because R/qtl assumes males are the hemizygous sex. The sex chromosome is marked as `X` in the input data and the

`read.cross` function is called on the input data with the option `convertXdata=TRUE` to code markers in the sex chromosome as required by R/qtl.

The probabilities of the true underlying genotypes at each marker were calculated using the `calc.genprob` function, assuming a genotyping error rate of 1×10^{-4} and using the Haldane mapping function. Standard interval mapping was done using the `scanone` function to estimate the likelihood of observing a QTL at a marker versus the likelihood of not observing a QTL in any marker. For quantitative traits such as colour and scale structure variation we used the standard normal model for QTL mapping which assumes that residual phenotypic variation follows a normal distribution. In the case of the hind-wing phenotype we used a non-parametric model. We included sex as an additive co-variate for both quantitative and discrete trait analyses. To determine a genome wide significance threshold we ran 1000 permutations and we set the option `perm.Xsp=TRUE` to get a separate significance threshold for the sex chromosome. The sex chromosome requires an additional number of permutations due to the difference in degrees of freedom of the linkage test in comparison to the autosomes (Broman et al., 2006). The exact number of additional replicates is not given, but it is roughly L/L_X times more than that used for the autosomes, where $L = \sum L_i$, L_i is the length of each chromosome in cM and L_X is the length of the sex chromosome (Broman et al., 2006). We did not consider sexes separately for QTL analysis because of the low sample numbers that we had in each family.

After sequencing and phenotyping the EC70 family for scale structure we noticed that its mother was probably an F2 rather than an F1. Since her alleles cannot be assigned with certainty to either Panama or Ecuador ancestry, we had to use only paternal alleles in the QTL analysis of EC70. For this we set all maternal alleles to 'Panama' (`A` in the R/qtl analysis) and treated EC70 as a back-cross family. This allowed us to perform a QTL analysis, which given the number of individuals (n = 73) may be the most powerful approach to reveal genetic associations. This likely produced loss of information because setting the maternal alleles to a single value removes information on the recombination event that took place in the meiosis of the maternal grandfather.

Explained variances for each QTL were estimated using the functions `makeqtl` to get genotype probabilities at the nearest pseudo-markers and then the function `fitqtl` to fit a single qtl model that returns the result as an ANOVA table containing LOD scores, percentage of variance explained and P-values. We verified the estimates of explained variances using the expression

$$1 - \frac{1}{10^{(2 \times LOD)/n}}$$

where n is the number of individuals used when fitting the model and LOD is the logarithm of odds of the QTL. Both estimates obtained were in good agreement. The

graphs of whole genome QTL scans and QTL effects were produced using the R/qtl2 R package (Broman et al., 2018).

The locations of QTL were estimated using the the function `bayesint` on the output from `scanone` for each significant QTL. The `bayesint` function computes an approximate Bayesian credible interval. The level of confidence used to estimate the intervals was set to 99%.

To further describe the genetic architecture of the analysed traits, we explore the allelic interactions at significant QTL markers, estimating a coefficient of dominance for traits and loci with significant associations. For this we assumed that the mean phenotype for a genotypic class is a good approximation to the expected phenotype, also known as the genotypic value (Lynch et al., 1998). Because we have two alleles for each locus, we can model the relationship between genotypic values and genotypes using the scheme shown in figure 3.1, adapted from Lynch et al., 1998.

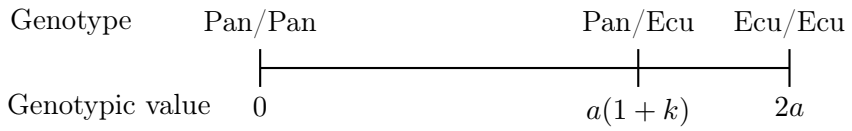

FIGURE 3.1: Representation of genotypic values for loci with Panama homozygotes, Ecuador homozygotes, and a heterozygote which in principle ranges between 0 and 2a.

For the genotypic value to range from 0 to $2a$ we subtract the mean phenotype of the Pan/Pan genotype ($\mu_{Pan/Pan}$) from the genotypic values of all genotypes, so that we have the following simplified expressions:

$$0 = \mu_{Pan/Pan} - \mu_{Pan/Pan}$$

$$a(1+k) = \mu_{Pan/Ecu} - \mu_{Pan/Pan}$$

$$2a = \mu_{Ecu/Ecu} - \mu_{Pan/Pan}$$

We solve for a in the last expression and substitute the value of a into the second expression to solve for k:

$$k = \frac{\mu_{Ecu/Pan} - \mu_{Pan/Pan}}{a} - 1$$

Using this approach we obtain the coefficient of dominance k, which in this case indicates dominance of Ecuador alleles over Panama alleles if $0 < k \leq 1$, dominance of Panama alleles over Ecuador alleles if $-1 \leq k < 0$ and additive effects of Ecuador and Panama alleles if $k = 0$. If $k > 1$ or $k < -1$ the locus is said to show over-dominance or under-dominance, respectively (Lynch et al., 1998). In the case of QTL on the sex chromosome we follow this approach using only male genotypes. In case

we do not have Pan/Pan homozygotes due to the structure of the inter-cross, we use the mean phenotypic values of hemizygous females carrying the Panama allele as a proxy.

3.3.6 Family-based GWAS analysis

Family-based association analysis

Since the QTL analysis of EC70 ignored the real mixture of "Panama" and "Ecuador" alleles in this family, we complemented it with a genome-wide association analysis taking into account pedigree structure to potentially reveal other loci controlling scale structure and structural colour in *H. melpomene*. The analysis we did consists of a score test based on kinship (Chen et al., 2007) which is done in two steps.

The first step uses a linear mixed model to get estimates of trait values after adjusting for covariates and random genetic effects. The model is described by the expression

$$Y_i = \mu + \sum_j \beta_j C_{ji} + G_i + e_i$$

Where Y_i is the array of phenotypic values for each individual i, μ is the mean phenotypic value for the population, C_{ij} is the value of the covariate j for the individual i, β_j is the effect of each covariate, G_i are random additive polygenic effects and e_i is the residual variance for each individual. This model produces trait residuals that are left over after accounting for covariates and random polygenic effects, they are denoted $\widehat{e_i}$ and are fit into a second model described by the expression

$$\widehat{e_i} = \mu + \beta g + e_i$$

Where β is the parameter for the effect of each SNP tested, g is a single SNP and e_i is the residual variation in phenotype for each individual i.

The association tests were done for the full set of *H. melpomene* crosses and for the EC70 family only. The phenotypes included were colour related phenotypes (BR value and luminance) for all the families, and colour related phenotypes and scale-structure related phenotypes (ridge spacing and cross-rib spacing) for EC70. We used the implementation of this score test available in the GenABEL R package (Aulchenko et al., 2007).

3.3.7 Gene count under QTL and top hits

We do not expect a QTL analysis to reveal single genes strongly associated with phenotype for quantitative traits such as scale structure and iridescence related colour measurements. However, to have an idea of what may be the number of genes under QTL, we did a simple search on LepBase (Challis et al., 2016) for genes appearing

within the 95% Bayesian confidence intervals around our QTL and report the gene count. In addition, since GWAS based approaches report associations in a SNP basis, we report the gene closest to or matching the position of the top scoring SNPs above the Bonferroni corrected thresholds.

3.3.8 Genes involved in wing pigmentation

Previous studies have shown that genes belonging to pigmentation pathways may have a dual effect on wing pigmentation and scale structure. Matsuoka and Monteiro (Matsuoka et al., 2018) tested the effect of 8 pigmentation genes on scale structure (Table S3.3). These genes belong to two pigmentation patwhays: the melanin-dopamine pathway (n = 5) and the ommochrome synthesis pathway (n = 3). They found that two genes belonging to the melanin pathway had an effect on scale structure in *B. anynana*.

We queried the same 8 pigmentation genes for localisation in the genomes of *H. erato* and *H. melpomene*. In addition we queried the *tan* gene, not reported by Matsuoka and Monteiro as having an effect on structure, but which is part of the melanin-dopamine pathway, is involved in cuticular melanisation (Thurmond et al., 2018) and is up-regulated in melanic regions of *Heliconius* butterflies (L. C. Ferguson et al., 2011). Our prediction is that the position of these genes doesn't overlap the Bayesian confidence interval estimated for our found QTL and if this is the case we can discard the possibility that they have an effect on structural colour in our co-mimic species.

We used the common names of these genes to find their position and length by using a simple search using the Ensembl tool available on LepBase (Challis et al., 2016). When the search for these names did not produce matches on LepBase, we did the same search by common name in FlyBase (FB2020_05) (Thurmond et al., 2018). We verified manually the top hits using the description of the gene. We then obtained its nucleotide sequence and did a BLAST-N search (Altschul et al., 1990) against a database comprising all butterfly genomes available on LepBase. We assumed the top hit on our two species is homologous to the query and used the physical information of these top hits to find the localisation of pigmentation genes in our butterfly genomes.

3.4 Results

3.4.1 QTL mapping

Linkage maps of *H. erato* and *H. melpomene*

The linkage map of *H. erato* was constructed from 65892 SNPs and it has 5648 markers, it has a length of 1162.37 cM, which is a similar size to that reported for the reference genome of this species (physical aprox 383Mb, Map 946cM) (Van Belleghem et al., 2017). The linkage map of *H. melpomene* was constructed from 63224 SNPs, it has 2163 markers and a length of 1469.88 cM, again similar to that reported for

the reference genome of this species (physical aprox 268Mb, Map 1364.2cM) (Davey et al., 2016). Both maps are organised in 21 linkage groups, which correspond exactly to the number of chromosomes of both species. Full details of the linkage maps can be found in tables S3.1 and S3.2.

Hind-wing variation mapping confirms the correctness of linkage maps of *H. erato* and *H. melpomene*

We found strong evidence for association of hind-wing phenotype with a QTL in chromosome 15 in both species. This is expected as the variation of the yellow bar and the white margin were previously mapped to a locus in this chromosome (L. Ferguson et al., 2010), and yellow bar variation is known to be controlled by the *cortex* gene (Nadeau et al., 2016), which in both species is located on chromosome 15. In *H. erato* we found an additional association which was marginally significant on chromosome 18 (Fig. S3.3). In *H. melpomene* we only found a single peak in chromosome 15 (Fig. S3.3).

In *H. erato* the Ecuador homozygote genotypes at the marker with the highest LOD score were mostly associated with a hind-wing distal white margin such as the one found in the parental Ecuadorian race *H. e. cyrbia*. Some intermediate forms (*Cr* genotype = 1.0) were also found to be associated with Ecuador homozygote alleles (Fig. S3.3). Heterozygotes were mostly found to be associated with intermediate forms, although there are also individuals with parental phenotypes that carry Ecuador and Panama alleles. Homozygous Panama individuals at this marker were found to be mostly associated with a proximal hind-wing yellow bar such as the one shown by the parental race *H. e. demophoon*, although 4 individuals showed a hind-wing phenotype that was scored as intermediate (Fig. S3.3).

In *H. melpomene* the Panama homozygote genotypes are mostly associated with the presence of the hind-wing yellow bar (*Yb* genotype = 0.0). There were also several individuals associated with an intermediate phenotype and a single individual showing an Ecuador type hind-wing (Fig. S3.3). This is possibly due to our relaxed assumption of EC70 as a back-cross masking true heterozygotes as Panama homozygotes at this marker. Heterozygote individuals show either association with an Ecuador type hind-wing or an intermediate hind-wing but no Panama type hind-wings (Fig. S3.3).

A locus in the sex chromosome underlies ridge spacing and luminance variation in *H. erato*

We found strong evidence for a ridge spacing QTL in the Z chromosome of *H. erato* at the Herato2101_7491127 marker (Fig. 3.2, A). This QTL explains 34.8% of variance in ridge spacing in the EC17 F2 brood. Although the QTL scan graph reveals two peaks in the Z chromosome, numerical results and further analyses confirm a significant association at a single marker (Table 3.1). Cross-rib spacing was not found to be

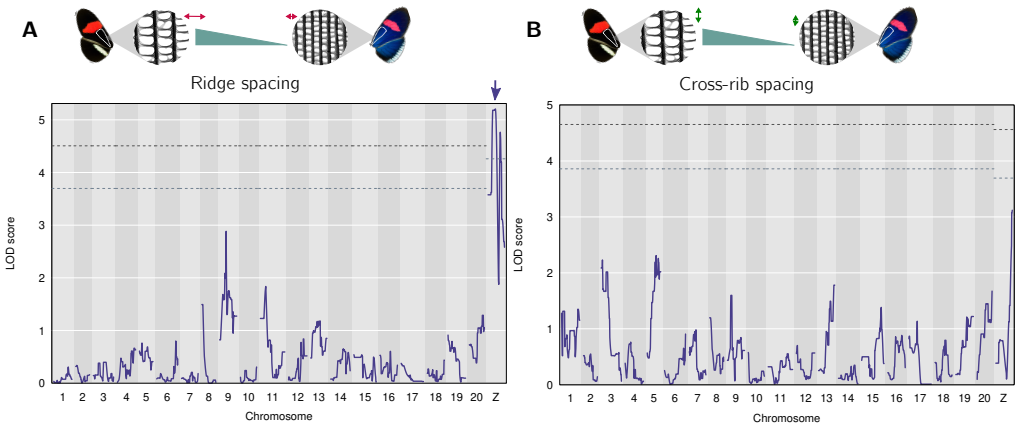

FIGURE 3.2: Scale structure QTL in *H. erato*: Evidence for genetic association was found in the sex chromosome for ridge spacing (A) but no strong associations were found for cross-rib spacing (B).

strongly associated with any QTL. The signals with the highest LOD scores are in the chromosomes 3, 5 and Z (Fig. 3.2, B).

We did not find QTL associated with BR-value for *H. erato* (Fig. 3.3, A). We found strong evidence for a luminance QTL in the Z chromosome of *H. erato* at the same marker significantly associated with variation in ridge spacing (Fig. 3.3, B; Table 3.1). This QTL explains 44.7% of variation in luminance in the EC17 brood. This is slightly different to results obtained previously in our research group using a larger sample containing more broods (Brien et al., 2021). In the analysis using larger sample sizes, QTL associated with BR-value were found on chromosomes 20 and Z, and a QTL associated with luminance was found in the Z chromosome as we did here.

Bayesian 99% credible intervals for the ridge spacing QTL span 42.34 Mb (Table 3.1) with the marker Herato2101_1133070 being the closest to the lower limit and Herato2101_12672960 being closest to the upper limit. For the luminance QTL, the Bayesian credible interval is narrower than that for the ridge spacing QTL, spanning 37.8 Mb (Table 3.1) and has Herato2101_4831239 as the closest marker to the lower limit and Herato2101_12968595 as the closest marker to the upper limit.

Our analysis of dominance revealed that Ecuador alleles show dominance over Panama alleles for ridge spacing (coefficient of dominance $k = 0.76$). This can be observed in our effect plots; males of EC17 family show little difference in ridge spacing despite their genotype (Fig. 3.4). The dominance effect seems to disappear when the Panama allele is not compensated for dosage in the hemizygous females (Fig. 3.4).

As opposed to ridge spacing, we found that Panama alleles behave dominantly over Ecuador alleles for luminance (coefficient of dominance $k = -0.57$). This is observed in figure 3.4; male homozygotes for the Ecuador allele and hemizygous Ecuador females show increased luminance compared to heterozygote males and hemizygous Panama females (Table 3.2).

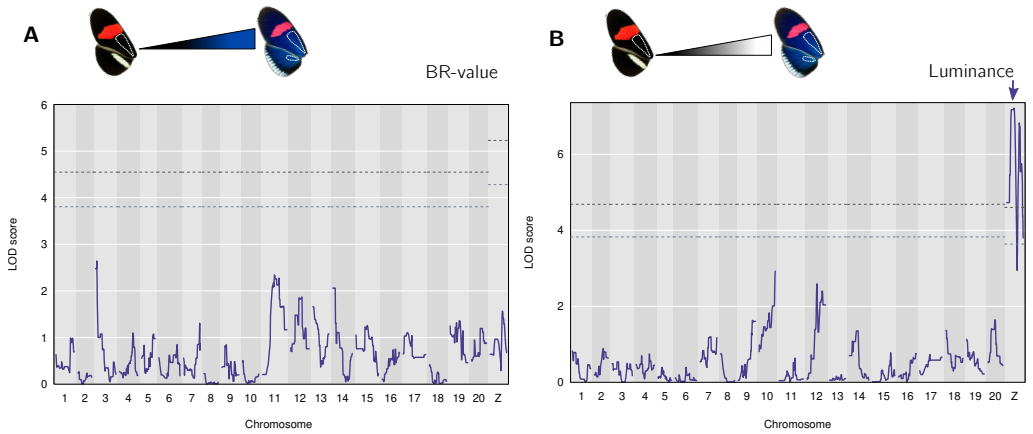

FIGURE 3.3: Iridescence QTL in *H. erato*: No significant QTL were found for BR value (A) but strong associations were found for luminance on chromosome Z (B).

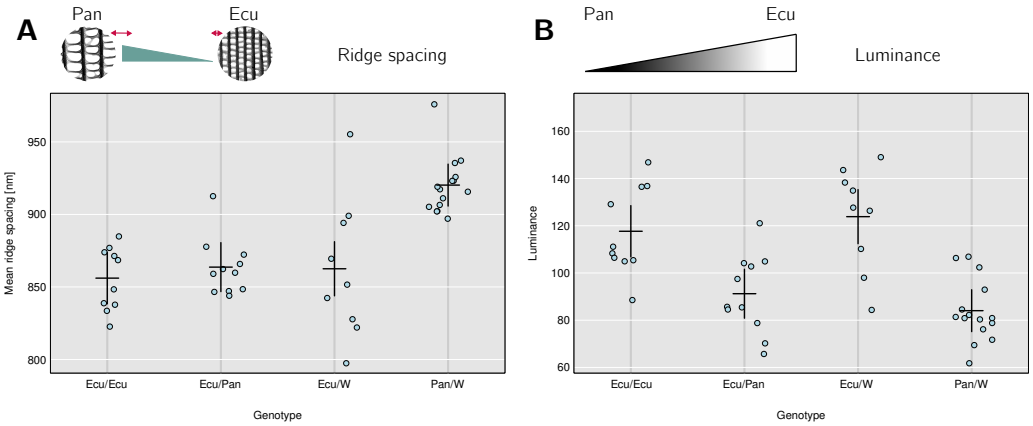

FIGURE 3.4: Genotypic associations at the marker closest to significant QTL in *H. erato*. Ecuador alleles are associated with narrower ridge spacing and Panama alleles are associated with wider spacing only when in hemizygous state (A). Ecuador alleles are associated with increased luminance when homozygotes or hemizygous and Panama alleles are associated with darker wings (B).

TABLE 3.1: Locations, p-values and confidence intervals for significant QTL in *H. erato*. The position of the QTL and the bounds of the confidence intervals are given in centi-Morgans. Significance thresholds given as superscripts in the Position column: $p = 0.05^{\dagger}$, $p < 0.05^{*}$, $p < 0.01^{**}$, $p < 0.001^{***}$.

Marker	LG	Position (LOD)	C. I. limits (LOD)		Span	Gene count
			Lower	Upper	cM - Mbp	
Cr						
Herato1524_-647681	15	69.0 (4.47)***	59.80 (2.39)	69.02 (4.47)	9.22 - 2.0	-
Herato1805_-3923683	18	21.0 (3.19)†	0.00 (1.80)	41.27 (1.29)	41.27 - 14.9	-
Luminance						
Herato2101_-7491127	21	23 (7.21)***	10.75 (5.45)	48.55 (5.25)	37.8 - 8.14	421
Ridge spacing						
Herato2101_-7491127	21	23 (5.20)*	0.00 (3.58)	42.34 (3.11)	42.34 - 11.53	618

TABLE 3.2: Mean ridge spacing and mean luminance of EC17 offspring for each genotype class at marker Herato2101_7491127. Females are hemizygous at this marker (-/W).

Genotype	Ridge spacing		Luminance	
	Mean	Std. error	Mean	Std. error
Pan/W	920.22	5.06	84.03	3.40
Ecu/Pan	863.67	5.94	91.22	5.02
Ecu/W	862.54	16.07	123.85	7.25
Ecu/Ecu	856.08	6.90	117.66	5.89

Unlinked autosomal loci control ridge spacing and luminance in *H. melpomene*

We found strong evidence for a QTL associated with ridge spacing variation in chromosome 7 of *H. melpomene* at the Hmel207001o_11550301 marker (Fig. 3.5, A). This QTL explains 30.2% of the variation in phenotype among the EC70 offspring. As in the case of *H. erato*, we did not find any strong evidence for QTL controlling variation in cross-rib spacing. The chromosomes containing loci with the highest LOD scores for this trait were 15 and Z (Fig. 3.5, B).

A significant association was found for luminance in the EC70 family at the marker Hmel203003o_2717321 on chromosome 3 (Fig. 3.6, B; Table 3.3). This QTL explains 31.6% of variation for luminance in EC70. A previous analysis in our research group revealed a QTL for BR value on chromosome 3. In contrast to the analysis of the full set of families, our analysis did not reveal significant associations for BR-value in EC70. However we did observe that the highest LOD score was found in chromosome 3 in a position that appears coincident with that of the QTL for luminance (Fig. 3.6, A).

Bayesian 99% credible intervals for the ridge spacing QTL span 14.24 Mb (Table 3.3) with the marker Hmel207001o_7968319 being the closest to the lower limit and Hmel207001o_13166323 being closest to the upper limit. For the luminance QTL, the

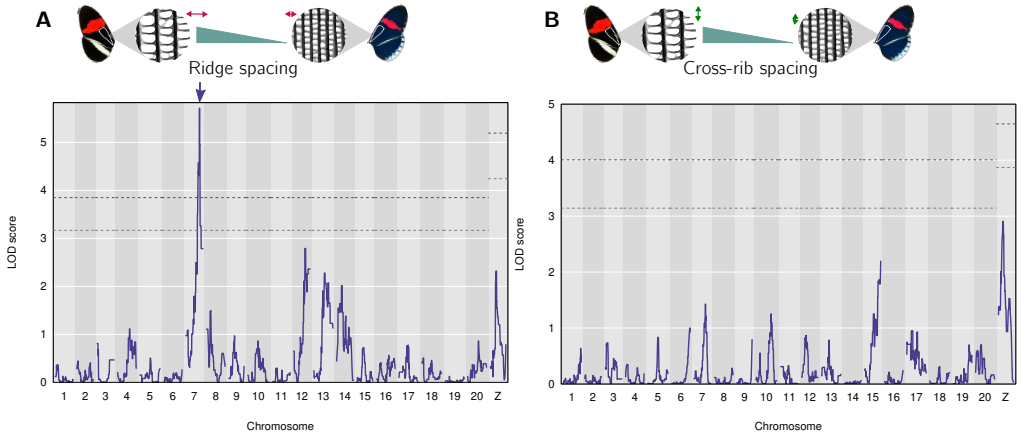

FIGURE 3.5: Scale structure QTL in *H. melpomene*: Evidence for genetic association was found in chromosome 7 for ridge spacing (A) but no strong associations were found for cross-rib spacing. The highest LOD scores in this case were found in chromosomes 15 and Z but these are not significant (B).

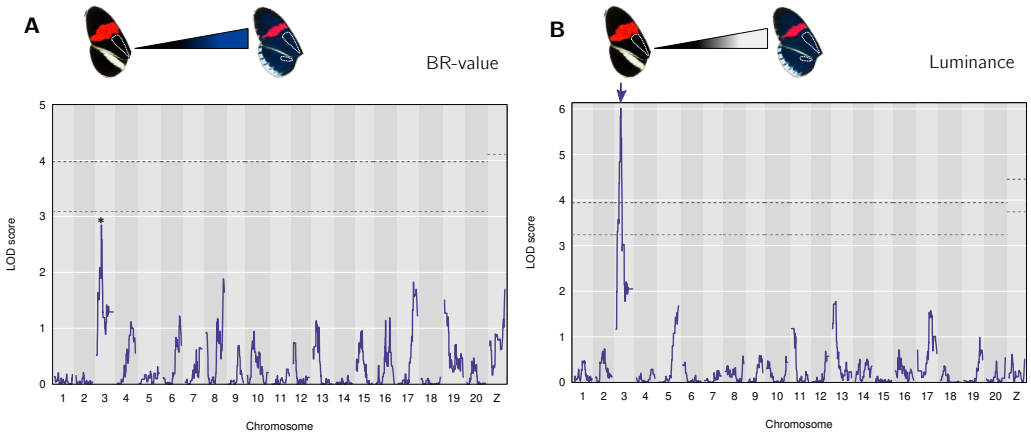

FIGURE 3.6: Iridescence QTL in *H. melpomene*: No evidence for genetic association was found for BR value (A) but chromosome 3 contains a QTL strongly associated with luminance (B) BR value shows a peak in chromosome 3 which is below the significance thresholds (*).

Bayesian credible interval is narrower than that for the ridge spacing QTL, spanning 14.72 Mb (Table 3.3) and has Hmel203003o_1264960 as the closest marker to the lower limit and Hmel203003o_4154626 as the closest marker to the upper limit.

TABLE 3.3: Locations, p-values and confidence intervals for significant QTL in *H. melpomene*. The position of the QTL and the bounds of the confidence intervals are given in centi-Morgans. Significance thresholds given as superscripts in the Position column: $p = 0.05^{\dagger}$, $p < 0.05^{*}$, $p < 0.01^{**}$, $p < 0.001^{***}$.

Marker	LG	Position (LOD)	C. I. limits (LOD)		Span	Gene count
			Lower	Upper	cM - Mbp	
Yb						
Hmel215003o_590099	15	4.0 (7.42)***	0.00 (6.52)	18.89 (5.09)	18.89 - 3.2	-
Luminance						
Hmel203003o_2717321	3	38.18 (6.01)***	28.88 (3.57)	43.60 (3.81)	14.72 - 2.89	162
Ridge spacing						
Hmel207001o_11550301	7	53.61 (5.71)***	45.34 (3.50)	59.58 (3.26)	14.24 - 5.2	423

Given that we set all maternal alleles to "Panama", we have true heterozygotes masked as Panama homozygotes and true Ecuador homozygotes masked as heterozygotes. Despite this, we expect to have true Panama homozygotes labelled correctly and we also expect to have true heterozygotes labelled correctly in the Pan/Ecu category. Moreover, individuals labelled as Pan/Ecu will always be carriers of Ecuador alleles, regardless of the number of true Ecuador alleles that each individual may have. We can thus give a description of possible associations of phenotype and allelic configurations, acknowledging that the possible relationships will be biased.

We found that individuals with an assumed homozygote Panama genotype have an increased ridge spacing compared to carriers of Ecuador alleles (Fig. 3.7; Table 3.4). This is in line with the expectation that individuals carrying Ecuador alleles should show a phenotype more similar to that of the parental race *H. m cythera*. This result also resembles the one found for *H. erato*, in which carriers of Ecuador alleles show narrower spacing between their ridges.

Carriers of Ecuador alleles at a marker significant for luminance association are expected to resemble the blue race *H. m. cythera* more than the matt-black *H. m. rosina*. Hence, individuals with higher luminance are expected to show an association with Ecuador genotypes. We found the opposite trend in the effect of genotypes on luminance in EC70. Panama homozygotes show higher mean luminance than heterozygotes (Fig. 3.7; Table 3.4).

We may use estimates of ridge spacing and luminance from wild caught individuals and make assumptions about their genotypes to get an idea of what may be the allelic interactions at the QTL that control iridescence and scale structure in *H. melpomene*. We may assume that crossed individuals with Ecuador alleles at loci controlling ridge spacing and luminance have estimates similar to those of wild caught *H. m. cythera*

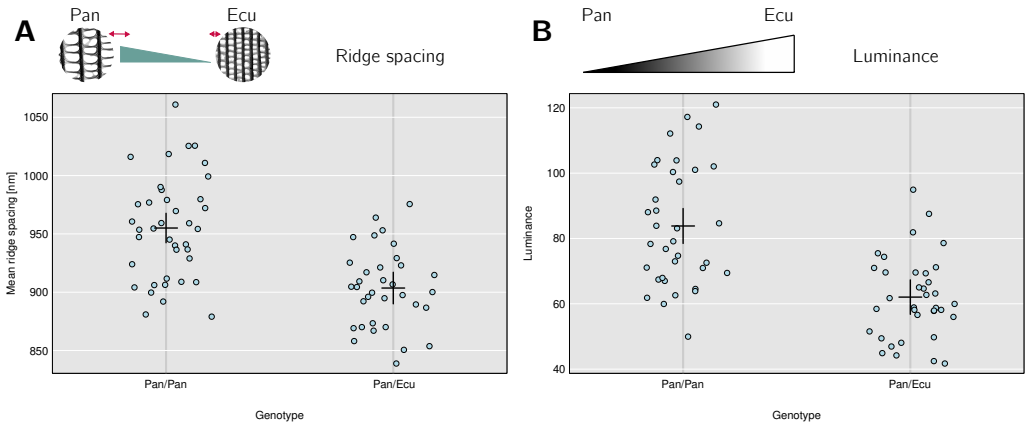

FIGURE 3.7: Genotypic associations at markers closest to significant QTL in *H. melpomene*. Ecuador alleles are associated with narrower ridge spacing at marker in chromosome 7 (A). Ecuador alleles are associated with decreased luminance in comparison to Panama homozygotes at the marker on chromosome 3 (B). The approach followed means that true heterozygotes are masked as Panama homozygotes and true Ecuador homozygotes are masked as heterozygotes.

(ridge spacing $\sim$ 823 nm according to Parnell et al., 2018, luminance $\sim$ 116.25 *a.u.* according to data from Emma Curran and Melanie Brien). Next, we calculate coefficients of dominance as we did in *H. erato*, which yield values of $k = -0.24$ for ridge spacing (close to additivity but skewed towards Panama dominance) and $k = -2.33$ for luminance (under-dominance). This suggests that alleles of *H. melpomene* interact differently to those of *H. erato*, which shows interactions closer to dominance. We note here that for these calculations we are assuming values for Ecuador homozygotes and that the phenotypic values associated with heterozygotes and Panama homozygotes are biased because of the setting of maternal alleles to Panama.

TABLE 3.4: Mean ridge spacing, mean luminance and corresponding standard errors of EC70 offspring for each genotype class at markers Hmel207001o_11550301 (ridge spacing) and Hmel203003o_2717321 (luminance).

Genotype	Ridge spacing		Luminance	
	Mean	Std. error	Mean	Std. error
Pan/Pan	952.63	7.18	83.82	3.14
Pan/Ecu	903.57	5.74	62.04	2.09

3.4.2 GWAS for EC70 family in *H. melpomene*

We also examined iridescence and scale structure variation using a Genome-wide association analysis in EC70 to explore the effect that ignoring maternal markers may have had on the QTL results, and whether additional information could be gained by including these markers. Our GWAS on EC70 controlling for family structure did not reveal significant genetic associations for any of the scale structure traits as shown in figure 3.8. The SNPs with the lowest p-values were found in chromosomes 1, 7, 17 and

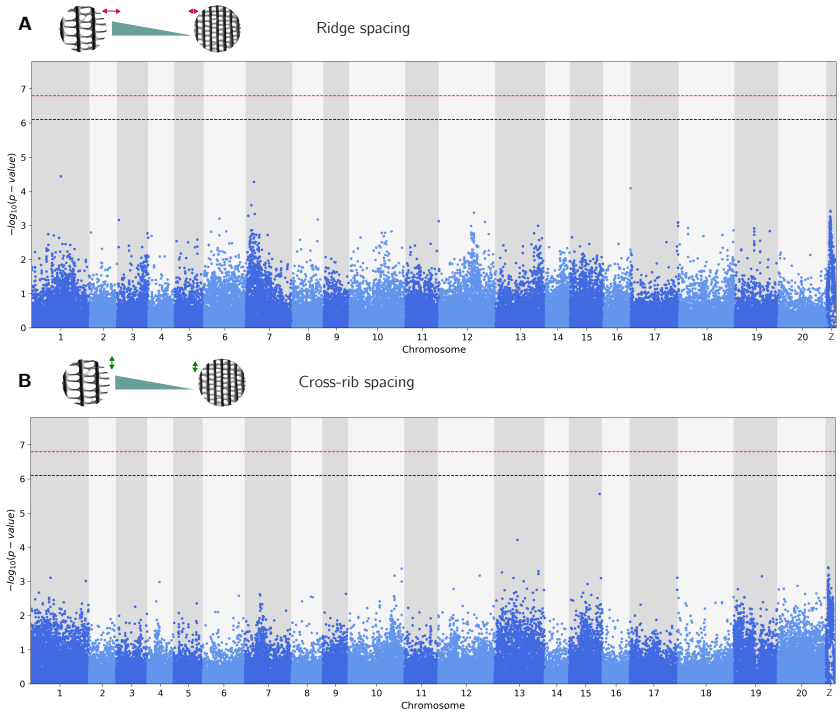

FIGURE 3.8: Genome wide patterns of association for scale structure in the EC70 family. No significant associations were found for ridge spacing (A) or cross-rib spacing (B).

Z for ridge spacing (Fig. 3.8 A), and in chromosomes 13 and Z for cross-rib spacing (Fig. 3.8 B).

We did not find significant associations between SNPs and BR-value in EC70. The smallest p-values (higher $-log_{10}(p\text{-}value)$) can be observed across most of chromosome 3 and also on chromosome 10 (Fig. 3.9, A). In contrast, we did find SNPs significantly associated with variation in luminance on chromosome 3. There is a single SNP which scores above both conservative genome-wide Bonferroni corrected thresholds (Fig. 3.9 B; $\alpha = 0.05$ black dashed line, $\alpha = 0.01$ red dashed line). Other SNPs with low p-values for association with luminance can be observed on chromosome 20.

When analysing all *H. melpomene* families together accounting for pedigree structure, we found significant associations for both iridescence traits on chromosome 3 (Fig. S3.5). Stronger support for association was found for luminance in comparison to BR-value. Since we do not have scale structure data for this larger data-set, we had to limit the GWAS with all families to colour variation traits only.

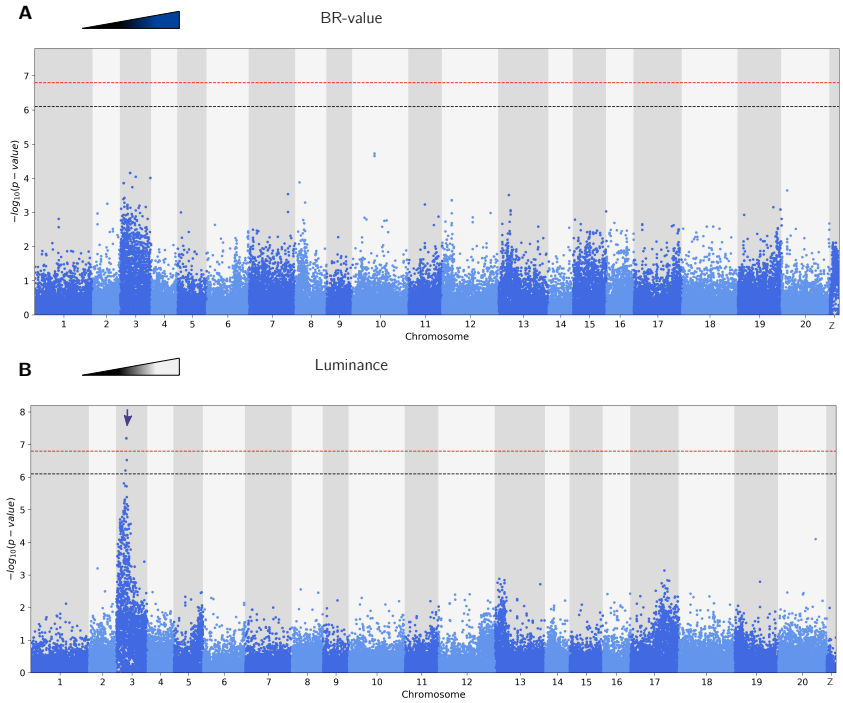

FIGURE 3.9: Genome wide patterns of association for iridescence traits in the EC70 family. No significant associations were found for BR-value (A), but a strong association with luminance variation was found in chromosome 3 (B).

3.4.3 Genes that control pigment and scale structure

We found that the pigmentation genes belonging to the ommochrome and melanin pathways have similar physical positions in the genomes of *H. erato* and *H. melpomene*, as expected due to their high level of synteny (Table 3.5). None of these genes are located within the Bayesian confidence intervals estimated for the QTL found in either species for colour or scale structure variation.

We found however that the *pale* and *tan* genes, both belonging to the melanin pathway, are both located on chromosome 21 at a physical position that is 1 Mbp and and 724 kbp from the upper limits of the Bayesian confidence intervals of the ridge spacing and luminance QTL of *H. erato* respectively, and the *tan* gene is located approximately 1.76 and 1.2 Mbp from the lower limits of the confidence intervals of the same QTL (Tables 3.1 and 3.5).

TABLE 3.5: Names and locations of pigmentation genes analysed for effects on scale structure in the 2018 study of Matsuoka and Monteiro. *Heliconius* gene names are based on gene annotations and predictions found in the reference versions Herato.v1 and Hmel.v2.5. Physical location corresponds to bp positions in the mentioned scaffold.

Gene name		Scaffold	Physical location
Common	*Heliconius*		
Melanin pathway			
DDC	evm.TU.Herato0101.485	Herato0101	13 654 807 - 13 667 714
	HMEL012487g1	Hmel201001o	10 291 883 - 10 303 233
yellow	evm.TU.Herato1701.151	Herato1701	5 730 510 - 5 741 296
	HMEL005860g1	Hmel217001o	4 228 039 - 4 236 260
aaNAT	evm.model.Herato1601.112	Herato1601	5 155 459 - 5 240 963
	HMEL004850g2	Hmel216002o	3 252 122 - 3 279 891
pale/TH	evm.model.Herato2101.432.1	Herato2101	13 692 635 - 13 700 795
	HMEL009822g1	Hmel221001o	10 528 143 - 10 535 436
ebony	evm.model.Herato1901.66	Herato1901	2 269 873 - 2 343 038
	HMEL016976g1	Hmel219001o	1 693 084 - 1 706 186
tan	evm.TU.Herato2101.123	Herato2101	3 628 492 - 3 638 492
	HMEL008807g1	Hmel221001o	2 486 855 - 2 494 204
Ommochrome synthesis pathway			
vermillion	evm.model.Herato1301.735	Herato1301	21 683 051 - 21 703 103
	HMEL010716g1	Hmel213001o	16 428 807 - 16 431 609
white	evm.model.Herato2001.443	Herato2001	11 740 220 - 11 763 714
	HMEL012487g1	Hmel220003o	8 843 443 - 8 852 044
scarlet	evm.TU.Herato2001.442	Herato2001	11 693 775 - 11 719 904
	HMEL035243g1	Hmel220003o	8 803 623 - 8 826 021

3.5 Discussion

We found QTL for ridge spacing and luminance in both species. QTL were located in different chromosomes and none overlapped or was physically linked to any colour pattern genes or pathway pigmentation genes. In *H. erato* QTL for ridge spacing and luminance overlap and both map to the sex chromosome. In *H. melpomene* the QTL are unlinked and are located on different autosomes. We did not find evidence of QTL for cross-rib spacing. Although there may be a difference in cross-rib spacing between iridescent and non-iridescent races (Brien et al., 2018), it is unclear what is its relationship to structural colour; as of yet it has has not been suggested to be related to the development of blue wing phenotypes. Cross-rib spacing has been found to be augmented in butterflies with ultra-black patches as a mechanism that may help with the reduction of reflection of light from wings with black backgrounds (Davis et al., 2020). It is possible that the genetic basis of cross-rib spacing is highly complex and substantially more sampling is required to uncover it. We also didn't find QTL for BR value probably because of a combination of low sample size and reduced content of information in comparison to luminance.

3.5.1 Genetic architecture of scale structure variation

In recent years, reverse genetics research has revealed a surprising connection between the molecular machinery underlying the development of pigmented wing patterns and the ultra-structure of butterfly scales in various species (Concha et al., 2019; Fenner et al., 2020; Matsuoka et al., 2018; Zhang et al., 2017). It is plausible that these genes could have an effect on scale architecture modifications that result in the production of structural colours in *Heliconius* and other butterfly species if there is a shared genetic architecture for structural and pigmentary colours.

In some butterflies, it seems to be the case that there is a shared architecture underlying both kinds of traits. For example, the transcription factor *optix* has been shown to act both as a switch that dictates the position and delimitation of wing patterns (Zhang et al., 2017) and as a modulator of lamina thickness involved in the production of a wide range of structural colours (Thayer et al., 2020; Zhang et al., 2017). It has also been shown that disruptions of the *WntA* ligand result in changes in pigment based and structural UV reflection in *Z. cesonia* (Fenner et al., 2020). Furthermore, not only pigmentation patterns change in *Heliconius* knockouts, but scale morphology also suffers modifications (Concha et al., 2019), albeit this change in scale morphology is not related to structural colour.

Our QTL are not associated with any known colour pattern gene of large or small effect. QTL found for luminance and ridge spacing variation are located on the sex chromosome in *H. erato*, while in *H. melpomene* the QTL with the largest effect on ridge spacing variation was found on chromosome 7 and the largest QTL associated with luminance is located on chromosome 3. None of the known major colour pattern controlling loci in *Heliconius* are found in these regions. In addition, QTL found here don't overlap QTL for pigment pattern variation that were found in a super-set of the families that we have used in our analyses (Bainbridge et al., 2020), further supporting the idea that structural colour variation and wing pattern variation is unlinked in both species. Hence, our findings show that *H. erato* and *H. melpomene* do not use the molecular machinery of wing pattern production for sculpting specialised nano-structures and iridescent wings.

In addition, genes involved in pigment production pathways in insects have also been found to have an effect on the architecture of the butterfly scale. Knockouts for two genes of the melanin-dopamine pathway produced modifications of the scale architecture (Matsuoka et al., 2018). The mutants for *yellow* and *DDC* genes showed modified scale architecture in comparison to wild-type individuals, suggesting the possibility of an association of pigmentation genes with scale structure variation in other butterfly species.

Our examination of the locations of melanin and ommochrome production genes did not reveal an overlap with QTL or their estimated confidence intervals in any of our crosses. One melanin pathway gene is located on the same linkage group as one of the

QTL we found. The *pale* gene was found 700 kb and 1000 kb from the upper limit of the confidence intervals estimated for luminance and ridge spacing respectively in the *H. erato* genome and the *tan* gene was found 1.76 Mb and 1.2 Mb from the lower limits of the same QTL. Despite their position on the same linkage group, the evidence at hand suggests these gene are not involved in scale structure modification in *Heliconius* as they fall outside the confidence region of the QTL interval.

The evidence we present here, together with the reverse genetics research done on *Heliconius* suggest that the genetic architecture of iridescent structural colour produced by ridge reflection in *H. erato* and *H. melpomene* is completely decoupled from that of mimicry related wing pattern regulation and that of pigment production. The position of QTL in each species' genome also suggests that in contrast to other adaptive traits co-evolved by these two co-mimics, the genetic architecture of structural colour is not shared between them.

Our observations for both species may result from several smaller effect QTL linked together as well as from genes of large effect within each QTL. The results we present are based on F2 crosses which are limited in resolution due to the low number of recombination events produced during the cross. The span of the confidence intervals of all of our significant QTL is rather large, each containing a large number of genes (tables 3.1 and 3.3). These QTL regions possibly harbour several mutations that contribute to structural colour variation spread across several genes. This putative genetic architecture may act as an artefact from which wrong conclusions about pleiotropy could be made when assuming that a significant QTL is due to a single gene of large effect (Hermisson et al., 2008). Thus, it is sensible to predict that a finer dissection of these QTL intervals and their associated traits using higher resolution mapping will result in picking apart loci controlling ridge spacing and loci controlling other aspects of scale morphology that are important for structural colour. This approach has resulted in breaking down large QTL into several loci of smaller effect in other organisms (Mackay, 2004; Orgogozo et al., 2006; Shahandeh et al., 2020). We anticipate this to be the case for both species, regardless of the differences we found between them.

In *H. erato* the same marker was associated with variation in ridge spacing and luminance. Previous studies (Brien et al., 2018; Parnell et al., 2018) and chapter 2 report significant negative correlations between ridge spacing and various chromatic and achromatic measurements of structural colour for *H. erato*. These two points together suggest the possibility of a single locus controlling ridge spacing and brightness in this species. However, if the same locus within the QTL truly controls both traits, we would expect alleles of the associated markers to show similar allelic interactions for both traits. We found that this marker shows allelic interactions that are different for each trait: for ridge spacing the alleles from Ecuador behave dominantly, and for luminance the Panama alleles behave dominantly (Fig. 3.4, Table 3.2). If a single gene underlies variation for both traits, then its alleles must necessarily be acting in

concert with products from other genes to produce the patterns of dominance with opposite directions shown here. This also suggests a more complex and indirect relationship between ridge spacing and brightness: although there is a strong correlation between these two traits, other aspects of scale morphology likely also contribute to variation in brightness and their genetic control possibly also overlap the QTL found on the Z chromosome. In *H. melpomene* two un-linked QTL were associated with differences in ridge spacing and luminance among individuals of the outcross EC70 family. This evidence for un-linked architecture further supports the idea that ridge spacing does not control brightness in a simple and direct manner as reported before (Parnell et al., 2018).

When comparing the possible interactions between alleles of Ecuador or Panama ancestry we also find evidence suggestive of differences between species. While for *H. erato* the estimates of k for ridge spacing and luminance suggest dominance interaction in both cases, *H. melpomene* possibly has alleles that tend to behave additively for ridge spacing and show under-dominance for luminance. This claim relies on assumptions about the phenotypic values of homozygote classes in both species and on estimates of k that are slightly biased due to our QTL analysis approach for *H. melpomene*. However, the evidence is suggestive of further differences in genetic architecture between species.

Our family-based GWAS analysis on EC70 failed to reveal additional QTL on top of those we found assuming that EC70 was a backcross family. Our results did not reproduce the significant association detected for ridge spacing (Fig. 3.8, A), although one of the top associated SNPs is on chromosome 7. We did not find significant associations with cross-rib spacing (Fig. 3.8, B) or BR-value (Fig. 3.9, A). They did, however, reproduce the significant association that we found for luminance on chromosome 3 (Fig. 3.9, B). This is possibly due to a combination of the level of information underlying each trait estimate, the genetic architecture and mode of inheritance of each trait, and the number of individuals available for analysis. In a follow-up family based GWAS involving all *H. melpomene* families we were able to recreate the significant QTL found by Melanie Brien for BR-value and luminance on chromosome 3 (Fig. S3.5). It is known that genome wide association studies rely heavily on large numbers of individuals to avoid false negatives due to lack of statistical power. Although no significant associations were found for scale structure variation, there is an elevated association pattern observable on chromosome Z for both ridge spacing and cross-rib spacing. This suggests the possibility of a genetic architecture of scale structure that is partially shared between *H. erato* and *H. melpomene*.

The difference in genetic architecture between species may be expected given that the two species show differences in correlations between traits reported in chapter 2 for crossed individuals: while ridge spacing and luminance are strongly correlated in *H. erato*, there is no correlation between these estimates for *H. melpomene*.

3.5.2 Lack of gene reuse and genetic parallelism

Many instances of parallel evolution involve the use of the same genes and developmental pathways in the production of similar phenotypes (Conte et al., 2012; A. Martin et al., 2013). This is the case for wing patterns involved in warning signal and mating in *Heliconius* co-mimics (Hines et al., 2011; Kronforst et al., 2015; Supple et al., 2013), in which evolution has repeatedly recruited the same set of hot-spot genes (Jiggins et al., 2017). A main result of our analysis of structural colour variation in controlled crosses is that this mechanism may not underlie complex traits such as scale structure and luminance. We explore different possibilities as to why we may observe this.

It is possible that we detect different QTL in both species due to the complexity of the traits analysed, the number of samples used and to inherent limitations of QTL analyses. In a QTL experiment there is a bias against loci of smaller effect; normally only those loci explaining the largest phenotypic variances are revealed as significant (Xu, 2003). The QTL we detected likely explain the most variation in these particular families and other QTL that remain undetected could have possibly been shared between species, thus we cannot discard a scenario of a partially shared genetic architecture for scale structure and luminance. Alternatively, since we only have a limited amount of variation segregating due to our experimental design, our analyses could have revealed only particular regions segregating in the parents that we crossed, and other genetic variance that underlies changes in structural colour possibly was left un-sampled.

Evolution of iridescent structural colour and other quantitative complex traits may not have a high chance of predictability if the effects of loci are small. Wing pattern traits are known to be mainly controlled by master genes of large effect but these traits have also been shown to have some degree of variation that maps to loci explaining smaller portions of variance and which have been deemed as loci with smaller effects. When comparing these smaller effect loci between species, lack of parallelism starts to show up (Bainbridge et al., 2020), yet it is not complete because the loci of largest effect remain the same across species (Bainbridge et al., 2020). The takeaway from this result is that large effect loci remain the same across species because they are frequent targets of evolution, whilst smaller effect loci are less likely to be targeted repeatedly by evolution. We suggest that a possibility for the lack of gene reuse of quantitative complex traits such as ridge spacing and luminance is that their underlying loci have modest effects at most. This makes evolutionary pathways less constrained: Assuming that genetic effect sizes are correlated with fitness effects, the emergence of deleterious mutations would only have minor negative consequences for fitness. This mode of evolution may require that there are several loci across the genome which could potentially harbour mutations that produce similar phenotypic outcomes across species (Conte et al., 2012).

Although our observations on lack of genetic parallelism are possibly strongly related with the small effects of QTL underlying trait variation, we think that there are additional contexts worth considering for discussing our results. The mutational and evolutionary spectrum is influenced or constrained by the ecology of populations (Stern et al., 2009). Thus, it is possible that differences in ecology and selection regimes between pigmented patterns and structural colour in *Heliconius* may explain the contrasts between their modes of evolution, genetic architecture, and the lack of gene reuse that we have observed in our QTL experiments.

3.5.3 Sexual dimorphism and sex linkage

There is sex linkage of ridge spacing and luminance in *H. erato* and not in *H. melpomene*. This may relate to the role that structural colour is playing in the life history of each species. The sex chromosome linkage may have to do with structural colour being sexually dimorphic in *H. erato* and not in *H. melpomene*. We found in our crosses that *H. erato* F2s showed significant differences between males and females which was not observed in the *H. melpomene* outcross. Although we may be observing these differences between sexes due to the crosses having a different structure, we think that the observed pattern likely reflects a true difference and not an artefact; sexual dimorphism in achromatic and chromatic aspects of structural colour has been observed in *H. erato* but not in *H. melpomene* in wild caught individuals, albeit this claim is based on a rather small sample size (Brien, 2019).

Sexual dimorphism could act as an artefact showing non-existent sex chromosome associations as significant. This could affect our analysis if the assumptions used for autosomal linkage groups were extended to the analysis of sex chromosomes (Broman et al., 2006). We added sex as a covariate in all our analyses, so we expect that this possible artefact in the sex chromosome is accounted for. We observe that despite the increased 1% and 5% LOD thresholds, the associations for ridge spacing and luminance are still statistically significant showing strong support for the association found in the sex chromosome. In addition, our *H. erato* data reveals that there are significant differences for both traits within sexes. Females with Ecu/W genotypes have significantly reduced spacing compared to Pan/W females (Table 3.2). For luminance, homozygote Ecuador males have significantly increased luminance compared to heterozygote males, and Ecu/W females have also significantly increased luminance compared to Pan/W females (Table 3.2). These results indicate that the significance of the QTL in the sex chromosome is due to genetic differences between iridescent and non-iridescent races that have evolved in the sex chromosome rather than being the result of an artefact produced by the inherent differences in configuration of sex chromosomes between males and females.

Traits with sexual dimorphism present in only one of these co-mimic species have been studied and reported before. Retinal mosaics and UV opsins are an example of this. A comparative analysis including several species of *Heliconius* butterflies

revealed differences between males and females in only some of the species analysed. The compound eye of *H. erato* females was found to contain cell sub-types and opsins that are not present in males. This is in contrast to *H. melpomene*, in which both males and females show identical components and receptor pigments, one of which is not expressed in the eyes of *H. erato* males (McCulloch et al., 2017). Additionally, the structural colours of butterflies, in particular those with short wavelengths (e.g. UV, violet, blue), have been reported to have roles in intraspecific recognition (Rutowski, 1977; Sweeney et al., 2003) and sexual behaviour (Kemp, 2007; Kemp et al., 2007; Papke et al., 2007; Rutowski et al., 2010), and in some instances they have been suggested to be part of aposematic warning signals, albeit this is not yet supported by evidence (Rutowski et al., 2010). We suggest that the evolution of structural colour in *Heliconius* is related to the evolution of the visual mechanism involved in mate choice/recognition previously described (Finkbeiner et al., 2017; McCulloch et al., 2017). In particular, differences in sex and the major QTL found in the sex chromosome in *H. erato* but not in *H. melpomene* suggest that structural colour is being used differently in these two species and is possibly important as a sexual signal in *H. erato*. The presence of a QTL in the sex chromosome is expected to be favoured in sexually selected traits since it can more easily overcome sexual conflict (Rice, 1984).

3.6 Conclusion and next steps

Evolution has targeted different sets of genes to develop scale architecture suitable for structural colour production in *H. erato* and *H. melpomene*. The lack of gene reuse in the evolution of this complex quantitative trait may be due to a joint effect of the ecological role of structural colour shaping the mutational landscape differently in both species, and also of a presumed less constrained evolutionary pathway due to the increased availability of loci of small effect that can potentially evolve iridescent blue phenotypes in a concerted manner without incurring in negative pleiotropy.

Reverse genetics approaches have uncovered surprising, unprecedented connections between wing patterning and pigment pathway genes of large effect. Although these loci clearly have effects on scale ultra-structure, none of them has been shown to be related to sculpting multi-layer ridge reflectors as of yet. Although our forward genetics approach does not single out specific genes, it has revealed novel loci of morphological evolution in butterflies. One limitation of our approach is that the accuracy of QTL analyses is limited, particularly when fewer individuals are used, resulting in inflated estimates of explained variance (Slate, 2013); the explained variance we hereby report is likely an overestimate due to the Beavis effect (Beavis, 1994). Follow-up studies may focus on finer scale mapping of iridescence related traits which will help narrow down the location of the genetic changes underlying phenotypic variation.

SAXS data and microscopy can reveal interesting features of scale structure and allow

for a better understanding of the relationship between scale architecture and structural colour. However, we consider that standardised photographs are an excellent method for characterising phenotypic variation related to iridescence and its genetic underpinnings. In our study both methods complemented well, revealing that different aspects of this complex trait have taken different evolutionary pathways in contrast to pigmented wing patterns for which the same genetic machinery has been reused in these two butterfly species. Other methods such as optical spectroscopy may reveal additional relationships between genetics and more detailed aspects of colour such as hue or saturation.

From a phenotyping perspective, another limitation to our approach is that the SAXS experiment did not allow the interrogation of smaller features of scale architecture such as the organisation of the lamellae; their dimensions and the size of the air gaps between them are expected to influence greatly the properties of the colour produced. Despite ridge spacing being associated with variation in structural colour and being a good proxy for variation in ultra-structure related to iridescence, interrogating the lamellae structure and characterising the variations in ridge morphology will likely result in a more precise description of phenotypic variance. This finer description of scale structure changes could possibly reflect finer segregation patterns in the crosses that could in turn help to reveal additional QTL.

Future efforts should focus in revealing candidate genes, functionally validating these using approaches such as CRISPR on individuals that express or lack expression of structural colour to see how their visual appearance is affected and also which aspects of ultra-structure change in knock-out individuals.

3.7 Contributions to this chapter

The rearing of broods and collection and analysis of colour variation and SAXS data was done as specified in Chapter 2. The extraction of genomic DNA was done by Melanie Brien. Library preparation and sequencing was done by Edinburgh Genomics. Linkage map construction was done by Melanie Brien with assistance from Pasi Rastas. The QTL analysis, family based association analysis, analyses of dominance and assessment of overlap with loci with pigmentation pattern genes were done by Juan Enciso.

3.8 Supplementary material

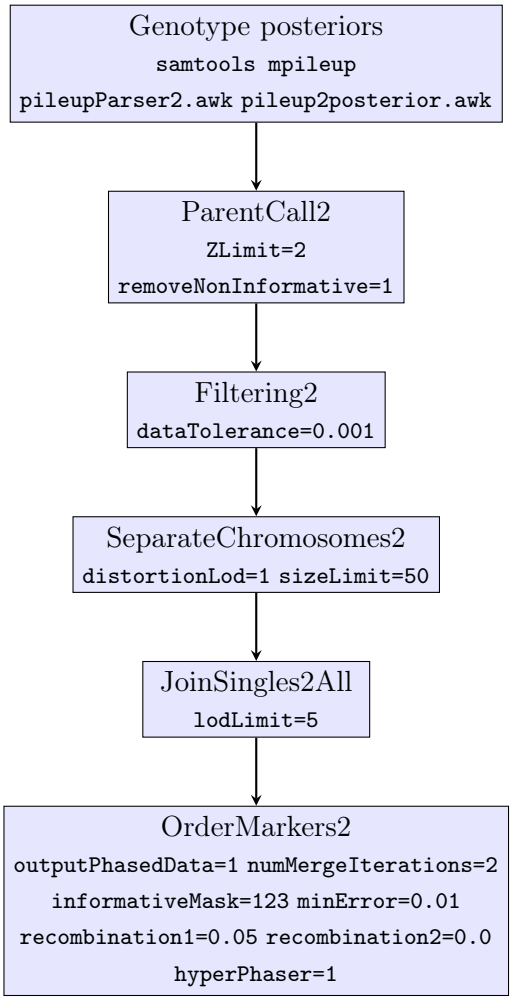

FIGURE S3.1: LepMap3 pipeline scheme. The steps followed and the modules called for linkage map construction are shown in order. The scripts used and the option values set for each module are included in each box.

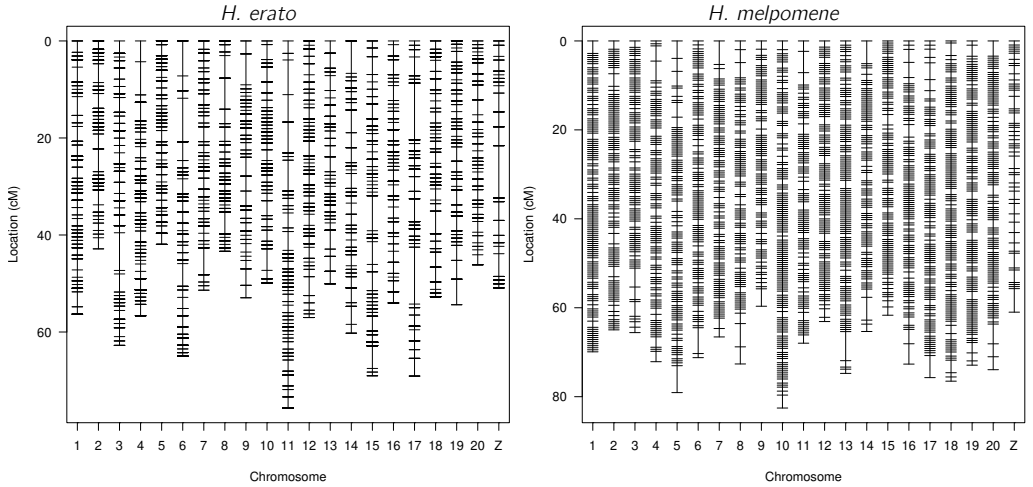

FIGURE S3.2: Linkage maps of *H. erato* and *H. melpomene* with markers distributed across 21 linkage groups.

TABLE S3.1: Details of marker spacing and length per linkage group for the linkage map of *H. erato*.

Linkage group	Markers	Length (cM)	Mean marker spacing (cM)	Max marker spacing (cM)
1	303	56.31	0.19	3.88
2	247	42.86	0.17	4.69
3	219	62.76	0.29	7.77
4	438	56.66	0.13	6.83
5	371	41.94	0.11	2.29
6	333	64.99	0.20	8.96
7	228	51.38	0.23	5.52
8	333	43.39	0.13	6.36
9	208	52.94	0.26	6.37
10	373	49.89	0.13	4.47
11	265	75.67	0.29	7.15
12	340	57.01	0.17	3.88
13	244	50.06	0.21	3.88
14	180	60.24	0.34	6.68
15	335	69.02	0.21	7.21
16	229	54.01	0.24	3.08
17	199	69.08	0.35	11.73
18	234	52.73	0.23	4.69
19	299	54.38	0.18	5.27
20	160	46.14	0.29	3.08
Z	110	50.91	0.47	10.79
Total	5648	1162.37	0.23	11.73

TABLE S3.2: Details of marker spacing and length per linkage group for the linkage map of *H. melpomene*.

Linkage group	Markers	Length (cM)	Mean marker spacing (cM)	Max marker spacing (cM)
1	123	69.91	0.57	2.81
2	103	64.97	0.64	2.82
3	97	65.59	0.68	4.25
4	100	72.13	0.73	4.43
5	99	79.08	0.81	6.05
6	108	71.22	0.67	5.81
7	100	66.56	0.67	5.29
8	90	72.64	0.82	5.23
9	87	59.66	0.69	3.92
10	134	82.55	0.62	2.91
11	90	67.97	0.76	4.79
12	107	63.10	0.60	1.92
13	122	74.76	0.62	6.54
14	89	65.34	0.74	5.13
15	102	61.68	0.61	2.34
16	99	72.67	0.74	4.57
17	107	75.71	0.71	4.96
18	125	76.51	0.62	2.82
19	119	72.91	0.62	2.49
20	111	73.93	0.67	4.44
Z	51	61.00	1.22	5.29
Total	2163	1469.89	0.70	6.54

Table S3.3: Names and biological functions of pigmentation genes analysed for effects on scale structure in the 2018 study of Matsuoka and Monteiro. Function terms were recovered from FlyBase (FB2020_05) and are based on experimental evidence.

Gene	Biological function (*Drosophila*)
Melanin pathway	
DDC	Adult chitin-containing cuticle pigmentation
	Dopamine biosynthetic process from tyrosine
	Serotonin biosynthetic process from tryptophan
	Thermosensory behaviour
	Wing disc development
yellow	Cuticle pigmentation
	Developmental pigmentation
	Male mating behaviour, veined wing extension
	Melanin biosynthesis
aaNAT	Developmental pigmentation
	Regulation of circadian cycle
	Serotonin catabolic process
pale/TH	Adult chitin-containing cuticle pigmentation
	Dopamine metabolism
	Male courtship behaviour
	Thermosensory behaviour
	Wing disc development
ebony	Dopamine synthase activity
tan	Dopamine synthase activity
	Cuticular melanisation
	Vision
	Neurotransmitter recycling
Ommochrome synthesis pathway	
vermillion	Kynurenine metabolic process
	Ommochrome biosynthetic process
	Tryptophan catabolic process to kynurenin
white	Compound eye pigmentation
	Gravitaxis
	Histamine uptake
	Male courtship behaviour
	Ommochrome biosynthetic process
scarlet	Aminergic neurotransmitter
	Eye pigment precursor transport
	Ommochrome biosynthetic process

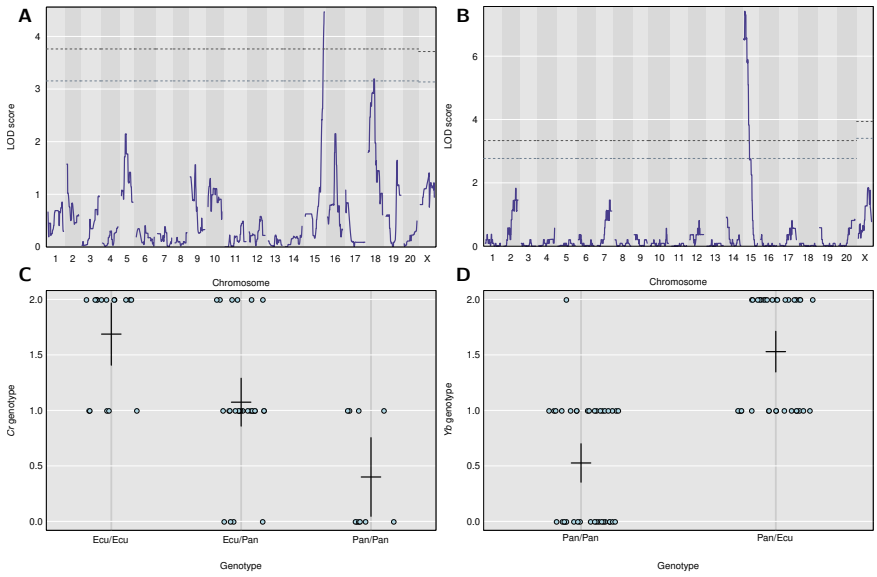

FIGURE S3.3: QTL for variation in hind-wing bar phenotype and corresponding effects on genotype in *H. erato* and *H. melpomene*. Significant evidence for association in chromosome 15 and chromosome 18 was found in *H. erato* (A). In *H. melpomene* evidence for association with hind-wing phenotype was found in chromosome 15 only (B). Association of genotypes with hind-wing phenotype confirm expectations of Ecuador alleles underlying white margin phenotypes (scores of 2.0) and Panama alleles underlying yellow bar phenotypes (scores of 0.0) in both species (C and D).

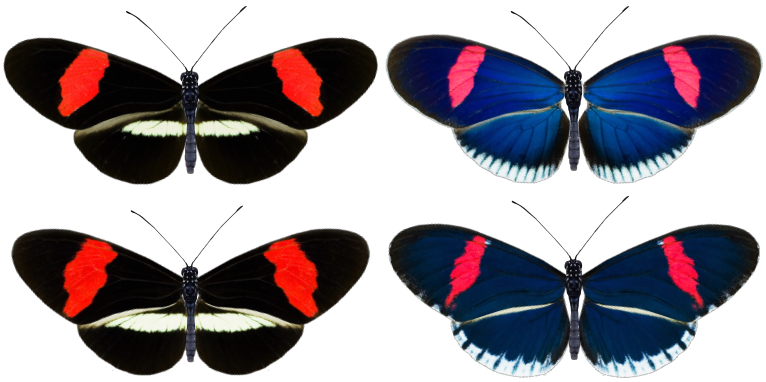

FIGURE S3.4: Wings of co-mimic sympatric races of *H. erato* (top) and *H. melpomene* (bottom). The Panamanian races *H. e. demophoon* and *H. m. rosina* are shown on the left and the Ecuadorian co-mimics *H. e. cyrbia* and *H. m. cythera* are shown on the right. Several differences can be observed between the wings of both species, especially between the Ecuadorian co-mimics. The intensity and hue of blue colour being perhaps the most prominent.

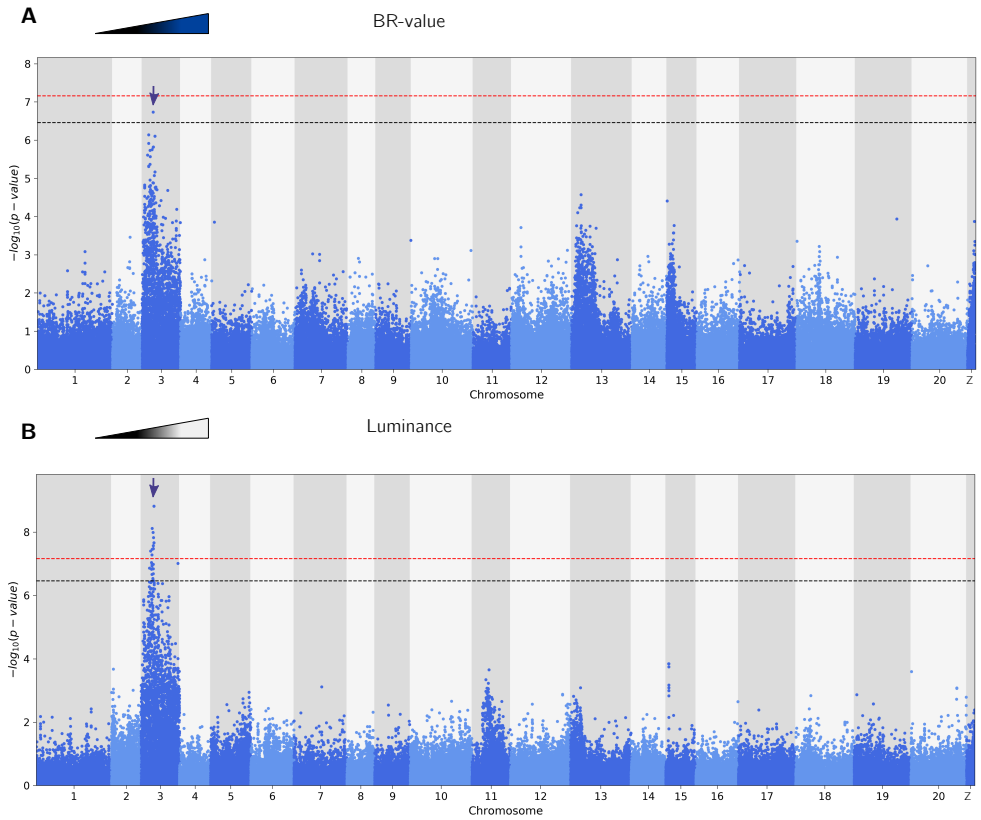

FIGURE S3.5: Genome wide patterns of association for iridescence traits of all families of the *H. melpomene* crosses. Blue-red value (A) and luminance (B) show strong associations at chromosome 3.

Chapter 4

Genetic analysis of structural colour variation in wild caught *H. erato* and *H. melpomene*

4.1 Abstract

In this chapter we used the phenotypic variation found in two co-mimic butterfly species across a natural gradient of structural colour variation between matt-black to bright blue to search for genetic polymorphisms associated with phenotypic variation. To this end we gathered re-sequencing data from a comprehensive set of samples from both species across this natural range, and performed SNP based GWAS to explore possible associations. In addition, we performed admixture and genetic structure analyses to incorporate the latter into the GWAS model to decrease the chance of getting spurious results. We phenotyped our individuals using optical spectroscopy to maximise the amount of colour data obtained per-individual and to possibly reduce the impact of damaged and worn wings in the observed data. We did not find significant associations with structural colour variation in *H. erato* or *H. melpomene* despite controlling for population structure and excluding the populations showing the highest population structure with respect to the rest. In contrast, we were able to find significant associations for a known Mendelian trait. We conclude that it is possible that structural colour has a polygenic basis and is controlled by genes of small effect. The association signal coming from these loci may have been confounded with the genetic structure that has evolved between populations despite applying controls for population structure to the GWAS. We list variants and genes of potential interest that scored highest in our association analysis.

4.2 Introduction

Finding the loci that control morphological variation remains a major goal and a challenge in evolutionary biology. One of the most impressive instances of morphological variation is structural colour, which is produced by the interaction of light and nanostructures present in various organisms. Although structural colour is present and has been studied in a wide variety of organisms, Lepidoptera, the clade of butterflies and moths, is one of the groups with the most striking diversity in structural colour. The lepidopteran scale has developed a wide array of modifications to produce diverse visual effects without the need of pigment (Ghiradella, 1991).

Although lepidopteran structural colour has been studied for nearly 100 years, little was known about its genetic underpinnings until recently. We have started to unveil the developmental mechanisms and genes involved in structural colour in several butterfly species. The results of these investigations show that butterflies, and possibly moths, can recruit a wide variety of genes to modify their scale structure and produce diverse colours. For example, a paralog of *doublesex* gene and the *bric-a-brac* gene have been identified as switches of sexually dimorphic UV colouration (Ficarrotta et al., 2021; Rodriguez-Caro et al., 2021), and the *optix* gene has been shown to modify the thickness of the lower lamina of the scale producing blue and green iridescent colour (Thayer et al., 2020; Zhang et al., 2017). The enormous diversity of phenotypic variation in structural colour in butterflies warrants the exploration of the genetics of structural colour in other species. This will enable the assessment of conservatism or diversity of genetic mechanisms used to control this trait in lepidoptera.

Heliconius is one of many groups of butterflies that have evolved structural colour. The physical mechanisms that produce structural colour in *Heliconius* butterflies have been described to some extent; different species of *Heliconius* modify scale architecture differently in order to produce structural colouration (Parnell et al., 2018; Wilts, Vey, et al., 2017). In particular, the Müllerian co-mimics *H. erato* and *H. melpomene* show iridescence as a spatially structured quantitative trait; populations of both species show a latitudinal gradient in structural colour from matt-black in Panama to blue in Western Colombia and Ecuador. Local forms of each species converge in structural colour, albeit not to the extent that they converge in their pigmented wing patterns. This convergence in structural colour can be partly explained by the convergence shown in the morphology of the scale; both *H. erato* and *H. melpomene* use the ridges of the scale to produce blue colour, and in both species narrower ridge spacing is associated with blue colour, as shown in Chapter 2, and by Parnell and colleagues (2018).

The genetic basis of structural colour in *H. erato* and *H. melpomene* has been studied previously using controlled crosses. In Chapter 3 we presented evidence for significant QTL associated with variation in scale structure and structural colour in *H. erato* and *H. melpomene*. Furthermore, we showed that this variation maps to different genomic

regions in both species which indicates a different genetic basis for the evolution of structural colour and lack of parallelism in a system that is established as a model for Müllerian mimicry and a repeated evolution of colour patterns. In this chapter we aim to characterise this divergent variation on a finer scale, possibly pinpointing genes or putative cis-regulatory regions associated with structural colour variation in *Heliconius*, as well as other loci that possibly were not detected using QTL analyses.

QTL studies have a number of limitations for identification of specific genes or putative regulatory regions controlling a trait. QTL analyses done using inbred line crosses, such as those used in Chapter 3 and in Brien et al. (2018), may not give accurate descriptions of the genetic architecture in the parental populations in their natural environment; this is because the limited number of individuals used as parents may not contain a complete set of alleles at every locus controlling the trait of interest if there is variation at these loci in the parental populations (Slate, 2004). Also, it is not uncommon to find several tightly linked genes under a single QTL, all having an effect on phenotypic variation (Hermisson et al., 2008; Mackay, 2004). Therefore, the QTL require dissection to find specific genes or markers associated with trait variation. Several potential routes may be used to complement QTL analyses and narrow down the loci controlling phenotypic variation. Association mapping is particularly useful when a large number of unrelated individuals is available (Slate, 2004), which is the case for our analysis.

Association mapping using genome-wide SNP marker data (GWAS) has been done before as a method for revealing the genetic architecture of iridescent structural in *H. erato* and *H. melpomene*, albeit without any significant results. In her PhD thesis, Emma Curran used RAD-Seq data and a measure of phenotypic variation obtained from digital photographs (Curran, 2018). Among several reasons that were mentioned behind the lack of significant results were that possibly the RAD-Seq data was excluding important allelic variants due to allele dropout (Cariou et al., 2016; Davey et al., 2012). It is also possible that the reduced representation of genomic DNA did not capture the relevant loci if restriction enzymes didn't have cut sites nearby loci of large effect on structural colour. This is likely given LD decays rapidly in both species (Counterman et al., 2010). Finally, iridescent colour is angle dependent and its variation possibly is more difficult to quantify for wild caught samples if only using digital photographs, this is because there will be more variation due to age and wear compared to the QTL analysis, in which butterflies are killed right after eclosion and wings are preserved as they emerge from the pupa, minimising the effects of wear.

We propose changes to methodological aspects in phenotyping and genotyping with respect to the aforementioned analysis. In this chapter we use a subset of samples used by Curran (2018), plus new samples for both species to do a GWAS of structural colour variation. We use optical spectroscopy for estimating phenotypic variation in our samples, focusing on regions of the wing that have the least signs of wear and the brightest iridescent colour. We expect this to maximise the amount of colour data

obtained per individual and to minimise the effect of damage present in some wings. We use whole genome re-sequencing data to improve coverage and increase the chance of sampling variants that are linked to the loci controlling structural colour.

We predict that SNPs with significant associations with phenotypic variation, as measured by colourimetric variables, will co-localise with the QTL we found in Chapter 3: A locus on the sex chromosome for *H. erato* and loci on chromosomes 3 and 7 for *H. melpomene*. Additionally we predict that significant associations appear on QTL that weren't found with the samples analysed on Chapter 3, but that were found and reported by Melanie Brien (2019) on her PhD thesis: A significant QTL on chromosome 20 for *H. erato*, and a suggestive QTL on chromosome 10 for *H. melpomene*. If the QTL we found and reported contain genes of moderate to large effect, we expect that the potential SNP associations will allow us to single out genes or point to narrow genomic regions that contain candidate genes for variation in structural colour. In addition, in dogface butterflies, a paralog of the *dsx* gene mediates the sex-specific expression of ultraviolet structural colour (Rodriguez-Caro et al., 2021). Thererfore, SNPs associated with structural colour variation may be found in genes described as *dsx* or doublesex-like in the *Heliconius* genomes. Finally, we expect to find significant genetic associations near genes with functions related to the actin cytoskeleton because it is suggested that actin dynamics are strongly related to the production of structural colour in the lepidopteran scale (Lloyd et al., 2021).

4.3 Methods

4.3.1 Sample collection

Individuals of *H. erato* (n = 275) and *H. melpomene* (n = 140) were collected from several localities across Panama, Colombia and Ecuador, aiming to cover the spectrum of phenotypic variation ranging from matt-black to iridescent blue. Upon collection, wings were removed and stored in glassine envelopes. The bodies were preserved in a solution of 20% dimethyl sulfoxide (DMSO) 0.25M EDTA saturated with NaCl. The details of collection localities are given in table 4.2 and Figure 4.1.

4.3.2 Phenotyping individuals

Optical spectroscopy

Different properties of structural colour can be analysed from the reflectance spectra of wings. We took reflectance measurements from the discal cell (Fig. S4.2) of the right fore-wings of collected butterflies. Left fore-wings were measured only when the right fore-wing was highly damaged, worn or unavailable. We set the wings on a rectangular piece of paper containing a fore-wing model for consistency of the position of the wing with respect to the probe of the spectrophotometer (Fig. S4.2). The wings were fixed to the paper using tack between the wing and the paper and Scotch Magic

tape covered with paper to avoid removing scales from the dorsal side of the wing. The piece of paper with the wing was fixed to an optical mount on a rotating stage for allowing the measurement of optical spectrum over a range of angles. It was observed that there are differences in the angle at which iridescent wings of each species attain maximum reflectance. Iridescent individuals of *H. erato* are most reflective between 8 and 20 degrees of rotation of the measuring stage, whereas *H. melpomene* showed peak reflectance between -4 and 10 degrees. Thus, we took measurements in ranges from 0 to 24 degrees for *H. erato* and from -4 to 10 degrees for *H. melpomene*, increasing the angle by 2 degrees to ensure measuring the angle of maximum reflectance. The rotation of the wing was done parallel to the orientation of the scales, which was previously determined to have the same orientation of the veins of *Heliconius* wings (Parnell et al., 2018).

We used an Ocean Optics (USA) USB2000+ optical spectrophotometer to record the reflectance spectra. The spectrophotometer was connected to a PX-2 pulsed xenon light source through a bifurcated fibre-optic probe with the third end of the probe fixed perpendicular to the optical mount at 0°. All measurements were normalised using the reflectance spectrum of a diffuse white standard of polytetrafluoroethylene (Labsphere Spectralon 99%) at 250–1600 nm. The wings were rotated so that the proximal part of the wing moved closer towards the light source/probe to ensure the recording of the peak reflectance as done previously by Parnell and colleagues (2018). The OceanView software (v1.6.7) was used to record the reflectance spectra, set to average 5 individual scans with a boxcar width of 3 and an integration time of 350 ms. We wrote a script to automate the normalisation using the white standard and to organise the recorded spectra by sample and angle of measurement.

We measured repeatability by taking three technical replicates from five randomly selected individuals. We followed the procedure described in chapter 15 of Whitlock and Schluter (2015), whereby a random effects ANOVA is used to estimate variance within groups (σ^2) and variance among groups (σ^2_A). A group in this case is the set of replicates taken from each sample. Then we estimated repeatability using the expression

$$Repeatability = \frac{\sigma^2_A}{\sigma^2_A + \sigma^2}$$

Estimates of repeatability were obtained for the six colour variables used to describe phenotypic variation, specified below in table 4.1.

Scoring of the yellow hind-wing bar

The scoring of yellow hind-wing bar phenotype is based on the nomenclature used by Mallet when describing the hybrid zones of *H. erato* and *H. melpomene* along Panama and West Colombia (Mallet, 1986). We scored the hind-wing bar phenotype according to the presence, complete or partial, of yellow bars on either dorsal or ventral sides of the wing, or both. In the case of samples coming from Ecuador a white margin can be

observed on the distal part of the wing on the dorsal side, and the yellow hind-wing bar is only present on the ventral side, being thinner and blurred compared to the yellow bars observed in Colombian and Panamanian races. Each hind-wing phenotype was assigned a score from 1 to 4 to jointly describe hind-wing bar variation of dorsal and ventral sides similar to that assigned by Mallet (1986). The Ecuador phenotype was scored as the number 5. Hind-wing phenotypes and their scores are shown in Figure S4.1.

4.3.3 Analysis of spectral data

We pre-processed the spectral data by choosing manually the angle at which maximum reflectance was attained for each individual. Since the structural colour of *H. erato* and *H. melpomene* is within the violet to green range, we selected the angle of peak reflectance as that which showed the maximum reflectance at wavelengths between 300 nm and 570 nm; which corresponds to wavelength ranges of violet, blue and green butterfly-visible light (Hecht, 2002).

We used the R package Pavo (v2.0) (Maia et al., 2019) for further processing and analysis of spectral data. We used one spectrum per individual as input and processed the spectra using the `procspec` function. It is recommended to smooth the spectra so that the noise does not affect the quality of the downstream analyses; we visually inspected the data under various smoothing parameter values and set the smoothing parameter `span` to 0.25. We toggled the `min` option to subtract the minimum value from all spectra. Negative values of reflectance were set to zero using the option `fixneg="zero"`.

We limited the wavelength range of the spectra to values between 300 nm and 605 nm, thus filtering out the wavelengths corresponding to orange, red and infrared. Pavo decomposes the spectra into 23 colourimetric variables through its `summary` function. The colourimetric variables correspond to different estimates of brightness, hue and saturation (Montgomerie, 2006). We did an initial exploration of the data distribution across the 23 variables and restricted our analysis to those described in table 4.1, using the same set of variables for both species. The S1 variable used to quantify saturation is divided arbitrarily into discrete ranges of colour by Pavo; here we used only three ranges corresponding to violet, blue and green colours. In the case of hue (H1) some matt-black individuals showed a peak reflectance of 300 nm while others showed a peak reflectance of 605 nm; these two values correspond to both ends of the spectral range analysed and are an artefact of the procedure rather than real hue values. Leaving values at these two extremes for matt-black individuals would produce a distribution that is unsuitable for association analyses. We thus changed the values of hue for matt-black individuals; their values were chosen at random from a uniform distribution between 298 nm and 302 nm.

Brightness was measured using two different variables in an attempt to account for the effect of age and wearing in the wings. We observed that the data coming from old and worn wings frequently show an elevated reflectance over the whole spectrum, likely because they contain regions that are devoid of scales in which the wing surface is exposed. B2 is a measure of brightness that comes from estimating the average of reflectance over the whole spectral range and B3 is the reflectance at the wavelength with the highest reflectance across the spectrum. We expect B2 to be slightly inflated in old and/or worn individuals because of the elevated reflectance across the spectrum. B3 on the other hand is the estimate of reflectance at a single point; the wavelength of maximum reflectance. B3 may result in a more accurate estimate of brightness as it does not depend on the estimations across all points throughout the wavelength range.

TABLE 4.1: Description of colourimetric variables used to measure variation in structural colour.

Variable	Name	Description
B2	Mean brightness	Mean reflectance over the entire spectral range
B3	Intensity	Reflectance at the wavelength of maximum reflectance
S1	Chroma (V, B, G)	Relative contribution of spectral range to total brightness
H1	Peak wavelength, hue	Wavelength of maximum reflectance

4.3.4 DNA extraction and sequencing

Genomic DNA was extracted using the QIAGEN DNeasy blood and tissue kit (QIAGEN) following the protocol issued by the manufacturer with an addition of QIAGEN RNase A for digestion of RNA. The DNA was quantified using a Qubit fluorometer and checked for contaminant residuals using a Nanodrop spectrophotometer. Illumina paired-end library preparation and sequencing were carried out by Novogene (China) using an Illumina HiSeq platform. Paired-end 150bp reads were generated with an insert size of 350bp. A fraction of the samples come from whole genome re-sequencing experiments done before and these were either obtained from the European Nucleotide Archive (ENA) or were kindly shared by colleagues at University of Cambridge and Universidad del Rosario (Colombia). Reads were checked for quality using FASTQC (v0.11.19) (Andrews et al., 2012). A portion of the data that was shared from colleagues contained traces of adapters from the Nextera library preparation kit. These data were cleaned and trimmed using Trimmomatic (v0.39) (Bolger et al., 2014) with the option `ILLUMINACLIP` set to `NexteraPE-PE.fa:2:30:10:2:keepBothReads`. Bases with a quality below 3 on 5' and 3' ends or with a quality below 15 over a 4 base sliding window were discarded and we kept reads with lengths equal to or above 40bp.

4.3.5 Genomic data processing

We mapped the quality checked reads of *H. erato* and *H. melpomene* individuals to the most recent reference genomes available for each species: *H. erato* referenge genome

v1.0 and *H. melpomene* reference genome v2.5 (Davey et al., 2017; Van Belleghem et al., 2017) using the `mem` function of the bwa alignment software (Li and Durbin, 2009). We removed PCR duplicates using the `MarkDuplicates` tool in the picard toolkit (*The Picard Toolkit* 2019) (v2.18.15) and we indexed and sorted the mapped genomes using the `index` and `sort` tools implemented in samtools (v1.8) (Li, Handsaker, et al., 2009). After checking quality and integrity of mapped data we retained 271 individuals of *H. erato* and 140 individuals of *H. melpomene*. Mapping quality and coverage were assessed using Qualimap (v2.2.1) (Okonechnikov et al., 2015) and sequencing and mapping statistics were summarised with multiqc (v1.8) (Ewels et al., 2016). They can be found on table 4.2.

We estimated genotype likelihoods using angsd (v0.921) (Korneliussen et al., 2014) using the GATK model. We retained only sites that were polymorphic according to a likelihood ratio test statistic higher than 24 (p-value $< 1 \times 10^{-6}$), had a minimum base quality of 20 and a minimum mapping quality of 30, had a minimum minor allele frequency of 0.05 and were genotyped for at least 90% of the individuals.

For the genetic association analysis SNP calling was required. We used the SNP calling based on genotype likelihoods implemented in angsd (Kim et al., 2011). The settings were as in the estimation of genotype likelihoods but with the added requirement that sites had to be supported by a minimum depth of 5.0 per sample to be called.

TABLE 4.2: Details on sex, collection locations and sequencing statistics of samples.

Individual	Race	Sex	Lat.	Lon.	Locality	M. cov.	No. reads	Insert	Map Q.	Err.	% align
H. erato											
guarica.M3121	guarica	M	2.94	−75.59	Huila	31.28	87 073 554.00	268.00	46.08	0.05	96.59
guarica.M3125	guarica	M	2.94	−75.59	Huila	40.77	114 856 664.00	288.00	46.02	0.05	96.32
guarica.M3375	guarica	F	4.21	−74.97	Tolima	42.25	110 849 537.00	274.00	45.13	0.05	95.57
guarica.M3376	guarica	M	4.21	−74.97	Tolima	36.95	101 111 784.00	288.00	46.20	0.05	96.49
guarica.M3428	guarica	M	4.21	−74.97	Tolima	46.50	122 081 261.00	291.00	45.95	0.05	96.41
guarXcolo.4165	guaricaXcolombina	F	5.70	−74.20	Otanche	9.11	23 181 371.00	292.00	46.09	0.05	97.16
guarXcolo.4166	guaricaXcolombina	F	5.70	−74.20	Otanche	10.27	27 514 237.00	298.00	46.39	0.05	93.85
guarXcolo.4181	guaricaXcolombina	M	5.74	−74.23	Otanche	10.50	27 353 220.00	344.00	46.16	0.05	96.95
guarXcolo.4192	guaricaXcolombina	M	5.78	−74.30	Otanche	11.07	28 933 561.00	291.00	46.30	0.05	96.56
colombina.M4164	colombina	F	5.77	−74.24	Otanche	18.26	50 347 533.00	237.00	46.85	0.05	97.81
demo.PetED6	demophoon	M	9.12	−79.70	Panama	40.81	145 549 823.00	138.00	45.53	0.04	97.66
demo.SW1284	demophoon	M	9.12	−78.72	Panama	35.18	141 212 706.00	370.00	46.54	0.04	94.59
demo.PetED4	demophoon	M	9.12	−79.70	Panama	44.33	157 303 614.00	139.00	45.87	0.04	96.29
demo.PetED3	demophoon	M	9.12	−79.70	Panama	44.77	161 157 699.00	140.00	45.81	0.04	97.61
demo.PetED5	demophoon	M	9.12	−79.70	Panama	34.71	123 030 492.00	140.00	45.32	0.04	97.26
demo.SW0087	demophoon	M	9.12	−78.72	Panama	35.72	120 195 619.00	293.00	46.34	0.04	95.93
demo.SW0082	demophoon	M	9.12	−78.72	Panama	22.48	69 814 164.00	332.00	46.40	0.04	96.33
hyd.SW0088	hydara	M	9.12	−78.72	Panama	41.92	130 982 032.00	290.00	46.36	0.04	95.93
hyd.SW0040	hydara	M	9.12	−78.72	Panama	31.52	110 529 704.00	176.00	45.25	0.04	95.99
hyd.SW5193	hydara	M	9.12	−78.72	Panama	30.85	101 897 029.00	308.00	46.32	0.04	95.61
hyd.0042	hydara	M	9.12	−78.72	Panama	34.50	111 983 840.00	176.00	44.93	0.04	95.52
hydXpet18006	hydaraXdemophoon	F	8.61	−78.14	Darien	10.97	26 969 553.00	326.00	46.23	0.05	97.17
demo.5362	demophoon	F	9.12	−78.72	Panama	36.63	129 235 797.00	216.00	45.23	0.04	94.83
hyd.5351	hydara	M	9.12	−78.72	Panama	24.67	86 603 799.00	343.00	46.36	0.04	95.58
hyd.0039	hydara	M	9.12	−78.72	Panama	29.53	107 868 236.00	174.00	45.04	0.04	96.46
demo.0033	demophoon	M	9.12	−78.72	Panama	28.86	101 766 288.00	175.00	45.26	0.04	96.39
hyd18008	hydara	M	8.61	−78.14	Darien	17.84	57 000 834.00	379.00	46.33	0.04	96.25
hydXpet18164	hydaraXdemophoon	M	8.28	−77.81	Darien	12.57	33 653 974.00	325.00	46.48	0.05	97.17
demo.5353	demophoon	F	9.12	−78.72	Panama	36.92	133 807 741.00	246.00	45.51	0.04	94.65
hydXpet18046	hydaraXdemophoon	F	8.61	−78.14	Darien	12.24	30 366 030.00	310.00	46.15	0.05	97.13
hydara18091	hydara	M	8.28	−77.81	Darien	11.75	30 799 339.00	328.00	46.35	0.05	97.05
hydXpet18059	hydaraXdemophoon	M	8.61	−78.14	Darien	10.87	29 398 683.00	307.00	46.38	0.05	97.26
hyd18009	hydara	M	8.61	−78.14	Darien	17.16	55 638 410.00	372.00	46.31	0.04	96.27
hyd18060	hydara	F	8.61	−78.14	Darien	17.90	56 100 620.00	377.00	46.32	0.04	96.31
hydXpet18026	hydaraXdemophoon	M	8.61	−78.14	Darien	11.02	29 436 401.00	312.00	46.33	0.05	97.14
hydXpet18050	hydaraXdemophoon	M	8.61	−78.14	Darien	10.60	27 559 050.00	313.00	46.48	0.05	97.29

Individual	Race	Sex	Lat.	Lon.	Locality	M. cov.	No. reads	Insert	Map Q.	Err.	% align
hydXpet18057	hydaraXdemophoon	M	8.61	−78.14	Darien	12.82	35 333 112.00	289.00	46.45	0.05	97.57
hydara18018	hydara	F	8.61	−78.14	Darien	10.19	28 057 172.00	296.00	46.31	0.05	97.31
hyd18121	hydara	M	8.16	−77.69	Darien	21.86	69 322 063.00	379.00	46.26	0.04	96.34
hydXpet18089	hydaraXdemophoon	M	8.02	−77.73	Darien	10.27	27 614 672.00	317.00	46.40	0.05	96.95
hyd18125	hydara	F	8.16	−77.69	Darien	20.46	58 175 688.00	378.00	46.07	0.04	95.78
hydara18106	hydara	M	8.02	−77.73	Darien	11.40	31 058 417.00	292.00	46.35	0.05	97.04
hydara18104	hydara	F	8.02	−77.73	Darien	11.87	29 209 624.00	298.00	46.16	0.05	97.10
hydara.15N375	hydara	M	7.55	−78.15	Jaque	12.33	32 553 172.00	326.00	46.31	0.05	96.95
venus.15N449	venus	M	7.49	−78.13	Jaque	10.55	28 117 348.00	348.00	45.88	0.05	96.74
hydara.15N433	hydara	F	7.53	−78.17	Jaque	12.27	29 539 331.00	347.00	45.57	0.05	96.66
hydara.15N358	hydara	M	7.53	−78.17	Jaque	10.58	27 536 225.00	298.00	46.13	0.05	96.20
hydara.15N346	hydara	M	7.50	−78.14	Jaque	10.21	26 800 793.00	298.00	46.00	0.05	96.73
hydara.15N396	hydara	M	7.55	−78.15	Jaque	10.53	26 129 753.00	324.00	46.01	0.05	97.02
hydara.15N331	hydara	F	7.49	−78.13	Jaque	11.24	27 492 574.00	280.00	45.96	0.05	96.18
hydara.15N392	hydara	M	7.55	−78.15	Jaque	9.83	25 418 529.00	319.00	46.08	0.05	97.31
hydara.15N344	hydara	F	7.50	−78.14	Jaque	11.34	26 555 710.00	293.00	45.91	0.05	96.75
venus.15N431	venus	M	7.53	−78.17	Jaque	10.66	27 545 357.00	298.00	45.92	0.05	96.92
venus.15N414	venus	M	7.52	−78.17	Jaque	12.46	31 850 153.00	314.00	45.90	0.05	97.09
hydara.15N332	hydara	F	7.49	−78.13	Jaque	12.73	31 973 678.00	287.00	45.91	0.05	96.97
hydara.15N430	hydara	M	7.53	−78.17	Jaque	11.96	29 739 048.00	305.00	45.95	0.05	97.23
venus.15N368	venus	M	7.53	−78.17	Jaque	10.30	26 679 906.00	330.00	45.83	0.05	97.14
hydara.15N357	hydara	F	7.53	−78.17	Jaque	12.26	31 370 037.00	369.00	45.82	0.05	96.88
hydara.15N454	hydara	F	7.49	−78.13	Jaque	11.70	28 514 499.00	298.00	45.78	0.05	96.96
hyd.15N322	hydara	M	7.49	−78.13	Jaque	20.35	63 820 475.00	378.00	45.89	0.04	96.07
hydara.15N424	hydara	M	7.53	−78.17	Jaque	10.95	28 485 544.00	303.00	45.87	0.05	96.93
hydara.15N436	hydara	M	7.53	−78.17	Jaque	11.27	28 844 725.00	335.00	45.85	0.05	96.44
venus.15N356	venus	F	7.53	−78.17	Jaque	11.34	27 242 823.00	296.00	45.75	0.05	97.06
hydara.15N441	hydara	F	7.50	−78.14	Jaque	11.94	29 356 701.00	332.00	45.57	0.05	96.85
hydara.15N444	hydara	M	7.50	−78.14	Jaque	11.24	29 352 852.00	350.00	45.96	0.05	96.67
hydara.15N412	hydara	M	7.52	−78.17	Jaque	11.15	29 566 780.00	316.00	46.05	0.05	97.20
venus.15N391	venus	M	7.55	−78.15	Jaque	9.94	25 646 836.00	286.00	46.05	0.05	96.77
hydara.15N425	hydara	M	7.53	−78.17	Jaque	11.11	29 708 241.00	318.00	45.67	0.05	96.76
hydara.15N381	hydara	F	7.55	−78.15	Jaque	13.16	30 067 747.00	331.00	45.83	0.05	96.67
petiverana.15N371	demophoon	F	7.53	−78.17	Jaque	10.81	26 617 570.00	332.00	45.72	0.05	97.20
hydara.15N419	hydara	F	7.53	−78.17	Jaque	10.55	26 363 262.00	298.00	45.70	0.05	97.25
hydara.15N378	hydara	F	7.55	−78.15	Jaque	11.50	27 223 069.00	320.00	45.79	0.05	95.37
hydara.15N324	hydara	F	7.49	−78.13	Jaque	10.79	26 329 194.00	285.00	45.87	0.05	97.06
hydara.15N360	hydara	F	7.53	−78.17	Jaque	10.44	24 986 661.00	298.00	45.86	0.05	97.12
hydara.15N416	hydara	F	7.52	−78.17	Jaque	10.28	17 055 056.00	235.00	45.20	0.05	76.82
hydara.15N348	hydara	M	7.49	−78.13	Jaque	10.48	26 364 576.00	300.00	45.82	0.05	96.89
hydara.15N446	hydara	M	7.50	−78.14	Jaque	11.78	31 350 129.00	347.00	45.79	0.05	96.91
hydara.15N385	hydara	F	7.55	−78.15	Jaque	10.50	25 764 850.00	312.00	45.80	0.05	96.95
hydara.15N413	hydara	F	7.52	−78.17	Jaque	11.56	27 931 693.00	337.00	45.67	0.05	96.81
venus.15N445	venus	F	7.50	−78.14	Jaque	12.65	29 333 794.00	346.00	45.56	0.05	96.52
hydara.15N442	hydara	M	7.53	−78.17	Jaque	11.54	30 397 101.00	339.00	45.72	0.05	96.94
hydara.15N349	hydara	F	7.49	−78.13	Jaque	10.93	26 481 951.00	298.00	45.87	0.05	97.09
hydara.15N365	hydara	M	7.53	−78.17	Jaque	10.85	27 360 778.00	344.00	45.84	0.05	96.88
hydara.15N407	hydara	M	7.52	−78.17	Jaque	11.01	28 660 147.00	333.00	45.79	0.05	97.09
hydara.15N369	hydara	M	7.53	−78.17	Jaque	12.15	31 163 494.00	338.00	45.88	0.05	97.00
venus.15N450	venus	M	7.49	−78.13	Jaque	11.47	29 578 960.00	300.00	45.88	0.05	96.36
hydara.15N405	hydara	M	7.55	−78.15	Jaque	10.18	26 968 658.00	329.00	45.77	0.05	97.10
venus.15N395	venus	M	7.55	−78.15	Jaque	10.63	27 324 510.00	292.00	45.95	0.05	97.01
hydara.15N330	hydara	M	7.49	−78.13	Jaque	9.79	25 720 282.00	327.00	46.00	0.05	97.23
venus.15N320	venus	F	7.49	−78.13	Jaque	22.15	63 622 812.00	370.00	45.78	0.04	96.01
hydara.15N359	hydara	F	7.53	−78.17	Jaque	9.84	24 982 598.00	281.00	45.90	0.05	97.28
hydara.15N428	hydara	F	7.53	−78.17	Jaque	12.93	30 794 162.00	325.00	45.81	0.05	96.85
hydara.15N447	hydara	M	7.53	−78.17	Jaque	11.48	29 660 034.00	347.00	45.90	0.05	96.86
hydara.15N374	hydara	M	7.55	−78.15	Jaque	10.02	25 492 158.00	314.00	45.90	0.05	97.00
hydara.15N400	hydara	F	7.55	−78.15	Jaque	14.49	32 235 874.00	285.00	45.90	0.05	96.47
hydara.15N434	hydara	F	7.53	−78.17	Jaque	11.58	28 427 533.00	333.00	45.64	0.05	96.93
venus.15N323	venus	M	7.49	−78.13	Jaque	13.19	63 335 558.00	365.00	45.78	0.04	65.84
hyd.15N321	hydara	F	7.49	−78.13	Jaque	21.66	61 240 363.00	372.00	45.77	0.04	95.96
hydara.15N362	hydara	M	7.53	−78.17	Jaque	10.49	28 354 729.00	283.00	45.91	0.05	97.25
hydara.15N347	hydara	F	7.49	−78.13	Jaque	10.80	25 008 026.00	301.00	45.91	0.05	96.87
venusXhyd.15N336	venusXhydara	M	7.49	−78.13	Jaque	10.83	27 176 939.00	301.00	45.84	0.05	96.94
hydara.15N422	hydara	M	7.53	−78.17	Jaque	9.81	25 896 315.00	321.00	45.90	0.05	97.00
hydara.15N418	hydara	F	7.52	−78.17	Jaque	10.36	25 646 945.00	334.00	45.85	0.05	96.73
venus.15N327	venus	M	7.49	−78.13	Jaque	10.71	28 388 391.00	307.00	45.94	0.05	96.79
hydara.15N393	hydara	F	7.55	−78.15	Jaque	12.34	28 975 045.00	309.00	45.62	0.05	96.75
hydara.15N401	hydara	F	7.55	−78.15	Jaque	11.07	25 424 653.00	297.00	45.75	0.05	96.87
hydara.15N345	hydara	M	7.50	−78.14	Jaque	9.87	26 553 329.00	331.00	45.59	0.05	96.93
hydara.15N406	hydara	F	7.55	−78.15	Jaque	11.87	28 126 663.00	304.00	45.86	0.05	97.06
hydara.15N386	hydara	M	7.55	−78.15	Jaque	10.11	26 642 928.00	339.00	45.79	0.05	97.00
hydara.15N363	hydara	M	7.53	−78.17	Jaque	10.77	26 015 620.00	321.00	45.70	0.05	97.00
hydara.15N361	hydara	M	7.53	−78.17	Jaque	11.03	26 746 121.00	328.00	45.95	0.05	97.06
hydara.15N402	hydara	M	7.55	−78.15	Jaque	12.79	31 764 233.00	295.00	46.13	0.05	96.83
hydara.15N337	hydara	M	7.49	−78.13	Jaque	12.93	33 039 736.00	302.00	45.96	0.05	96.95
venus.15N452	venus	M	7.49	−78.13	Jaque	10.02	26 671 658.00	325.00	45.84	0.05	95.64
hydara.15N448	hydara	F	7.49	−78.13	Jaque	12.14	28 107 918.00	331.00	45.63	0.05	96.86
hydara.15N364	hydara	M	7.53	−78.17	Jaque	9.81	25 407 354.00	294.00	45.82	0.05	96.81

Individual	Race	Sex	Lat.	Lon.	Locality	M. cov.	No. reads	Insert	Map Q.	Err.	% align
hydara.15N453	hydara	M	7.49	−78.13	Jaque	10.16	25 428 337.00	292.00	45.97	0.05	97.12
hydara.15N388	hydara	M	7.55	−78.15	Jaque	10.02	24 768 385.00	317.00	45.46	0.05	96.82
venus.15N261	venus	M	5.57	−77.50	Amargal	21.49	62 522 643.00	369.00	45.06	0.05	95.77
venus.15N238	venus	F	5.57	−77.50	Amargal	22.65	63 328 135.00	370.00	45.03	0.04	95.75
venus.15N239	venus	F	5.57	−77.50	Amargal	24.29	68 920 190.00	385.00	44.93	0.05	95.76
venus.15N241	venus	F	5.57	−77.50	Amargal	21.76	61 188 984.00	365.00	45.02	0.04	95.89
venus.CS635	venus	M	3.94	−77.37	Ladrilleros	7.85	20 662 377.00	210.00	44.86	0.05	86.81
venus.CS632	venus	M	3.94	−77.37	Ladrilleros	9.56	26 435 706.00	213.00	44.30	0.05	84.22
venus.CS634	venus	F	3.94	−77.37	Ladrilleros	1.84	14 643 155.00	75	42.15	0.04	45.90
venus.15N194	venus	M	3.84	−77.26	Ladrilleros	20.80	60 472 498.00	385.00	45.04	0.05	95.36
venus.CS284	venus	M	3.94	−77.37	Ladrilleros	6.62	15 253 386.00	202.00	45.53	0.05	98.00
venus.CS46	venus	M	3.94	−77.37	Ladrilleros	5.38	13 498 015.00	201.00	45.51	0.05	97.05
venus.CS630	venus	M	3.94	−77.37	Ladrilleros	5.79	13 140 578.00	194.00	45.56	0.05	97.87
venus.15N192	venus	M	3.84	−77.26	Ladrilleros	21.76	62 261 073.00	369.00	45.09	0.05	95.52
venus.15N193	venus	F	3.84	−77.26	Ladrilleros	23.12	62 937 709.00	378.00	44.91	0.05	95.74
venus.15N195	venus	M	3.84	−77.26	Ladrilleros	19.38	58 507 570.00	372.00	45.03	0.05	95.63
venus4536	venus	F	3.94	−77.36	Ladrilleros	13.81	32 597 998.00	338.00	45.17	0.05	96.81
venus4545	venus	M	3.94	−77.36	Ladrilleros	11.64	27 861 528.00	344.00	45.07	0.05	96.82
venus4549	venus	F	3.94	−77.36	Ladrilleros	15.09	34 460 696.00	338.00	45.02	0.05	96.75
venus4553	venus	F	3.94	−77.36	Ladrilleros	14.96	35 169 951.00	323.00	45.15	0.05	97.01
venus4576	venus	F	3.94	−77.36	Ladrilleros	14.11	32 424 685.00	325.00	44.99	0.05	96.32
venus4577	venus	F	3.94	−77.36	Ladrilleros	11.66	26 924 814.00	328.00	44.95	0.05	96.70
venus.CS265	venus	F	3.96	−77.37	Ladrilleros	7.35	16 421 844.00	210.00	45.39	0.05	97.82
venus.CS274	venus	M	3.96	−77.37	Ladrilleros	6.54	14 962 927.00	207.00	45.26	0.05	97.27
venus.CS275	venus	M	3.94	−77.37	Ladrilleros	5.81	13 763 117.00	190.00	45.48	0.05	98.27
venus.CS285	venus	M	3.94	−77.37	Ladrilleros	6.20	14 849 369.00	211.00	45.32	0.05	97.60
venus.CS287	venus	M	3.94	−77.37	Ladrilleros	6.47	14 402 800.00	196.00	45.46	0.05	97.91
venus.CS289	venus	M	3.94	−77.37	Ladrilleros	6.99	16 756 826.00	206.00	45.52	0.05	97.96
venus.CS460	venus	F	3.94	−77.37	Ladrilleros	6.39	14 217 907.00	191.00	45.47	0.05	98.05
venus.CS47	venus	F	3.94	−77.37	Ladrilleros	5.53	12 798 587.00	205.00	45.27	0.05	97.46
venus.CS627	venus	M	3.94	−77.37	Ladrilleros	6.28	14 918 780.00	209.00	44.87	0.05	97.86
venus.CS628	venus	M	3.94	−77.37	Ladrilleros	5.69	13 884 758.00	445.00	44.94	0.05	94.56
venus3656	venus	M	3.53	−76.75	La Elsa	36.65	127 887 921.00	201.00	44.41	0.04	94.50
venus3357	venus	F	3.53	−76.75	La Elsa	8.61	18 875 246.00	201.00	45.09	0.05	97.99
venus3659	venus	M	3.53	−76.75	La Elsa	38.44	139 086 417.00	210.00	44.63	0.04	93.98
venus3356	venus	M	3.50	−76.76	La Elsa	7.81	17 789 476.00	190.00	45.18	0.05	97.38
venus3130	venus	M	3.50	−76.76	La Elsa	6.85	15 518 464.00	195.00	45.18	0.05	97.95
venus.15N111	venus	M	3.53	−76.75	La Elsa	19.55	58 985 637.00	367.00	44.97	0.05	95.70
venus3350	venus	M	3.50	−76.76	La Elsa	7.84	18 477 473.00	201.00	45.15	0.05	98.13
venus3348	venus	M	3.50	−76.76	La Elsa	9.01	21 138 491.00	202.00	45.10	0.05	97.33
venus.15N113	venus	F	3.53	−76.75	La Elsa	19.55	54 589 430.00	376.00	44.79	0.05	95.09
venus.15N120	venus	F	3.53	−76.75	La Elsa	25.97	69 527 080.00	385.00	44.76	0.05	95.55
venus.15N121	venus	M	3.53	−76.75	La Elsa	24.56	72 977 016.00	369.00	44.95	0.05	95.70
venus3654	venus	M	3.53	−76.75	La Elsa	34.91	125 338 775.00	200.00	44.46	0.04	94.74
venus3657	venus	M	3.53	−76.75	La Elsa	53.29	182 143 876.00	184.00	44.27	0.04	94.62
venus3128	venus	M	3.50	−76.76	La Elsa	9.18	19 301 315.00	195.00	45.18	0.05	98.13
venus3655	venus	F	3.53	−76.75	La Elsa	43.84	150 437 126.00	212.00	44.41	0.04	94.24
venus3351	venus	F	3.50	−76.76	La Elsa	8.33	18 525 520.00	209.00	45.14	0.05	97.94
venus3349	venus	M	3.50	−76.76	La Elsa	7.98	17 340 335.00	204.00	45.05	0.05	97.85
venus.15N112	venus	M	3.53	−76.75	La Elsa	19.16	54 970 956.00	373.00	45.06	0.05	95.60
venus3352	venus	M	3.50	−76.76	La Elsa	7.29	16 853 792.00	204.00	45.15	0.05	97.36
venus4860	venus	M	3.90	−76.69	R. Calima	22.05	61 380 928.00	289.00	45.05	0.05	83.77
venus4873	venus	M	3.90	−76.69	R. Calima	18.26	45 029 935.00	298.00	44.87	0.05	96.40
venus4869	venus	M	3.90	−76.69	R. Calima	20.28	50 235 514.00	293.00	44.98	0.05	96.07
venus4870	venus	M	3.90	−76.69	R. Calima	17.25	42 895 434.00	293.00	45.23	0.05	96.60
cyrbia.CAM040686	cyrbia	F	0.21	−78.96	Tortugo	5.95	13 549 168.00	214.00	45.71	0.05	98.05
cyrbia.CAM040841	cyrbia	M	0.85	−79.80	Tonsupa	4.05	10 017 962.00	177.00	46.62	0.05	98.02
cyrbia.CAM040744	cyrbia	F	0.11	−79.23	PuertoQuito	7.54	18 677 977.00	192.00	46.70	0.05	98.58
cyrbia.CAM040749	cyrbia	M	0.11	−79.23	PuertoQuito	6.41	15 568 439.00	202.00	46.00	0.05	98.11
cyrbia.14N014	cyrbia	M	0.18	−78.85	Mashpi	20.62	61 334 737.00	373.00	44.83	0.05	95.27
cyrbia004	cyrbia	M	−3.73	−79.84	Balsas	37.11	116 067 730.00	190.00	43.56	0.04	95.46
cyrbia.CAM040934	cyrbia	M	−0.06	−78.79	Mindo	7.02	16 789 245.00	205.00	46.04	0.05	98.40
cyrbia.CAM040321	cyrbia	M	−0.05	−78.77	Mindo	8.95	21 760 426.00	220.00	45.85	0.05	97.93
cyrbia.CAM040748	cyrbia	F	0.11	−79.23	PuertoQuito	4.98	11 496 309.00	199.00	45.95	0.05	98.12
cyrbia.CAM040371	cyrbia	M	0.21	−78.94	Tortugo	6.98	16 941 367.00	236.00	45.65	0.05	97.42
cyrbia.CAM040745	cyrbia	M	0.11	−79.23	PuertoQuito	6.42	15 742 837.00	203.00	46.09	0.05	98.16
cyrbia.CAM040847	cyrbia	M	0.85	−79.80	Tonsupa	5.44	13 954 602.00	177.00	46.89	0.05	98.87
cyrbia.C40861	cyrbia	M	0.85	−79.80	Tonsupa	23.92	58 974 959.00	273.00	45.10	0.05	96.84
cyrbia.CAM040957	cyrbia	F	−0.05	−78.79	Mindo	6.37	16 119 221.00	201.00	46.24	0.05	98.43
cyrbia026	cyrbia	M	−3.73	−79.84	Balsas	9.67	30 271 600.00	177.00	43.32	0.04	95.80
cyrbia.C40853	cyrbia	M	0.85	−79.80	Tonsupa	23.38	56 554 177.00	256.00	45.07	0.05	96.96
cyrbia.CAM040839	cyrbia	M	0.85	−79.80	Tonsupa	4.16	10 192 449.00	181.00	46.86	0.05	98.86
cyrbia.15N016	cyrbia	M	0.18	−78.91	Mashpi	21.90	64 346 486.00	375.00	44.87	0.05	95.60
cyrbia.CAM040754	cyrbia	M	0.11	−79.23	PuertoQuito	1.08	2 667 410.00	162.00	47.27	0.05	95.88
cyrbia.CAM040751	cyrbia	M	0.11	−79.23	PuertoQuito	10.61	26 194 855.00	201.00	46.07	0.05	98.37
cyrbia.CAM040679	cyrbia	M	0.21	−78.96	Tortugo	5.87	14 575 368.00	192.00	46.16	0.05	98.48
cyrbia.15N017	cyrbia	F	0.18	−78.91	Mashpi	21.59	61 995 084.00	378.00	44.68	0.05	95.48
cyrbia.C40842	cyrbia	M	0.85	−79.80	Tonsupa	21.80	53 817 435.00	253.00	45.01	0.05	97.25
cyrbia.CAM040361	cyrbia	F	−0.05	−78.77	Mindo	8.89	19 268 812.00	242.00	45.46	0.05	97.41
cyrbia.CAM040357	cyrbia	M	0.21	−78.95	Tortugo	5.05	12 508 731.00	209.00	46.10	0.05	98.22

Individual	Race	Sex	Lat.	Lon.	Locality	M. cov.	No. reads	Insert	Map Q.	Err.	% align
cyrbia.CAM040856	cyrbia	M	0.85	−79.80	Tonsupa	7.78	18 872 806.00	186.00	45.99	0.05	98.46
cyrbia.CAM040674	cyrbia	M	0.21	−78.95	Tortugo	5.65	13 495 378.00	204.00	45.85	0.05	98.29
cyrbia.CAM040971	cyrbia	M	−0.05	−78.79	Mindo	5.55	13 077 680.00	185.00	46.22	0.05	98.68
cyrbia.CAM040698	cyrbia	M	0.21	−78.95	Tortugo	7.05	16 546 637.00	191.00	46.27	0.05	98.40
cyrbia.C40578	cyrbia	M	0.16	−78.76	Tortugo	22.21	56 236 060.00	271.00	44.91	0.05	97.07
cyrbia.C40854	cyrbia	M	0.85	−79.80	Tonsupa	21.70	52 903 020.00	255.00	45.24	0.05	97.27
cyrbia.C40836	cyrbia	M	0.85	−79.80	Tonsupa	20.36	50 541 949.00	275.00	45.12	0.05	97.05
cyrbia.CAM040449	cyrbia	F	0.21	−78.95	Tortugo	6.14	13 974 814.00	202.00	45.78	0.05	98.22
cyrbia.CAM040403	cyrbia	M	0.14	−78.76	Pacto	6.16	14 793 300.00	231.00	45.70	0.05	97.50
cyrbia005	cyrbia	M	−3.73	−79.84	Balsas	36.27	106 360 950.00	189.00	43.64	0.04	95.52
cyrbia023	cyrbia	M	−3.73	−79.84	Balsas	29.82	106 071 776.00	200.00	44.17	0.04	95.33
cyrbia024	cyrbia	M	−3.73	−79.84	Balsas	31.89	104 631 962.00	182.00	43.76	0.04	95.73
cyrbia.C40545	cyrbia	M	0.16	−78.76	Pacto	21.82	53 115 782.00	264.00	44.97	0.05	97.11
cyrbia.C40584	cyrbia	M	0.16	−78.76	Pacto	22.01	55 315 035.00	262.00	44.95	0.05	97.11
cyrbia.C40594	cyrbia	M	0.17	−78.76	Pacto	20.62	50 445 428.00	261.00	44.98	0.05	97.15
cyrbia.C40673	cyrbia	M	0.21	−78.95	Tortugo	22.95	58 161 375.00	244.00	45.20	0.05	97.40
cyrbia.C40678	cyrbia	M	0.21	−78.95	Tortugo	21.03	51 094 180.00	274.00	44.98	0.05	97.03
cyrbia.C40692	cyrbia	M	0.21	−78.95	Tortugo	21.90	54 689 833.00	270.00	45.00	0.05	97.12
cyrbia.C40695	cyrbia	M	0.21	−78.95	Tortugo	23.75	58 238 141.00	268.00	44.78	0.05	96.28
cyrbia.C40697	cyrbia	M	0.21	−78.95	Tortugo	19.72	46 919 793.00	271.00	45.07	0.05	97.01
cyrbia.C40743	cyrbia	M	0.11	−79.23	PuertoQuito	20.81	51 485 710.00	259.00	45.04	0.05	97.28
cyrbia.C40758	cyrbia	M	0.11	−79.23	PuertoQuito	17.92	46 662 987.00	263.00	45.10	0.05	97.16
cyrbia.C40834	cyrbia	F	0.85	−79.80	Tonsupa	23.20	53 041 646.00	274.00	45.00	0.05	96.95
cyrbia.C40835	cyrbia	F	0.85	−79.80	Tonsupa	25.17	59 075 556.00	255.00	44.99	0.05	96.90
cyrbia.C40850	cyrbia	F	0.85	−79.80	Tonsupa	23.65	56 025 793.00	271.00	44.94	0.05	97.01
cyrbia.C40852	cyrbia	F	0.85	−79.80	Tonsupa	22.83	53 513 391.00	278.00	45.00	0.05	96.62
cyrbia.C40858	cyrbia	M	0.85	−79.80	Tonsupa	19.74	49 420 648.00	269.00	45.10	0.05	96.96
cyrbia.C40860	cyrbia	M	0.85	−79.80	Tonsupa	22.79	54 877 023.00	277.00	44.94	0.05	95.86
cyrbia.C40952	cyrbia	F	−0.05	−78.79	Mindo	25.15	57 817 167.00	283.00	44.81	0.05	96.82
cyrbia.CAM040354	cyrbia	M	0.21	−78.95	Tortugo	9.23	22 666 116.00	224.00	45.87	0.05	97.78
cyrbia.CAM040355	cyrbia	M	0.21	−78.95	Tortugo	6.84	17 162 309.00	234.00	45.64	0.05	97.57
cyrbia.CAM040356	cyrbia	M	0.21	−78.95	Tortugo	4.21	9 903 226.00	191.00	45.88	0.05	98.65
cyrbia.CAM040358	cyrbia	M	0.21	−78.95	Tortugo	5.28	13 547 412.00	207.00	45.84	0.05	95.54
cyrbia.CAM040362	cyrbia	M	0.14	−78.76	Pacto	6.57	16 416 769.00	235.00	45.71	0.05	97.72
cyrbia.CAM040363	cyrbia	M	0.14	−78.76	Pacto	7.60	18 525 432.00	229.00	45.57	0.05	97.46
cyrbia.CAM040364	cyrbia	M	0.14	−78.76	Pacto	6.62	15 858 751.00	233.00	45.67	0.05	97.72
cyrbia.CAM040365	cyrbia	M	0.14	−78.76	Pacto	8.45	20 786 177.00	233.00	45.57	0.05	97.48
cyrbia.CAM040366	cyrbia	M	0.14	−78.76	Pacto	6.48	15 640 647.00	238.00	45.61	0.05	97.72
cyrbia.CAM040367	cyrbia	M	0.15	−78.75	Pacto	6.47	16 234 742.00	233.00	45.85	0.05	97.82
cyrbia.CAM040372	cyrbia	M	0.21	−78.94	Tortugo	6.58	16 607 840.00	228.00	45.79	0.05	97.71
cyrbia.CAM040373	cyrbia	M	0.21	−78.94	Tortugo	7.24	17 256 943.00	214.00	46.03	0.05	97.84
cyrbia.CAM040374	cyrbia	M	0.21	−78.94	Tortugo	8.03	20 161 236.00	237.00	45.71	0.05	97.58
cyrbia.CAM040375	cyrbia	M	0.21	−78.95	Tortugo	6.74	16 836 481.00	230.00	45.77	0.05	97.74
cyrbia.CAM040376	cyrbia	M	0.21	−78.95	Tortugo	5.95	14 095 647.00	227.00	45.67	0.05	97.84
cyrbia.CAM040380	cyrbia	M	0.21	−78.95	Tortugo	7.16	17 557 868.00	226.00	45.54	0.05	97.66
cyrbia.CAM040381	cyrbia	M	0.21	−78.94	Tortugo	6.60	16 593 952.00	243.00	45.73	0.05	97.50
cyrbia.CAM040404	cyrbia	M	0.15	−78.76	Pacto	8.05	20 179 978.00	234.00	45.66	0.05	97.59
cyrbia.CAM040406	cyrbia	M	0.14	−78.76	Pacto	7.60	19 066 796.00	233.00	45.81	0.05	97.61
cyrbia.CAM040411	cyrbia	F	0.15	−78.76	Pacto	7.35	17 657 617.00	243.00	45.52	0.05	97.02
cyrbia.CAM040412	cyrbia	F	0.21	−78.95	Tortugo	6.67	14 979 633.00	225.00	45.57	0.05	97.75
cyrbia.CAM040413	cyrbia	F	0.14	−78.76	Pacto	7.89	19 437 622.00	228.00	45.83	0.05	97.69
cyrbia.CAM040416	cyrbia	F	0.21	−78.95	Tortugo	6.17	17 055 056.00	235.00	45.20	0.05	76.82
cyrbia.CAM040445	cyrbia	F	0.21	−78.95	Tortugo	7.20	17 246 284.00	197.00	45.63	0.05	97.48
cyrbia.CAM040523	cyrbia	M	0.14	−78.67	Nanegal	6.69	16 069 374.00	204.00	46.03	0.05	98.33
cyrbia.CAM040524	cyrbia	M	0.14	−78.67	Nanegal	5.30	13 011 557.00	205.00	45.93	0.05	98.21
cyrbia.CAM040565	cyrbia	M	0.16	−78.76	Pacto	6.23	15 273 580.00	215.00	45.11	0.05	97.70
cyrbia.CAM040684	cyrbia	M	0.21	−78.96	Tortugo	5.34	12 478 503.00	192.00	45.83	0.05	98.51
cyrbia.CAM040690	cyrbia	F	0.21	−78.95	Tortugo	5.24	11 567 548.00	202.00	45.64	0.05	98.29
cyrbia.CAM040693	cyrbia	M	0.21	−78.95	Tortugo	2.69	6 566 412.00	195.00	46.40	0.05	98.55
cyrbia.CAM040696	cyrbia	M	0.21	−78.95	Tortugo	3.43	8 341 681.00	202.00	44.91	0.05	98.26
cyrbia.CAM040742	cyrbia	M	0.11	−79.23	PuertoQuito	4.39	10 578 713.00	178.00	46.26	0.05	98.75
cyrbia.CAM040746	cyrbia	F	0.11	−79.23	PuertoQuito	7.78	17 715 180.00	197.00	46.02	0.05	98.25
cyrbia.CAM040747	cyrbia	F	0.11	−79.23	PuertoQuito	4.65	10 827 339.00	198.00	45.79	0.05	97.87
cyrbia.CAM040750	cyrbia	M	0.11	−79.23	PuertoQuito	5.89	14 702 774.00	199.00	46.06	0.05	98.43
cyrbia.CAM040752	cyrbia	M	0.11	−79.23	PuertoQuito	11.66	29 325 172.00	205.00	46.19	0.05	98.17
cyrbia.CAM040753	cyrbia	M	0.11	−79.23	PuertoQuito	4.69	11 551 293.00	194.00	45.75	0.05	98.12
cyrbia.CAM040757	cyrbia	M	0.11	−79.23	PuertoQuito	6.38	15 398 568.00	211.00	45.89	0.05	97.94
cyrbia.CAM040759	cyrbia	M	0.11	−79.23	PuertoQuito	7.48	18 136 807.00	206.00	46.07	0.05	98.09
cyrbia.CAM040833	cyrbia	M	0.85	−79.80	Tonsupa	7.08	17 336 451.00	204.00	45.86	0.05	98.10
cyrbia.CAM040838	cyrbia	M	0.85	−79.80	Tonsupa	7.46	17 693 255.00	206.00	45.87	0.05	97.92
cyrbia.CAM040840	cyrbia	F	0.85	−79.80	Tonsupa	5.89	14 017 191.00	177.00	46.25	0.05	98.19
cyrbia.CAM040848	cyrbia	M	0.85	−79.80	Tonsupa	6.62	16 615 924.00	207.00	45.91	0.05	98.15
cyrbia.CAM040851	cyrbia	M	0.85	−79.80	Tonsupa	5.41	13 394 127.00	191.00	46.33	0.05	98.11
cyrbia.CAM040855	cyrbia	M	0.85	−79.80	Tonsupa	4.06	10 040 450.00	184.00	45.93	0.05	98.01
cyrbia.CAM040933	cyrbia	F	−0.06	−78.79	Mindo	6.09	14 556 508.00	195.00	46.28	0.05	98.51
cyrbia.CAM040935	cyrbia	M	−0.06	−78.79	Mindo	6.81	16 964 650.00	197.00	46.25	0.05	98.45
cyrbia.CAM040936	cyrbia	M	−0.06	−78.79	Mindo	7.54	17 383 022.00	192.00	46.04	0.05	98.42
cyrbia.CAM040972	cyrbia	M	−0.05	−78.79	Mindo	5.75	14 904 563.00	194.00	46.19	0.05	98.56
cyrbia.CAM040986	cyrbia	M	−0.05	−78.79	Mindo	3.80	9 026 673.00	182.00	45.87	0.05	98.66

Individual	Race	Sex	Lat.	Lon.	Locality	M. cov.	No. reads	Insert	Map Q.	Err.	% align
H. melpomene											
carosina.CS4169	ca-rosina	M	5.77	−74.24	Otanche	36.44	40 232 181.00	306.00	45.40	0.03	96.83
carosina.CS4201	ca-rosina	F	5.78	−74.30	Otanche	47.74	46 691 022.00	272.00	44.88	0.03	97.21
carosina.CS4228	ca-rosina	F	5.78	−74.30	Otanche	51.04	43 269 482.00	274.00	45.01	0.03	97.74
martinae4190	martinae	M	5.74	−74.23	Otanche	39.00	33 603 889.00	342.00	45.50	0.03	97.87
martinae4191	martinae	M	5.78	−74.30	Otanche	29.49	26 034 447.00	282.00	45.39	0.03	97.84
martinae4195	martinae	M	5.66	−74.18	Otanche	28.25	27 577 099.00	362.00	45.59	0.03	97.93
martinae4197	martinae	M	5.66	−74.18	Otanche	30.41	34 102 020.00	353.00	45.42	0.03	97.90
martinae4202	martinae	M	5.78	−74.30	Otanche	41.67	32 038 777.00	342.00	45.61	0.03	97.34
martinae4205	martinae	M	5.66	−74.18	Otanche	37.71	32 261 644.00	291.00	45.26	0.03	98.02
martinae4217	martinae	M	5.78	−74.29	Otanche	28.77	28 537 936.00	285.00	45.51	0.04	97.53
martinae.CS1239	martinae	M	5.04	−74.58	Guaduas	58.38	69 829 826.00	306.00	44.81	0.04	96.80
martinae.CS1240	martinae	M	5.04	−74.58	Guaduas	46.66	59 378 848.00	281.00	45.22	0.04	96.69
martinae.CS2945	martinae	M	5.05	−74.38	Guaduas	56.53	67 460 136.00	295.00	44.71	0.04	94.69
martiXcaros4170	martinaeXca-rosina	M	5.77	−74.24	Otanche	234.32	204 425 794.00	338.00	45.30	0.03	97.50
martiXcaros4229	martinaeXca-rosina	M	5.78	−74.30	Otanche	32.21	25 275 923.00	328.00	45.49	0.03	97.84
martinae4218	martinae	F	5.78	−74.30	Otanche	44.83	35 853 979.00	338.00	42.88	0.04	90.21
ros2059	rosina	M	9.11	−79.69	Panama	49.99	54 533 229.00	330.00	46.10	0.03	97.25
ros2045	rosina	M	9.11	−79.69	Panama	53.47	48 239 551.00	349.00	45.93	0.03	97.29
ros1880	rosina	M	9.08	−79.66	Panama	81.78	63 966 239.00	247.00	45.55	0.03	98.35
ros2552	rosina	M	9.01	−79.55	Panama	86.31	53 211 009.00	255.00	45.23	0.03	91.81
ros1841	rosina	M	9.08	−79.66	Panama	70.55	57 318 110.00	255.00	45.74	0.03	98.36
ros533	rosina	M	9.11	−79.69	Panama	62.89	81 749 063.00	134.00	43.99	0.03	96.34
ros531	rosina	M	9.11	−79.69	Panama	66.73	81 361 287.00	144.00	43.90	0.03	97.06
ros2519	rosina	M	9.01	−79.55	Panama	50.69	60 290 306.00	337.00	45.99	0.03	95.76
ros546	rosina	M	9.13	−79.69	Panama	70.22	80 459 050.00	137.00	44.00	0.03	96.91
ros2071	rosina	M	9.11	−79.69	Panama	89.47	110 516 437.00	149.00	44.19	0.03	98.06
melpXros18120	melpomeneXrosina	M	8.16	−77.69	Darien	41.47	62 610 169.00	374.00	45.70	0.03	96.99
melpXros18102	melpomeneXrosina	M	8.02	−77.73	Darien	48.68	63 575 328.00	384.00	45.42	0.03	96.44
melpXros18191	melpomeneXrosina	M	8.39	−77.84	Darien	48.59	66 282 171.00	383.00	45.67	0.03	97.23
melpomene.15N353	melpomene	M	7.53	−78.17	Jaque	35.61	59 824 561.00	388.00	45.76	0.03	96.94
melpomene18055	melpomene	M	8.61	−78.14	Darien	38.01	61 745 036.00	377.00	45.77	0.03	97.23
melpomene18160	melpomene	M	8.28	−77.81	Darien	45.77	64 286 334.00	378.00	45.51	0.03	96.97
melpomene18093	melpomene	M	8.28	−77.81	Darien	45.11	63 486 936.00	374.00	45.53	0.03	96.90
melpomene18005	melpomene	M	8.61	−78.14	Darien	41.67	62 871 046.00	377.00	45.49	0.03	97.28
melpomene18014	melpomene	M	8.61	−78.14	Darien	42.74	52 838 087.00	382.00	45.68	0.03	96.95
melpomene18085	melpomene	M	8.61	−78.14	Darien	41.50	62 311 472.00	362.00	45.76	0.03	97.21
melpomene18193	melpomene	M	8.28	−77.81	Darien	43.42	62 716 295.00	372.00	45.60	0.03	96.72
vulcXros.15N354	vulcanusXrosina	F	7.53	−78.17	Jaque	38.05	57 793 209.00	384.00	45.24	0.03	96.87
vulcXros18192	vulcanusXrosina	F	8.39	−77.84	Darien	52.79	70 087 797.00	382.00	44.91	0.03	97.07
vulcXros.15N443	vulcanusXrosina	M	7.50	−78.14	Jaque	42.49	56 441 024.00	385.00	45.48	0.03	97.07
vulcXmel.15N421	vulcanusXmelpomene	M	7.53	−78.17	Jaque	40.83	60 374 990.00	383.00	45.77	0.03	97.09
vulcXmel.15N355	vulcanusXmelpomene	M	7.53	−78.17	Jaque	38.04	59 118 711.00	383.00	45.43	0.03	97.35
vulcXmel18195	vulcanusXmelpomene	M	8.28	−77.81	Darien	47.70	53 568 061.00	329.00	45.45	0.03	97.80
vulcXmel.15N387	vulcanusXmelpomene	M	7.55	−78.15	Jaque	40.65	50 145 484.00	382.00	45.76	0.03	97.05
vulcXmel.15N338	vulcanusXmelpomene	M	7.49	−78.13	Jaque	44.78	57 878 961.00	382.00	45.64	0.03	97.07
vulcXmel.15N328	vulcanusXmelpomene	M	7.49	−78.13	Jaque	46.01	60 934 018.00	387.00	45.44	0.03	96.92
vulcXmel.15N420	vulcanusXmelpomene	M	7.53	−78.17	Jaque	39.71	52 882 795.00	392.00	45.52	0.03	97.11
vulcXmel.16N072	vulcanusXmelpomene	M	6.39	−77.40	B. Solano	79.70	67 895 036.00	291.00	45.55	0.04	97.51
vulcanus.15N435	vulcanus	M	7.53	−78.17	Jaque	39.43	58 699 821.00	378.00	45.47	0.03	97.09
vulcanus.16N020	vulcanus	M	6.39	−77.39	B. Solano	62.20	62 974 900.00	321.00	45.30	0.03	97.66
vulcanus.16N047	vulcanus	M	6.39	−77.38	B. Solano	60.87	60 800 373.00	320.00	45.72	0.04	97.53
vulcanus.16N080	vulcanus	F	6.39	−77.40	B. Solano	58.54	49 334 883.00	334.00	44.68	0.04	97.15
vulcanus.16N077	vulcanus	M	6.39	−77.40	B. Solano	48.70	55 295 722.00	300.00	45.35	0.03	97.85
vulcanus.16N048	vulcanus	M	6.39	−77.38	B. Solano	44.96	54 790 345.00	318.00	45.52	0.03	97.77
vulcanus.16N078	vulcanus	M	6.39	−77.40	B. Solano	50.09	59 858 105.00	314.00	45.30	0.03	97.52
vulcanus.16N093	vulcanus	M	6.35	−77.37	B. Solano	46.27	51 541 713.00	317.00	45.49	0.03	97.75
vulcanus.16N091	vulcanus	M	6.35	−77.37	B. Solano	48.89	57 816 309.00	336.00	45.56	0.03	97.57
vulcanus.16N068	vulcanus	M	6.39	−77.40	B. Solano	62.19	67 502 531.00	317.00	45.36	0.03	96.65
vulcanus.15N281	vulcanus	M	5.57	−77.50	Amargal	51.75	55 065 251.00	363.00	45.51	0.03	95.98
vulcanus.15N299	vulcanus	M	5.57	−77.50	Amargal	48.34	55 951 920.00	388.00	45.69	0.03	96.98
vulcanus.15N306	vulcanus	M	5.57	−77.50	Amargal	69.31	59 358 828.00	322.00	45.22	0.03	97.51
vulcanus.15N260	vulcanus	M	5.57	−77.50	Amargal	38.74	55 450 800.00	381.00	45.44	0.03	97.00
vulcanus.15N240	vulcanus	M	5.57	−77.50	Amargal	37.10	56 964 679.00	385.00	45.45	0.03	96.51
vulcanus.CS2278	vulcanus	M	3.94	−77.37	Ladrilleros	21.05	16 272 133.00	218.00	45.18	0.03	97.83
vulcanus.CS636	vulcanus	M	3.94	−77.37	Ladrilleros	17.96	17 278 198.00	208.00	45.12	0.03	92.58
vulcanus.CS648	vulcanus	M	3.94	−77.37	Ladrilleros	16.32	17 345 373.00	213.00	45.07	0.03	98.36
vulcanus.CS1001	vulcanus	M	3.83	−76.79	Ladrilleros	13.90	15 684 616.00	219.00	45.33	0.03	98.39
vulcanus.CS647	vulcanus	M	3.94	−77.37	Ladrilleros	15.20	16 004 757.00	202.00	45.24	0.03	98.40
vulcanus.15N152	vulcanus	M	3.58	−76.86	La Elsa	43.34	59 477 950.00	387.00	45.23	0.03	95.68
vulcanus.15N153	vulcanus	M	3.58	−76.86	La Elsa	37.97	65 855 964.00	378.00	45.40	0.03	96.92
vulcanus.15N151	vulcanus	M	3.58	−76.86	La Elsa	41.02	55 042 995.00	384.00	45.35	0.03	97.04
vulcanus.15N123	vulcanus	M	3.53	−76.75	La Elsa	35.35	58 563 595.00	387.00	45.48	0.03	95.90
vulcanus.15N156	vulcanus	M	3.58	−76.86	La Elsa	52.27	65 675 426.00	300.00	45.47	0.03	97.62
vulcanus.15N143	vulcanus	M	3.58	−76.86	La Elsa	40.60	61 739 009.00	388.00	45.56	0.03	97.04
vulcanus.15N144	vulcanus	M	3.58	−76.86	La Elsa	49.41	61 957 081.00	385.00	45.58	0.03	96.36
vulcanus.15N110	vulcanus	M	3.53	−76.75	La Elsa	48.33	58 958 512.00	385.00	45.50	0.03	96.69
vulcanus.15N154	vulcanus	M	3.58	−76.86	La Elsa	41.17	60 729 800.00	381.00	45.39	0.03	96.91
vulcanus.CS748	vulcanus	F	3.88	−76.59	R. Calima	12.01	12 480 103.00	149.00	35.26	0.06	82.16

Individual	Race	Sex	Lat.	Lon.	Locality	M. cov.	No. reads	Insert	Map Q.	Err.	% align
vulcanus.CS457	vulcanus	M	3.94	−77.37	Ladrilleros	0.48	24 007 038.00	19	33.52	0.03	7.05
vulcanus.CS749	vulcanus	M	3.88	−76.59	R. Calima	3.46	17 509 910.00	20	24.25	0.01	30.56
vulcanus.CS3621	vulcanus	M	3.88	−76.59	R. Calima	14.53	15 866 243.00	214.00	44.99	0.03	93.36
vulcanus.CS3622	vulcanus	M	3.88	−76.59	R. Calima	0.67	22 959 367.00	19	33.00	0.02	5.23
vulcanus.CS3614	vulcanus	M	3.88	−76.59	R. Calima	17.50	16 946 505.00	212.00	45.03	0.03	98.18
vulcanus.CS3617	vulcanus	M	3.88	−76.59	R. Calima	15.97	16 960 183.00	209.00	45.06	0.03	98.52
vulcanus.15N133	vulcanus	M	3.88	−76.59	R. Calima	42.56	65 746 209.00	382.00	45.32	0.03	97.10
vulcanus.15N172	vulcanus	M	3.88	−76.59	R. Calima	41.81	57 988 802.00	383.00	45.61	0.03	96.18
vulcanus.CS3601	vulcanus	F	3.88	−76.59	R. Calima	15.66	17 283 151.00	213.00	44.43	0.03	98.53
vulcanus.CS3603	vulcanus	M	3.88	−76.59	R. Calima	16.18	17 168 094.00	210.00	45.18	0.03	98.42
vulcanus.CS3605	vulcanus	M	3.88	−76.59	R. Calima	14.20	16 410 200.00	210.00	45.05	0.03	95.07
vulcanus.CS3606	vulcanus	M	3.88	−76.59	R. Calima	19.31	16 679 744.00	210.00	45.25	0.03	98.33
vulcanus.CS3612	vulcanus	M	3.88	−76.59	R. Calima	14.18	14 481 624.00	205.00	45.04	0.03	98.14
vulcanus.CS3615	vulcanus	M	3.88	−76.59	R. Calima	19.52	18 281 738.00	214.00	45.03	0.03	98.20
vulcanus.CS3616	vulcanus	M	3.88	−76.59	R. Calima	16.58	16 133 163.00	204.00	45.24	0.03	97.38
vulcanus.CS3618	vulcanus	M	3.88	−76.59	R. Calima	13.45	15 877 882.00	208.00	45.12	0.03	90.05
cythera.CAM040631	cythera	F	0.18	−78.85	Mashpi	17.05	12 955 160.00	201.00	43.80	0.03	98.26
cythera.CAM040944	cythera	F	−0.06	−78.79	Mindo	19.58	19 225 544.00	229.00	43.84	0.03	98.30
cythera.CAM040383	cythera	F	0.21	−78.94	Tortugo	13.39	13 689 468.00	200.00	44.14	0.03	98.03
cythera.CAM040652	cythera	M	0.21	−78.96	Tortugo	13.11	14 873 886.00	205.00	44.82	0.03	98.64
cythera.CAM040682	cythera	F	0.21	−78.96	Tortugo	16.20	16 577 485.00	215.00	43.72	0.03	98.49
cythera.CAM040680	cythera	M	0.21	−78.96	Tortugo	13.24	12 262 157.00	201.00	44.48	0.03	98.44
cyth.15N038	cythera	M	0.18	−78.91	Mashpi	82.41	80 120 282.00	311.00	45.22	0.04	97.61
cyth.14N004	cythera	M	0.18	−78.85	Mashpi	40.79	59 518 407.00	380.00	45.19	0.03	96.92
cyth.14N009	cythera	M	0.18	−78.85	Mashpi	38.91	58 228 850.00	364.00	45.12	0.03	96.36
cyth.14N015	cythera	M	0.18	−78.85	Mashpi	42.09	63 146 721.00	377.00	45.14	0.03	96.98
cyth.14N023	cythera	M	0.18	−78.85	Mashpi	34.85	62 509 754.00	372.00	45.25	0.03	97.17
cyth.14N037	cythera	M	0.22	−78.89	Guayllabamba	49.94	58 640 445.00	382.00	45.33	0.03	96.77
cyth.14N038	cythera	M	0.22	−78.89	Guayllabamba	43.59	64 905 082.00	378.00	45.18	0.03	96.99
cyth.14N039	cythera	M	0.22	−78.89	Guayllabamba	43.60	66 599 583.00	389.00	45.11	0.03	97.17
cyth.14N043	cythera	M	0.22	−78.89	Guayllabamba	41.97	54 055 344.00	381.00	45.20	0.03	96.45
cyth.14N044	cythera	M	0.22	−78.89	Guayllabamba	33.31	50 166 858.00	370.00	45.15	0.03	96.44
cyth.14N045	cythera	M	0.22	−78.89	Guayllabamba	59.73	59 818 030.00	333.00	45.04	0.04	97.31
cyth.14N506	cythera	F	0.22	−78.89	Guayllabamba	59.18	63 512 708.00	328.00	44.74	0.04	97.61
cyth.14N507	cythera	F	0.22	−78.89	Guayllabamba	67.42	58 723 431.00	323.00	45.11	0.04	97.53
cyth.15N020	cythera	M	0.22	−78.89	Guayllabamba	56.60	54 139 790.00	336.00	44.76	0.04	97.30
cyth.BV19	cythera	F	−3.73	−79.84	Balsas	63.36	61 923 953.00	318.00	44.65	0.04	97.76
cyth.BV20	cythera	F	−3.73	−79.84	Balsas	60.78	58 641 607.00	322.00	44.71	0.04	97.66
cythera.CAM040382	cythera	M	0.21	−78.94	Tortugo	13.26	14 826 902.00	213.00	44.55	0.03	98.41
cythera.CAM040456	cythera	M	0.15	−78.76	Pacto	11.34	12 691 026.00	198.00	44.86	0.03	98.85
cythera.CAM040457	cythera	M	0.15	−78.76	Pacto	14.45	15 022 734.00	207.00	44.80	0.03	98.64
cythera.CAM040458	cythera	M	0.15	−78.76	Pacto	14.18	14 793 505.00	214.00	44.95	0.03	98.30
cythera.CAM040459	cythera	M	0.15	−78.76	Pacto	14.51	14 665 651.00	207.00	44.86	0.03	98.66
cythera.CAM040460	cythera	M	0.15	−78.76	Pacto	18.00	18 934 610.00	207.00	44.40	0.03	98.44
cythera.CAM040474	cythera	F	0.15	−78.76	Pacto	9.78	9 415 210.00	205.00	44.02	0.03	98.64
cythera.CAM040475	cythera	F	0.15	−78.76	Pacto	10.15	11 026 961.00	209.00	44.06	0.03	98.56
cythera.CAM040516	cythera	M	0.14	−78.67	Nanegal	14.47	13 261 276.00	213.00	44.91	0.03	98.30
cythera.CAM040517	cythera	M	0.14	−78.67	Nanegal	16.96	17 565 951.00	217.00	44.51	0.03	98.58
cythera.CAM040518	cythera	M	0.14	−78.67	Nanegal	13.18	14 500 753.00	211.00	44.77	0.03	98.65
cythera.CAM040519	cythera	M	0.14	−78.67	Nanegal	15.55	14 782 873.00	222.00	44.62	0.03	98.44
cythera.CAM040520	cythera	M	0.14	−78.67	Nanegal	13.85	15 016 851.00	206.00	44.55	0.03	98.59
cythera.CAM040521	cythera	M	0.14	−78.67	Nanegal	16.38	15 515 804.00	217.00	44.69	0.03	98.41
cythera.CAM040522	cythera	M	0.14	−78.67	Nanegal	12.70	13 687 747.00	210.00	44.71	0.03	98.37
cythera.CAM040528	cythera	M	0.14	−78.67	Nanegal	15.09	16 509 634.00	209.00	44.72	0.03	98.58
cythera.CAM040529	cythera	F	0.14	−78.67	Nanegal	12.58	14 559 956.00	207.00	43.96	0.03	98.66
cythera.CAM040535	cythera	M	0.16	−78.76	Pacto	18.36	18 080 680.00	210.00	44.34	0.03	98.31
cythera.CAM040536	cythera	M	0.16	−78.76	Pacto	15.00	15 503 586.00	220.00	44.58	0.03	98.45
cythera.CAM040564	cythera	M	0.16	−78.76	Pacto	12.27	15 487 502.00	216.00	44.53	0.03	98.59
cythera.CAM040621	cythera	F	0.18	−78.85	Mashpi	12.50	13 769 308.00	211.00	44.48	0.03	98.62
cythera.CAM040622	cythera	F	0.18	−78.85	Mashpi	17.16	13 763 497.00	201.00	43.64	0.03	98.44
cythera.CAM040630	cythera	F	0.18	−78.85	Mashpi	14.78	13 687 444.00	202.00	43.80	0.03	98.60
cythera.CAM040651	cythera	M	0.18	−78.85	Mashpi	12.85	14 192 099.00	204.00	44.76	0.03	98.61

4.3.6 Population structure analysis

We aimed to determine the genetic structure of the sampled populations of both *H. erato* and *H. melpomene* to both decide which individuals to include in the genetic association analysis and to account for population structure when doing such analysis to reduce inflation of the association statistics (Price et al., 2006).

We performed a genetic clustering and admixture analysis using Ngsadmix (Skotte et

al., 2013), which uses genotype likelihoods to calculate the fraction of each individual genome that can be assigned to an ancestral population among a pre-defined number of populations (K). Ngsadmix was run separately for *H. erato* and *H. melpomene* with values of K ranging from 2 to 10. Each run was replicated 10 times, each time with a different random seed, as suggested in the manual of the program. The most likely number of genetic clusters describing the variation in our samples was determined using the ΔK comparison criterion (Evanno et al., 2005) implemented in Clumpak (Kopelman et al., 2015).

We performed a principal component analysis (PCA) on genetic data using the single read sampling approach implemented in angsd. We used this specific procedure because it is more robust when samples are sequenced at low coverage or the coverage is not uniform across samples. This approach produces a genetic covariance matrix using an allele frequency estimator f_m for each site m based on single reads calculated as

$$f_m = \frac{N_{minor}}{N_{minor} + N_{major}}$$

where N_{minor} and N_{major} are the number of reads at the site m with minor and major alleles respectively. The entries of the covariance matrix are calculated using the expression

$$cov(ij) = \frac{1}{M} \sum_{m}^{M} \frac{(h_m^i - f_m)(h_m^j - f_m)}{f_m(1 - f_m)}$$

where M is the number of sites with reads for both individuals i and j. h_m^i is 1 if individual i has the major allele at site m and 0 otherwise. We then calculated the eigenvectors and eigenvalues of the covariance matrix to obtain the principal components of variation of genetic structure and the contribution of each principal component to the observed variance.

4.3.7 GWAS

We used the called SNPs as input for the association analysis. For our association analysis we used the GenABEL R package (Aulchenko et al., 2007). We checked the integrity and quality of SNP data using the `descriptives.marker` function and applied quality control using the `check.marker` and `Xfix` functions. Briefly, the `Xfix` function sets to 'No Call' all the genotypes for which impossible heterozygotes occur on sex chromosomes of individuals known to be hemizygous. The `check.marker` function was run in two rounds: The first round was set to exclude individuals with call rates below 0.8 and sites that were not at least 80% genotyped and showing a minor allele frequency lower than 0.01. The second round included the criteria used during the first round but in addition it excluded sites that were not in Hardy-Weinberg equilibrium

according to a p-value threshold of 0.001. After applying filters we retained 410 832 SNPs across 254 *H. erato* individuals and 4 791 755 SNPs across 130 *H. melpomene* individuals.

The colourimetric variables were pre-processed before using them in the association analysis. All colourimetric variables except hue were transformed using the rank-based inverse normal transform implemented in the `rntransform` function of the GenABEL package. For hue, black individuals were excluded from the association analysis since it is not clear what should be defined as 'black' colour in terms of wavelength of peak reflectance across the radiation spectrum. In some studies, butterflies with reflectance estimates ranging from 1 to 3% are considered black butterflies (Davis et al., 2020). We set an arbitrary threshold of 2% reflectance to consider a butterfly as black. In addition, individuals whose hue had an estimate smaller than or equal to 302 nm were considered black and excluded from a genetic association analysis with hue (H1). These two criteria largely overlap, with individuals having lower estimates of hue ($\leq$ 302 nm) having also lower values of reflectance ($<$ 2%). The two criteria were used to partially account for the condition of the wing, because worn wings tend to show inflated estimates of reflectance across all the visible range despite being qualitatively black (low hue estimates with reflectance higher than 2%).

We used the fast score test for association implemented in the `qtscore` function of the GenABEL package. This function uses a single marker linear regression model to estimate SNP-phenotype association statistics using the model

$$y_i = \mu + bx_i + e$$

where y_i is the vector of phenotypic values for the individual i, μ is the phenotype mean, x_i is the SNP value for individual i, b is the effect of each variant and e is the error residual. The `qtscore` function allows for the inclusion of principal components of genetic variation to correct for population stratification. We added principal components as covariates to the model to apply this correction. For each species we added as many principal components as genetic clusters we found using the results of the admixture analysis for each species. To judge significance we used the genome-wide Bonferroni corrected threshold $\frac{\alpha}{n}$ where α is either 0.01 or 0.05 and n is the number of SNPs used for the association analysis. Since the Bonferroni correction approach tends to be conservative and introduces the possibility of false negatives, we used two additional approaches for judging significance in order to have a higher chance of detecting possible SNP associations with variation in structural colour. We used the false discovery rate (FDR) approach implemented in the function `qvaluebh95` of GenABEL. In short, this function takes the p-values of the original association test and computes their corresponding q-values given a desired FDR. We used FDR values of 0.1, 0.05, 0.01 and 0.002. In addition we used an approximation to the type-I error rate using a permutation test that randomized the individuals' phenotypes to

obtain a null distribution for each SNP. An empirical p-value is obtained by estimating the proportion of times that minimal p-values from re-sampled data are less than the original p-value. This procedure is implemented in the `emp.qtscore` function of GenABEL. We did a thousand iterations for the permutation test for each trait by setting the parameter `times=1000`.

4.3.8 Description of genes close to top GWAS results

We listed the neighbouring genes around the top scoring SNPs of our GWAS results. For this, we input the physical position of the SNP on the Lepbase (Challis et al., 2016) Ensembl tool using the reference genomes for *H. erato* and *H. melpomene* and retrieved the identities of the genes. We then used the UniProt identifiers of the genes when available and did a search on the UniProt Knowledge Base (Bateman et al., 2020) to enquire about the biological process that the gene is involved in.

4.4 Results

4.4.1 SNP calling and genotyping

The SNP calling procedure produced an initial 615 581 SNPs for *H. erato* and 4 792 720 SNPs for *H. melpomene*. The large difference in typed SNPs is surprising given the relatively similar genome sizes for both species. To our best knowledge there is not a large difference in effective population size between *H. erato* and *H. melpomene* (Belleghem et al., 2018). We think the observed difference in the amount of SNPs after genotyping may be a result of a combination of the difference in the number of samples and possibly a higher base quality in *H. melpomene*.

4.4.2 Geographic distribution and genetic structure

We observe structured populations of both species and different patterns of population structure and admixture between *H. erato* and *H. melpomene*. For *H. erato* we found that the most likely number of genetic clusters was $K = 3$ (Fig. S4.3, A) and for *H. melpomene* the most likely number of genetic clusters was $K = 4$ (Fig. S4.3, B). In *H. erato* the three genetic clusters represent groups that include samples from Panama and Central Colombia (Left panel, Fig. 4.1, green); West Colombia (Left panel, Fig. 4.1, blue) and Ecuador (Left panel, Fig. 4.1, red). For *H. melpomene* the four genetic clusters correspond to groups that include samples from Central Colombia (Right panel, Fig. 4.1, purple); Panama (Right panel, Fig. 4.1, green); West Colombia (Right panel, Fig. 4.1, blue) and Ecuador (Right panel, Fig. 4.1, red). There is evidence for hybridisation and admixture between these groups.

The principal component analysis on genetic variation revealed population stratification that largely reflects geographic structure between populations of both species. The PCA also shows different patterns of genetic structure between species that are possibly due to different demographic histories (Figs. 4.2 and 4.3). Note that in these

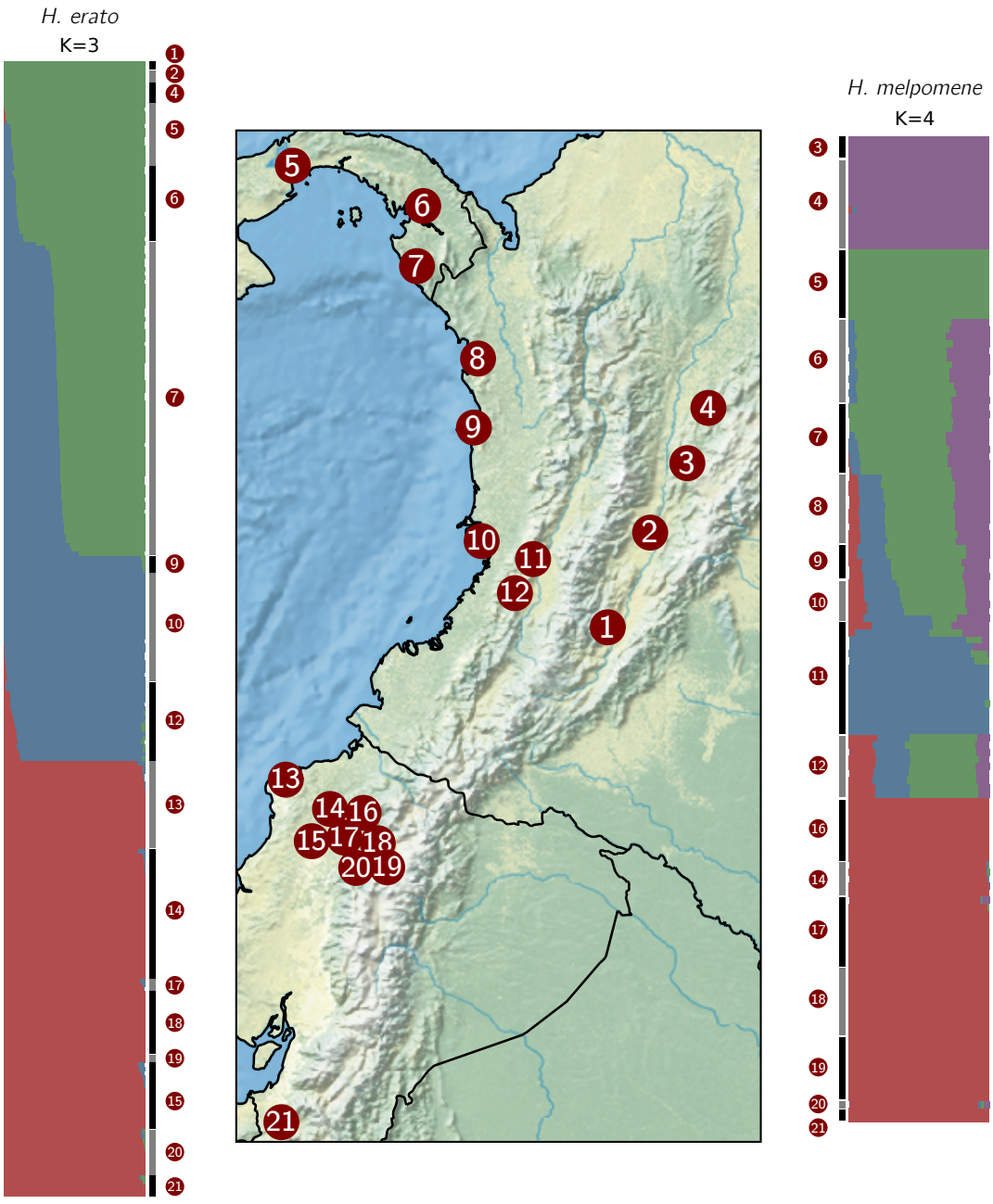

FIGURE 4.1: Admixture proportions of *H. erato* and *H. melpomene* estimated with NGSadmix. Individuals are sorted by locality and localities are numbered on the margins of the admixture plots. A map shows the geographic positions of each locality. Each individual is represented by a horizontal bar and the colours of the bars represent the genetic clusters found by the admixture analysis. Vertical bars group individuals that were sampled at the same locality.

figures the locality named Jaque (sampling point 7 in Figure 4.1) is shown along with other major localities. This locality harbours a large proportion of individuals that are hybrids between Colombian and Panamanian populations in both species. We aimed to visually assess whether the hybrid nature of individuals from this locality is reflected in the results of the PCA.

In *H. erato* the biplot of PC1 and PC2 (Fig. 4.2, A) shows clear-cut clusters of samples for each major locality. Geometrically, three vertices can be seen which correspond to samples from Central Colombia (goldenrod), West Colombia (blue) and Ecuador (red). Along the edge between Central Colombia and West Colombia, samples from Panama (green) and Jaque (pink) are spread. This pattern reflects the result obtained from the admixture analysis for *H. erato* (Fig. 4.1, left) whereby populations from Central Colombia (1-4) and West Colombia (9, 10, 12) each form a single genetic cluster (green, blue), whereas populations from Panama (5, 6) and Jaque (7) show shared ancestry between Central Colombia and West Colombia. When expanding the analysis of genetic structure by including PC3, we also find a clustering of samples that reflects geographic structure. PC3 splits the West Colombia cluster in two, with one of the clusters being closer to the Ecuador samples along the vertical direction (Fig. 4.2 B, C). This could be due to the pattern of shared ancestry with Ecuadorian populations that is seen in some samples from West Colombia (Fig. 4.1, left panel, location 12). The variance explained by the first principal component of the PCA is very high in *H. erato* (19.63%) compared to *H. melpomene* (5.25%).

In *H. melpomene* a clustering of samples that reflects geography can also be seen, albeit less clearly than *H. erato*. The two principal components that explain the most variation show a similar pattern to that of *H. erato* except that there are two clusters for West Colombia (blue, Fig. 4.3, A). Presumably these two clusters correspond to individuals with mixed ancestries from several populations (localities 8–10, 12, Fig. 4.1, right panel) and individuals with single or dominant blue ancestry (locality 11). The pattern of aggregation seen on the PC1 vs. PC3 plot shows a similar behaviour (Fig. 4.3, B) insofar it clusters most samples by geography and splits the Panama samples in two groups; one of them overlapping with the samples from Jaque. This again reflects the mixed ancestry of some Panamanian samples observed on the admixture analysis result, in which individuals from location 5 show single or dominant ancestry of the green group and samples from location 6 have some admixture with Central Colombia (Fig. 4.1, right panel).

Overall the admixture and PCA analyses reveal features of the genetic structure of populations that are important to consider when correcting for population stratification in the association analysis. Both species show clear patterns of structure and shared ancestry that can be accounted for by incorporating the information of the PCs on the GWAS as covariates. In addition, some groups of samples can be excluded in the association analysis depending on whether they show an elevated level of structure. Firstly we took out the individuals from Colombia's Magdalena Valley

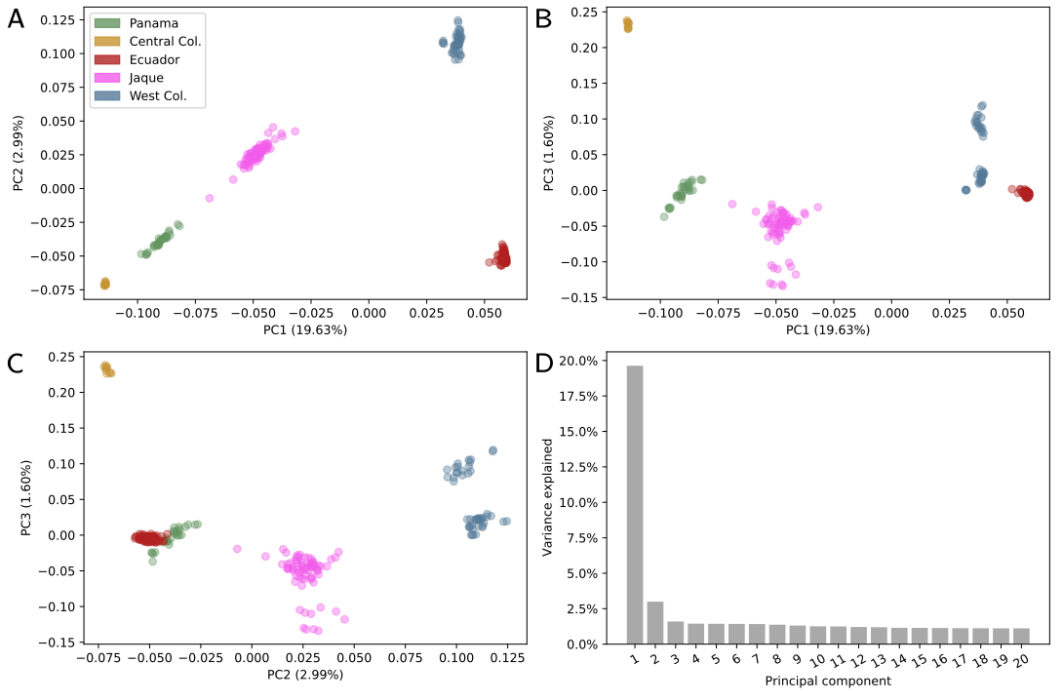

FIGURE 4.2: Principal component analysis of genetic variation in *H. erato*. Relationships between variation on principal components 1 and 2 (A), 1 and 3 (B), 2 and 3 (C), and a barplot of variance explained by the first 20 principal components (D) are shown. Samples are coloured by major geographic location.

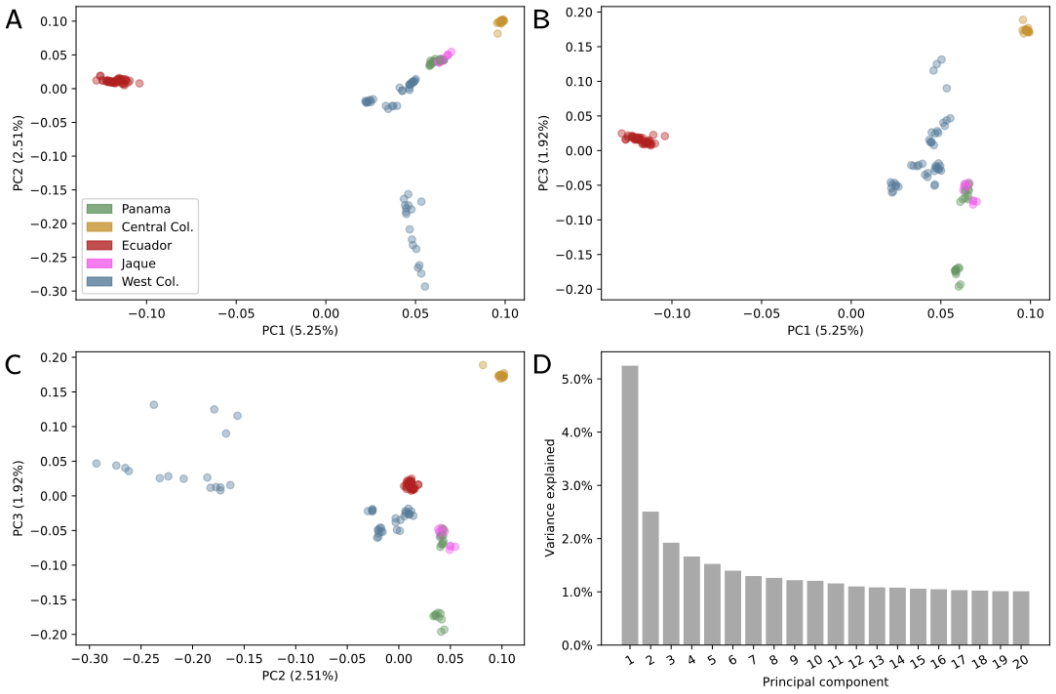

FIGURE 4.3: Principal component analysis of genetic variation in *H. melpomene*. Relationships between variation on principal components 1 and 2 (A), 1 and 3 (B), 2 and 3 (C), and a barplot of variance explained by the first 20 principal components (D) are shown. Samples are coloured by major geographic location.

(Central Colombia. Localities: Huila (1), Tolima (2), Guaduas (3) and Otanche (4) Fig. 4.1). Although not strong, genetic structure was found between this group and the individuals from Panama and North Colombia localities in *H. erato*. We suspect that isolation by distance may still introduce some level of noise to the analysis. In *H. melpomene* genetic structure was observed between these samples and those of other localities in Colombia. Taking into account the results of the analyses of genetic structure we did two association tests for all phenotypic measurements for both species with two sets of individuals: The first set included all the samples except those from Central Colombia and in the second set Ecuadorian samples, which form a genetic cluster on their own in both species and show little or no admixture with Colombian populations, were further excluded.

The patterns of genetic structure and admixture observed here are somewhat similar to those observed in a previous study (Curran et al., 2020). This study included *H. erato* and *H. melpomene* individuals from some of the geographical regions that we included here, and some individuals are shared between studies, although Curran's did not include samples from Ecuador or Central Colombia. Results of admixture between Panamanian and Western Colombian populations in both species is highly similar and shows the mixed ancestry of individuals from Jaque (loc. 7). The results from PCA are different between studies. In Curran et al. (2020) PCA explains little variation in both species and specifically for *H. erato* it doesn't seem to separate populations as expected, while in our analysis several clusters corresponding to geographically separated populations are revealed. These differences may be the result of including more samples in our study and also because the sequencing technique used in Curran is different from the one we used.

4.4.3 Variation in spectral properties and repeatability of phenotypic estimates

As expected, our samples showed variation in spectral properties along their geographic distribution. For *H. erato*, most colourimetric variables show an increasing trend in localities that have lower latitudes (southern latitudes) (x axis on Fig. 4.4): brightness (B2, B3 Fig. 4.4 A and B); blue saturation (S1B Fig. 4.4 D) and hue (H1 Fig. 4.4 F) all show this increasing trend. Estimates of brightness tend to stabilise at location 13 because all Ecuadorian samples belong to the iridescent race *H. e. cyrbia*. Saturation of violet colour (S1V) shows a more stable pattern of variation across localities; it decreases only slightly between localities 5 and 17 showing a subtle increase in the last three localities (Fig. 4.4 C). Green saturation (S1G) decays rapidly at localities 5–7 and remains low at subsequent locations, where individuals with brighter blue wings are found (Fig. 4.4 E).

For *H. melpomene* the behaviour of colourimetric variables is similar to that of *H. erato* despite the obvious differences in structural colour between the two species. Both estimates of brightness (B2 and B3) increase gradually as latitude increases

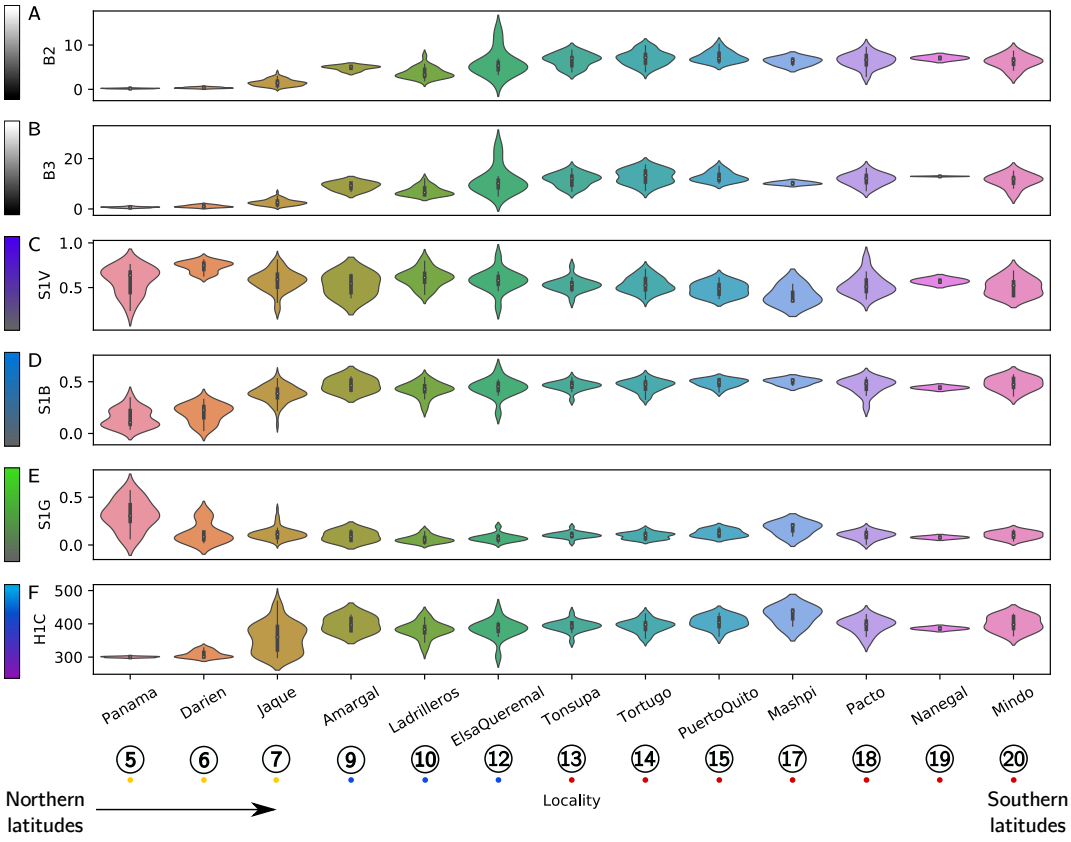

FIGURE 4.4: Distribution of colourimetric variables across several localities for *H. erato*. The numbers underneath represent the localities from which the samples come as shown in figure 4.1, and the localities are sorted by latitude. A and B panels show variation in estimates of brightness; C, D and E show variation in saturation and F shows variation in hue. Coloured dots underneath localities denote major geographical regions: Yellow: Panama, Blue: West Colombia, Red: Ecuador.

(Fig. 4.5 A, B). Violet saturation (S1V) shows a steep increase across Panamanian localities 5, 6 and 7 and remains high on average in southern latitudes, but some localities in West Colombia and Ecuador (9–14) show high variability (Fig. 4.5 C). Blue saturation shows a more gradual increase with latitude, showing high variability in localities 9–14 and stabilising in Ecuadorian localities (14–21) (Fig. 4.5 D) where the iridescent race *H. m. cythera* is found. A sharp decrease similar to that observed in *H. erato* is seen for green saturation (S1G), again dropping in Panamanian localities (5, 6), remaining stable in Colombian and Ecuadorian localities but showing high variability in localities 9–14 (Fig. 4.5 E). Hue (H1) shows variability in locations 10, 11, 12, 19 and 21 but remains low overall, with the exception of a slight increase in location 21 (Fig. 4.5 F). Estimates of phenotypic variation were highly repeatable (table 4.3).

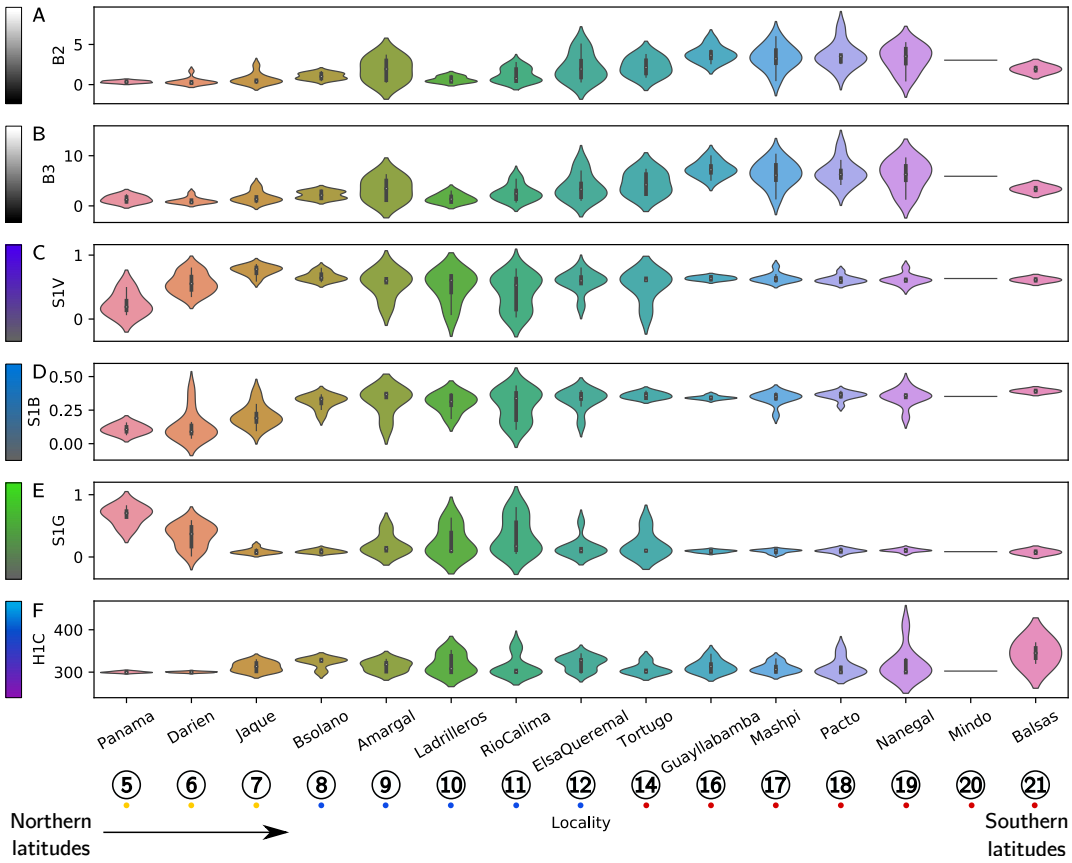

FIGURE 4.5: Distribution of colourimetric variables across several localities for *H. melpomene*. The numbers underneath represent the localities from which the samples come as shown in figure 4.1, and the localities are sorted by latitude. A and B panels show variation in estimates of brightness; C, D and E show variation in saturation and F shows variation in hue. Coloured dots underneath localities denote major geographical regions: Yellow: Panama, Blue: West Colombia, Red: Ecuador.

TABLE 4.3: The repeatability of colourimetric variables obtained from optical spectroscopy.

Measurement	Repeatability
B2	0.998
B3	0.997
S1V	0.981
S1B	0.973
S1G	0.997
H1	0.998

4.4.4 GWAS of all samples

Different patterns of association were observed for colourimetric variables and hind wing pattern. The density of markers may have implications for the results obtained in genome-wide association analyses, as larger distances between SNPs may decrease the chance of observing associations if LD is low. We obtained summary statistics for marker distributions along the genome in both species. As expected from the number of markers, *H. melpomene* showed a smaller inter-marker distance on average than *H. erato* (Table S4.1). Notably, the sex chromosome in *H. erato* (chr21) showed the largest gaps between markers (∼4kb on average and a maximum of ∼736kb) and the largest standard deviation in gap sizes (Fig. S4.4, Table S4.1).

Genetic association for hind-wing pattern

We found significant associations for the yellow hind-wing bar; a Mendelian trait known to be controlled by the *cortex* gene (chromosome 15) in both species (Nadeau et al., 2016). For *H. erato* we observe SNPs above both Bonferroni corrected thresholds (Fig. 4.6, A) and above both empirical significance thresholds on chromosome 15 (Fig. S4.5, A). All the SNPs showing significant associations are on the scaffold Herato1505, which is the scaffold that contains the *cortex* gene in these species. The associated SNPs appear clustered within an interval from position 2 262 194 to 2 420 418 on this scaffold. This interval does not overlap the span of the *cortex* gene in *H. erato*, which is from 2 074 108 to 2 087 841. For *H. melpomene* we observe a similar result, with all SNPs above Bonferroni corrected thresholds (Fig. 4.6, B) and above both empirical significance thresholds mapping to the same scaffold that contains *cortex* (Hmel215003o) on chromosome 15 (Fig. S4.5, B). The SNPs showing significant associations cluster within an interval that spans from 1 364 547 to 1 452 978 on this scaffold (Table 4.5). This interval partially overlaps the position of *cortex* in *H. melpomene*, which spans from 1 413 766 to 1 533 113. For both species, significant SNPs according to an FDR of ≤ 0.002 corresponded well with SNP associations that were significant according to other significance criteria. Setting the FDR above 0.002 resulted in significant associations of SNPs on chromosomes other than chromosome 15, which we considered to be false positives.

Genetic association for colourimetric variables

Given the significant QTL reported in Chapter 3 and the results reported by Brien (2019) on QTL for luminance and blue colour variation, we expected to find significant associations for brightness (B2, B3) and for variation in saturation of colour and hue (S1B, H1). We did not find significant genetic associations for the variation captured by colourimetric variables in full sets of wild caught samples of *H. erato* (Fig. 4.7) or *H. melpomene* (Fig. 4.8). This was the case despite having used less conservative significance criteria in addition to Bonferroni correction for multiple testing: We did not find SNPs significantly associated with structural colour variation at a lenient

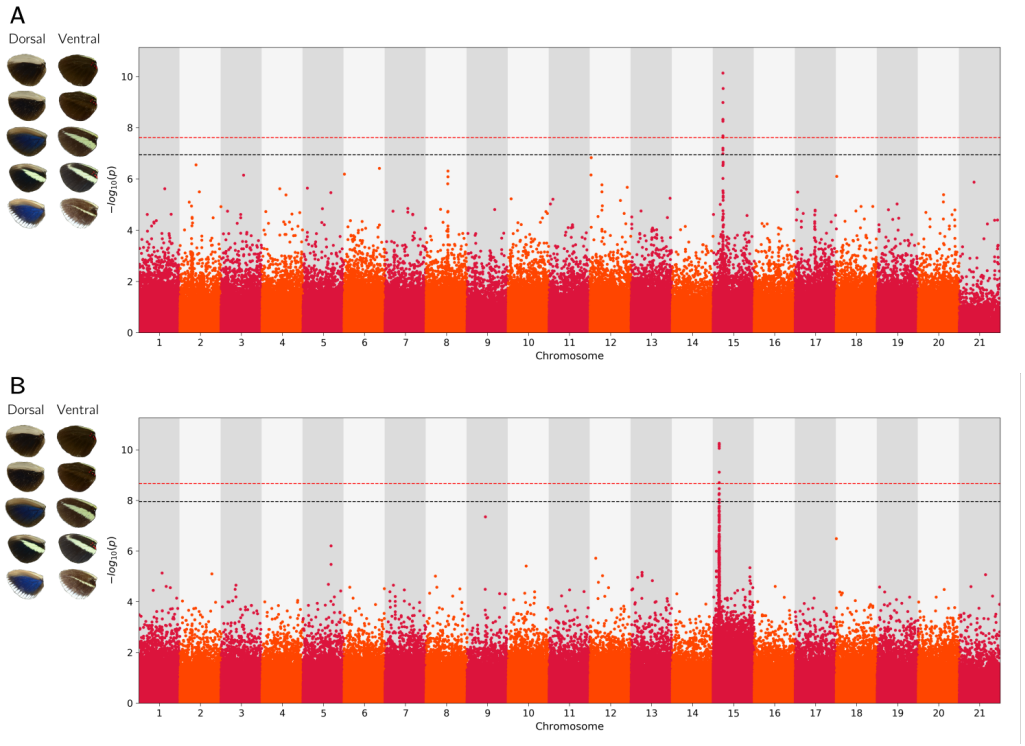

FIGURE 4.6: Genome wide association results for hind-wing yellow bar variation across samples from the full set of samples of *H. erato* (A) and *H. melpomene* (B). The negative logarithm of p-values is shown. Dashed lines correspond to Bonferroni corrected significance thresholds: Black, 0.05; red, 0.01.

false discovery rate of 0.1 or below an empirical p-value threshold of 0.05. Despite not having observed significant associations for variation in structural colour, we report the top scoring SNPs for association tests done for each colourimetric variable (Tables 4.4 and 4.5).

The strongest evidence that we observed previously for colour, luminance and scale structure variation in Chapter 3 was found on the sex chromosome in *H. erato*. In our analysis, the sex chromosome does not show any patterns that suggest an association with brightness (Fig. 4.7 A, B).

For the full set of *H. erato* the strongest associations (lowest p-values) are observed for brightness (B2) and hue, spread across several autosomes (Table 4.4). The top scoring SNPs for both variables measuring brightness are on chromosomes 1, 2, 3, 6 and 10 (Fig. 4.7 A, B; Table 4.4). For saturation, the most outstanding SNPs were observed on chromosomes 4, 6, 7, 17 and 18 in the case of violet saturation (Fig. 4.7 C; Table 4.4); chromosomes 8, 10, 11 and 18 for blue saturation (Fig. 4.7 D; Table 4.4); and chromosomes 10, 12, 16 and 18 for green saturation (Fig. 4.7, E; Table 4.4). Hue is the colourimetric variable that shows the SNPs with the strongest associations (Fig. 4.7, F; Table 4.4) on chromosomes 7, 8 and 17.

For *H. melpomene*, given the results shown in Chapter 3, we expected to find significant

SNP associations on chromosomes 3 and 7, as it is possible that these contain the loci with the largest effects on structural colour. Again, no significant associations were found at a false discovery rate of 0.1 or below the 0.05 empirical p-value threshold. In general, we observed weaker signals of association (higher p-values) in *H. melpomene* than those observed in *H. erato*. As in the case of *H. erato*, we report the top 5 SNPs showing the strongest evidence of association for each colourimetric variable.

For the full set of *H. melpomene* individuals the strongest associations were observed for brightness (B2) and violet and green saturation S1V and S1G (Fig. 4.8 A, C, E). Unlike *H. erato*, the full set of *H. melpomene* individuals does not show strong associations with hue variation (Table 4.5). B2 showed the highest scoring associations on chromosomes 5, 13, 14, and 21 (Fig. 4.8 A; Table 4.5). B3 showed the highest scoring SNPs on chromosomes 4, 7, 13, 14 and 21 (Fig. 4.8 B; 4.5). For violet saturation (S1V) the highest scoring SNPs were observed on chromosomes 3, 4, 10 and 13 (Fig. 4.8 C; Table 4.5). Blue saturation (S1B) showed the lowest p-values on its top associated SNPs on chromosomes 1, 3, 8 and 20 (Fig. 4.8 D; Table 4.5). Green saturation (S1G) showed the strongest associations on chromosomes 9, 10, 13 and 17 (Fig. 4.8 E; Table 4.5). For hue (H1) the top scoring SNPs were on chromosomes 2, 13, 20 and 21 (Fig. 4.8 F; Table 4.5).

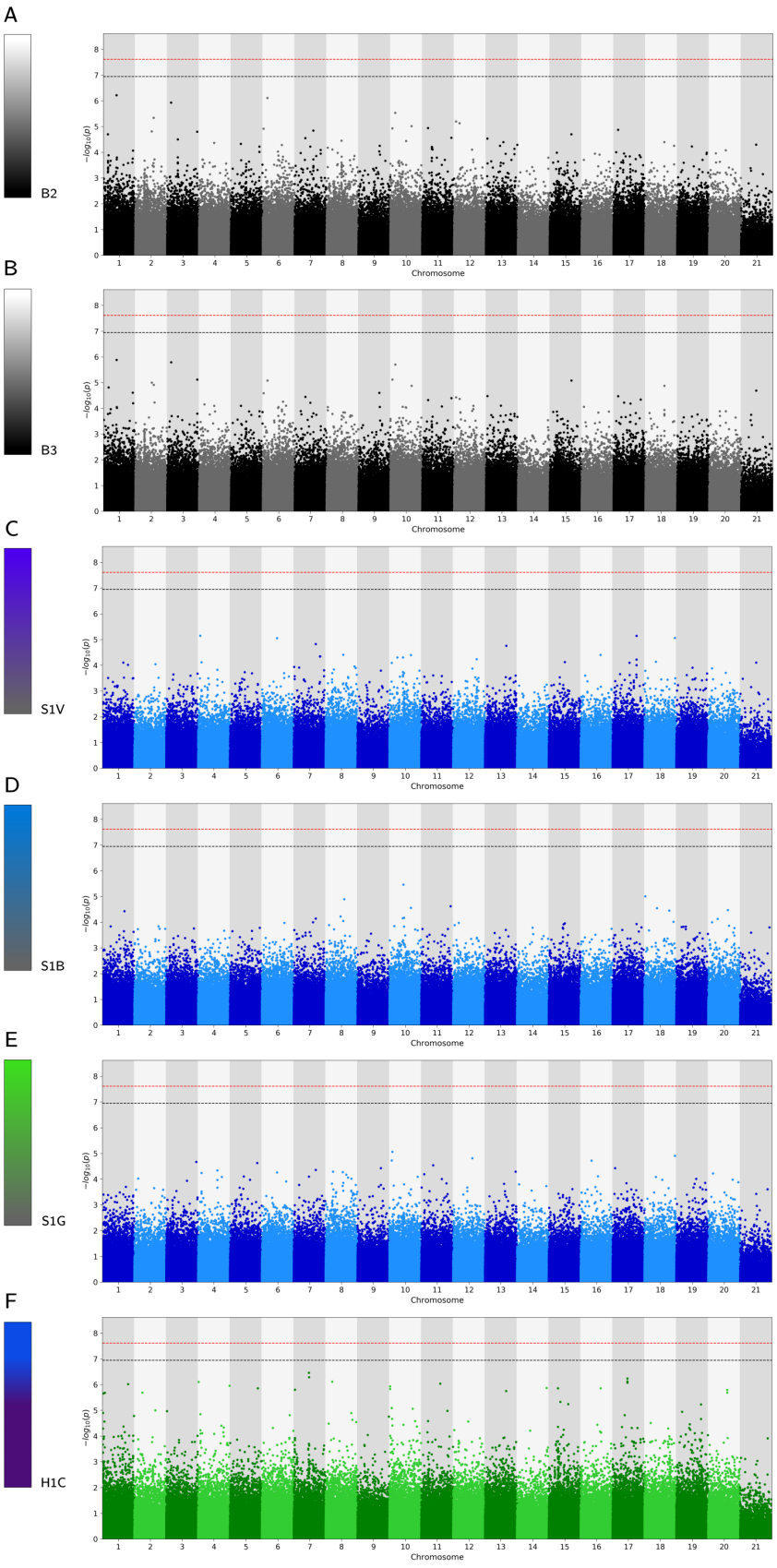

FIGURE 4.7: Genome wide association results for colourimetric variables in *H. erato*. No SNPs were significantly associated with variation in brightness (A, B) saturation (C, D, E) or hue (F). The negative logarithm of p-values is shown. Dashed lines correspond to Bonferroni corrected significance thresholds: Black, 0.05; red, 0.01.

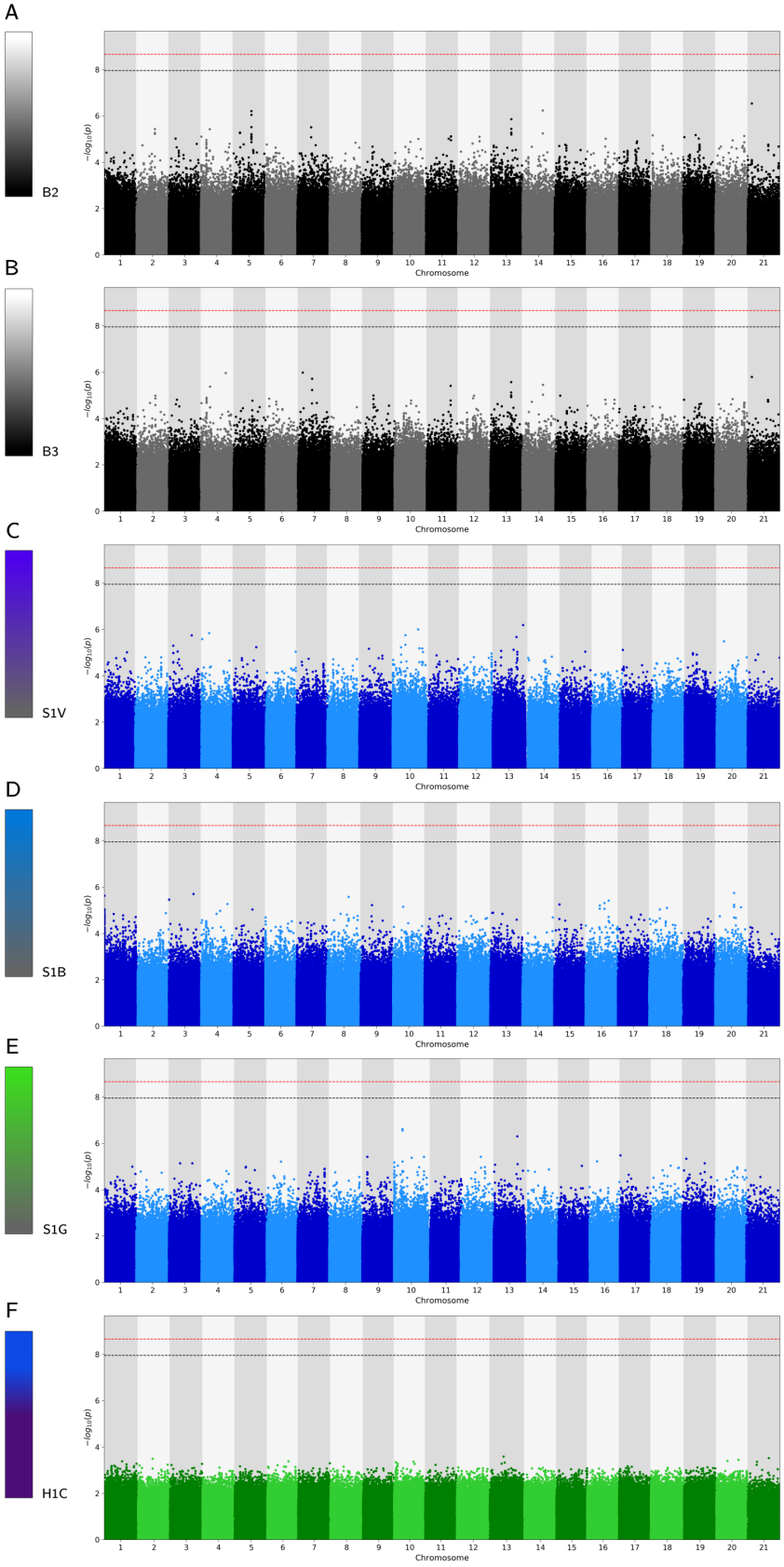

FIGURE 4.8: Genome wide association results for colourimetric variables in *H. melpomene*. No SNPs were significantly associated with variation in brightness (A, B) saturation (C, D, E) or hue (F). The negative logarithm of p-values is shown. Dashed lines correspond to Bonferroni corrected significance thresholds: Black, 0.05; red, 0.01.

4.4.5 GWAS on samples excluding Ecuador

The results observed for the GWAS analysis excluding samples from Ecuador are similar to those of the full sample set, but top scoring SNPs of colourimetric variables change largely from those found in the first analysis. Significant associations are found only for hue (H1) in *H. melpomene*. We present the plots corresponding to the empirical p-values obtained for all SNPs in the main text. The Manhattan plots with the original p-values can be found at the supplementary material section, figures S4.8; S4.9 and S4.10.

Genetic association for hind-wing pattern

We found significant associations for hind-wing bar variation on chromosome 15 for both *H. erato* (Fig. 4.9, A) and *H. melpomene* (Fig. 4.9, B). The top scoring SNPs in *H. erato* are again in the scaffold Herato1505, clustered within the segment 2 262 212 to 2 420 418 (Table 4.4), which doesn't physically overlap the *cortex* gene. For *H. melpomene* there is only a single SNP above the Bonferroni corrected threshold corresponding to $\alpha = 0.05$ (Fig. 4.9, B. Table 4.5) but the empirical p-value distribution reveals 27 SNPs whose p-value is below the 0.05 threshold. This suggests that reducing the number of samples in *H. melpomene* results in loss of statistical power. These SNPs are clustered within the segment 1 394 799 to 1 457 832 on the scaffold Hmel215003o, which partially overlaps with the physical position of the *cortex* gene similar to what was previously described for the full set of individuals. As in the case of the full sets of samples, significant SNPs according to an FDR of 0.002 are in good correspondence with significant associations according to the other two significance criteria and setting a more relaxed FDR leads to false positive association results.

Genetic association for colourimetric variables

The observed results from the second association test are similar to those observed in the test that included all samples; in most cases no significant associations were found. In *H. erato* the top scoring SNPs for association with brightness (B2 and B3) were observed on chromosomes 1, 2, 4, 11, 13, 14 and 21 (Fig. 4.10 A, B; Table 4.4). For violet saturation the top five SNPs were observed at chromosomes 6, 8, 13, 17, 18 (Fig. 4.7 C; Table 4.4); chromosomes 1, 10, 13, 16 and 17 for blue saturation (Fig. 4.10 D; Table 4.4) and chromosomes 2, 6, 8, 9 for green saturation (Fig. 4.10 E; Table 4.4). For hue the top associations were observed on chromosomes 2, 5, 8, 9 and 15 (Fig. 4.10 F; Table 4.4).

For *H. melpomene* we observed results similar to *H. erato*, except for green saturation and hue. Brightness showed the highest associations on chromosomes 7, 13, 17, 19 and 21 (Fig. 4.11 A, B; Table 4.5). For saturation the top SNPs were observed on chromosomes 6, 10 and 13 for violet saturation (Fig. 4.11 C; Table 4.5); chromosomes 4 and 10 for blue saturation (Fig. 4.11 D; Table 4.5); and a small cluster of SNPs on scaffold Hmel210001o (chromosome 10), between positions 143 378 and 157 493 with

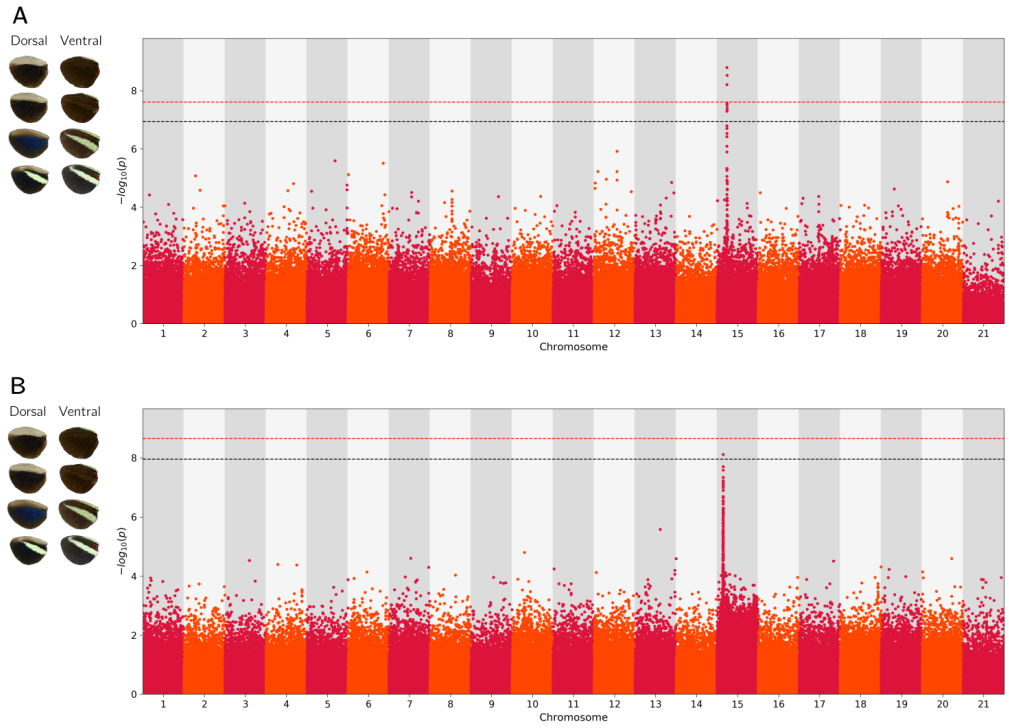

FIGURE 4.9: Genome wide association results for hind-wing yellow bar variation across samples from the set of samples excluding Ecuador localities of *H. erato* (A) and *H. melpomene* (B). The negative logarithm of p-values is shown. Dashed lines correspond to Bonferroni corrected significance thresholds: Black, 0.05; red, 0.01.

an additional SNP on the same scaffold at position 173 681 (Fig. 4.11 E; Table 4.5). For hue we observed significant associations at nine SNPs on chromosomes 2, 5, 6, 13, 18 and 20. These associations were significant at a Bonferroni corrected threhsold of 0.05 and an FDR of 0.005 (Fig. S4.10 F; Table 4.5). These nine SNPs were not found to be significant at an empirical p-value threshold of 0.05 (Fig. 4.11 F; Table 4.4).

4.4.6 Genes neighbouring top SNPs

Although none of our GWAS analyses results revealed significant associations with structural colour variation, we report the genes that are physically closest to the top scoring SNPs and their biological functions, provided that their annotations were available on Lepbase/UniProt. In general we found diverse biological processes associated with the genes neighbouring the top SNPs of our GWAS analysis. There is little overlap in SNPs, genes, and gene functions between sets within a single species (i.e. full sets vs. Ecuador samples removed) except for the yellow hind-wing bar in both species, and for violet saturation in *H. erato*. The full list of genes neighbouring top scoring SNPs and their associated biological processes can be found on tables 4.4 and 4.5.

TABLE 4.4: Top association results for seven traits in *H. erato*. Significance according to Bonferroni corrected thresholds (< 0.05, *), empirical p-value (< 0.05, §) and FDR (†) is indicated. Overlapping (o) or neighbouring genes and their associated biological process are shown.

Trait	Chromosome	SNP		p-value		Neighbouring genes		Biological process	
		All individuals	No Ecuador	All individuals	No Ecuador	Upstream	Downstream	Upstream	Downstream
Hindwing bar	15	Herato1505_2277787†§*	Herato1505_2277787†§*	7.3×10^{-11}	1.6×10^{-9}	evm.TU.Herato1505.85 (*cortex*)	evm.TU.Herato1505.86	Differentiation, meiosis, oogenesis	Nuclear-transcribed mRNA poly(A) tail shortening
	15	Herato1505_2420333†§*	Herato1505_2420333†§*	2.9×10^{-10}	2.7×10^{-8}	-	-	-	-
	15	Herato1505_2277767†§*	Herato1505_2277767†§*	1.0×10^{-9}	6.1×10^{-9}	-	-	-	-
	15	Herato1505_2262212†§*		4.6×10^{-9}		-	-	-	-
	15	Herato1505_2277874†§*		4.8×10^{-9}		-	-	-	-
	15	Herato1505_2262194†§*		5.5×10^{-9}		-	-	-	-
	15	Herato1505_2262277†§*		2.0×10^{-8}		-	-	-	-
	15	Herato1505_2420418†§*	Herato1505_2420418†§	2.3×10^{-8}	2.9×10^{-9}	-	-	-	-
	15	Herato1505_2277866§*		6.2×10^{-8}		-	-	-	-
	15	Herato1505_2262227§*		7.3×10^{-8}		-	-	-	-
	15		Herato1505_2295279†§*		3.0×10^{-8}	-	-	-	-
	15		Herato1505_2420369†§*		3.8×10^{-8}	-	-	-	-
	15		Herato1505_2420375†§*		4.5×10^{-8}	-	-	-	-
	15		Herato1505_2319300†§*		5.0×10^{-8}	-	-	-	-
B2	1	Herato0101_9978296		6.0×10^{-7}		evm.TU.Herato0101.288	evm.TU.Herato0101.289	Regulation of synapse assembly	NA
	6	Herato0601_3651263		7.6×10^{-7}		evm.TU.Herato0601.86	evm.TU.Herato0601.87	NA	Signal peptide processing
	3	Herato0301_1097312		1.2×10^{-6}		evm.TU.Herato0301.22	evm.TU.Herato0301.23	D-amino acid metabolic process	Response to oxidative stress
	10	Herato1001_3404807		2.9×10^{-6}		evm.TU.Herato1001.115	evm.TU.Herato1001.116	NA	NA
	2	Herato0211_1157291		4.5×10^{-6}		evm.TU.Herato0211.55 (o)	-	Negative regulation of cold-induced thermogenesis	-
	14		Herato1407_42514		3.9×10^{-7}	NA	NA	NA	NA
	4		Herato0417_127380		5.9×10^{-7}	NA	NA	NA	NA
	2		Herato0211_2906724		1.2×10^{-6}	evm.TU.Herato0211.99	evm.TU.Herato0211.100	NA	Potassium ion transmembrane transport
	13		Herato1301_468564		6.3×10^{-6}	evm.TU.Herato1301.18 (o)	-	Nervous system development	-
	21		Herato2101_9743064		8.4×10^{-6}	evm.TU.Herato2101.331 (o)	-	Microtubule-based movement	-
B3	1	Herato0101_9978296		1.0×10^{-6}		evm.TU.Herato0101.288	evm.TU.Herato0101.289	Regulation of synapse assembly	NA
	3	Herato0301_1097312		2.0×10^{-6}		evm.TU.Herato0301.22	evm.TU.Herato0301.23	D-amino acid metabolic process	Response to oxidative stress
	10	Herato1001_3404807		2.0×10^{-6}		evm.TU.Herato1001.115	evm.TU.Herato1001.116	NA	NA
	3	Herato0310_9650739		8.0×10^{-6}		evm.TU.Herato0310.295	evm.TU.Herato0310.296	NA	NA
	10	Herato1001_1006075		8.0×10^{-6}		evm.TU.Herato1001.47	evm.TU.Herato1001.48	NA	NA
	1		Herato0101_21154602		5.5×10^{-6}	evm.TU.Herato0101.816 (o)	-	Fatty acid biosynthetic process	-
	4		Herato0417_127380		6.1×10^{-7}	NA	NA	NA	NA
	21		Herato2101_9743064		9.7×10^{-6}	evm.TU.Herato2101.331 (o)	-	Microtubule-based movement	-
	14		Herato1407_42514		1.1×10^{-5}	NA	NA	NA	NA
	11		Herato1102_1158628		1.8×10^{-5}	novel_gene_123	NA	DNA integration, DNA recombination	NA
S1V	4	Herato0401_1505746		7.0×10^{-6}		evm.TU.Herato0401.31	evm.TU.Herato0401.32	Protein serine/threonine kinase activity	Flagellated sperm motility
	17	Herato1707_278837	Herato1707_278837	7.0×10^{-6}	2.9×10^{-5}	evm.TU.Herato1707.16	evm.TU.Herato1707.17	NA	NA
	18	Herato1807_4792975	Herato1807_4792975	9.0×10^{-6}	6.3×10^{-5}	evm.TU.Herato1807.116 (o)	-	NA	NA
	6	Herato0606_2614761	Herato0606_2614761	9.0×10^{-6}	2.5×10^{-5}	evm.TU.Herato0606.79	evm.TU.Herato0606.80	NA	Photoreceptor cell morphogenesis
	7	Herato0701_12458805		1.5×10^{-5}		evm.TU.Herato0701.588 (o)	-	Extracellular matrix disassembly, proteolysis	-
	8		Herato0807_34371		3.0×10^{-5}	evm.TU.Herato0807.1 (o)	-	NA	NA
	13		Herato1301_19402818		6.8×10^{-5}	evm.TU.Herato1301.671	NA	Central nervous system development	NA
S1B	10	Herato1003_4045076		3.0×10^{-6}		evm.TU.Herato1003.120 (o)	-	NA	NA
	18	Herato1801_425370		1.0×10^{-5}		evm.TU.Herato1801.20	evm.TU.Herato1801.21	RNA-directed DNA polymerase activity	Heme biosynthetic process
	8	Herato0802_15592		1.3×10^{-5}		evm.TU.Herato0802.1 (o)	-	NA	NA
	11	Herato1108_14018357		2.4×10^{-5}		evm.TU.Herato1108.594 (o)	-	Regulation of cytokine production	-
	10	Herato1005_1200053		2.8×10^{-5}		evm.TU.Herato1005.75 (o)	-	Cell adhesion	-
	16		Herato1605_2406958		8.0×10^{-6}	evm.TU.Herato1605.83	evm.TU.Herato1605.84	NA	NA
	13		Herato1301_3492206		3.5×10^{-5}	evm.TU.Herato1301.96	evm.TU.Herato1301.97	Anterior/posterior pattern specification	NA
	1		Herato0101_17534239		4.3×10^{-5}	evm.TU.Herato0101.689 (o)	-	Cell differentiation	-
	17		Herato1705_463171		4.5×10^{-5}	evm.TU.Herato1705.10	evm.TU.Herato1705.11	NA	NA
	10		Herato1007_3353016		4.7×10^{-5}	evm.TU.Herato1007.122 (o)	-	Cellular protein modification process	-
S1G	10	Herato1001_1699715		9.0×10^{-6}		evm.TU.Herato1001.64 (o)	-	Microtubule organizing center organization	-
	18	Herato1807_4792975		1.2×10^{-5}		evm.TU.Herato1807.116 (o)	-	NA	NA
	12	Herato1202_12403520		1.5×10^{-5}		evm.TU.Herato1202.471	evm.TU.Herato1202.472	NA	Carbohydrate metabolism
	10	Herato1001_1356893		1.9×10^{-5}		evm.TU.Herato1001.51	evm.TU.Herato1001.52	Extracellular matrix organization	NA
	16	Herato1601_5259724		1.9×10^{-5}		evm.TU.Herato1601.114	evm.TU.Herato1601.115	Regulation of mRNA stability	Feeding behavior
	8		Herato0801_6655120		1.2×10^{-5}	evm.TU.Herato0801.193 (o)	-	Negative regulation of apoptotic process	-
	2		Herato0204_610361		1.4×10^{-5}	evm.TU.Herato0204.27 (o)	-	Antennal development	-
	8		Herato0801_8459899		1.7×10^{-5}	evm.TU.Herato0801.295 (o)	-	L-threonine catabolic process to propionate	-
	6		Herato0601_3607111		3.3×10^{-5}	evm.TU.Herato0601.86 (o)	-	NA	NA
	9		Herato0901_10799881		3.7×10^{-5}	evm.TU.Herato0901.324	evm.TU.Herato0901.325	Cardiac muscle cell action potential	NA
H1	7	Herato0701_7907628		3.5×10^{-7}		evm.TU.Herato0701.359 (o)	-	Regulation of innate immune response	-
	7	Herato0701_7908593		5.1×10^{-7}		-	-	-	-
	17	Herato1701_11464731		5.7×10^{-7}		evm.TU.Herato1701.407	NA	NA	NA
	17	Herato1701_11464729		7.5×10^{-7}		-	NA	NA	NA
	8	Herato0801_4919339		7.6×10^{-7}		evm.TU.Herato0801.106	evm.TU.Herato0801.107	NA	Cell-cell adhesion
	5		Herato0511_9592		1.4×10^{-5}	evm.TU.Herato0511.1	evm.TU.Herato0511.2	NA	NA
	8		Herato0801_4888613		1.4×10^{-5}	evm.TU.Herato0801.106	evm.TU.Herato0801.107	NA	Cell-cell adhesion
	9		Herato0901_11273432		1.7×10^{-5}	evm.TU.Herato0901.334 (o)	-	Transmembrane transport	-
	2		Herato0215_3265819		2.0×10^{-5}	evm.TU.Herato0215.125 (o)	-	RNA processing	-
	15		Herato1505_2524575		2.3×10^{-5}	evm.TU.Herato1505.102 (o)	-	DNA catabolic process	-

TABLE 4.5: Top association results for seven traits in *H. melpomene*. Significance according to Bonferroni corrected thresholds (< 0.05, *), empirical p-value (< 0.05, §) and FDR (†) is indicated. Overlapping (o) or neighbouring genes and their associated biological process are shown.

Trait	Chromosome	SNP		p-value		Neighbouring genes		Biological process	
		All individuals	No Ecuador	All individuals	No Ecuador	Upstream	Downstream	Upstream	Downstream
Hindwing bar	15	Hmel215003o_1406664†§*		5.6×10^{-11}		HMEL032679g1	HMEL000025 (*cortex*)	NA	Positive regulation of ubiquitin protein ligase activity
	15	Hmel215003o_1406687†§*		6.2×10^{-11}		-	-	-	-
	15	Hmel215003o_1406685†§*		6.2×10^{-11}		-	-	-	-
	15	Hmel215003o_1406689†§*		7.4×10^{-11}		-	-	-	-
	15	Hmel215003o_1406690†§*		8.7×10^{-11}		-	-	-	-
	15	Hmel215003o_1401294†§*		7.5×10^{-10}		-	-	-	-
	15	Hmel215003o_1375761†§*		2.0×10^{-9}		-	-	-	-
	15	Hmel215003o_1375822†§*		3.4×10^{-9}		-	-	-	-
	15	Hmel215003o_1393191†§*		5.3×10^{-9}		-	-	-	-
	15	Hmel215003o_1364547†§*		5.8×10^{-9}		HMEL002023g1 (o)	-	NA	NA
	15		Hmel215003o_1448057†§*		7.5×10^{-9}	-	-	-	-
B2	21	Hmel221001o_1579498		2.9×10^{-7}		HMEL013511g2	HMEL013510g1	Smooth muscle contraction	Assembly and functioning of muscles
	14	Hmel214004o_5470445		5.7×10^{-7}		HMEL032489g1 (o)	-	Transmembrane transport	-
	5	Hmel205001o_6154547		6.2×10^{-7}		HMEL036739g1	HMEL036740g1	Protein O-linked glycosylation	Apoptotic process
	5	Hmel205001o_6154855		8.9×10^{-7}		HMEL036740g1 (o)	-	Apoptotic process	-
	13	Hmel213001o_12223208		1.4×10^{-6}		HMEL032111g1	HMEL032112g1	NA	NA
	19		Hmel219001o_12350039		1.2×10^{-5}	HMEL034817g1	HMEL003260g1	NA	NA
	21		Hmel221001o_923868		1.2×10^{-5}	HMEL011023g1	HMEL035441g1	NA	NA
	21		Hmel221001o_923743		1.2×10^{-5}	HMEL011023g1	HMEL035441g1	NA	NA
	7		Hmel207001o_3013998		1.5×10^{-5}	HMEL007133g1	HMEL007134g1	Hematopoietic progenitor cell differentiation	NA
	13		Hmel221001o_923856		1.5×10^{-5}	HMEL011023g1	HMEL035441g1	NA	NA
B3	7	Hmel207001o_2031048		1.0×10^{-6}		HMEL011248g2	HMEL037391g1	NA	NA
	4	Hmel204001o_7279928		1.1×10^{-6}		HMEL009923g2	HMEL022324g1	NA	Adaptive immune response
	21	Hmel221001o_1579498		1.6×10^{-6}		HMEL013511g2	HMEL013510g1	Protein phosphorylation	-
	7	Hmel207001o_5516296		1.9×10^{-6}		HMEL037474g1	HMEL037474g1	NA	NA
	13	Hmel213001o_12223208		2.7×10^{-6}		HMEL032111g1	HMEL032112g1	NA	NA
	17		Hmel217001o_11131648		7.3×10^{-6}	HMEL034019g1	HMEL034020g1	NA	NA
	7		Hmel207001o_3013998		8.3×10^{-6}	HMEL007133g1	HMEL007134g1	Hematopoietic progenitor cell differentiation	Structural constituent of cuticle
	13		Hmel213001o_12223223		8.5×10^{-6}	HMEL032111g1	HMEL032112g1	NA	NA
	17		Hmel217001o_11257183		9.6×10^{-6}	HMEL010146g1 (o)	-	NA	NA
	7		Hmel207001o_3013992		1.1×10^{-5}	HMEL007133g1	HMEL007134g1	Hematopoietic progenitor cell differentiation	Structural constituent of cuticle
S1V	13	Hmel213001o_16897208		6.3×10^{-7}		HMEL032253g1 (o)	-	Negative regulation of autophagy	-
	10	Hmel210001o_12693273		9.8×10^{-7}		HMEL006927g3 (o)	-	Morphogenesis of embryonic epithelium	-
	4	Hmel204001o_2226238		1.4×10^{-6}		HMEL015899g1 (o)	-	NA	NA
	10	Hmel210001o_6008870		1.7×10^{-6}		HMEL018081g1 (o)	-	Carbohydrate metabolic process	-
	3	Hmel203003o_7204327		1.8×10^{-6}		HMEL025053 (o) (*Dfd*)	-	Regulation of transcription	-
	13		Hmel213001o_16897208		2.8×10^{-6}	HMEL032253g1 (o)	-	Negative regulation of autophagy	-
	10		Hmel210001o_157376		1.2×10^{-5}	HMEL013626g1	HMEL013627g1	Biosynthetic process	NA
	6		Hmel206001o_13514935		1.3×10^{-5}	HMEL014411 (*Dcr-1*) (o)	-	Anatomical structure development	-
	10		Hmel210001o_5481154		1.4×10^{-5}	HMEL030668g1 (o)	-	NA	-
	10		Hmel210001o_12693273		1.5×10^{-5}	HMEL006927g3 (o)	-	Morphogenesis of embryonic epithelium	-
S1B	20	Hmel220003o_8659226		1.8×10^{-6}		HMEL035242g1	HMEL012769g1	Golgi localization	NA
	3	Hmel203003o_7806561		1.9×10^{-6}		HmGr36_1	HmGr27_1	NA	NA
	1	Hmel201001o_56603		2.3×10^{-6}		HMEL030005g1 (o)	-	DNA biosynthetic process	-
	8	Hmel208001o_6534792		2.6×10^{-6}		HMEL022065g1	HMEL035858g1	NA	NA
	3	Hmel203003o_31177		3.4×10^{-6}		HMEL035998g1	HMEL021764g1	NA	NA
	10		Hmel210001o_15988590		3.7×10^{-6}	HMEL009079g4	HMEL030919g1	Lipid catabolic process	NA
	10		Hmel210001o_15988585		4.7×10^{-6}	HMEL009079g4	HMEL030919g1	Lipid catabolic process	NA
	10		Hmel210001o_15988639		4.7×10^{-6}	HMEL009079g4	HMEL030919g1	Lipid catabolic process	NA
	4		Hmel204001o_7272366		5.0×10^{-6}	HMEL009923g2	HMEL022324g1	NA	Adaptive immune response
	4		Hmel204001o_7272366		5.0×10^{-6}	-	-	-	-
S1G	10	Hmel210001o_4244748		2.4×10^{-7}		HmelUGT33G1	HMEL022620	Transferase activity	UDP-glycosyltransferase activity
	10	Hmel210001o_4244761		2.8×10^{-7}		-	-	-	-
	13	Hmel213001o_13777974		4.9×10^{-7}		HMEL014714g1	HMEL032155g1	NA	NA
	17	Hmel217001o_528682		3.3×10^{-6}		HMEL033711g1	HMEL033712g1	NA	NA
	9	Hmel209001o_1076433		3.8×10^{-6}		HMEL007018g1 (o)	-	Cell-cell adhesion	-
	10		Hmel210001o_157376		1.0×10^{-6}	HMEL013626g1	HMEL013627g1	Alpha-amino acid metabolic process	NA
	10		Hmel210001o_157266		1.6×10^{-6}	-	-	-	-
	10		Hmel210001o_156916		2.6×10^{-6}	-	-	-	-
	10		Hmel210001o_157493		2.7×10^{-6}	-	-	-	-
	10		Hmel210001o_143378		1.7×10^{-6}	HMEL030576g1	HMEL013626g1	NA	Alpha-amino acid metabolic process
H1	13	Hmel213001o_7903775		2.6×10^{-4}		HMEL008634g1	HMEL008632g1	Neuropeptide signaling pathway	NA
	21	Hmel221001o_8612951		3.0×10^{-4}		HMEL008471g6 (o)	-	Nervous system development	NA
	2	Hmel202001o_4067972		3.2×10^{-4}		HMEL009425g1 (o)	-	Innate immune response	NA
	20	Hmel220003o_10305570		3.5×10^{-4}		HMEL008161g2	HMEL035292g1	NA	NA
	20	Hmel220003o_4593578		4.0×10^{-4}		HMEL014725g1	HMEL035090g1	Actin cytoskeleton organization	NA
	5		Hmel205001o_7410962†*		9.5×10^{-11}	HMEL036806g1	HMEL036807g1	NA	NA
	6		Hmel206001o_9725979†*		5.4×10^{-9}	HMEL008033 (NIM-2)	HMEL014654g1	Actin cytoskeleton organization	NA
	6		Hmel206001o_10629244†*		5.7×10^{-9}	HMEL037178g1	HMEL037179g1	NA	Monooxigenase, oxidoreductase
	6		Hmel206001o_5252579†*		7.8×10^{-9}	HMEL016776g1	HMEL037024g1	Regulation of transcription	
	6		Hmel206001o_5252608†*		1.0×10^{-8}	HMEL016776g1	HMEL037024g1	Covalent chromatin modification	NA
	18		Hmel218003o_10661095†*		5.5×10^{-9}	HMEL015560g1	HMEL015559g1	Protein demethylation	Carbohydrate transmembrane transport
	20		Hmel220003o_1075234†*		1.0×10^{-8}	HMEL034993g1 (o)	-	Neural crest cell migration	-
	2		Hmel202001o_8309539†*		1.0×10^{-8}	HMEL009603g1 (o)	-	Actin filament organization	-
	13		Hmel213001o_13294837†*		8.6×10^{-9}	HMEL032144g1 (o)	-	Intracellular signal transduction	-

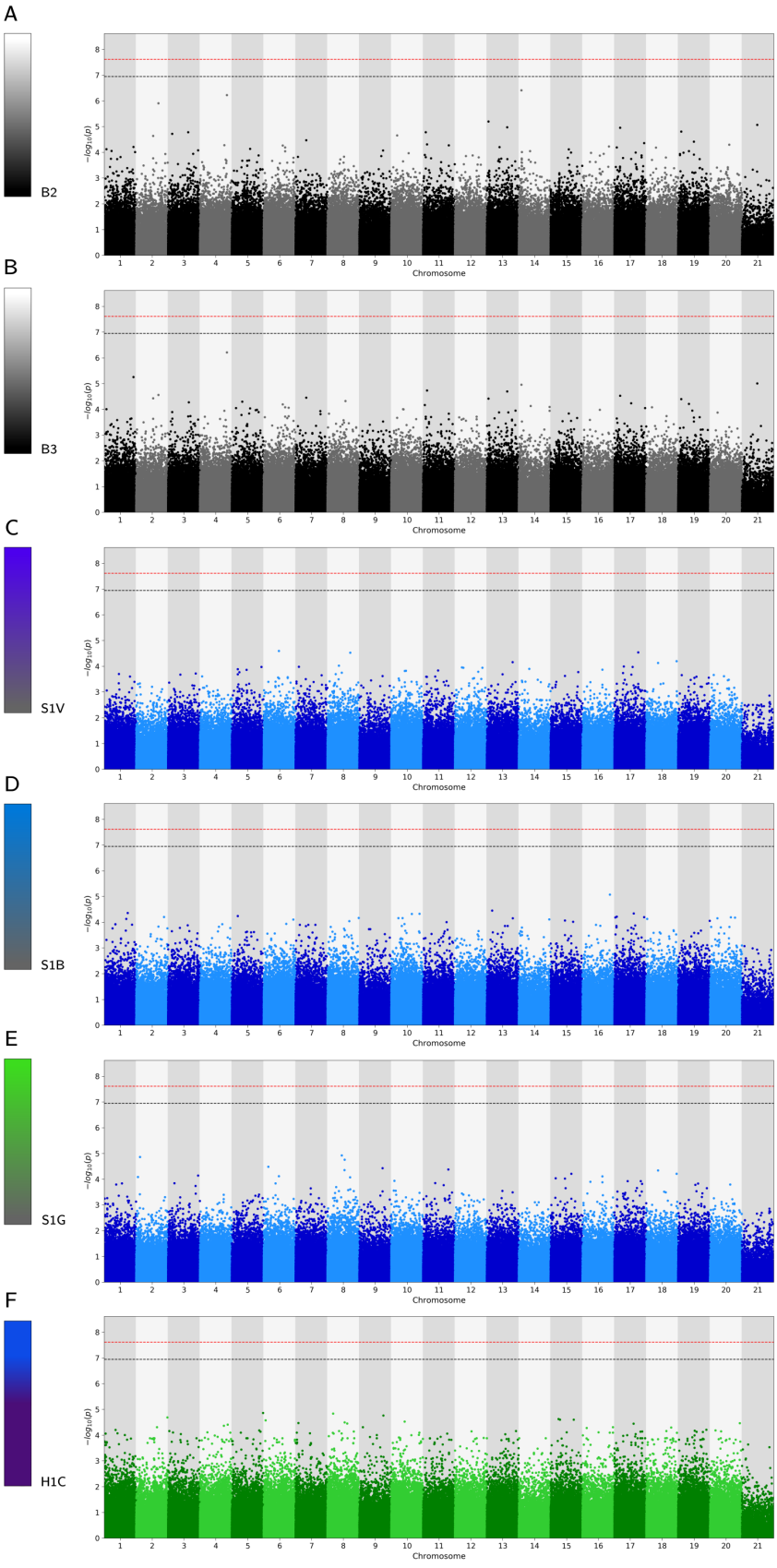

FIGURE 4.10: Genome wide association results for for colourimetric variables in *H. erato* excluding samples coming from Ecuador (*H. e. cyrbia*). No SNPs were significantly associated with variation in brightness (A, B) saturation (C, D, E) or hue (F). The negative logarithm of p-values is shown. Dashed lines correspond to Bonferroni corrected significance thresholds: Black, 0.05; red, 0.01.

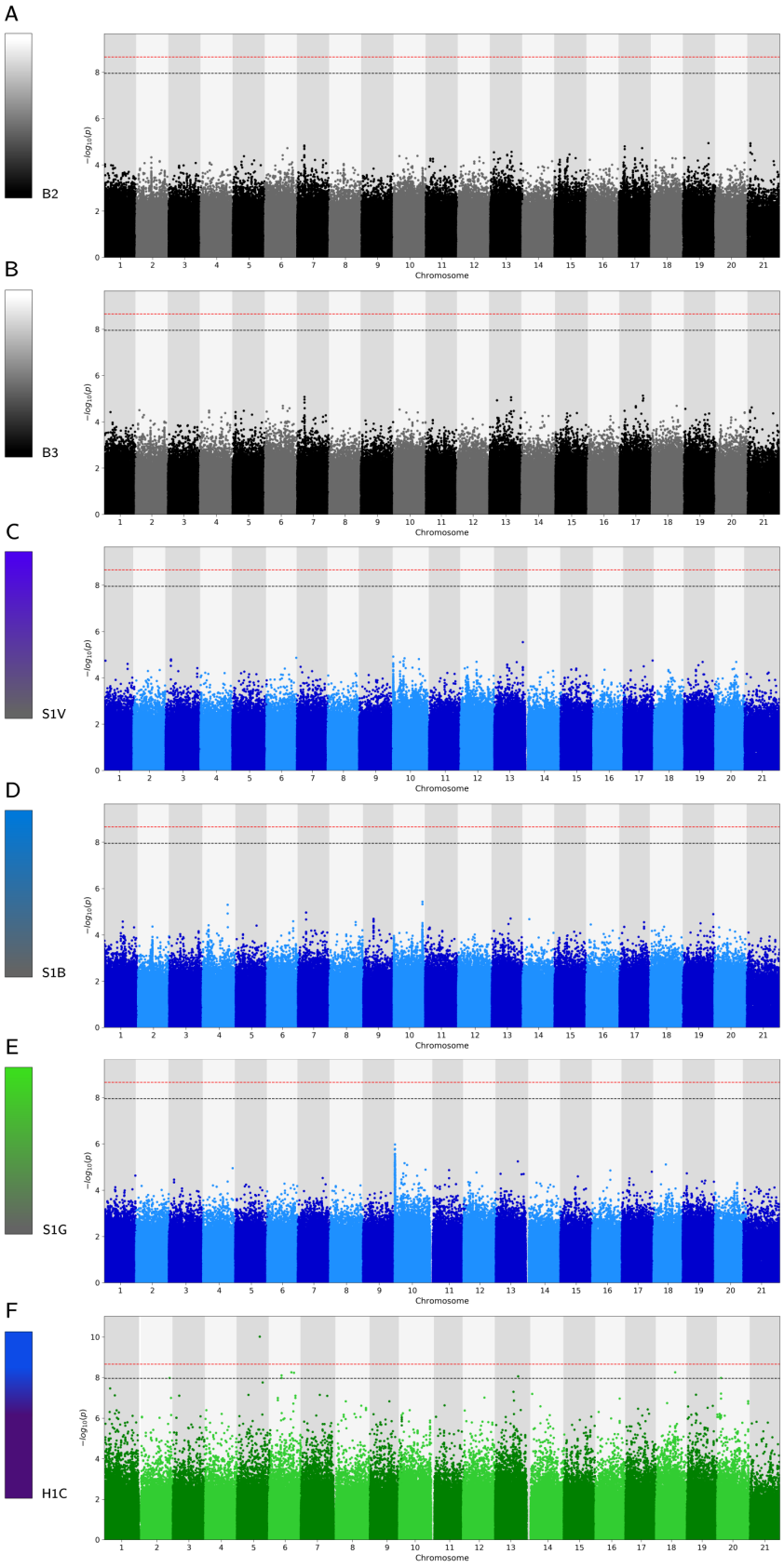

FIGURE 4.11: Genome wide association results for for colourimetric variables in *H. melpomene* excluding samples coming from Ecuador (*H. m. cythera*). No SNPs were significantly associated with variation in brightness (A, B) saturation (C, D, E) or hue (F). The negative logarithm of p-values is shown. Dashed lines correspond to Bonferroni corrected significance thresholds: Black, 0.05; red, 0.01.

4.5 Discussion

In this chapter our main aim was to discover genetic variants in both species that were associated with variation in structural colour, potentially having an effect on this trait. We also aimed to describe the variation in structural colour across a natural range for two *Heliconius* butterfly species using optical spectroscopy and to use this phenotypic variation for our genetic association analyses. We used population genetics analyses to assess the level of genetic structure in the natural populations, to analyse the GWAS results in the light of this natural genetic variation and to apply corrections for population structure in the genome-wide association analysis. Although we get good descriptions of the phenotypic variation and genetic structure across populations of both species, we do not identify significant associations of genetic variants with variation in structural colour in either of them. Nevertheless, we mention genes in both species that could potentially be associated with structural colour variation based on the top results of the association analysis.

4.5.1 Phenotypic variation in natural populations

Our analysis of structural colour as a set of colourimetric variables has allowed a precise description of its variation along a natural range. The estimates of structural colour variation we present are in good correspondence with the phenotypic gradient described for blue colour variation from photographs over similar geographic ranges of *H. erato* and *H. melpomene* (Curran et al., 2020). Properties of colour such as brightness, blue saturation and hue show a gradient of colour ranging from matt-black to blue along different localities across Panama, Colombia and Ecuador.

The ecological role of structural colour may have an effect on fine aspects of variation of this trait in nature, and may have had an impact on our measurements. At the moment, the ecology of structural colour in *Heliconius* butterflies remains largely unknown. We may hypothesise about possible interactions between ecology and observed phenotypic variation based on evidence from other butterfly species. For example, structural colour in *Colias eurytheme* is condition dependent and is involved in mate choice and quality signalling to potential mates (Kemp, 2007; Kemp et al., 2007). If structural colour is used similarly by *H. erato* and *H. melpomene* then it is reasonable to consider the possibility that our measurements of phenotypic variation could have been affected by variation in adult development conditions; previous work carried out in our research group suggests that this is the case for the species *Heliconius sara* and *Heliconius erato* (Brien, 2019). There was no way to correct for possible effects of condition dependence in our samples because they are collected as adults from the wild. We recognise the possibility that there is an effect of this on the phenotypic measurements that we took, and that its extent is unknown. In addition, the wearing of wings also has an effect on the visual properties of structural colour, particularly for older individuals and for those damaged due to manipulation. Age

and wear are two factors that could possibly be modelled so that their effects are accounted for in future measurements of structural colour.

4.5.2 Admixture and genetic structure

We found that relatively high levels of genetic structure have evolved between populations along the sampled range for both species. The structure patterns were similar for *H. erato* and *H. melpomene*; for both there appear clusters that are associated with the geographical distribution of their populations. This was observed in the admixture analysis and in the genetic PCA results.

The variance explained by PC1 was considerably high (19.63%) in *H. erato*. It is not uncommon to see explained variances with similar magnitudes in PCA using resequencing data in *Heliconius* butterflies (see Martin et al. 2016 and Van Belleghem et al. 2018). In these studies the variance is highest along the axis that differentiates populations with greater genetic structure and deeper phylogenetic splits the most (PC1). We believe that our PCA analysis shows that, in general, the sampled populations of *H. erato* have higher levels of genetic structure than populations of *H. melpomene*; this remark has also been done in previous studies involving both species (Curran et al., 2020). Although our observations are similar to those found by other researchers, we think that it is also possible that the there is an effect of the difference in the number of genotyped SNPs (higher for *H. melpomene*) on the difference in variance explained between species (19.63% vs. 5.25%).

The genetic structure patterns between populations of each species may have implications for the GWAS analysis. Despite the similarity in genetic structure patterns between species as observed in the PCA and admixture analyses, we found a greater extent of population structure for *H. erato* (higher variance explained in the first three principal components). This means that, in particular for this species, more spurious associations may be expected due to population structure and true associations will be more difficult to pick apart when applying a correction for population structure. Although this is expected when analysing both Mendelian and quantitative traits, the effect is likely higher for quantitative traits because they are expected to be controlled by several loci with mixed effect sizes. In the extreme case of genetic architecture fitting an infinitesimal model, it would be impossible to distinguish background genetic structure from association with loci controlling the quantitative trait. Although we did not formally test it, our data shows that variation in admixture proportion is possibly correlated with the phenotypic variation in structural colour. It is possible that including the population structure PCA as covariates masked real associations if these are also associated with the underlying population structure.

Our admixture analyses show a sharp shift in ancestry between Panamanian and

Colombian populations of both species. These populations show a phenotypic transition between black colour in Panama and blue colour in Colombia, showing a black-blue gradient that becomes brighter as latitude decreases (towards the south). The presence of a hybrid zone between black and blue populations should have been advantageous as we sampled hybrid individuals and possibly gene flow reduces the genetic structure between populations. Additionally, by including hybrids in our GWAS analysis we expected to have recombinant haplotypes that were possibly informative for SNPs associated with structural colour variation. Nevertheless, we think a more exhaustive sampling of hybrid individuals was required for our study. Lack of sampling in key localities between Panama and Colombia may have prevented us from having a more comprehensive set of genotype-phenotype combinations to be tested. This is especially important if the trait has variation due to the environment, as even more samples are needed for the linear models of the GWAS to estimate associations accurately. Sampling some areas between Jaque (Panama, loc. 7) and Bahía Solano (Colombia, loc. 8) would have been ideal for this study, as hybrid individuals with more West Colombian ancestry and possibly varying degrees of iridescence are expected to be found there. At the moment the region between these localities cannot be accessed safely due to public unrest.

It is still unclear whether structural colour evolves by recruiting the same genes in different populations of a single species. Sharp discontinuities in admixture proportions are observed between Colombian and Ecuadorian populations of both species. West-Colombian and Ecuadorian populations share the attribute of displaying iridescent blue colour in both species, albeit with differences in optical properties as seen in our results (Figs. 4.4 and 4.5) and as shown previously (Parnell et al., 2018). If the strong genetic structure and lack of admixed individuals we observe truly reflects a lack of contact between West Colombian and Ecuadorian populations it is possible that structural colour evolved independently in these populations. Therefore, our predictions of finding SNPs under the same QTL reported on Chapter 3 may deviate from potential significant associations, as only Panamanian and Ecuadorian populations were used for the crosses in that analysis. It is possible that different loci produce structural colour in West Colombian populations, and an interesting question could be whether replicate QTL and loci associated with structural colour are found in West Colombian and Ecuadorian populations.

4.5.3 Association analysis in traits with complex genetic architecture

We expected that having both 'pure' individuals and individuals with mixed ancestry would contribute to reveal genetic associations in either or both species. This expectation stems from the nature of the genomic assortment of haplotypes from different source populations, which requires the assumption of admixture between divergent lineages that are phenotypically different and come into contact in hybrid zones: In *H. erato* and *H. melpomene*, populations of West Colombia and Panama come into

contact in southern Panama (Jaque) producing individuals that are recombinant genetically and phenotypically (Curran et al., 2020; Mallet, 1986). If admixture LD is present (i.e. recombinant individuals have relatively large blocks of genomic material from parental populations), then the haplotypes harbouring alleles associated with structural colour should contribute to the observation of significant results in the association analyses (Buerkle et al., 2008).

The lack of significant results despite the presence of pure and recombinant individuals with varying levels of structural colour may be the result of the joint effect of a putatively complex genetic architecture and the breaking down of admixture LD across a high number of generations since admixture. We did not test for the presence/absence of admixture LD or the assortment of local ancestry across the genome in recombinant individuals, but we argue that it is possible that a high number of generations since contact between divergent populations have eroded admixture LD in individuals of the hybrid zone that we sampled. Using data from the same geographical area and assuming these hybrid zones are the result from secondary contact, it has been estimated that time since admixture can be up to 26 000 generations (Mallet, 1986). When compared to the number of generations since contact of other natural hybrids that have been used to map complex traits using hybrid populations (Bresadola et al., 2019; Lindtke et al., 2013) this number is substantially higher. As time since admixture increases, the power of studies using natural hybrids tends to decrease, possibly due to recombination of QTL and markers available (Lindtke et al., 2013).

In addition to being condition dependent in *Heliconius*, there is evidence for sexual dimorphism in *H. erato* as suggested by the results observed on Chapter 3 and those in Brien et al. (2018). This may have had an impact in our analysis. Condition dependent traits, especially those that are sexually selected, are expected to have a sparse genetic architecture with a large number of loci with additive small effects (Rowe et al., 1996). Castle-Wright estimators have been calculated for *H. erato* and *H. melpomene*. In both species the estimates suggest that the trait is controlled by more than one locus. Specifically, the estimates of loci underlying variation in structural colour were 4.6 for *H. erato* (Brien et al., 2018) and 6.9 for *H. melpomene* (Brien, 2019) and both of these are possibly underestimates of the true number of loci underlying structural colour (Brien et al., 2018). The fact that we have detected significant associations for the yellow hind-wing bar phenotype at a locus of large effect (the locus containing *cortex* gene) means that our study design has power to detect associations for loci of large effect despite high levels of population structure, especially when samples from the populations with the highest level of genetic differentiation are excluded. Nevertheless, the high number of loci that control structural colour in *Heliconius* and the presumed small additive effects that each locus contributes may have required more power to be detected.

4.5.4 Genes close to SNPs with highest score of association

We predicted that using GWAS we would find significant associations on chromosome 21 for *H. erato*, as suggested by evidence presented on Chapter 3 and also on chromosome 20, as suggested by a QTL analysis done using black-blue variation from digital photographs (Brien et al., 2021). For *H. melpomene*, evidence from Chapter 3 and from QTL analyses (Brien et al., 2021) suggests that loci are expected on chromosomes 3 and 7; this is under the assumption that the loci within the QTL are of large effect, which may not be the case if the high variance explained by the QTL is due to the Beavis effect. The *dsx* gene or its putative paralogs are also candidates for harbouring SNPs significantly associated with variation in structural colour as in other butterfly species these have been found to be involved in UV structural colour production (Rodriguez-Caro et al., 2021). Genes that are involved in processes related to the actin cytoskeleton are also predicted to have a role in structural colour, as evidence suggests that there is an active role of the actin cytoskeleton and chitin synthases in the production of the ridge morphology required for structural colour in lepidoptera (Lloyd et al., 2021).

Genes with the lowest p-values of association and that had a putative function potentially related to structural colour were found on chromosomes 1, 7, 9, 10 and 21 for *H. erato* and chromosomes 2, 6, 7 and 20 for *H. melpomene*. These SNPs largely miss the predictions made based on QTL positions, genes involved in structural colour production in other butterfly species, and genes with functions predicted to play key roles in the development of structural colour. There are two reasons why this may be the case: It is possible that these SNPs are truly not associated with structural colour (even if the function of nearby genes, as inferred from the biological processes found in UniProt, suggests a possible involvement). On the other hand they may contribute modestly to the additive genetic variation of structural colour and they missed the stringent significance thresholds used in our analysis or were swamped by the corrections applied for population structure. If structural colour in *H. erato* and *H. melpomene* is a trait with a sparse genetic architecture, some of these genes may harbour variants related to structural colour that may be further explored in future studies. However, in the absence of convincing evidence of association, even mentioning them as potential candidates is highly speculative.

We found little overlap with QTL of structural colour previously reported. The only SNP among those reported as top scoring that is within the confidence interval of the QTL reported on Chapter 3 and a QTL analysis of colour variation (Brien et al., 2021) in *H. erato* is Herato2101_9743064, within the z-chromosome QTL. This site is within the span of the gene evm.TU.Herato2101.331 (*dnah5*). In *Drosophila* this gene is involved in hearing (Senthilan et al., 2012), and it is predicted to enable microtubule motor activity (Gaudet et al., 2011). In *H. melpomene* the SNPs Hmel207001o_3013992 and Hmel207001o_3013998 were among the top scoring and are located on the same scaffold that the QTL reported for ridge spacing variation,

but they fall outside the 95% confidence interval estimated for this QTL and are ∼5.3 Mbp away from the lower bound of the QTL interval. The nearest genes to these SNPs are HMEL007133g1 and HMEL007134g1. HMEL007133g1 is the *ewc* gene, which is involved in imaginal disc morphogenesis and development of flight muscles in *Drosophila* (DeSimone et al., 1993). HMEL007134g1 is the gene *pcp52*, which is involved in the formation of the pupal cuticle in the wax moth *Galleria mellonella* (Kollberg et al., 1995).

The development of a butterfly scale involves the transformation of a single cell into a rigid chitin frame. In the early pupal stages cells protrude from the wing epithelium and progressively become flattened sac-like structures as the pupa develops. In the final stages the scale cell dies and leaves an air-filled chitin structure; the adult wing scale. During this process microtubules and actin bundles (Dinwiddie et al., 2014; Greenstein, 1972a; Overton, 1966) as well as enzymes involved in the synthesis of chitin play a central role in the sculpting of scales (reviewed in Lloyd et al. 2021). In particular, the actin cytoskeleton has been linked to the development of the scale structures that produce structural colour. In *H. melpomene* high scoring SNPs were found in close proximity to genes that are related to actin cytoskeleton and actin filament organization according to their UniProt description. We further explored the function of these genes in *Drosophila* and other insects such as *Bombyx mori* (where possible) to assess the possibility that they have a role in *Heliconius* that is relevant for structural colour production. HMEL014725g1 is the gene *itpka*, which in *Drosophila* regulates autophagy in cells of the salivary gland (Nelson et al., 2014). HMEL008033 is the *nimrod-2* gene, which is involved in immune response against bacteria in *Drosophila* (Hashimoto et al., 2009), the silkworm *Bombyx mori* (Gul et al., 2021), and possibly has the same function across a large phylogenetic scale in insects. HMEL009603g1 is the gene *coronin*, which has a role in actin cytoskeleton re-organisation during axon growth in *Drosophila* (Rothenberg et al., 2003). Again, to our best knowledge none of these biological processes is relevant to the production of structural colour.

4.6 Conclusions and next steps

Structural colour possibly has a complex genetic architecture including genes of small effect in the co-mimics *H. erato* and *H. melpomene*. The complexity of the trait may not be limited to its genetic architecture. Different populations within a single species show different optical properties of structural colour, raising the question of whether they have evolved only once or multiple times, perhaps using different genes, within a single species. The possibility that this trait has evolved using different genes in different populations is an interesting future research question to address, as it would allow to explore in more detail the mode of evolution of quantitative traits.

Our samples were a comprehensive set which included the full range of natural variation in structural colour in nature but significant results were not observed. We hypothesise that the putative small effects of loci controlling the trait were swamped by the high levels of genetic structure. Either a more exhaustive sampling in hybrid zones or alternative methods could alleviate this.

One possibility to dissect the complex genetic architecture of structural colour in *Heliconius* using unrelated samples is to use genomic prediction. In particular, genomic prediction methods that are capable of modelling Mendelian and quantitative traits are promising. Similarly to GWAS these methods also require low levels of genetic structure among samples and a high number of individuals. They have been used successfully to describe the genetic architecture of traits with varying levels of heritabilities and effect sizes (Hunter et al., 2021; Moser et al., 2015).

4.7 Contributions to this chapter

Wings, DNA extractions and sequencing of the majority of the Ecuadorian individuals were contributed by Gabriela Montejo-Kovacevich and Chris Jiggins from the Buterfly Genetics Group at the University of Cambridge. DNA extractions of a large part of individuals from Panama and Colombia were done by Emma Curran. Wings and tissue of individuals from Central Colombia and some of the samples from West Colombia were contributed by Camilo Salazar and Carolina Pardo from the Evolutionary Genetics Group at Universidad del Rosario (Colombia). Phenotyping, DNA extractions and data analysis were done by Juan Enciso. Sequencing was done by NovoGene.

4.8 Supplementary material

FIGURE S4.1: Hindwing phenotypes on the dorsal and ventral sides across the whole range of samples used. The phenotypes shown here are from *H. erato*, but for the co-mimic species *H. melpomene* equivalent phenotypes are found. The phenotypes are labelled taking into account dorsal and ventral sides jointly.

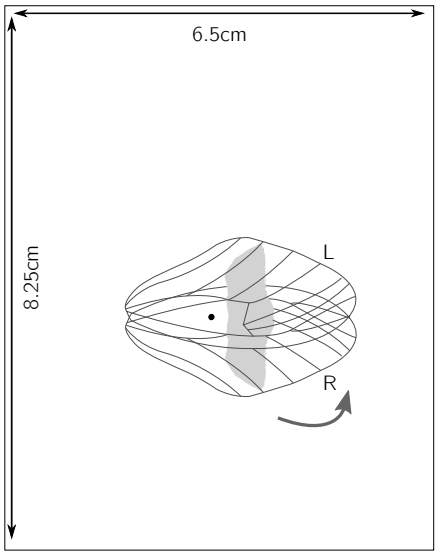

FIGURE S4.2: Scheme of the setting used when probing forewings with the spectrophotometer. The grey curved arrow shows the direction of rotation for sampling several angles. The black circle represents the initial position of the probe on the discal wing. Left and right fore-wing positions are demarcated with wing models (L,R); both are set using the same horizontal orientation.

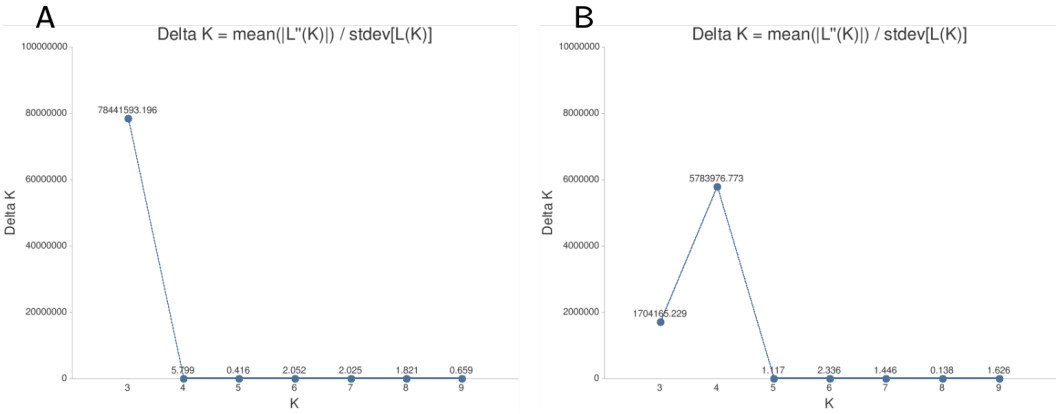

FIGURE S4.3: Best K according to Evanno test for *H. erato* (A) and *H. melpomene* (B).

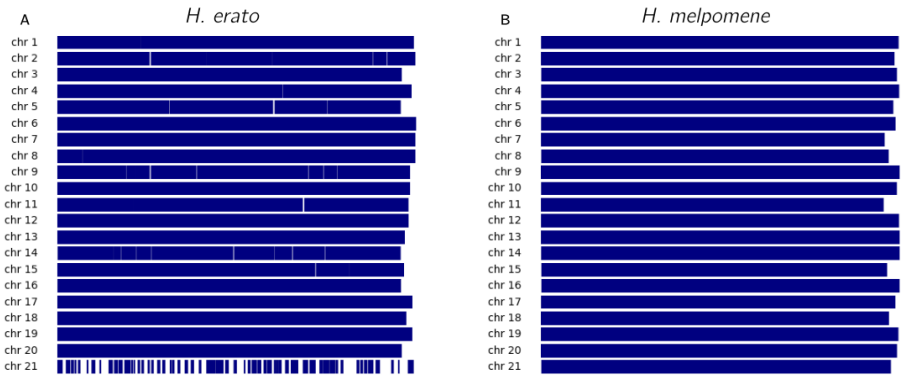

FIGURE S4.4: SNP densities per chromosome in *H. erato* (A) and *H. melpomene* (B).

TABLE S4.1: Descriptive statistics of density of markers used for the association analysis in *H. erato* and *H. melpomene*. For all chromosomes in both species the minimum distance between markers was 0.

Chromosome	Average	Maximum	Median	Std. deviation
H. erato				
1	1062	115 928	15	4056
2	845	132 250	13	4595
3	846	97 571	10	4304
4	742	89 098	9	3975
5	805	126 033	10	4249
6	732	88 150	11	3451
7	1029	78 756	14	3942
8	508	83 703	7	3175
9	1229	114 816	12	5635
10	877	54 870	15	3195
11	982	142 390	10	4843
12	937	87 710	13	3739
13	1014	118 730	13	3791
14	1233	106 243	11	5794
15	861	121 863	11	4697
16	833	89 325	11	3868
17	803	87 068	13	3530
18	1025	91 361	14	3664
19	958	78 599	13	3728
20	1103	74 951	13	4168
21	4516	763 442	8	34 151
H. melpomene				
1	555	26 564	166	987
2	571	17 860	138	1092
3	629	22 808	160	1207
4	553	39 216	146	1064
5	531	21 032	135	1037
6	605	29 945	166	1168
7	539	19 034	152	1018
8	524	32 150	129	1128
9	527	26 220	134	990
10	571	21 670	167	990
11	595	36 497	153	1086
12	567	28 290	157	1006
13	621	40 463	180	1252
14	571	42 365	137	1228
15	565	52 565	133	1309
16	553	24 841	149	1015
17	608	46 766	169	1179
18	573	43 133	170	1042
19	625	26 671	184	1148
20	566	49 610	163	1131
21	1543	35 319	543	2410

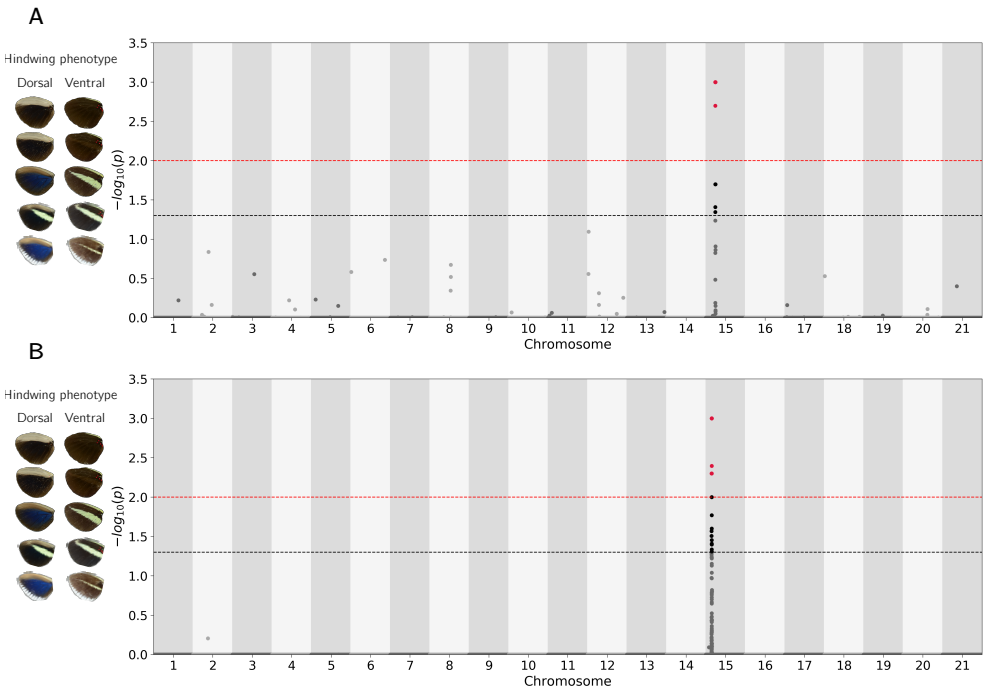

FIGURE S4.5: Genome wide association results for hind-wing yellow bar variation across samples from the full set of samples of *H. erato* (A) and *H. melpomene* (B). The negative logarithm of empirical p-values is shown. Dashed lines correspond to significance thresholds: Black, 0.05; red, 0.01.

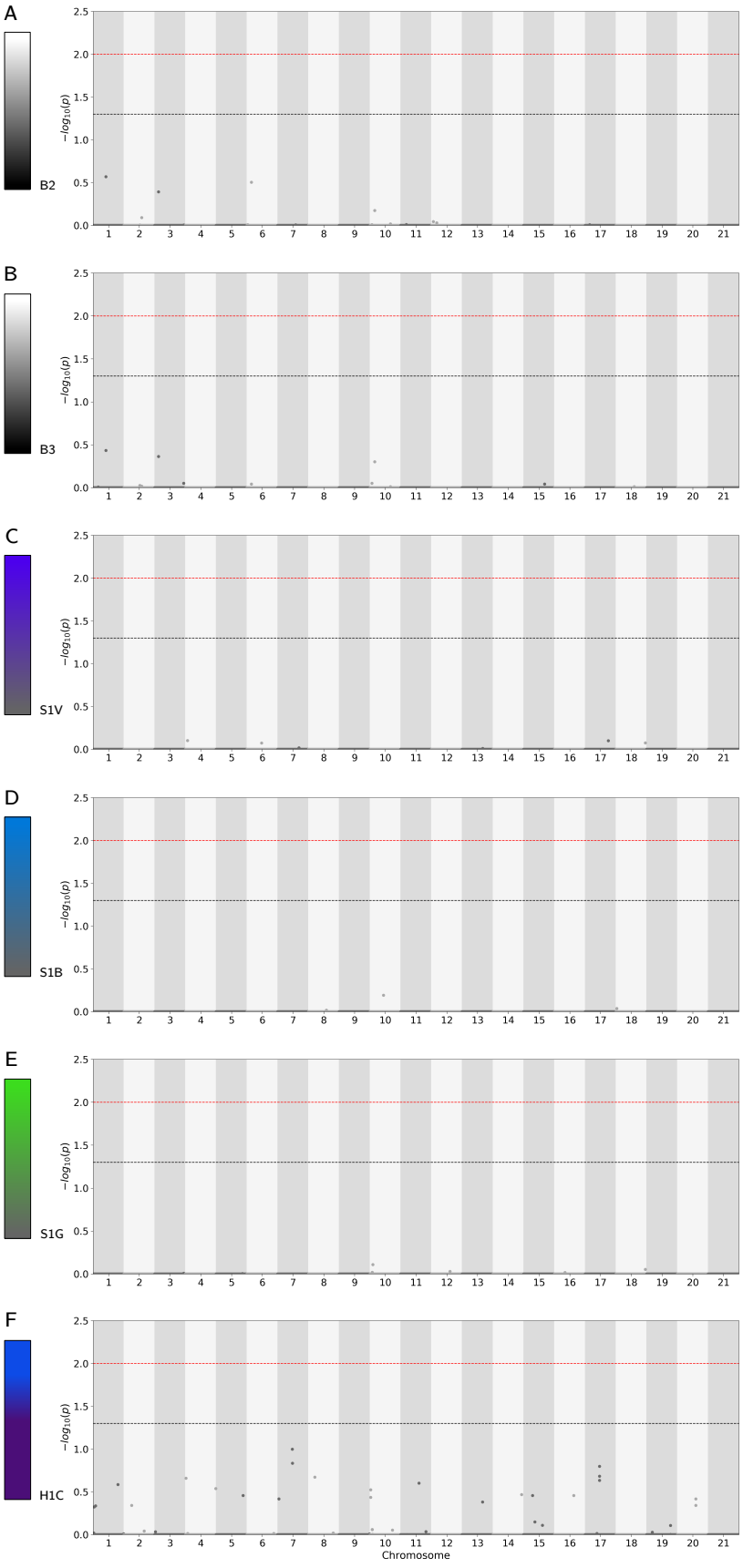

FIGURE S4.6: Genome wide association results for colourimetric variables in *H. erato*. No SNPs were significantly associated with variation in brightness (A, B) saturation (C, D, E) or hue (F). The negative logarithm of empirical p-values is shown. Dashed lines correspond to significance thresholds: Black, 0.05; red, 0.01.

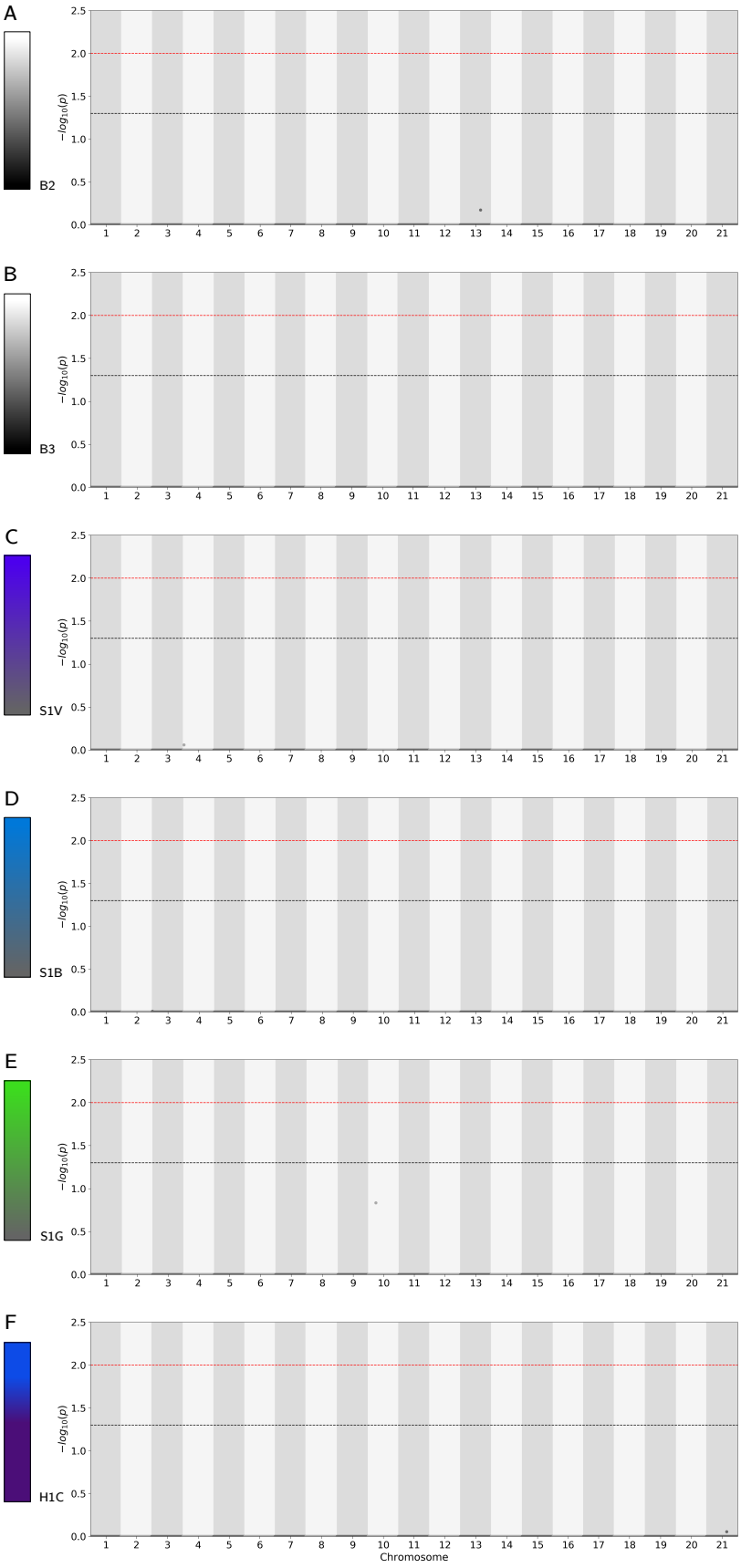

FIGURE S4.7: Genome wide association results for colourimetric variables in *H. melpomene*. No SNPs were significantly associated with variation in brightness (A, B) saturation (C, D, E) or hue (F). The negative logarithm of empirical p-values is shown. Dashed lines correspond to significance thresholds: Black, 0.05; red, 0.01.

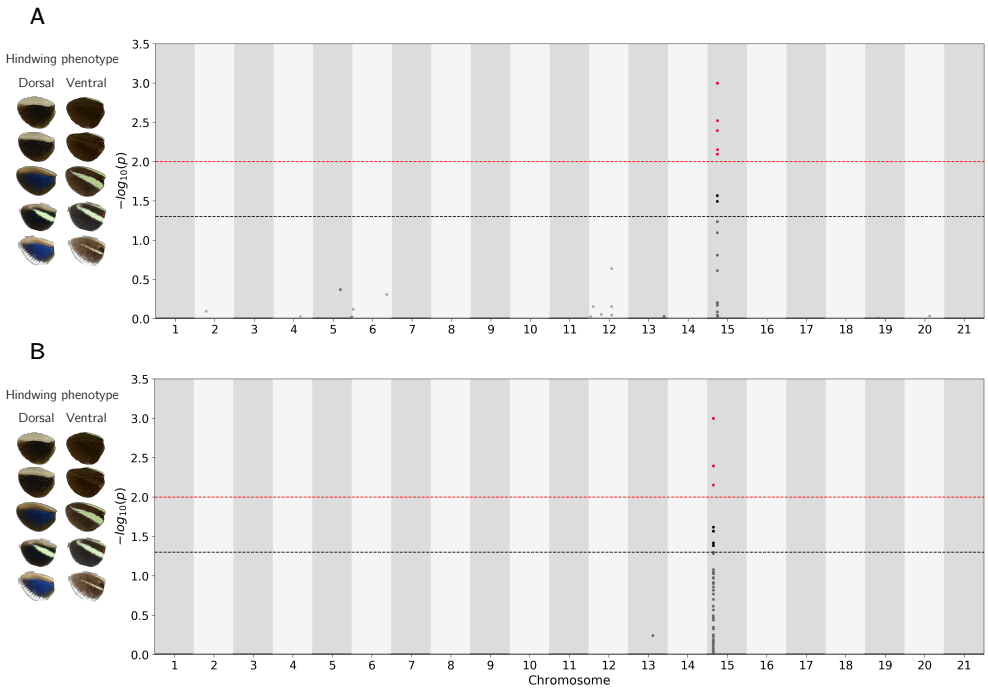

FIGURE S4.8: Genome wide association results for hind-wing yellow bar variation across samples from the set of samples excluding Ecuador localities of *H. erato* (A) and *H. melpomene* (B). The negative logarithm of empirical p-values is shown. Dashed lines correspond to significance thresholds: Black, 0.05; red, 0.01.

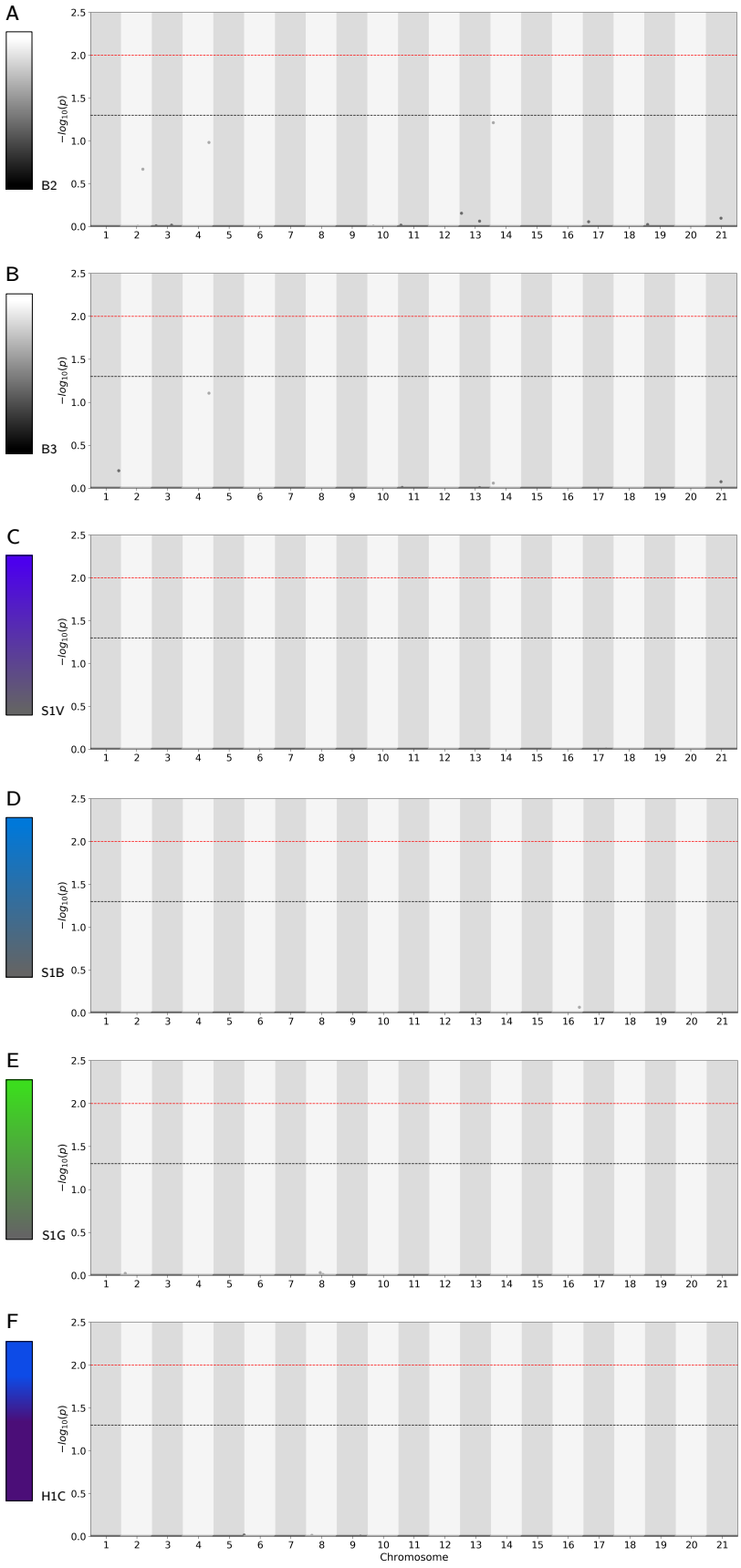

FIGURE S4.9: Genome wide association results for for colourimetric variables in *H. erato* excluding samples coming from Ecuador (*H. e. cyrbia*). No SNPs were significantly associated with variation in brightness (A, B) saturation (C, D, E) or hue (F). The negative logarithm of empirical p-values is shown. Dashed lines correspond to significance thresholds: Black, 0.05; red, 0.01.

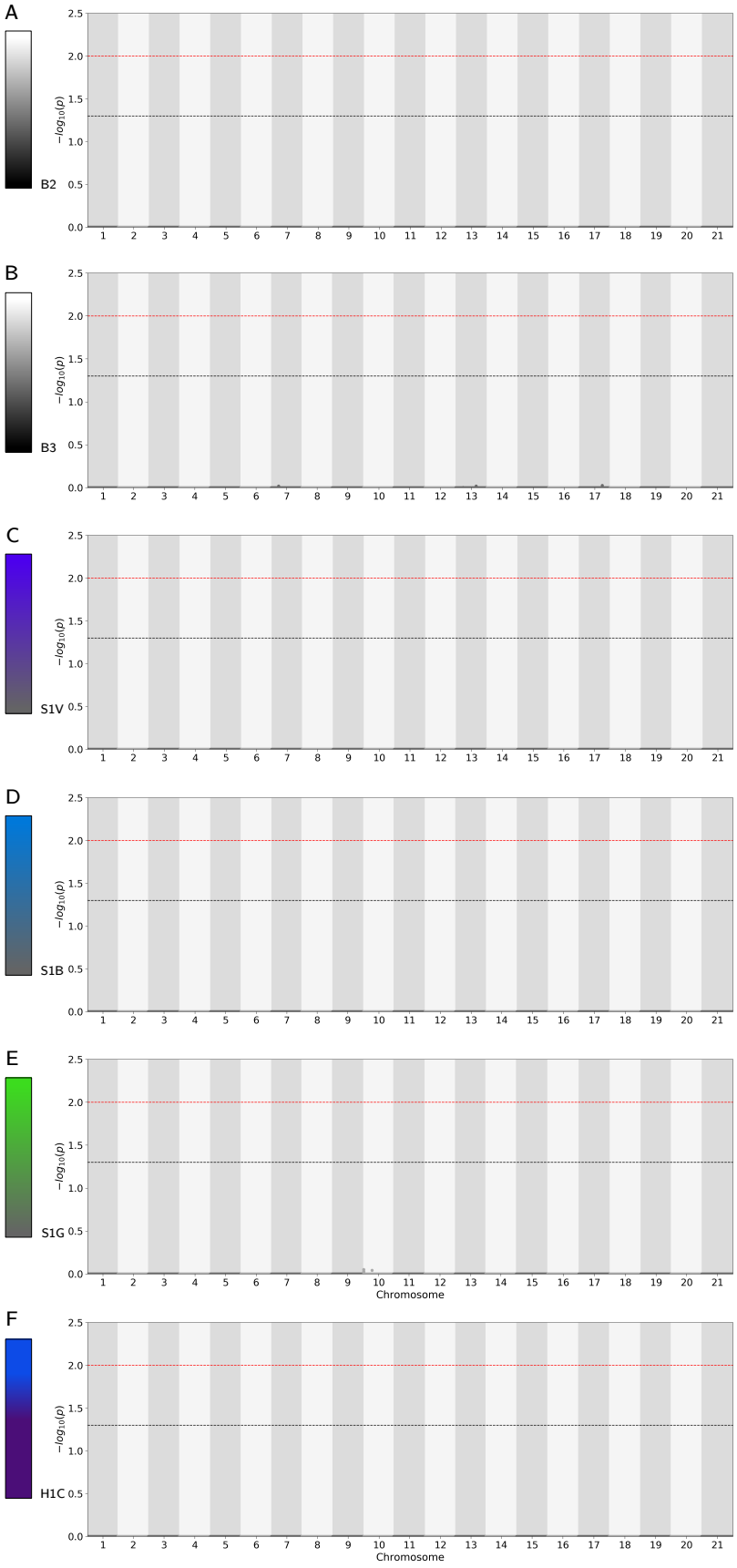

FIGURE S4.10: Genome wide association results for for colourimetric variables in *H. melpomene* excluding samples coming from Ecuador (*H. m. cythera*). No SNPs were significantly associated with variation in brightness (A, B) saturation (C, D, E) or hue (F). The negative logarithm of empirical p-values is shown. Dashed lines correspond to significance thresholds: Black, 0.05; red, 0.01.

Chapter 5

General discussion

5.1 Research summary and significance of thesis findings

In Chapter 2 I characterised and analysed variation in scale structure and structural colour in two co-mimic *Heliconius* species. I combined microscopy (SEM), X-ray diffraction (USAXS) and colour variation data to describe phenotypic variation in wild caught individuals and offspring from crosses between blue and matt-black races. Like other butterfly species that produce structural colour using multi-layered ridges (Ghiradella et al., 1972; Kemp et al., 2006; Kinoshita, Yoshioka, and Kawagoe, 2002), blue individuals of *H. erato* and *H. melpomene* show narrow ridge spacing. This reinforces the idea of narrow ridge spacing as a trait strongly associated with structural colouration. This association was observed in the analysis of variation in scale structure using individuals from several natural populations of *H. erato* and *H. melpomene* from Panama, Colombia and Ecuador, and also in individuals from artificial populations produced via controlled crosses. Observations of narrow ridge spacing in structurally coloured scales are not limited to fully developed adults. Developing scales localised in silver patches of *Vanessa cardui* show F-actin bundles with a tighter distribution than those observed in scales that contain pigment colour only (Dinwiddie et al., 2014). Cross-rib spacing variation show weak or no correlation with colour variation in most cases, which suggests that this aspect of scale structure is not very important for structural colour production and that significant correlations observed are possibly due to correlations with ridge spacing, where present. High variance in scale morphology within localities, in hybrid populations and F2 cohorts suggest that a complex genetic basis underlies ridge spacing variation.

In Chapter 3 I investigated the genetic basis of the scale morphology and colour variation described in Chapter 2 using QTL analyses. Scale morphology, specifically ridge spacing, has a genetic basis that could partially be described in both species. In contrast, cross-rib spacing does not seem to be associated to any particular locus. This could be due to a lack of genetic variation for this trait in our crosses, or individual loci have small effects, which we lack the power to detect due to low numbers of samples.

For colour variation, I found strong evidence for QTL associated to luminance but not for blue colour variation in both species. Differences between the co-mimic *H. erato* and *H. melpomene* were found both in genetic architecture of scale morphology and colour; while in *H. erato* both ridge spacing and luminance map to the sex chromosome, in *H. melpomene* ridge spacing and luminance map to two separate autosomes. A major result of this chapter is that there is a lack of genetic parallelism for scale morphology and structural colour in two co-mimic species whose adaptive morphological evolution has been largely driven by genetic parallelism.

None of the QTL contained or overlapped known loci of large effect that control pigmented wing patterns in *Heliconius* butterflies. In *Heliconius* some genes of large effect like *cortex* and *WntA* have been reported to modify scale structure (Concha et al., 2019; Livraghi et al., 2021). In other nymphalid butterflies like *Bicyclus anynana* genes in the melanin and ommochrome pathways have been shown to modify scale size, ridge spacing, cross-rib spacing and thickness of cross-ribs in pigmented scales (Matsuoka et al., 2018). Although several genes involved in pigment pathways seem to have effects on scale morphology, these effects are likely specific to pigment deposition in the scales and unrelated to structural colour production. Furthermore, pigment genes that have effects on aspects of scale morphology that are relevant for structural colour production (e. g. ridge spacing) may lack important interactions with other genes or pathways that control other aspects that may be also necessary for structural colour (e. g. the multi layer lamellae within each ridge) or may not be the only genes affecting said morphological aspects.

In Chapter 4 I aimed at both finding additional loci significantly associated with structural colour variation and also refining the positions of the loci found in Chapter 3 by finding significant SNPs within the confidence intervals estimated for each QTL. I did GWAS analyses using continuous variation in structural colour in both *H. erato* and *H. melpomene* including populations from Panama, West and Central Colombia, and West Ecuador which comprise the full range of structural colour variation in these species. I performed population genomics analyses to understand, quantify and use population structure in the GWAS as a covariate for reducing inflation of the association statistics due to genetic divergence among individuals. We observed relatively high levels of genetic structure in both species, albeit consistently higher in *H. erato*, which confirms previous observations (Curran et al., 2020) and may imply that in this species I could have a higher chance of type I error. Therefore, in a GWAS I expected either false positive significant associations or losing true positive associations due to over-correction for genetic structure, especially because phenotypic variation and genetic structure seem to correlate. This effect is expected to be higher for quantitative traits if these are controlled by several genes of medium or small effect. I didn't find significant associations for structural colour variation in either species, even when excluding the populations with the highest observed population stratification. This is in contrast to results of an additional GWAS done on a discrete trait with a known

Mendelian genetic basis for which I consistently found significant associations at the expected locus. I interpret these results jointly and argue that structural colour variation possibly has a polygenic genetic basis where SNPs of moderate to small effect may not have been detected due to a combination of factors that may affect GWAS (Santure et al., 2018). Specifically, our observations are probably chiefly due to lack of power, which has been shown to be one of the main factors affecting GWAS when effect sizes are small (François et al., 2018). Several populations showing varying levels of structural colour were included in the GWAS and lumped together to increase statistical power. I also argue that it is possible that structural colour has evolved via different genetic pathways in different populations, although that assertion is highly speculative and would need to be tested in future studies.

5.2 *Heliconius* structural colour: Outstanding questions and next steps

5.2.1 Studying phenotypic variation

During this thesis I used different approaches to measure and quantify phenotypic variation related to structural colour in the co-mimics *H. erato* and *H. melpomene*. It has been suggested that colour measurements from butterfly wings, especially those of wild caught individuals, may be distorted due to damage on the wing or age of the individual and that one way to overcome these potential problems is characterising variation in scale nano-structures (Curran, 2018). In Chapters 2 and 3 I focused on variation in scale structure, and complemented these observations with measurements of colour taken previously on the samples I worked with. This allowed me to characterise to some extent how scale morphology co-varies with structural colour in natural populations and resulted in insights on what are the possible developmental boundaries of scale architecture of both species, which aspects selection may be targeting and more importantly that the underlying genetic architecture behind this variation is probably not the same between *H. erato* and *H. melpomene*. Despite our efforts to characterise scale structure variation in minute detail, important aspects of scale structure of our samples remain unexplored.

In butterflies that use their ridges to produce structural colour (like *H. erato* and *H. melpomene*), it is known that the cuticle lamellae in the ridges of the scale make up a multi-layer structure that produces colour by constructive interference of a visible wavelength (Ghiradella, 1974; Kinoshita, Yoshioka, and Kawagoe, 2002; Vukusic et al., 1999). Specifically, the reflectance of the colour increases rapidly with a small increase in the number of layers (Kinoshita et al., 2005), and the hue depends on the thickness of the lamellae (Vukusic et al., 1999). Therefore, identifying how the inner structure of the ridges and the multi-layered lamellae varies across the matt-black — blue phenotypic gradient remains a key goal for understanding structural colour variation. Although our SEM and USAXS experiments allowed the recognition

and description of important differences, they did not allow this important detailed examination. I propose two approaches that can be followed so that a more complete description of scale structure can possibly be achieved.

First, I propose to add a complementary microscopy experiment to the results that we present in Chapter 2 of this thesis. Transmission electron microscopy (TEM) has been successfully used in the past to study cross-sections of scales of several species of iridescent butterflies and describe their physical and optical properties (Ghiradella et al., 1972; Vukusic et al., 1999). TEM would allow us to reveal the inner structure of the ridges in *Heliconius* thus enabling us to describe the morphological changes that take place between iridescent and non-iridescent butterflies with more precision. Alternatively, a similar experimental approach such as ion microscopy could be used to this end. For example, focused ion beam microscopy has been used recently to analyse the cross section of iridescent scales of some butterfly species, revealing important details of nano-structure variation (Parnell et al., 2018; Thayer et al., 2020). The success of these methods is highly contingent on available budget and availability of equipment and an experienced microscopist.

A second approach I suggest involves the use of an *in silico* procedure. This technique may complement the results obtained in TEM experiments or the observations of variation that I report on chapter 2. Ideally, the results of TEM experiments can be used as templates to FDTD (finite difference time domain) simulations. In these simulations, light as an electromagnetic wave is simulated to pass through a di-electric material (chitin). The structure of the scale can be set to have the physical properties of chitin, such as a defined diffraction index and an electromagnetic constant. A portion of the incoming radiation is expected to be reflected back from the chitin template and reveal the properties of the structural colour that could be expected from such interaction. This approach has been used in the field to simulate the effect of the nano-structures in the wings of the iconic *Morpho* butterflies (Zhu et al., 2009), the effect of scale trabeculae in ultra-black butterfly scales (Davis et al., 2020) and the production of structural white colour in beetles (Burg et al., 2019). If TEM results are not available some aspects of the ridge architecture can be drawn from the literature to complement the estimates of ridge spacing and cross-rib spacing variation that I report and an FDTD analysis can be run with these parameters to further investigate the role that ridge spacing and cross-rib spacing play for *Heliconius* iridescence.

5.2.2 Finding the genetic architecture and molecular basis of structural colour production

Despite using different approaches to study and describe the genetic basis of structural colour, the results reported in this thesis are limited to single out QTL of colour and scale structure variation, and describing their putative genetic basis in two *Heliconius* co-mimics. Since the amount of explained variation from QTL was relatively high, we expected to find SNP associations within their span, but such associations were

not found. The lack of concordance between QTL and GWAS may be due to several factors. It has been suggested that mapping efforts in wild populations could benefit from using extreme phenotypes to increase the chance of finding statistical associations with a modest number of samples (Emond et al., 2012). Although this approach may have proven effective in particular scenarios, it is prone to lose power when analysing sparse genetic architectures and high levels of genetic structure are present (Kardos et al., 2015). The inclusion of extreme phenotypes in my analyses implied using populations with high genetic divergence, which could have produced similar issues. I believe that modifying the sampling scheme can help alleviate this problem in future GWAS analyses. Future efforts of GWAS on structural colour should focus on sampling large numbers of individuals with mixed ancestry that display relevant and sufficient phenotypic variation. Using a large proportion of samples with mixed ancestry or exclusively individuals from hybrid zones has enabled the mapping of complex traits in several species (Brelsford et al., 2017; Bresadola et al., 2019; Lindtke et al., 2013; Pallares et al., 2014). A disadvantage of this approach in the particular case of *Heliconius* is that hybrid zones of iridescent and matt-black individuals are located in areas where access is very limited due to public unrest.

In the short term and with the data available we can use alternative methods to GWAS to describe the genetic basis of a complex trait like structural colour. Chromosome partitioning is a useful method for testing for polygenic architecture; this is done by regressing the phenotypic variance explained per chromosome against the length of each chromosome (Kemppainen et al., 2018; Yang et al., 2011). Chromosome partitioning is known to be sensitive to several factors including trait heritability, chromosome size ranges and sample size (Kemppainen et al., 2018). Sample size is low in our case and so results would require a careful and conservative interpretation. Bayesian methods that estimate genetic variance explained by groups of SNPs and model the effects of SNP variants as a mixture of effect distributions may also be useful for describing the genetic basis of structural colour. These methods have been used to identify genetic variants associated with complex diseases in humans, infer their genetic basis and predict phenotypes and risk of disease given the genetic information of sampled individuals (Moser et al., 2015). These methods are not without challenges, as they also depend on sufficient sampling and moderate to high trait heritability.

The challenges imposed by restricted access to important sampling areas and other caveats inherent to analysing variation in wild individuals may be overcome using molecular methods that allow an exploration gene expression or gene accessibility during wing or scale development. For example, transcriptomics analyses have been utilised in conjunction with genome-wide association studies to characterise colour pattern genes (Nadeau et al., 2016; Saenko et al., 2019), and to further explore the dynamics between genes during development of different wing patterns (Hanly et al., 2019). Expression profiles of iridescent and matt-black individuals of Ecuadorian and Panamanian races have been analysed jointly with the QTL found on Chapter 3 of

this thesis and those found previously for iridescent colour variation revealing genes that may be involved in structural colour production (Brien et al., 2021). Another technique that could be used is an assay for transposase-accesible chromatin with high-throughput sequencing (ATAC-Seq). It has been noted that during the development of scales only a small fraction of DNA is accessible (Greenstein, 1972b), which possibly harbours genes and regulatory regions that may be different between blue and matt-black individuals. These differences could possibly be assessed and described by sequencing free DNA during scale development. ATAC-Seq has allowed detailed characterisation of the role of the *cortex* gene and its neighbouring putative regulatory elements on wing patterns and scale structure in *Heliconius* butterflies (Livraghi et al., 2021). These assays can be made more precise by the use of single cell sequencing techniques, which allow the interrogation of a targeted population of cells in the wing (Kalisky et al., 2011).

The repeatability of evolution is a matter of debate in biology and structural colour in *Heliconius* offers an opportunity to explore it beyond the results reported in Chapter 3 of this thesis. In Chapter 4 I suggest that it is possible that different populations of *H. erato* and *H. melpomene* have evolved structural colour independently using different genes, and that this could have had consequences on the lack of significant peaks in the GWAS analyses. Further research questions can be formulated that aim to address the repeatability of evolution in a different phylogenetic context than was addressed on Chapter 3: have different populations within each of these *Heliconius* species evolved structural colour using different genetic pathways? This is difficult to predict as the literature has seemingly contrasting answers. While in some organisms a high degree of genetic parallelism is observed between closely related lineages (Deagle et al., 2013), in others there is partial or no reuse of the same loci during adaptation (Elmer et al., 2011; Gagnaire et al., 2013). It has been suggested that the same genetic mechanisms are more likely to be used if there is a shared pool of standing variation prior to lineage splitting, which in turn is more common with less time of divergence between lineages (Conte et al., 2012). Additional QTL experiments can be done for each species using different races or populations that show iridescence and crossing these with matt-black populations. Then the resulting QTL can be compared within each species to further explore the degree of genetic parallelism, or lack thereof, that underlies phenotypic evolution in each of the iridescent populations.

5.2.3 The ecology and adaptive role of structural colour

It is still unclear what role structural colour plays for *Heliconius* butterflies. Although the scope of this thesis is the characterisation of structural colour variation and its genetic basis, understanding aspects such as its ecological relevance and adaptive value can give insights into its evolution in natural populations, its putative genetic architecture and the differences and relationships that may exist with other important traits (Linnen et al., 2009) such as pigmented wing patterns in this particular case.

There are different hypotheses about the function of structural colour in *Heliconius*. Evidence from visual models and hybrid zone analyses suggests that selection regimes of pigmented and structural colour are coupled and perhaps are both part of the warning signal since they are both visible by potential predators (Curran et al., 2020; Parnell et al., 2018). On the other hand it has been suggested that structural colour is involved in long distance mate recognition (Sweeney et al., 2003) and that it is sex-linked and condition dependent (Brien, 2019; Brien et al., 2018). Sex linkage may suggest a role of structural colour in sexual selection in *Heliconius*, although this is speculative and needs to be tested; for the sake of the argument we may assume this is true. In addition, we may consider that condition dependent sexually selected traits are possibly controlled by a large number of loci with small effects (Rowe et al., 1996). This would explain the striking differences in genetic architectures between pigmented patterns and structural colour observed in this thesis. More efforts studying the ecological role of structural colour in *Heliconius* and its relationship with pigmented patterns are required to confirm this and would help build a more general understanding of relationships between ecology, evolutionary dynamics and genetic architecture of adaptive traits.

5.3 Conclusions

The study of phenotypic variation in scale structure and structural colour in this thesis has allowed the understanding of biological aspects of the *Heliconius* scale and structural colour; its distribution in natural populations, mechanisms of inheritance, genetic architecture and evolutionary dynamics. It also contributes to long standing discussions in evolutionary biology such as the mode of evolution of adaptive traits and their genetic architecture. My work on structural colour builds on top of and complements previous theses in Nicola Nadeau's laboratory showing that co-mimics *H. erato* and *H. erato* have evolved adaptive traits both by selective sweeps at warning colour loci (Moest et al., 2020) and likely by polygenic adaptation in the case of structural colour. Future work should focus on more detailed characterisations of scale structure and more refined molecular techniques to further discover the genes and developmental pathways involved.

Bibliography

Altschul, S. F. et al. (Oct. 1990). "Basic local alignment search tool". In: *Journal of Molecular Biology* 215.3, pp. 403–410.

Anderson, T. F. and A. G. Richards (1942). "An Electron Microscope Study of Some Structural Colors of Insects". In: *Journal of Applied Physics* 13.12, pp. 748–758.

Andrews, S. et al. (Jan. 2012). *FastQC*. Babraham Institute. Babraham, UK.

Araki, Y. and T. Sota (Dec. 2020). "Population genetic structure underlying the geographic variation in beetle structural colour with multiple transition zones". In: *Molecular Ecology*.

Aulchenko, Y. S., D.-J. de Koning, and C. Haley (July 2007). "Genomewide Rapid Association Using Mixed Model and Regression: A Fast and Simple Method For Genomewide Pedigree-Based Quantitative Trait Loci Association Analysis". In: *Genetics* 177.1, pp. 577–585.

Badyaev, A. V. (May 2005). "Stress-induced variation in evolution: from behavioural plasticity to genetic assimilation". In: *Proceedings of the Royal Society B: Biological Sciences* 272.1566, pp. 877–886.

Bainbridge, H. E. et al. (Oct. 2020). "Limited genetic parallels underlie convergent evolution of quantitative pattern variation in mimetic butterflies". In: *Journal of Evolutionary Biology* 33.11, pp. 1516–1529.

Bateman, A. et al. (Nov. 2020). "UniProt: the universal protein knowledgebase in 2021". In: *Nucleic Acids Research* 49.D1, pp. D480–D489.

Baxter, S. W. et al. (Apr. 2011). "Linkage Mapping and Comparative Genomics Using Next-Generation RAD Sequencing of a Non-Model Organism". In: *PLoS ONE* 6.4. Ed. by P. K. Ingvarsson, e19315.

Beavis, W. D. (1994). "The power and deceit of QTL experiments: lessons from comparative QTL studies." In: *Proceedings of the forty-ninth annual corn and sorghum industry research conference*, pp. 260–266.

Belleghem, S. M. V. et al. (Apr. 2018). "Patterns of Z chromosome divergence among Heliconius species highlight the importance of historical demography". In: *Molecular Ecology* 27.19, pp. 3852–3872.

Berthier, S., E. Charron, and A. D. Silva (2003). "Determination of the cuticle index of the scales of the iridescent butterfly Morpho menelaus". In: *Optics Communications* 228.4, pp. 349–356.

Bolger, A. M., M. Lohse, and B. Usadel (Apr. 2014). "Trimmomatic: a flexible trimmer for Illumina sequence data". In: *Bioinformatics* 30.15, pp. 2114–2120.

Bowers, M. D. and Z. Larin (Apr. 1989). "Acquired chemical defense in the lycaenid butterfly,Eumaeus atala". In: *Journal of Chemical Ecology* 15.4, pp. 1133–1146.

Brelsford, A., D. P. L. Toews, and D. E. Irwin (Nov. 2017). "Admixture mapping in a hybrid zone reveals loci associated with avian feather coloration". In: *Proceedings of the Royal Society B: Biological Sciences* 284.1866, p. 20171106.

Bresadola, L. et al. (May 2019). "Admixture mapping in interspecific Populus hybrids identifies classes of genomic architectures for phytochemical, morphological and growth traits". In: *New Phytologist*.

Brien, M. N. (2019). "The genetics and evolution of iridescent structural colour in *Heliconius* butterflies". PhD thesis. University of Sheffield.

Brien, M. N. et al. (Dec. 2018). "Phenotypic variation in Heliconius erato crosses shows that iridescent structural colour is sex-linked and controlled by multiple genes". In: *Interface Focus* 9.1, p. 20180047.

Brien, M. N. et al. (Apr. 2021). "The genetic basis of structural colour variation in mimetic Heliconius butterflies". In: *bioRxiv*.

Broman, K. W. et al. (May 2003). "R/qtl: QTL mapping in experimental crosses". In: *Bioinformatics* 19.7, pp. 889–890.

Broman, K. W. et al. (Oct. 2006). "The X Chromosome in Quantitative Trait Locus Mapping". In: *Genetics* 174.4, pp. 2151–2158.

Broman, K. W. et al. (Dec. 2018). "R/qtl2: Software for Mapping Quantitative Trait Loci with High-Dimensional Data and Multiparent Populations". In: *Genetics* 211.2, pp. 495–502.

Buerkle, C. A. and C. Lexer (Dec. 2008). "Admixture as the basis for genetic mapping". In: *Trends in Ecology & Evolution* 23.12, pp. 686–694.

Burg, S. L. et al. (Aug. 2019). "Liquid–liquid phase separation morphologies in ultra-white beetle scales and a synthetic equivalent". In: *Communications Chemistry* 2.1.

Cariou, M., L. Duret, and S. Charlat (Nov. 2016). "How and how much does RAD-seq bias genetic diversity estimates?" In: *BMC Evolutionary Biology* 16.1.

Challis, R. J. et al. (June 2016). "Lepbase: the Lepidopteran genome database". In.

Chazot, N. et al. (Jan. 2016). "Morpho morphometrics: Shared ancestry and selection drive the evolution of wing size and shape inMorphobutterflies". In: *Evolution* 70.1, pp. 181–194.

Chen, W.-M. and G. R. Abecasis (Nov. 2007). "Family-Based Association Tests for Genomewide Association Scans". In: *The American Journal of Human Genetics* 81.5, pp. 913–926.

Cho, E. H. and H. F. Nijhout (Jan. 2013). "Development of polyploidy of scale-building cells in the wings of Manduca sexta". In: *Arthropod Structure & Development* 42.1, pp. 37–46.

Comeault, A. A. et al. (May 2016). "Color phenotypes are under similar genetic control in two distantly related species of *Timema* stick insect". In: *Evolution* 70.6, pp. 1283–1296.

Concha, C. et al. (Dec. 2019). "Interplay between Developmental Flexibility and Determinism in the Evolution of Mimetic Heliconius Wing Patterns". In: *Current Biology* 29.23, 3996–4009.e4.

Consortium, T. H. G. (May 2012). "Butterfly genome reveals promiscuous exchange of mimicry adaptations among species". In: *Nature* 487, pp. 94–.

Conte, G. L. et al. (Oct. 2012). "The probability of genetic parallelism and convergence in natural populations". In: *Proceedings of the Royal Society B: Biological Sciences* 279.1749, pp. 5039–5047.

Counterman, B. A. et al. (Feb. 2010). "Genomic Hotspots for Adaptation: The Population Genetics of Müllerian Mimicry in Heliconius erato". In: *PLoS Genetics* 6.2. Ed. by M. W. Nachman, e1000796.

Curran, E. V. (2018). "An exploration of the parallel evolution of iridescent structural colour in *Heliconius* butterflies". PhD thesis. University of Sheffield.

Curran, E. V. et al. (June 2020). "Müllerian mimicry of a quantitative trait despite contrasting levels of genomic divergence and selection". In: *Molecular Ecology* 29.11, pp. 2016–2030.

Davey, J. W. et al. (Oct. 2012). "Special features of RAD Sequencing data: implications for genotyping". In: *Molecular Ecology* 22.11, pp. 3151–3164.

Davey, J. W. et al. (2016). "Major Improvements to the Heliconius melpomene Genome Assembly Used to Confirm 10 Chromosome Fusion Events in 6 Million Years of Butterfly Evolution". In: *G3: Genes, Genomes, Genetics*.

Davey, J. W. et al. (June 2017). "No evidence for maintenance of a sympatric *Heliconius* species barrier by chromosomal inversions". In: *Evolution Letters* 1.3, pp. 138–154.

Davis, A. L., H. F. Nijhout, and S. Johnsen (Mar. 2020). "Diverse nanostructures underlie thin ultra-black scales in butterflies". In: *Nature Communications* 11.1.

Day, C. R. et al. (June 2019). "Sub-micrometer insights into the cytoskeletal dynamics and ultrastructural diversity of butterfly wing scales". In: *Developmental Dynamics* 248.8, pp. 657–670.

Deagle, B. E. et al. (Mar. 2013). "Phylogeography and adaptation genetics of stickleback from the H aida G waii archipelago revealed using genome-wide single nucleotide polymorphism genotyping". In: *Molecular Ecology* 22.7, pp. 1917–1932.

Dembeck, L. M. et al. (May 2015). "Genetic Architecture of Abdominal Pigmentation in Drosophila melanogaster". In: *PLOS Genetics* 11.5. Ed. by C. D. Jones, e1005163.

DeSimone, S. M. and K. White (June 1993). "The Drosophila erect wing gene, which is important for both neuronal and muscle development, encodes a protein which is similar to the sea urchin P3A2 DNA binding protein." In: 13.6, pp. 3641–3649.

Dinwiddie, A. et al. (2014). "Dynamics of F-actin prefigure the structure of butterfly wing scales". In: *Developmental Biology* 392.2, pp. 404–418.

Doucet, S. M. and M. G. Meadows (Feb. 2009). "Iridescence: a functional perspective". In: *Journal of The Royal Society Interface* 6.Suppl 2, S115–S132.

Elmer, K. R. and A. Meyer (June 2011). "Adaptation in the age of ecological genomics: insights from parallelism and convergence". In: *Trends in Ecology & Evolution* 26.6, pp. 298–306.

Emond, M. J. et al. (July 2012). "Exome sequencing of extreme phenotypes identifies DCTN4 as a modifier of chronic Pseudomonas aeruginosa infection in cystic fibrosis". In: *Nature Genetics* 44.8, pp. 886–889.

Emsley, M. G. (1965). "The geographical distribution of the color-pattern components of *Heloconius erato* and *Heliconius melpomene* with genetical evidence for the systematic relationship between the two species". In: *Zoologica : scientific contributions of the New York Zoological Society.* 49, pp. 245–286.

Engler, H. S., K. C. Spencer, and L. E. Gilbert (July 2000). "Preventing cyanide release from leaves". In: *Nature* 406.6792, pp. 144–145.

Evanno, G., S. Regnaut, and J. Goudet (July 2005). "Detecting the number of clusters of individuals using the software structure: a simulation study". In: *Molecular Ecology* 14.8, pp. 2611–2620.

Ewels, P. et al. (June 2016). "MultiQC: summarize analysis results for multiple tools and samples in a single report". In: *Bioinformatics* 32.19, pp. 3047–3048.

Fenner, J., L. Rodriguez-Caro, and B. Counterman (July 2019). "Plasticity and divergence in ultraviolet reflecting structures on Dogface butterfly wings". In: *Arthropod Structure & Development* 51, pp. 14–22.

Fenner, J. et al. (June 2020). "Wnt Genes in Wing Pattern Development of Coliadinae Butterflies". In: *Frontiers in Ecology and Evolution* 8.

Ferguson, L. et al. (Mar. 2010). "Characterization of a hotspot for mimicry: assembly of a butterfly wing transcriptome to genomic sequence at the *HmYb/Sb* locus". In: *Molecular Ecology* 19, pp. 240–254.

Ferguson, L. C., L. Maroja, and C. D. Jiggins (Dec. 2011). "Convergent, modular expression of ebony and tan in the mimetic wing patterns of Heliconius butterflies". In: *Development Genes and Evolution* 221.5-6, pp. 297–308.

Ficarrotta, V. et al. (May 2021). "A genetic switch for male UV-iridescence in an incipient species pair of sulphur butterflies". In.

Finkbeiner, S. D. et al. (Jan. 2017). "Ultraviolet and yellow reflectance but not fluorescence is important for visual discrimination of conspecifics byHeliconius erato". In: *The Journal of Experimental Biology* 220.7, pp. 1267–1276.

François, O. and K. Caye (May 2018). "Naturalgwas: An R package for evaluating genomewide association methods with empirical data". In: *Molecular Ecology Resources* 18.4, pp. 789–797.

Frank, F. and H. Ruska (Apr. 1939). "Übermikroskopische Untersuchung der Blaustruktur der Vogelfeder". In: *Die Naturwissenschaften* 27.14, pp. 229–230.

Gagnaire, P.-A. et al. (Mar. 2013). "THE GENETIC ARCHITECTURE OF REPRODUCTIVE ISOLATION DURING SPECIATION-WITH-GENE-FLOW IN LAKE

WHITEFISH SPECIES PAIRS ASSESSED BY RAD SEQUENCING". In: *Evolution* 67.9, pp. 2483–2497.

Gaudet, P. et al. (Aug. 2011). "Phylogenetic-based propagation of functional annotations within the Gene Ontology consortium". In: 12.5, pp. 449–462.

Ghiradella, H. (1985). "Structure and Development of Iridescent Lepidopteran Scales: the Papilionidae as a Showcase Family". In: *Annals of the Entomological Society of America* 78.2, pp. 252–264.

Ghiradella, H. et al. (Dec. 1972). "Ultraviolet Reflection of a Male Butterfly: Interference Color Caused by Thin-Layer Elaboration of Wing Scales". In: *Science* 178.4066, pp. 1214–1217.

Ghiradella, H. (Apr. 1974). "Development of ultraviolet-reflecting butterfly scales: How to make an interference filter". In: *Journal of Morphology* 142.4, pp. 395–409.

– (1989). "Structure and development of iridescent butterfly scales: Lattices and laminae". In: *Journal of Morphology* 202.1, pp. 69–88.

– (Aug. 1991). "Light and color on the wing: structural colors in butterflies and moths". In: *Appl. Opt.* 30.24, pp. 3492–3500.

– (Apr. 1994). "Structure of butterfly scales: Patterning in an insect cuticle". In: *Microscopy Research and Technique* 27.5, pp. 429–438.

Gilbert, L. et al. (1988). "Correlations of ultrastructure and pigmentation suggest how genes control development of wing scales of *Heliconius* butterflies". In: *J. Res. Lepid* 26.1.

Greenstein, M. E. (Jan. 1972a). "The ultrastructure of developing wings in the giant silkmoth, *Hyalophora cecropia*. II. Scale-forming and socket-forming cells". In: *Journal of Morphology* 136.1, pp. 23–51.

– (Jan. 1972b). "The ultrastructure of developing wings in the giant silkmoth,Hyalophora cecropia. I. Generalized epidermal cells". In: *Journal of Morphology* 136.1, pp. 1–21.

Gul, I. et al. (Dec. 2021). "Identification and the immunological role of two Nimrod family genes in the silkworm, Bombyx mori". In: 193, pp. 154–165.

Gur, D. et al. (Dec. 2020). "In situ differentiation of iridophore crystallotypes underlies zebrafish stripe patterning". In: *Nature Communications* 11.1.

Hanly, J. J. et al. (July 2019). "Conservation and flexibility in the gene regulatory landscape of heliconiine butterfly wings". In: *EvoDevo* 10.1.

Hashimoto, Y. et al. (Nov. 2009). "Identification of Lipoteichoic Acid as a Ligand for Draper in the Phagocytosis ofStaphylococcus aureusbyDrosophilaHemocytes". In: 183.11, pp. 7451–7460.

Hecht, E. (2002). *Optics*. Reading, Mass: Addison-Wesley.

Henning, F. et al. (Mar. 2013). "Transcriptomics of morphological color change in polychromatic Midas cichlids". In: *BMC Genomics* 14.1.

Hermisson, J. and A. P. McGregor (Dec. 2008). "Pleiotropic scaling and QTL data". In: *Nature* 456.7222, E3–E3.

Hines, H. M. et al. (Dec. 2011). "Wing patterning gene redefines the mimetic history of Heliconius butterflies". In: *Proceedings of the National Academy of Sciences* 108.49, pp. 19666–19671.

Hoekstra, H. E. (July 2006). "Genetics, development and evolution of adaptive pigmentation in vertebrates". In: *Heredity* 97, pp. 222–.

Hof, A. E. van't et al. (June 2016). "The industrial melanism mutation in British peppered moths is a transposable element". In: *Nature* 534.7605, pp. 102–105.

Hunter, D. et al. (Jan. 2021). "Using genomic prediction to detect microevolutionary change of a quantitative trait". In.

Ingram, A. L. and A. R. Parker (2008). "A review of the diversity and evolution of photonic structures in butterflies, incorporating the work of John Huxley (The Natural History Museum, London from 1961 to 1990)". In: *Philosophical Transactions of the Royal Society of London B: Biological Sciences* 363.1502, pp. 2465–2480.

Jackson, I. (Sept. 1997). "Homologous pigmentation mutations in human, mouse and other model organisms". In: *Human Molecular Genetics* 6.10, pp. 1613–1624.

Jiggins, C. D., R. W. R. Wallbank, and J. J. Hanly (Feb. 2017). "Waiting in the wings: what can we learn about gene co-option from the diversification of butterfly wing patterns?" In: *Philosophical transactions of the Royal Society of London. Series B, Biological sciences* 372 (1713). ppublish.

Joron, M. et al. (Sept. 2006). "A Conserved Supergene Locus Controls Colour Pattern Diversity in Heliconius Butterflies". In: *PLoS Biology* 4.10. Ed. by M. A. F. Noor, e303.

Kalisky, T. and S. R. Quake (Mar. 2011). "Single-cell genomics". In: *Nature Methods* 8.4, pp. 311–314.

Kapan, D. D. (Jan. 2001). "Three-butterfly system provides a field test of Müllerian mimicry". In: *Nature* 409, pp. 338–.

Kardos, M. et al. (Dec. 2015). "Whole-genome resequencing of extreme phenotypes in collared flycatchers highlights the difficulty of detecting quantitative trait loci in natural populations". In: 16.3, pp. 727–741.

Kemp D. J., D. J., P. Vukusic, and R. L. Rutowski (2006). "Stress-mediated covariance between nano-structural architecture and ultraviolet butterfly coloration". In: *Functional Ecology* 20.2, pp. 282–289.

Kemp, D. J. (Jan. 2007). "Female butterflies prefer males bearing bright iridescent ornamentation". In: *Proceedings of the Royal Society B: Biological Sciences* 274.1613, pp. 1043–1047.

Kemp, D. J. and R. L. Rutowski (Jan. 2007). "Condition dependence, quantitative genetics, and the potential signal content of iridescent ultraviolet butterfly coloration". In: *Evolution* 61.1, pp. 168–183.

Kemppainen, P. and A. Husby (Mar. 2018). "Inference of genetic architecture from chromosome partitioning analyses is sensitive to genome variation, sample size, heritability and effect size distribution". In: *Molecular Ecology Resources* 18.4, pp. 767–777.

Kertész, K. et al. (Mar. 2021). "Multi-instrumental techniques for evaluating butterfly structural colors: A case study on Polyommatus bellargus (Rottemburg, 1775) (Lepidoptera: Lycaenidae: Polyommatinae)". In: *Arthropod Structure & Development* 61, p. 101010.

Kértesz, K. et al. (2017). "Changes in structural and pigmentary colours in response to cold stress in Polyommatus icarus butterflies". In: *Scientific Reports* 7.1, pp. 1118–.

Kieffer, J. and D. Karkoulis (Mar. 2013). "PyFAI, a versatile library for azimuthal regrouping". In: *Journal of Physics: Conference Series* 425.20, p. 202012.

Kim, S. Y. et al. (June 2011). "Estimation of allele frequency and association mapping using next-generation sequencing data". In: *BMC Bioinformatics* 12.1.

Kinoshita, S., S. Yoshioka, and J. Miyazaki (2008). "Physics of structural colors". In: *Reports on Progress in Physics* 71.7, p. 076401.

Kinoshita, S. and S. Yoshioka (Aug. 2005). "Structural Colors in Nature: The Role of Regularity and Irregularity in the Structure". In: *ChemPhysChem* 6.8, pp. 1442–1459.

Kinoshita, S., S. Yoshioka, Y. Fujii, et al. (Sept. 2002). "Photophysics of Structural Color in the Morpho Butterflies". In: *FORMA* 17.2, pp. 103–121.

Kinoshita, S., S. Yoshioka, and K. Kawagoe (July 2002). "Mechanisms of structural colour in the Morpho butterfly: cooperation of regularity and irregularity in an iridescent scale". In: *Proceedings of the Royal Society of London. Series B: Biological Sciences* 269.1499, pp. 1417–1421.

Knudsen, E. B. et al. (Feb. 2013). "FabIO: easy access to two-dimensional X-ray detector images in Python". In: *Journal of Applied Crystallography* 46.2, pp. 537–539.

Kollberg, U. et al. (Mar. 1995). "Expression cloning and characterization of a pupal cuticle protein cDNA of Galleria mellonella L". In: 25.3, pp. 355–363.

Kopelman, N. M. et al. (Feb. 2015). "Clumpak : a program for identifying clustering modes and packaging population structure inferences across K". In: *Molecular Ecology Resources* 15.5, pp. 1179–1191.

Korneliussen, T. S., A. Albrechtsen, and R. Nielsen (Nov. 2014). "ANGSD: Analysis of Next Generation Sequencing Data". In: *BMC Bioinformatics* 15.1.

Kottler, V. A. et al. (July 2013). "Pigment Pattern Formation in the Guppy, Poecilia reticulata, Involves the Kita and Csf1ra Receptor Tyrosine Kinases". In: *Genetics* 194.3, pp. 631–646.

Kozak, K. M. et al. (Jan. 2015). "Multilocus Species Trees Show the Recent Adaptive Radiation of the Mimetic Heliconius Butterflies". In: *Systematic Biology* 64.3, pp. 505–524.

Krishna, A. et al. (Jan. 2020). "Infrared optical and thermal properties of microstructures in butterfly wings". In: *Proceedings of the National Academy of Sciences* 117.3, pp. 1566–1572.

Kronforst, M. R. and R. Papa (May 2015). "The Functional Basis of Wing Patterning in Heliconius Butterflies: The Molecules Behind Mimicry". In: *Genetics* 200.1, pp. 1–19.

Kunte, K. et al. (Mar. 2014). "doublesex is a mimicry supergene". In: *Nature* 507.7491, pp. 229–232.

Land, M. (1972). "The physics and biology of animal reflectors". In: *Progress in Biophysics and Molecular Biology* 24.Supplement C, pp. 75–106.

Langmead, B. and S. L. Salzberg (Mar. 2012). "Fast gapped-read alignment with Bowtie 2". In: *Nature Methods* 9.4, pp. 357–359.

Li, H. (Sept. 2011). "A statistical framework for SNP calling, mutation discovery, association mapping and population genetical parameter estimation from sequencing data". In: *Bioinformatics* 27.21, pp. 2987–2993.

Li, H. and R. Durbin (May 2009). "Fast and accurate short read alignment with Burrows-Wheeler transform". In: *Bioinformatics* 25.14, pp. 1754–1760.

Li, H., B. Handsaker, et al. (June 2009). "The Sequence Alignment/Map format and SAMtools". In: *Bioinformatics* 25.16, pp. 2078–2079.

Lindtke, D. et al. (July 2013). "Admixture mapping of quantitative traits in Populus hybrid zones: power and limitations". In: *Heredity* 111.6, pp. 474–485.

Linnen, C. R. and H. E. Hoekstra (Jan. 2009). "Measuring Natural Selection on Genotypes and Phenotypes in the Wild". In: *Cold Spring Harbor Symposia on Quantitative Biology* 74.0, pp. 155–168.

Livraghi, L. et al. (July 2021). "Cortex cis-regulatory switches establish scale colour identity and pattern diversity in Heliconius". In: *eLife* 10.

Lloyd, V. J. and N. J. Nadeau (Aug. 2021). "The evolution of structural colour in butterflies". In: *Current Opinion in Genetics & Development* 69, pp. 28–34.

Locke, M. (Apr. 1966). "The structure and formation of the cuticulin layer in the epicuticle of an insect,Calpodes ethlius (Lepidoptera, Hesperiidae)". In: *Journal of Morphology* 118.4, pp. 461–494.

Lynch, M. and B. Walsh (1998). *Genetics and analysis of quantitative traits*. Sunderland, Mass: Sinauer.

Mackay, T. (June 2004). "The genetic architecture of quantitative traits: lessons from Drosophila". In: *Current Opinion in Genetics & Development* 14.3, pp. 253–257.

Maia, R. et al. (Apr. 2019). "pavo 2: New tools for the spectral and spatial analysis of colour in r". In: *Methods in Ecology and Evolution* 10.7. Ed. by R. B. O'Hara, pp. 1097–1107.

Mallet, J. (Apr. 1986). "Hybrid zones of Heliconius butterflies in Panama and the stability and movement of warning colour clines". In: *Heredity* 56.2, pp. 191–202.

Mallet, J. et al. (2007). "Natural hybridization in heliconiine butterflies: the species boundary as a continuum". In: *BMC Evolutionary Biology* 7.1, p. 28.

Martin, A. and V. Orgogozo (2013). "The loci of repeated evolution: A catalog of genetic hotspots of phenotypic variation". In: *Evolution* 67.5, pp. 1235–1250.

Martin, A. et al. (Feb. 2014). "Multiple recent co-options of Optix associated with novel traits in adaptive butterfly wing radiations". In: *EvoDevo* 5.1, p. 7.

Martin, S. H. et al. (Mar. 2016). "Natural selection and genetic diversity in the butterfly Heliconius melpomene". In: *Genetics* 203.1, pp. 525–541.

Mason, C. W. (1925). "Structural Colors in Insects. I". In: *The Journal of Physical Chemistry* 30.3, pp. 383–395.

– (1926). "Structural Colors in Insects. II". In: *The Journal of Physical Chemistry* 31.3, pp. 321–354.

Matsuoka, Y. and A. Monteiro (July 2018). "Melanin Pathway Genes Regulate Color and Morphology of Butterfly Wing Scales". In: *Cell Reports* 24.1, pp. 56–65.

McCulloch, K. J. et al. (May 2017). "Sexual Dimorphism and Retinal Mosaic Diversification following the Evolution of a Violet Receptor in Butterflies". In: *Molecular Biology and Evolution* 34.9, pp. 2271–2284.

Merrill, R. M. et al. (2015). "The diversification of Heliconius butterflies: what have we learned in 150 years?" In: *Journal of Evolutionary Biology* 28.8, pp. 1417–1438.

Merrill, R. M. et al. (2011). "Mate preference across the speciation continuum in a clade of mimetic butterflies". In: *Evolution* 65.5, pp. 1489–1500.

Moest, M. et al. (Feb. 2020). "Selective sweeps on novel and introgressed variation shape mimicry loci in a butterfly adaptive radiation". In: *PLOS Biology* 18.2. Ed. by N. J. Besansky, e3000597.

Montgomerie, R. (2006). "Bird Coloration, Volume 1: Mechanisms and Measurements". In: ed. by G. E. Hill and K. J. McGraw. Harvard University Press. Chap. Analyzing colors.

Morris, J. et al. (Jan. 2019). "The genetic architecture of adaptation: convergence and pleiotropy in Heliconius wing pattern evolution". In: *Heredity*.

Moser, G. et al. (Apr. 2015). "Simultaneous Discovery, Estimation and Prediction Analysis of Complex Traits Using a Bayesian Mixture Model". In: *PLOS Genetics* 11.4. Ed. by C. Haley, e1004969.

Mundy, N. I. et al. (June 2016). "Red Carotenoid Coloration in the Zebra Finch Is Controlled by a Cytochrome P450 Gene Cluster". In: *Current Biology* 26.11, pp. 1435–1440.

Nadeau, N. J., F. Minvielle, and N. I. Mundy (June 2006). "Association of a Glu92Lys substitution in MC1R with extended brown in Japanese quail (Coturnix japonica)". In: *Animal Genetics* 37.3, pp. 287–289.

Nadeau, N. J. (Oct. 2016). "Genes controlling mimetic colour pattern variation in butterflies". In: *Current Opinion in Insect Science* 17, pp. 24–31.

Nadeau, N. J. et al. (June 2016). "The gene cortex controls mimicry and crypsis in butterflies and moths". In: *Nature* 534, pp. 106–.

Nelson, C., V. Ambros, and E. H. Baehrecke (Nov. 2014). "miR-14 Regulates Autophagy during Developmental Cell Death by Targeting ip3-kinase 2". In: 56.3, pp. 376–388.

Nijhout, H. F. (1990). "A comprehensive model for colour pattern formation in butterflies". In: *Proceedings of the Royal Society of London B: Biological Sciences* 239.1294, pp. 81–113.

Okonechnikov, K., A. Conesa, and F. García-Alcalde (Oct. 2015). "Qualimap 2: advanced multi-sample quality control for high-throughput sequencing data". In: *Bioinformatics*, btv566.

Orgogozo, V., K. W. Broman, and D. L. Stern (Feb. 2006). "High-Resolution Quantitative Trait Locus Mapping Reveals Sign Epistasis Controlling Ovariole Number Between Two Drosophila Species". In: *Genetics* 173.1, pp. 197–205.

Orr, H. A. (Feb. 2005). "The genetic theory of adaptation: a brief history". In: *Nature Reviews Genetics* 6.2, pp. 119–127.

Overton, J. (May 1966). "Microtubules and microfibrils in the morphogenesis of the scale cells of *Ephestia kühniella*". In: *Journal of Cell Biology* 29.2, pp. 293–305.

Pallares, L. F. et al. (Nov. 2014). "Use of a natural hybrid zone for genomewide association mapping of craniofacial traits in the house mouse". In: *Molecular Ecology* 23.23, pp. 5756–5770.

Papke, R. S., D. J. Kemp, and R. L. Rutowski (Jan. 2007). "Multimodal signalling: structural ultraviolet reflectance predicts male mating success better than pheromones in the butterfly Colias eurytheme L. (Pieridae)". In: *Animal Behaviour* 73.1, pp. 47–54.

Pardo-Diaz, C. et al. (June 2012). "Adaptive Introgression across Species Boundaries in Heliconius Butterflies". In: *PLOS Genetics* 8.6, pp. 1–13.

Parker, A. R. (1998). "The diversity and implications of animal structural colours." In: *Journal of Experimental Biology* 201.16, pp. 2343–2347.

– (2000). "515 million years of structural colour". In: *Journal of Optics A: Pure and Applied Optics* 2.6, R15.

Parnell, A. J. et al. (Dec. 2015). "Spatially modulated structural colour in bird feathers". In: *Scientific Reports* 5.1.

Parnell, A. J. et al. (Apr. 2018). "Wing scale ultrastructure underlying convergent and divergent iridescent colours in mimetic Heliconius butterflies". In: *Journal of The Royal Society Interface* 15.141, p. 20170948.

Pauw, B. R. (Aug. 2013). "Everything SAXS: small-angle scattering pattern collection and correction". In: *Journal of Physics: Condensed Matter* 25.38, p. 383201.

Pedregosa, F. et al. (2011). "Scikit-learn: Machine Learning in Python". In: *Journal of Machine Learning Research* 12, pp. 2825–2830.

Prakash, A. and A. Monteiro (Feb. 2018). "apterous A specifies dorsal wing patterns and sexual traits in butterflies". In: *Proceedings of the Royal Society B: Biological Sciences* 285.1873, p. 20172685.

Prakash, A. et al. (Oct. 2021). "Antennapedia regulates metallic silver wing scale development and cell shape in Bicyclus anynana butterflies". In.

Price, A. L. et al. (July 2006). "Principal components analysis corrects for stratification in genome-wide association studies". In: *Nature Genetics* 38.8, pp. 904–909.

Quek, S.-P. et al. (Apr. 2010). "Dissecting comimetic radiations in Heliconius reveals divergent histories of convergent butterflies". In: *Proceedings of the National Academy of Sciences* 107.16, pp. 7365–7370.

R Core Team (2019). *R: A Language and Environment for Statistical Computing*. R Foundation for Statistical Computing. Vienna, Austria.

Rastas, P. (Aug. 2017). "Lep-MAP3: robust linkage mapping even for low-coverage whole genome sequencing data". In: *Bioinformatics* 33.23. Ed. by B. Berger, pp. 3726–3732.

Reed, R. D. et al. (2011). "optix Drives the Repeated Convergent Evolution of Butterfly Wing Pattern Mimicry". In: *Science* 333.6046, pp. 1137–1141.

Rice, W. R. (July 1984). "Sex chromosomes and the evolution of sexual dimorphism". In: *Evolution* 38.4, pp. 735–742.

Rodriguez-Caro, F. et al. (July 2021). "Novel Doublesex Duplication Associated with Sexually Dimorphic Development of Dogface Butterfly Wings". In: *Molecular Biology and Evolution*. Ed. by J. True.

Rothenberg, M. E. et al. (Aug. 2003). "Drosophila Pod-1 Crosslinks Both Actin and Microtubules and Controls the Targeting of Axons". In: 39.5, pp. 779–791.

Rowe, L. and D. Houle (Oct. 1996). "The lek paradox and the capture of genetic variance by condition dependent traits". In: *Proceedings of the Royal Society of London. Series B: Biological Sciences* 263.1375, pp. 1415–1421.

Rutowski, R. L. (1977). "The use of visual cues in sexual and species discrimination by males of the small sulphur butterfly *Eurema lisa* (lepidoptera, pieridae)". In: *Journal of Comparative Physiology* 115.1, pp. 61–74.

– (Apr. 1985). "Evidence for Mate Choice in a Sulphur Butterfly (Colias eurytheme)". In: *Zeitschrift für Tierpsychologie* 70.2, pp. 103–114.

Rutowski, R. L. and D. J. Kemp (Apr. 2017). "Female iridescent colour ornamentation in a butterfly that displays mutual ornamentation: is it a sexual signal?" In: *Animal Behaviour* 126, pp. 301–307.

Rutowski, R. L., A. C. Nahm, and J. M. Macedonia (Feb. 2010). "Iridescent hindwing patches in the Pipevine Swallowtail: differences in dorsal and ventral surfaces relate to signal function and context". In: *Functional Ecology* 24.4, pp. 767–775.

Saenko, S. V. et al. (Aug. 2019). "Unravelling the genes forming the wing pattern supergene in the polymorphic butterfly Heliconius numata". In: *EvoDevo* 10.1.

San-Jose, L. M. and A. Roulin (May 2017). "Genomics of coloration in natural animal populations". In: *Philosophical Transactions of the Royal Society B: Biological Sciences* 372.1724, p. 20160337.

Santure, A. W. and D. Garant (June 2018). "Wild GWAS—association mapping in natural populations". In: *Molecular Ecology Resources* 18.4, pp. 729–738.

Saranathan, V. et al. (June 2010). "Structure, function, and self-assembly of single network gyroid (I4132) photonic crystals in butterfly wing scales". In: *Proceedings of the National Academy of Sciences* 107.26, pp. 11676–11681.

Schindelin, J. et al. (June 2012). "Fiji: an open-source platform for biological-image analysis". In: *Nature Methods* 9.7, pp. 676–682.

Schneider, C. A., W. S. Rasband, and K. W. Eliceiri (June 2012). "NIH Image to ImageJ: 25 years of image analysis". In: *Nature Methods* 9.7, pp. 671–675.

Sekimura, T. and N. H. Frederik, eds. (2017). *Diversity and Evolution of Butterfly Wing Patterns*. Springer.

Senthilan, P. R. et al. (Aug. 2012). "Drosophila Auditory Organ Genes and Genetic Hearing Defects". In: 150.5, pp. 1042–1054.

Shahandeh, M. P. and T. L. Turner (Mar. 2020). "The complex genetic architecture of male mate choice evolution between Drosophila species". In: *Heredity* 124.6, pp. 737–750.

Silberglied, R. E. and O. R. Taylor (Feb. 1973). "Ultraviolet Differences between the Sulphur Butterflies, Colias eurytheme and C. philodice, and a Possible Isolating Mechanism". In: *Nature* 241.5389, pp. 406–408.

Silberglied, R. E. and O. R. Taylor (Sept. 1978). "Ultraviolet reflection and its behavioral role in the courtship of the sulfur butterflies Colias eurytheme and C. philodice (Lepidoptera, Pieridae)". In: *Behavioral Ecology and Sociobiology* 3.3, pp. 203–243.

Sivia, D. S. (2011). *Elementary Scattering Theory*. Oxford University Press. 216 pp.

Skotte, L., T. S. Korneliussen, and A. Albrechtsen (Sept. 2013). "Estimating Individual Admixture Proportions from Next Generation Sequencing Data". In: *Genetics* 195.3, pp. 693–702.

Slate, J. (Nov. 2004). "Quantitative trait locus mapping in natural populations: progress, caveats and future directions". In: *Molecular Ecology* 14.2, pp. 363–379.

– (Feb. 2013). "From Beavis to beak color: A simulation study to examine how much QTL mapping can reveal about the genetic architecture of quantitative traits." In: *Evolution*.

Stavenga, D. G., H. L. Leertouwer, and B. D. Wilts (2014). "Coloration principles of nymphaline butterflies – thin films, melanin, ommochromes and wing scale stacking". In: *Journal of Experimental Biology* 217.12, pp. 2171–2180.

Stern, D. L. and V. Orgogozo (2009). "Is Genetic Evolution Predictable?" In: *Science* 323.5915, pp. 746–751.

Suomalainen, E., L. M. Cook, and J. R. G. Turner (Feb. 2009). "Achiasmatic oogenesis in the Heliconiine butterflies". In: *Hereditas* 74.2, pp. 302–304.

Supple, M. A. et al. (2013). "Genomic architecture of adaptive color pattern divergence and convergence in Heliconius butterflies". In: *Genome Research* 23.8, pp. 1248–1257.

Sweeney, A., C. Jiggins, and S. Johnsen (May 2003). "Polarized light as a butterfly mating signal". In: *Nature* 423, pp. 31–.

Thayer, R. C., F. I. Allen, and N. H. Patel (Apr. 2020). "Structural color in Junonia butterflies evolves by tuning scale lamina thickness". In: *eLife* 9.

The Picard Toolkit (2019). `http://broadinstitute.github.io/picard/`.

Thurmond, J. et al. (Oct. 2018). "FlyBase 2.0: the next generation". In: *Nucleic Acids Research* 47.D1, pp. D759–D765.

Van Belleghem, S. M. et al. (Aug. 2021). "Heliconius butterflies: a window into the evolution and development of diversity". In: *Current Opinion in Genetics & Development* 69, pp. 72–81.

Van Belleghem, S. M. et al. (Jan. 2017). "Complex modular architecture around a simple toolkit of wing pattern genes". In: *Nature Ecology & Evolution* 1, pp. 0052–.

Vincent, T. et al. (Feb. 2020). *silx-kit/silx: v0.13.0 beta 0: 21/02/2020*.

Vischer, N. (Nov. 2013). *PeakFinder*. `https://sils.fnwi.uva.nl/bcb/objectj/examples/PeakFinder/PeakFinderTool.txt`.

Vukusic, P., J. R. Sambles, and C. R. Lawrence (May 2004). "Structurally assisted blackness in butterfly scales". In: *Proceedings of the Royal Society of London. Series B: Biological Sciences* 271.suppl_4.

Vukusic, P. et al. (1999). "Quantified interference and diffraction in single Morpho butterfly scales". In: *Proceedings of the Royal Society of London B: Biological Sciences* 266.1427, pp. 1403–1411.

Vukusic, P. and J. R. Sambles (Aug. 2003). "Photonic structures in biology". In: *Nature* 424.6950, pp. 852–855.

Wallbank, R. W. R. et al. (Jan. 2016). "Evolutionary Novelty in a Butterfly Wing Pattern through Enhancer Shuffling". In: *PLOS Biology* 14.1. Ed. by N. H. Barton, e1002353.

Wasik, B. R. et al. (2014). "Artificial selection for structural color on butterfly wings and comparison with natural evolution". In: *Proceedings of the National Academy of Sciences* 111.33, pp. 12109–12114.

Whitlock, M. and D. Schluter (2015). *The analysis of biological data*. 2nd ed.

Wilts, B. D., A. J. M. Vey, et al. (Nov. 2017). "Longwing (Heliconius) butterflies combine a restricted set of pigmentary and structural coloration mechanisms". In: *BMC Evolutionary Biology* 17.1.

Wilts, B. D., B. A. Zubiri, et al. (Apr. 2017). "Butterfly gyroid nanostructures as a time-frozen glimpse of intracellular membrane development". In: *Science Advances* 3.4.

Wood, T. E., J. M. Burke, and L. H. Rieseberg (2005). "Parallel genotypic adaptation: when evolution repeats itself". In: *Georgia Genetics Review III*. Springer-Verlag, pp. 157–170.

Xu, S. (Dec. 2003). "Theoretical basis of the Beavis effect." In: *Genetics* 165 (4), pp. 2259–2268. ppublish.

Yang, J. et al. (May 2011). "Genome partitioning of genetic variation for complex traits using common SNPs". In: *Nature Genetics* 43.6, pp. 519–525.

Yoshioka, S. and S. Kinoshita (2004). "Wavelength-selective and anisotropic light-diffusing scale on the wing of the Morpho butterfly". In: *Proceedings of the Royal Society of London B: Biological Sciences* 271.1539, pp. 581–587.

Zhang, L., A. Mazo-Vargas, and R. D. Reed (2017). "Single master regulatory gene coordinates the evolution and development of butterfly color and iridescence". In: *Proceedings of the National Academy of Sciences* 114.40, pp. 10707–10712.

Zhu, D. et al. (Nov. 2009). "Investigation of structural colors in *Morpho* butterflies using the nonstandard-finite-difference time-domain method: Effects of alternately stacked shelves and ridge density". In: *Physical Review E* 80.5.

Appendix A

The genetic basis of structural colour variation in mimetic *Heliconius* butterflies

Manuscript submitted to the journal Philosophical Transactions of The Royal Society B. Accepted for publication.

The genetic basis of structural colour variation in mimetic *Heliconius* butterflies

Melanie N. Brien[1*], Juan Enciso Romero[1,2,*], Victoria J. Lloyd[1*], Emma V. Curran[1], Andrew J. Parnell[3], Carlos Morochz[4], Patricio A. Salazar[1], Pasi Rastas[5], Thomas Zinn[6], Nicola J. Nadeau[1†]

[1]Ecology and Evolutionary Biology, School of Biosciences, The University of Sheffield, Alfred Denny Building, Western Bank, Sheffield, S10 2TN, United Kingdom

[2]Biology Program, Faculty of Natural Sciences, Universidad del Rosario, Bogotá, Colombia

[3]Department of Physics and Astronomy, The University of Sheffield, Hicks Building, Hounsfield Road, Sheffield, S3 7RH, United Kingdom

[4]Biology & Research Department, Mashpi Lodge, Ecuador

[5]Institute of Biotechnology, University of Helsinki, Finland

[6]ESRF - The European Synchrotron, 38043, Grenoble Cedex 9, France

[*]These authors contributed equally.

[†]Corresponding author: n.nadeau@sheffield.ac.uk.

Short title: Structural colour genetics in *Heliconius* butterflies.

Keywords: Structural colour, iridescence, gene expression, *Heliconius,* QTL, convergence.

Abstract

Structural colours, produced by the reflection of light from ultrastructures, have evolved multiple times in butterflies. Unlike pigmentary colours and patterns, little is known about the genetic basis of these colours. Reflective structures on wing-scale ridges are responsible for iridescent structural colour in many butterflies, including the Müllerian mimics *Heliconius erato* and *Heliconius melpomene.* Here we quantify aspects of scale ultrastructure variation and colour in crosses between iridescent and non-iridescent subspecies of both of these species and perform quantitative trait locus (QTL) mapping. We show that iridescent structural colour has a complex genetic basis in both species, with offspring from crosses having wide variation in blue colour (both hue and brightness) and scale structure measurements. We detect two different genomic regions in each species that explain modest amounts of this variation, with a sex-linked QTL in *H. erato* but not *H. melpomene.* We also find differences between species in the relationships between structure and colour, overall suggesting that these species have followed different evolutionary trajectories in their evolution of structural colour. We then identify genes within the QTL intervals that are differentially expressed between subspecies and/or wing regions, revealing likely candidates for genes controlling structural colour formation.

Introduction

Structural colours are some of the most vivid and striking colours found in nature. They are formed from the reflection and refraction of light from physical ultrastructures and examples of these can be found in nearly all groups of organisms. The structural colours of butterflies and moths are among the best described and play diverse roles, including initiation of courtship and mating behaviour (Silberglied and Taylor, 1978; Obara *et al.*, 2008), sex and species discrimination (Rutowski, 1977),

long distance mate recognition (Sweeney, Jiggins and Johnsen, 2003) and signalling of quality and adult condition (Kemp and Rutowski, 2007).

Butterflies and moths have evolved several mechanisms of structural colour production by modifying different components of wing scale morphology (Ghiradella, 1991). Scales typically consist of a flat lower lamina connected to an upper lamina by pillar-like trabeculae, with a small space separating the upper and lower laminae (Figure 1). The lower lamina can act as a thin film reflector that produces hues ranging from violet to green depending on its thickness (Stavenga, Leertouwer and Wilts, 2014; Wasik *et al.*, 2014; Thayer, Allen and Patel, 2020). The upper lamina has a more complex structure; it consists of a parallel array of ridges connected by cross-ribs, and modifications to these can yield diverse optical effects. For example, a lamellar structure in the ridges forms multilayer reflectors that produce the iridescent (angle dependent) blue in *Morpho* butterflies (Vukusic *et al.*, 1999) and UV reflectance in *Colias eurytheme* (Eisner *et al.*, 1969; Ghiradella, 1974). The variations in hue and brightness of colour produced in the intricate structures of the upper lamina depend on an interplay between the number of lamellae, the thickness of each layer and the spacing between the ridges (Parnell *et al.*, 2018).

Recent studies have begun to uncover the genetic and developmental basis of structural colours in some species (Lloyd and Nadeau, 2021), revealing a common pattern in *Bicyclus anynana* and *Junonia coenia*; artificial selection for colourful phenotypes quickly resulted in changes in lower lamina thickness, and consequently hue, in a relatively small number of generations (Wasik *et al.*, 2014; Thayer, Allen and Patel, 2020). Knockouts of known colour pattern genes (Concha *et al.*, 2019), and genes involved in pigment synthesis pathways (Zhang, Mazo-Vargas and Reed, 2017; Matsuoka and Monteiro, 2018), have shown that modification of these can result in altered scale ultrastructure, and moreover has brought about unexpected instances of structural colour (Zhang, Mazo-Vargas and Reed, 2017). Interestingly, there are groups of butterflies for which the gene *optix,* a known major colour pattern gene (Reed *et al.*, 2011), can jointly control pigment based colouration and thickness of

the lower lamina, producing blue structural colour (Thayer, Allen and Patel, 2020). It remains unclear whether this joint control extends to other butterfly taxa that produce structural colour using lower lamina reflection. In species with ridge reflectors, such as *Heliconius,* this does not seem to be the case (Zhang, Mazo-Vargas and Reed, 2017). More efforts are required to understand the genetic underpinnings and evolution of upper lamina architecture and the organisation of reflective nanostructures in the scales of iridescent butterflies.

Wing colour patterns have been widely studied in the *Heliconius* butterflies, a group of butterflies with a diverse set of aposematic colour patterns. These patterns show examples of both convergent evolution between distantly related species, and divergent evolution within species. Some species form mimicry rings, in which wing patterning is under strong positive frequency-dependent selection due to predation (Mallet and Barton, 1989). Pigment colour patterns are largely determined by a small number of genes which are homologous across species. Extensive research has uncovered a toolkit of five loci which control much of the colour pattern variation in *Heliconius* species, and some other Lepidoptera (Nadeau, 2016). *Heliconius* also display structural colour, and in comparison to the well-studied pigmentary colours, very little is known about the development and genetic basis of these. While overall scale morphology is similar between iridescent and non-iridescent scales in *Heliconius*, those with blue structural colour have overlapping ridge lamellae which act as multilayer reflectors (as in *Morpho*), along with a greater density of ridges on the scale (narrower ridge spacing) (Brien *et al.*, 2018; Parnell *et al.*, 2018).

Structural colour has evolved multiple times within the *Heliconius* genus (Parnell *et al.*, 2018). In some species, all subspecies have iridescent colour, while others exhibit interspecific variation in iridescence. *Heliconius erato* and *Heliconius melpomene* are two co-mimicking species which diverged around 10-13 Mya (Kozak *et al.*, 2015) with each evolving around 25 different colour pattern morphs (Sheppard *et al.*, 1985). Most of the different colour patterns are produced by pigment colours, but subspecies found west of the Andes in Ecuador and Colombia also have an iridescent

blue structural colour. *H. erato cyrbia* and *H. melpomene cythera* found in Western Ecuador have the brightest iridescence, while subspecies *H. erato demophoon* and *H. melpomene rosina,* found to the north in Panama, are matt black in the homologous wing regions (Figure 1). A hybrid zone forms between the iridescent and non-iridescent groups where they meet near the border between Panama and Colombia, and here, populations with intermediate levels of iridescence can be found (Curran *et al.*, 2020). Continuous variation in iridescent colour is observed in the centre of the hybrid zone and in experimental crosses (Brien *et al.*, 2018), suggesting that this trait is controlled by multiple genes. The evolution of pigmentation and simple colour pattern traits have frequently been shown to involve the re-use of a small number of genes across animal species (Hubbard *et al.*, 2010; Manceau *et al.*, 2010; Nadeau, 2016). However, we may expect the genetic basis of a quantitative trait controlled by multiple genes, such as iridescence in these species, to be less predictable (Conte *et al.*, 2012). In addition, iridescence in *H. e. cybria* is much brighter than in *H. m. cythera* (Parnell et al., 2018), suggesting some differences in scale structure and presumably genetic control of this structure formation process.

Here, we use crosses between subspecies of iridescent and non-iridescent *Heliconius* to determine the genetics of both colour and scale ultrastructure traits for the first time. We measure the intensity of blue colour and overall luminance (brightness) to assess variation in colour. We complement our estimates of colour variation with high throughput measurements of ridge spacing and cross-rib spacing using ultra small-angle X-ray scattering (USAXS). Using a quantitative trait locus (QTL) mapping approach, we can identify the location and effect sizes of loci in the genome that are controlling variation in iridescent colour. We then use RNA sequencing data from the same subspecies of each species to identify genes that are differentially expressed, both between subspecies and between wing regions that differ in scale type. Comparison of the genetic basis of these traits between *H. melpomene* and *H. erato*, two distantly related mimetic species, allows us to ask whether, like

pigment colour patterns, variation in iridescent colour and scale structure is also an example of gene reuse.

Methods

Experimental crosses

Experimental crosses were performed using geographical morphs of both *Heliconius erato* and *Heliconius melpomene*. In both species, morphs from Panama (*H. e. demophoon* and *H. m. rosina*) were crossed with morphs from Western Ecuador (*H. e. cyrbia* and *H. m. cythera*), then the F1 generation crossed with each other to produce an F2. For *H. erato*, we also analysed a backcross between the F1 and *H. e. cyrbia* (Figure 1). Due to a mix-up in the insectary, one of our largest *H. melpomene* broods, named 'EC70', was obtained from a cross between an F1 father and a mother of unknown parentage, likely an F2 individual. Further details of the crosses are in Table S1. A total of 155 *H. erato* individuals from 5 broods were used to generate linkage maps and perform QTL mapping (3 *demophoon* and 3 *cyrbia* grandparents, 11 F1 parents, and 40 backcross and 99 F2 offspring). For *H. melpomene*, data from 4 broods made up of 228 individuals were used (1 *rosina* and 2 *cythera* grandparents, 6 parents and 219 offspring, Table S1). Some of these crosses have previously been used for an analysis of quantitative pattern variation (Bainbridge *et al.*, 2020). Details of sequencing and linkage map construction are given in Bainbridge et al. (Bainbridge *et al.*, 2020) and in the Supplementary Material.

Phenotypic measurements

In the offspring of these crosses, we measured four phenotypes - blue colour (BR), luminance, ridge spacing and cross-rib spacing. Wings were photographed under standard lighting conditions (full details in (Brien *et al.*, 2018)). A colour checker in each photograph was used to standardise the photographs using the levels tool in Adobe Photoshop (CS3). RGB values were extracted from two blue/black areas of each wing (proximal areas of both the forewing and hindwing, Figure S1) and

averaged. Blue-red (BR) values were used as a measure of blue iridescent colour. These were calculated as (B-R)/(B+R), where 1 is completely blue and -1 is completely red. Luminance measured overall brightness and was calculated as R+G+B, with each colour having a maximum value of 255.

Scale structure measurements were extracted from ultra small-angle X-ray scattering (USAXS) data, from a single family of each species (n=56 *H. erato* F2 and n=73 *H. melpomene* (mother of unknown ancestry)). We measured between 33 and 113 points per individual along a linear proximodistal path across the proximal part of the forewing, which has the most vivid iridescence in the blue subspecies (Figure S1). The raw images were corrected for dark current and spatial distortion. SEM data from a subset of individuals was used to interpret the scattering patterns and develop robust methods for extracting mean ridge and cross-rib spacing values for the dorsal wing scales of all individuals (see Supplementary Material for details).

Quantitative Trait Locus mapping

The R package R/qtl was used for the QTL analysis (Broman *et al.*, 2003). For *H. erato*, initially the F2 crosses were analysed together and the backcross analysed separately. Genotype probabilities were calculated for these two groups using *calc.genoprob*. We ran standard interval mapping to estimate LOD (logarithm of the odds) scores using the *scanone* function with the Haley-Knott regression method. In the F2 analysis, sex and family were included as additive covariates, and family was included as an interactive covariate, to allow multiple families to be analysed together. Sex was included as a covariate in the backcross analysis to account for any sexual dimorphism. To determine the significance level for the QTL, we ran 1000 permutations, with *perm.Xsp=T* to get a separate threshold for the Z chromosome. A single F2 family (n=56) was used to analyse scale structure variation (ridge spacing and cross-rib spacing) using the same method, albeit a higher number of permutations was used for determining the significance level of the QTL (4000). For analyses of BR colour and luminance, LOD scores for the F2 crosses and the backcross were added together, to allow analysis of all individuals together to increase power, and the significance level recalculated in R/qtl.

Confidence intervals for the positions of QTL were determined with the *bayesint* function and we used a *fitqtl* model to calculate the phenotypic variance that each QTL explained. Genome scan plots and genotype plots were made with R/qtl2 (Broman *et al.*, 2019). Genetic distances in the QTL results are based on the observed recombination rate and expressed in centimorgans (cM), which is the distance between two markers that recombine once per generation. These were related to physical distances based on the marker positions in the assembled reference genome of each species.

The same method was used to run genome scans for BR colour and luminance in *H. melpomene*. Since the parentage of the mother of the EC70 brood is unknown, the maternal alleles in the offspring could not be assigned as being from either a *cythera* or a *rosina* grandparent. Therefore, in this family only paternal alleles were taken into account (and all maternal alleles were assigned to a *rosina* grandparent), and the cross was treated as if a backcross. LOD scores of the three F2 families were added to the LOD score from the EC70 family, as in *H. erato*, and the significance level recalculated. Again, a single family was used for analysis of scale structures (EC70, n=73).

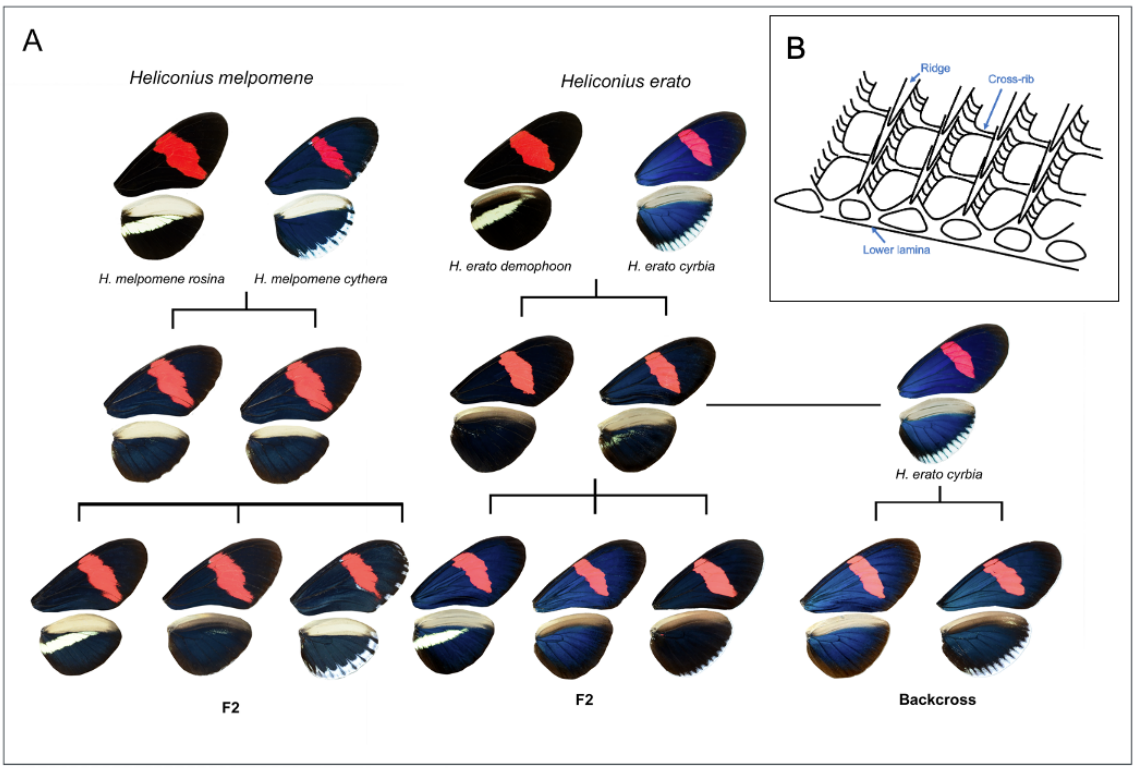

Figure 1. (A) Crosses between iridescent and non-iridescent morphs of *Heliconius melpomene* and *Heliconius erato*. For *H. melpomene* we used F2 crosses, plus one cross thought to be F1xF2 (not shown). For *H. erato*, we used F2 crosses and a backcross to the iridescent subspecies. (B) Scales are formed of a lower lamina and an upper lamina, which is made up of longitudinal ridges connected by cross-ribs.

Gene expression analysis

RNA sequence data was generated from 32 *H. erato* pupal wing samples (16 *H. e. demophoon,* 16 *H. e. cyrbia*) and *H. melpomene* pupal wing samples (16 *H. m. rosina*, 16 *H. m. cythera*), with individuals sampled from the same captive populations as those used for the crosses. Each of these samples contained 2 wing regions (the anterior hind-wing or "androconial" region, which has a different scale type, was dissected from the rest of the wing and sampled separately, Figure S1), and two developmental stages, 5 days post pupation (DPP) (50 % total pupation time) and 7 DPP (70 % total pupation time). Overall this gave four biological replicates for each tissue type/developmental stage/subspecies combination (Table S2).

Quality-trimmed reads were aligned to the respective *Heliconius* reference genomes using HISAT2 (version 2.1.0). Clustering of samples by Multi-Dimensional Scaling (MDS) on expression levels

revealed one of the *H. m. rosina* individuals had been incorrectly labelled (which was also confirmed by analysis of nucleotide variants) and was removed from subsequent analyses. Each species was analysed separately to identify genes that were differentially expressed between subspecies and between the wing regions for the iridescent blue subspecies (Figure S1), using the quasi-likelihood (QL) F-test in R/Bioconductor package EdgeR (version 3.28.1). For the wing region comparison, we used a general linear model approach, with the two wing regions nested within "individual ID" for each individual. We then determined if any significantly differentially expressed genes (between subspecies or wing region) were within the mapped QTL intervals. We further determined if any genes were differentially expressed in parallel between species. Details of further analyses of these data including gene set enrichment analysis are given in the Supplementary Material.

Results

QTL mapping in H. erato

We found significant correlations between scale structure and colour measurements: ridge spacing is negatively correlated with both luminance and BR values (Figure S2). Cross-rib spacing is positively correlated with ridge spacing and also negatively correlates with BR values (supplementary text). Significant QTL were found for three phenotypes in *H. erato* - BR colour, luminance and ridge spacing (Figure 2, Table 1, Table S3). When analysing the colour measurements, F2 and backcross genome scans were combined, and for BR values these showed 2 significant QTL on chromosomes 20 and the Z sex chromosome. These QTL were also found when analysing the F2 broods separately from the backcross brood (Figure S3). At both markers, individuals with Panama-type genotypes (Pan/Pan and Pan(W)) had lower BR values than Ecuador-type and heterozygous genotypes, following the expected trend (Figure 2). The QTL on the Z chromosome explained the largest proportion of the phenotypic variation in BR colour in both the F2 crosses (19.5%) and the backcross (24.6%), and the chromosome 20 QTL explained a further 12.3% in the F2 crosses.

Luminance (overall brightness of the wing region) was highly associated with the Z chromosome (Figure 2B). The significant marker did not map exactly to the same position as for the BR values but was apart by only 3.6cM, and confidence intervals for each overlap. Individuals with Ecuador-type alleles had higher luminance values than those with Panama-type alleles, showing the same trend as the BR values (Figure 2G). This QTL explained 40.2% of the variance in luminance values in the F2 crosses and 24.2% in the backcross. This was the only significant QTL for luminance, with nothing appearing on chromosome 20.

A single QTL on the Z chromosome was also significant for ridge spacing (Figure 2C). This marker was at a different position to the markers for BR and luminance, but mapped to the same marker as luminance when using the same individuals (Figure S3). All genotypes with one or two Ecuador-type alleles had similar ridge spacing, but those with a hemizygous Panama-type genotype ('Pan(W)' in Figure 2H) had significantly wider ridge spacing. This QTL explained 34.8% of variance in ridge spacing in this family. No significant QTL were found for cross-rib spacing, although the highest LOD score was seen on the Z chromosome (Figure 2D).

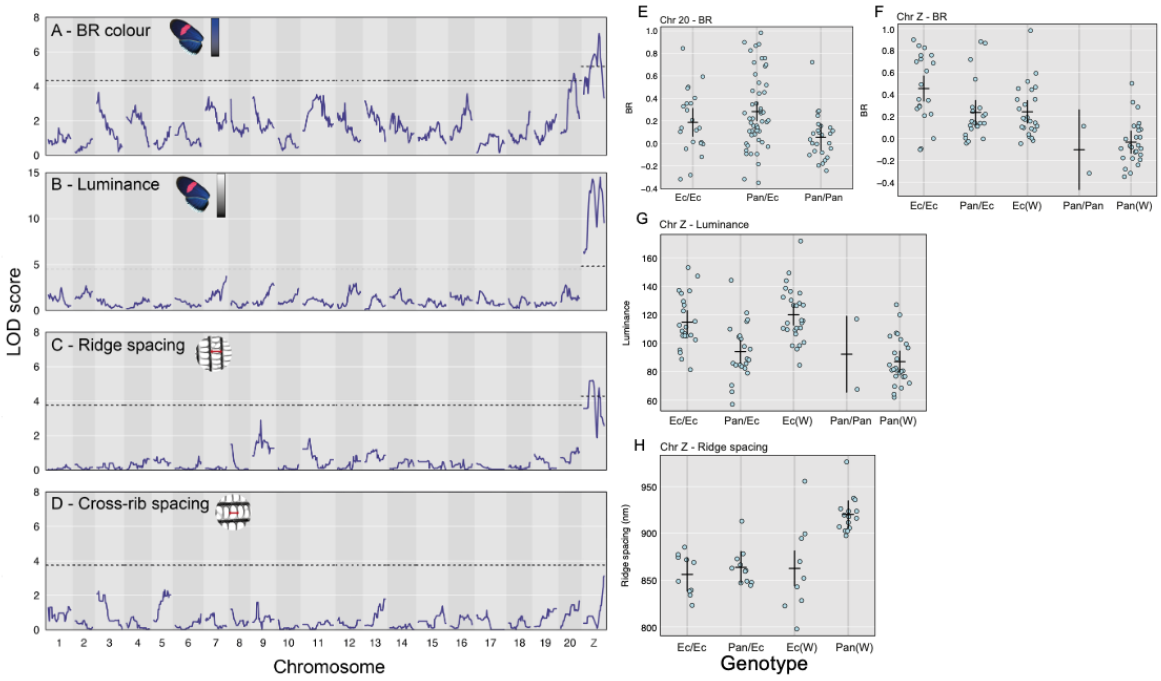

Figure 2. *H. erato* QTL plots including all families for BR colour (A) and luminance (B). QTL plots for a single family for ridge spacing (C) and cross-rib spacing (D). Dotted line shows p=0.05 significance level. The phenotypes of F2 individuals with different genotypes at the most significant

markers within each *H. erato* QTL. The QTL for BR on the chromosome 20 (E) and the Z (F). Significant Z markers for luminance (G) and ridge spacing (H). 'Pan' denotes alleles from the Panama subspecies *demophoon*, and 'Ec' the Ecuador subspecies *cyrbia*. Only two individuals have homozygous Panama-type *demophoon* genotypes at the Z chromosome marker due to the small number of individuals with a *demophoon* maternal grandfather (Table S1). Marker positions are shown in Table 1.

Phenotype	Marker	Chromosome	Position (cM)	LOD	p
Heliconius erato					
BR colour (all families)	Herato2101_12449252	Z	38.0	7.07	0.001
	Herato2001_12633065	20	32.9	4.75	0.022
Luminance (all families)	Herato2101_12449398	Z	41.6	14.50	<0.001
Ridge Spacing (single family)	Herato2101_7491127	Z	23.0	5.21	0.013
Heliconius melpomene					
BR (all families)	Hmel203003o_2119654	3	15.22	7.26	0.001
Luminance (all families)	Hmel203003o_2635435	3	17.97	13.61	<0.001
Ridge spacing (EC70)	Hmel207001o_11550301	7	53.61	5.71	<0.001

Table 1: Significant QTL found for three phenotypes in *H. erato* and *H. melpomene*.

QTL mapping in H. melpomene

In contrast to *H. erato*, scale structure measurements in *H. melpomene* did not correlate with either of the colour measurements (Figure S2, supplementary text). A single significant QTL for BR colour was found on chromosome 3 (Figure 3A, Table 1, Table S4) when combining the F2 families with EC70 (and for EC70 only, Figure S4). The marker explains 15.3% of phenotypic variation in EC70 (which should be an underestimate due to all maternal alleles being ignored) and 9.2% in the three F2 families. Luminance was also strongly associated with markers on chromosome 3 (Figure 3B, Figure S4). The associated marker was 2.75cM from the marker for BR colour, and the confidence intervals overlap. In contrast, for ridge spacing we found a significant QTL on chromosome 7 (using just the EC70 brood), explaining 30.3% of variation (Figure 3G). Again, no significant QTL were found for cross-rib spacing (Figure 3D). These results were generally supported by a genome-wide association

analysis using all SNP variation (which allowed maternal variation in EC70 to be included) and did not reveal any additional loci (Figure S5, see Supplementary Material for full results and methods).

Individuals with homozygous Panama-type genotypes at the mapped chromosome 3 markers had lower BR and luminance values (Figure 3). Individuals carrying Ecuador-type alleles at the mapped chromosome 7 marker showed reduced ridge spacing, consistent with the observation that the Panama subspecies has greater ridge spacing.

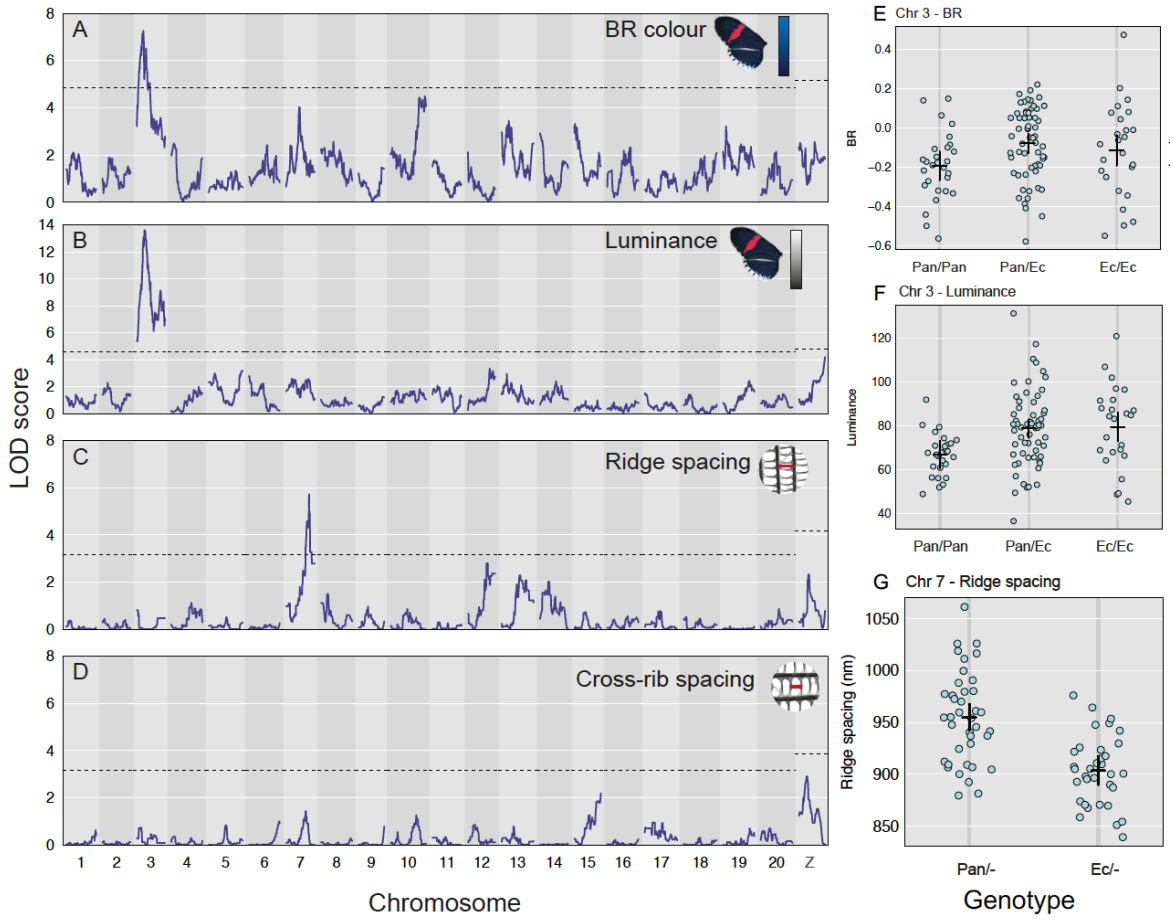

Figure 3. *H. melpomene* QTL plots including all families for BR colour (A) and luminance (B). QTL plots for a single family for ridge spacing (C) and cross-rib spacing (D). Genotype x phenotype plots for significant *H. melpomene* QTL. For the F2 families: (E) BR colour and (F) luminance. 'Pan' denotes alleles from the Panama subspecies *rosina*, and 'Ec' the Ecuador subspecies *cythera*. (G) Ridge spacing in the EC70 brood. Here we only know the origin of the paternal allele. Marker positions shown in Table 1.

Differential expression

A total of 24,118 genes were expressed in the wings of *H. erato* and 30,721 in the wings of *H. melpomene*. In both *H. erato* and *H. melpomene,* multidimensional scaling (MDS) analysis of expression levels revealed strong clustering by stage (dimension 1) and subspecies (dimension 2), leading to four distinct clusters (Figure S6). 907 and 1043 genes were differentially expressed (DE, FDR<0.05) between *H. erato cyrbia* and *H. erato demophoon* at 5 and 7 days post pupation, respectively (Table S5, S6). In *H. melpomene*, 203 and 29 genes were DE between *H. m. cythera* and *H. m. rosina* at 5 and 7 DPP, respectively (Table S7, S8). Comparing between wing regions, in *H. erato cyrbia* there was one gene at 5 DPP and 70 genes at 7 DPP DE (Table S9, S10); in *H. melpomene cythera*, there were six genes at 5 DPP and 50 genes at 7 DPP DE (Table S11, S12). Much of this DE will be due to the genome-wide divergence between subspecies (which is greater in *H. erato* than in *H. melpomene*, (Parnell *et al.*, 2018; Curran *et al.*, 2020)), we therefore used further comparisons to narrow down these lists of genes.

We may expect that genes involved in scale structure regulation would be DE both between subspecies and wing regions that differ in scale structure, but very few genes were found in both sets (Figure S7, Table S13). At 7 DPP, there were two genes upregulated in *H. erato* in both comparisons, *chitin deacetylase 1*, with a likely function in the deacetylation of chitin to chitosan and with potential structural roles in the cuticle (Thurmond *et al.*, 2018). The other gene had similarity with the circadian clock-controlled gene *daywake*. There was no overlap in significant, downregulated genes expressed at 7 DPP in *H. erato*. At 5 DPP in *H. erato,* there were no significant, concordantly DE genes. However, a *doublesex*-like gene on chromosome 8 narrowly missed the significance cutoff and was downregulated (LogFC < -1.5) in both comparisons (FDR = 0.02 between subspecies, FDR = 0.08 between wing regions). In *H. melpomene* at both 7 and 5 DPP there was no overlap between genes that were DE between subspecies and wing regions.

Genes involved in controlling scale structure may be similarly differentially expressed between species. Between subspecies, at 7 DPP there were no concordantly DE genes in either species. However, at 5 DPP, there were 2 concordant genes significantly DE, *Fatty acid synthase* and *Gamma-glutamylcyclotransferase* (Table S14). For the wing region comparison, at 7 DPP there were 4 concordant genes significantly DE in both species, the homeobox gene *invected, Transglutaminase, uncharacterized LOC113401078* and the *doublesex*-like gene, which was also DE between *H. erato* subspecies (at 5 DPP), but none at 5 DPP (although the *doublesex*-like gene is again DE in *H. melpomene*, Table S14).

DE genes in the QTL intervals

In order to identify candidate genes in the QTL intervals, we identified DE genes within these genomic regions. In *H. erato*, there were 2 and 5 DE genes in the 'BR' interval on chromosome 20 at 5 DPP and 7 DPP, respectively (Table S15). One of the genes at 7 DPP was *Fringe*, a boundary specific signalling molecule which modulates the Notch signalling pathway and has roles in eyespot formation and scale cell spacing in butterflies (Reed and Serfas, 2004; Thurmond *et al.*, 2018).

On the Z chromosome, at 5 DPP there were 27, 25, and 17 genes significantly DE between subspecies in the 'ridge spacing', 'luminance' and 'BR' intervals, respectively, with 16 genes shared between all 3 intervals (Figure 4, Table S15). Of note, the microtubule motor protein, *dynein heavy chain 6* was within all three QTL intervals and highly-upregulated (LogFC > 3.0, FDR < 0.05) in the iridescent subspecies. Additionally, an *O-GlcNAc transferase*, with strong similarity to *Drosophila* polycomb group gene *super sex combs* was highly differentially expressed (LogFC = -9.32, FDR<0.004) and matched the exact physical location of the 'BR' and 'luminance' marker within the genome.

At 7 DPP, on the Z chromosome there were 24, 23, and 14 genes significantly DE in the 'ridge spacing', 'luminance' and 'BR' intervals, respectively, with 14 shared across all 3 regions (Table

S15). The gene *trio*, which functions in actin structure regulation through activation of Rho-family GTPases (Thurmond *et al.*, 2018), was found in all three intervals with particular proximity to the 'ridge spacing' marker (405 kbp away from the start of this gene). In addition to the functional role of *trio*, its high expression and large fold change (logCPM = 7.34, LogFC = -2.29, FDR = 0.0015) makes it a particularly good candidate for a role in optical nanostructure development in *H. erato*. Furthermore, a novel gene (MSTRG.21985) was also DE expressed (LogFC= -1.28, FDR = 0.0115) and may be part of a Rho GTPase activating protein (182 bp upstream of a gene with this annotation).

In *H. melpomene,* there were no DE genes between subspecies in the 'ridge spacing' interval on chromosome 7 at either stage. However, 7 DPP, the gene *ringmaker,* which functions in microtubule organisation (Thurmond *et al.*, 2018) showed slight DE (logFC = -1.43, FDR = 0.144). On chromosome 3, in the BR interval there was 1 novel gene (MSTRG.3173) DE at 5 DPP (but this falls outside the luminance interval) and no DE genes at 7 DPP (Table S16). The gene *miniature,* which in fly bristles is a component of the cuticulin envelope functioning in interactions between the depositing cuticle, membrane and cytoskeleton (Roch, Alonso and Akam, 2003), falls in the overlap of the luminance and BR regions and shows slight DE at 5 DPP (logFC = 1.60, FDR = 0.192).

For the wing region comparison, in *H. erato* there were no genes DE at either stage within any of the QTL intervals. For *H. melpomene,* there was 1 DE gene in the 'BR' interval (but outside the 'luminance' interval) on chromosome 3 at 7 DPP (a *lactase-phlorizin hydrolase-like* gene) and no DE genes at 5 DPP. For the 'Ridge Spacing' interval on chromosome 7 there was 1 DE gene at 5 DPP, an *F-actin-uncapping protein LRRC16A* and 1 gene at 7 DPP, a *cuticle protein 18.6-like* gene (Table S17).

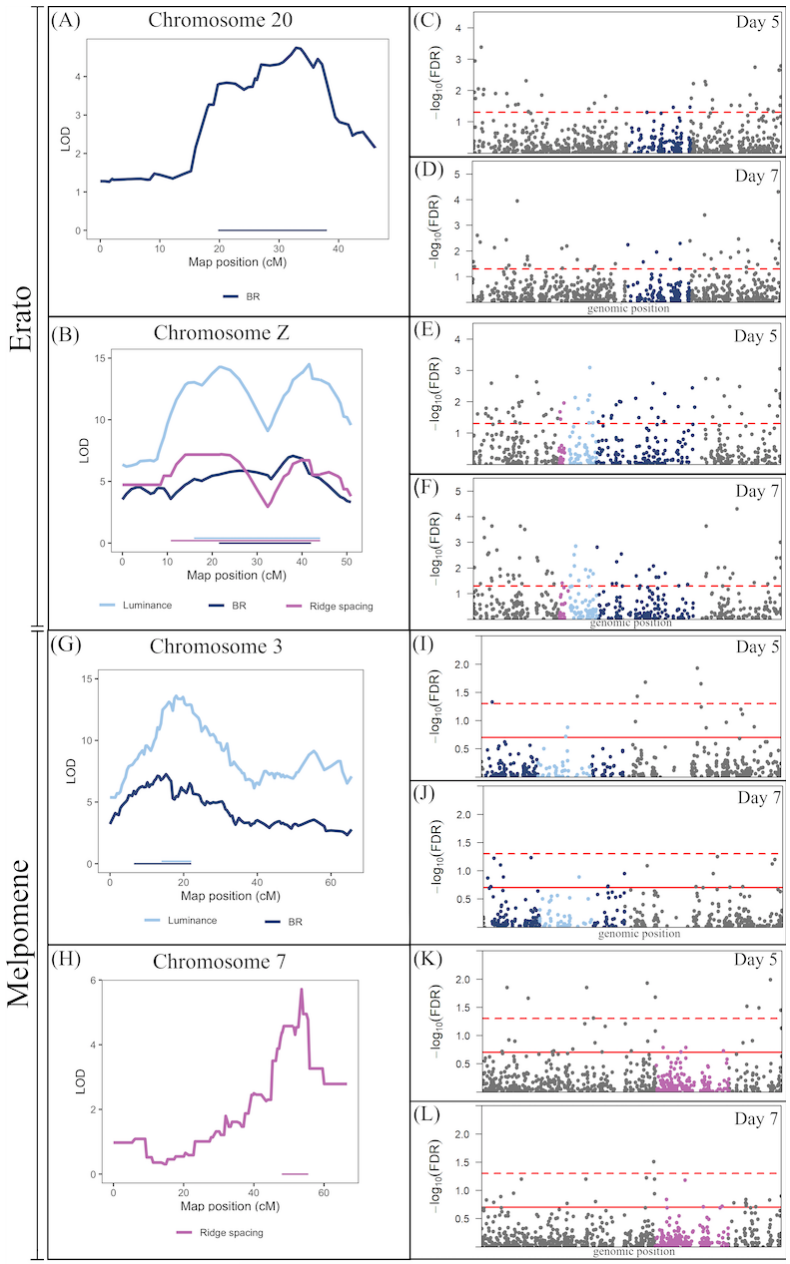

Figure 4. Differential expression of genes in the QTL in *Heliconius erato* (A-F) and *Heliconius melpomene* (G-L). Left panels: LOD scores and QTL intervals in *H. erato* (A, B) and *H. melpomene* (G, H). Right panels: -$\log_{10}$ False Discovery Rate (FDR) for differential expression. Genes are coloured within the QTL intervals for *H. erato* (C-F) and *H. melpomene* (I-L), with colours matching those of the intervals in the panels on the left. In E and F the QTL overlap, such that all genes in the BR and ridge spacing intervals also fall within the luminance interval, see Table S15 for details. In I

and J the luminance interval is within the BR interval. The dashed red line indicates FDR = 0.05 (significance), solid red line indicates FDR = 0.2.

Discussion

In one of the first studies to look at the genetics of structural colour variation in terms of both colour and structure, we show that the trait is controlled by multiple genes in the co-mimics *Heliconius erato* and *Heliconius melpomene*. While we found only a small number of QTL, these explain relatively little of the overall phenotypic variation, suggesting there are more loci which remain undetected. Some of these may be the genes that we detected as differentially expressed, but that fall outside the detected QTL intervals. Of particular interest are genes that we detected as differentially expressed both between subspecies and between wing regions that differ in scale type. *Chitin deacetylase 1* is one such candidate in *H. erato*, which is on chromosome 5 (not in a QTL interval). Chitin is the main component of the cuticle and the differential expression of a potential chitin-degrading gene could alter the formation of the scale ridges (Yu *et al.*, 2016).

Within each species, we find that hue and brightness (BR and luminance) are controlled by loci on the same chromosomes. In *H. erato*, this was on the Z chromosome, confirming our previous phenotypic analysis (Brien *et al.*, 2018), and in *H. melpomene*, on chromosome 3. An additional locus on chromosome 20 was also found to affect blue colour but not brightness in *H. erato*. The Z chromosome locus in *H. erato* appears to control ridge spacing, which could have a direct effect on the brightness of the reflectance by increasing the density of reflective structures. Indeed, in the single-family analyses, luminance and ridge spacing mapped to exactly the same marker. However, the observed correlation between brightness and ridge spacing in *H. erato* may be a product of an unobserved association between tighter ridge spacing and other aspects of scale nanostructure, specifically the number of lamellae layers within the ridges. Theoretical analyses and simulations of the optical properties of multilayers have revealed that increasing the number of layers will result in a

rapid increase of brightness; adding even a small number of layers produces a significant increase in the amount of reflected light (Kinoshita and Yoshioka, 2005). Therefore, the Z chromosome locus may be affecting multiple aspects of scale structure, producing the observed correlations between the different colour and structure measurements. Indeed, some DE genes in the Z locus may control multiple aspects of scale structure. For example, *trio* acts in several signalling pathways to promote reorganisation of the actin cytoskeleton through Rho GTPase activation. Its regulatory function may be repeatedly employed during scale development in the formation of different aspects of scale ultrastructure guided by the actin cytoskeleton. Interestingly, potentially related signalling genes, such as the novel gene located immediately before a Rho GTPase activating protein, also fall within this locus and are DE, potentially suggesting there are several functional genes linked together in this region.

In contrast, in *H. melpomene* we found different loci controlling colour and ridge spacing, suggesting a more dispersed genetic architecture and different loci controlling different aspects of scale structure. We found strong evidence for a locus on chromosome 3 controlling BR and luminance, but this locus appeared to have no effect on our measurements of scale structure and so is likely controlling other aspects of scale structure not quantified here. Instead, we find a locus on chromosome 7 that partially controls ridge spacing. We see a small, but not significant, effect of this chromosome on BR colour, suggesting that ridge spacing may have a small and relatively weak effect on colour in *H. melpomene*, despite the parental populations showing a similar difference in ridge spacing to that seen in *H. erato*. If *H. erato* has a locus on the Z chromosome that can control multiple aspects of scale structure, while *H. melpomene* requires mutations at loci dispersed around the genome, this could provide one explanation for how *H. erato* has been able to evolve brighter structural colour than that observed in *H. melpomene*.

In contrast to many of the loci for pigment colour patterns which are homologous across multiple *Heliconius* species, the loci controlling iridescence in *H. erato* and *H. melpomene* appear to be largely

different. Differences in the physical scale architecture and brightness of colour between the species perhaps makes these genetic differences unsurprising (Parnell *et al.*, 2018; Curran *et al.*, 2020). A lack of genetic parallelism may also be more likely for a quantitative trait such as iridescence (Conte *et al.*, 2012). Nevertheless, on the Z chromosome in *H. melpomene*, we do observe elevated LOD scores in the QTL analysis and low p-value SNPs in the GWAS for both scale structure traits, but neither of the colour traits. This suggests that *H. melpomene* may have a locus homologous to that in *H. erato,* which is controlling some aspects of scale structure variation, but with apparently little or no effect on colour variation. In addition, we find some genes that appear to show parallel expression patterns between species. Of particular interest is a *doublesex*-like gene that is DE between wing regions in both species and between *H. erato* subspecies. A different duplication of *doublesex* has been found to control structural colour in the Dogface butterfly (Rodriguez-Caro *et al.*, 2021), making this an interesting, potentially parallel candidate between species. It is possible that the evolutionary pathways may be different between species, but have triggered expression changes in similar downstream developmental pathways. However, we found very few genes that show concordant expression patterns between species.

In recent years, reverse genetics research has revealed a surprising connection between the molecular machinery underlying the development of pigmented wing patterns and the ultrastructure of butterfly scales in various species (Zhang, Mazo-Vargas and Reed, 2017; Concha *et al.*, 2019; Fenner *et al.*, 2020; Livraghi *et al.*, 2021). However, our QTL are not associated with any known colour pattern gene of large or small effect in *Heliconius* (*aristaless, WntA, vvl*, *cortex* and *optix* - located on chromosomes 1, 10, 13, 15 and 18 respectively) (Nadeau, 2016). Our findings show that *H. erato* and *H. melpomene* do not use the known molecular machinery of wing pattern production for sculpting specialised nanostructures and iridescent wings, and that the production of structural colour is completely decoupled from that of mimicry related wing pattern regulation and pigment production.

Overall, we show major differences in the genetic basis of structural colour in *H. erato* and *H. melpomene*. Combining this with gene expression analyses, we have been able to identify novel candidate genes for the control of structural colour variation with potential functions in chitin metabolism, cytoskeleton formation, gene expression regulation and cell signalling.

Acknowledgements

We thank the governments of Ecuador and Panama for permission to collect butterflies. Thanks to Darwin Chalá, Juan López and Gabriela Irazábal for their assistance with the crosses. We are grateful to the European Synchrotron Radiation Facility for provision of X-ray beamtime under proposal LS2720, and to Andrew Dennison for assistance with USAXS data collection. We also thank Alexandre Thiery for his assistance with the differential expression analysis. Library preparation and sequencing was performed by staff at the Edinburgh Genomics Facility, at the University of Edinburgh. We thank Alan Dunbar for use of the scanning electron microscope.

Data availability

Genomic sequence data from the crosses are deposited in the European Nucleotide Archive under project number PRJEB38330. RNA sequence data are deposited under project number XXXX Photographs of all samples can be found at https://doi.org/10.5281/zenodo.3799188. USAXS data handling scripts can be found at https://github.com/juanenciso14/butterfly_usaxs. Linkage maps, QTL scripts and all phenotypic measurements used will be available on publication.

Author contributions

MNB and JER performed the QTL analyses and wrote the manuscript with NJN and VJL. PR and MNB constructed the linkage maps. AJP co-ordinated collection of the USAXS data, which were collected by TZ, AJP, EVC, NJN and MNB. JER analysed the USAXS and SEM data and ran the association analysis. PAS, CM, MNB, EVC and NJN performed the crosses. NJN collected the tissue and extracted the RNA for the gene expression analysis, VJL performed all gene expression analyses. NJN devised and co-ordinated the study. All authors read and commented on the manuscript.

Funding disclosure

This work was funded by the "Speciation and adaptation genes: from loci to causative mutations" issue of Philosophical Transactions B through an Independent Research Fellowship (NE/K008498/1) to NJN. MNB, EVC and VJL were funded by the NERC doctoral training partnership, ACCE (NE/L002450/1). JER is funded through the Leverhulme Centre for Advanced Biological Modelling as well as scholarships from Universidad del Rosario and the University of Sheffield. The scanning electron microscope is funded via a EPSRC 4CU grant (EP/K001329/1).

References

Bainbridge, H. E. *et al.* (2020) 'Limited genetic parallels underlie convergent evolution of quantitative pattern variation in mimetic butterflies', *Journal of evolutionary biology*. doi: 10.1111/jeb.13704.

Brien, M. N. *et al.* (2018) 'Phenotypic variation in crosses shows that iridescent structural colour is sex-linked and controlled by multiple genes', *Interface focus*, 9(1), p. 20180047.

Broman, K. W. *et al.* (2003) 'R/qtl: QTL mapping in experimental crosses', *Bioinformatics*, pp. 889–890. doi: 10.1093/bioinformatics/btg112.

Broman, K. W. *et al.* (2019) 'R/qtl2: Software for Mapping Quantitative Trait Loci with High-Dimensional Data and Multiparent Populations', *Genetics*, pp. 495–502. doi: 10.1534/genetics.118.301595.

Concha, C. *et al.* (2019) 'Interplay between Developmental Flexibility and Determinism in the Evolution of Mimetic Heliconius Wing Patterns', *Current biology: CB*, 29(23), pp. 3996–4009.e4.

Conte, G. L. *et al.* (2012) 'The probability of genetic parallelism and convergence in natural populations', *Proceedings. Biological sciences / The Royal Society*, 279(1749), pp. 5039–5047.

Curran, E. V. *et al.* (2020) 'Müllerian mimicry of a quantitative trait despite contrasting levels of genomic divergence and selection', *Molecular ecology*, 29(11), pp. 2016–2030.

Eisner, T. *et al.* (1969) 'Ultraviolet video-viewing: the television camera as an insect eve', *Science*, 166(3909), pp. 1172–1174.

Fenner, J. *et al.* (2020) 'Wnt Genes in Wing Pattern Development of Coliadinae Butterflies', *Frontiers in Ecology and Evolution*. doi: 10.3389/fevo.2020.00197.

Ghiradella, H. (1974) 'Development of ultraviolet-reflecting butterfly scales: How to make an interference filter', *Journal of morphology*, 142(4), pp. 395–409.

Ghiradella, H. (1991) 'Light and color on the wing: structural colors in butterflies and moths', *Applied optics*, 30(24), pp. 3492–3500.

Hubbard, J. K. *et al.* (2010) 'Vertebrate pigmentation: from underlying genes to adaptive function',

Trends in genetics: TIG, 26(5), pp. 231–239.

Kemp, D. J. and Rutowski, R. L. (2007) 'Condition dependence, quantitative genetics, and the potential signal content of iridescent ultraviolet butterfly coloration', *Evolution; international journal of organic evolution*, 61(1), pp. 168–183.

Kinoshita, S. and Yoshioka, S. (2005) 'Structural colors in nature: the role of regularity and irregularity in the structure', *Chemphyschem: a European journal of chemical physics and physical chemistry*, 6(8), pp. 1442–1459.

Kozak, K. M. *et al.* (2015) 'Multilocus species trees show the recent adaptive radiation of the mimetic heliconius butterflies', *Systematic biology*, 64(3), pp. 505–524.

Livraghi, L. *et al.* (2021) 'Cortex cis-regulatory switches establish scale colour identity and pattern diversity in', *eLife*, 10. doi: 10.7554/eLife.68549.

Lloyd, V. J. and Nadeau, N. J. (2021) 'The evolution of structural colour in butterflies', *Current opinion in genetics & development*, 69, pp. 28–34.

Mallet, J. and Barton, N. H. (1989) 'STRONG NATURAL SELECTION IN A WARNING-COLOR HYBRID ZONE', *Evolution; international journal of organic evolution*, 43(2), pp. 421–431.

Manceau, M. *et al.* (2010) 'Convergence in pigmentation at multiple levels: mutations, genes and function', *Philosophical Transactions of the Royal Society B: Biological Sciences*, pp. 2439–2450. doi: 10.1098/rstb.2010.0104.

Matsuoka, Y. and Monteiro, A. (2018) 'Melanin Pathway Genes Regulate Color and Morphology of Butterfly Wing Scales', *Cell reports*, 24(1), pp. 56–65.

Nadeau, N. J. (2016) 'Genes controlling mimetic colour pattern variation in butterflies', *Current opinion in insect science*, 17, pp. 24–31.

Obara, Y. *et al.* (2008) 'Mate preference in males of the cabbage butterfly, Pieris rapae crucivora, changes seasonally with the change in female UV color', *Zoological science*, 25(1), pp. 1–5.

Parnell, A. J. *et al.* (2018) 'Wing scale ultrastructure underlying convergent and divergent iridescent colours in mimetic butterflies', *Journal of the Royal Society, Interface / the Royal Society*, 15(141). doi: 10.1098/rsif.2017.0948.

Reed, R. D. *et al.* (2011) 'optix drives the repeated convergent evolution of butterfly wing pattern mimicry', *Science*, 333(6046), pp. 1137–1141.

Reed, R. D. and Serfas, M. S. (2004) 'Butterfly wing pattern evolution is associated with changes in a Notch/Distal-less temporal pattern formation process', *Current biology: CB*, 14(13), pp. 1159–1166.

Roch, F., Alonso, C. R. and Akam, M. (2003) 'Drosophila miniature and dusky encode ZP proteins required for cytoskeletal reorganisation during wing morphogenesis', *Journal of cell science*, 116(Pt 7), pp. 1199–1207.

Rodriguez-Caro, F. *et al.* (2021) 'Novel doublesex duplication associated with sexually dimorphic development of dogface butterfly wings', *Molecular biology and evolution*. doi: 10.1093/molbev/msab228.

Rutowski, R. L. (1977) 'The use of visual cues in sexual and species discrimination by males of the small sulphur butterfly Eurema lisa (lepidoptera, pieridae)', *Journal of Comparative Physiology*,

115(1), pp. 61–74.

Sheppard, P. M. *et al.* (1985) 'Genetics and the evolution of muellerian mimicry in heliconius butterflies', *Philosophical Transactions of the Royal Society of London. B, Biological Sciences*, pp. 433–610. doi: 10.1098/rstb.1985.0066.

Silberglied, R. E. and Taylor, O. R., Jr. (1978) 'Ultraviolet reflection and its behavioral role in the courtship of the sulfur butterflies Colias eurytheme and C. philodice (Lepidoptera, Pieridae)', *Behavioral ecology and sociobiology*, 3(3), pp. 203–243.

Stavenga, D. G., Leertouwer, H. L. and Wilts, B. D. (2014) 'Coloration principles of nymphaline butterflies - thin films, melanin, ommochromes and wing scale stacking', *The Journal of experimental biology*, 217(Pt 12), pp. 2171–2180.

Sweeney, A., Jiggins, C. and Johnsen, S. (2003) 'Insect communication: Polarized light as a butterfly mating signal', *Nature*, 423(6935), pp. 31–32.

Thayer, R. C., Allen, F. I. and Patel, N. H. (2020) 'Structural color in butterflies evolves by tuning scale lamina thickness', *eLife*, 9. doi: 10.7554/eLife.52187.

Thurmond, J. *et al.* (2018) 'FlyBase 2.0: the next generation', *Nucleic acids research*, 47(D1), pp. D759–D765.

Vukusic, P. *et al.* (1999) 'Quantified interference and diffraction in single Morpho butterfly scales', *Proceedings of the Royal Society of London. Series B, Containing papers of a Biological character. Royal Society* , 266(1427), pp. 1403–1411.

Wasik, B. R. *et al.* (2014) 'Artificial selection for structural color on butterfly wings and comparison with natural evolution', *Proceedings of the National Academy of Sciences of the United States of America*, 111(33), pp. 12109–12114.

Yu, R. *et al.* (2016) 'Helicoidal Organization of Chitin in the Cuticle of the Migratory Locust Requires the Function of the Chitin Deacetylase2 Enzyme (LmCDA2)', *The Journal of biological chemistry*, 291(47), pp. 24352–24363.

Zhang, L., Mazo-Vargas, A. and Reed, R. D. (2017) 'Single master regulatory gene coordinates the evolution and development of butterfly color and iridescence', *Proceedings of the National Academy of Sciences of the United States of America*, 114(40), pp. 10707–10712.

Appendix B

Phenotypic variation in *Heliconius erato* crosses shows that iridescent structral colour is sex-linked and controlled by multiple genes

Paper in the format published in the journal Interface Focus.

INTERFACE FOCUS

rsfs.royalsocietypublishing.org

Research

Cite this article: Brien MN *et al*. 2018 Phenotypic variation in *Heliconius erato* crosses shows that iridescent structural colour is sex-linked and controlled by multiple genes. *Interface Focus* **9**: 20180047.
http://dx.doi.org/10.1098/rsfs.2018.0047

Accepted: 29 October 2018

One contribution of 11 to a theme issue 'Living light: optics, ecology and design principles of natural photonic structures'.

Subject Areas:
biophysics

Keywords:
structural colour, *Heliconius*, butterflies, iridescence, evolution, quantitative genetics

Authors for correspondence:
Melanie N. Brien
e-mail: mnbrien1@sheffield.ac.uk
Nicola J. Nadeau
e-mail: n.nadeau@sheffield.ac.uk

Electronic supplementary material is available online at https://dx.doi.org/10.6084/m9.figshare.c.4302737.

THE ROYAL SOCIETY PUBLISHING

Phenotypic variation in *Heliconius erato* crosses shows that iridescent structural colour is sex-linked and controlled by multiple genes

Melanie N. Brien[1], Juan Enciso-Romero[1,2], Andrew J. Parnell[3], Patricio A. Salazar[1,4], Carlos Morochz[5], Darwin Chalá[5], Hannah E. Bainbridge[1], Thomas Zinn[6], Emma V. Curran[1] and Nicola J. Nadeau[1]

[1]Department of Animal and Plant Sciences, University of Sheffield, Alfred Denny Building, Western Bank, Sheffield S10 2TN, UK
[2]Biology Program, Faculty of Natural Sciences and Mathematics, Universidad del Rosario, Bogotá, Colombia
[3]Department of Physics and Astronomy, University of Sheffield, Hicks Building, Hounsfield Road, Sheffield S3 7RH, UK
[4]Centro de Investigación en Biodiversidad y Cambio Climático (BioCamb), Universidad Tecnológica Indoamérica, Quito, Ecuador
[5]Mashpi Reserve, Ecuador
[6]ESRF — The European Synchrotron, 38043 Grenoble Cedex 9, France

MNB, 0000-0002-3089-4776; JE-R, 0000-0002-4143-3705; AJP, 0000-0001-8606-8644; NJN, 0000-0002-9319-921X

Bright, highly reflective iridescent colours can be seen across nature and are produced by the scattering of light from nanostructures. *Heliconius* butterflies have been widely studied for their diversity and mimicry of wing colour patterns. Despite iridescence evolving multiple times in this genus, little is known about the genetic basis of the colour and the development of the structures which produce it. *Heliconius erato* can be found across Central and South America, but only races found in western Ecuador and Colombia have developed blue iridescent colour. Here, we use crosses between iridescent and non-iridescent races of *H. erato* to study phenotypic variation in the resulting F_2 generation. Using measurements of blue colour from photographs, we find that iridescent structural colour is a quantitative trait controlled by multiple genes, with strong evidence for loci on the Z sex chromosome. Iridescence is not linked to the Mendelian colour pattern locus that also segregates in these crosses (controlled by the gene *cortex*). Small-angle X-ray scattering data show that spacing between longitudinal ridges on the scales, which affects the intensity of the blue reflectance, also varies quantitatively in F_2 crosses.

1. Introduction

Structural colours are bright and highly reflective colours produced by the interaction of light with nanostructures. They can be seen across a range of taxa, including fish, birds, molluscs and insects, and have numerous functions covering visual communication and recognition, mate choice and thermoregulation [1–3]. Despite this, little is known about the genetic basis of structural colour, or how genetic variation translates into developmental differences of the nanostructures.

Examples of the different ways structural colour is produced can be seen across butterfly species. Multilayer reflectors produce the bright blue colour in *Morpho* butterflies [4], while *Callophrys rubi* have a highly connected gyroid structure contained within the upper and lower lamina [5]. Scales on butterfly wings are formed as a long, flattened extension of the cuticle. Generally, they are composed of longitudinal ridges which are linked transversely by cross-ribs (figure 1). These nanostructures make up a variety of repeating elements which can vary in

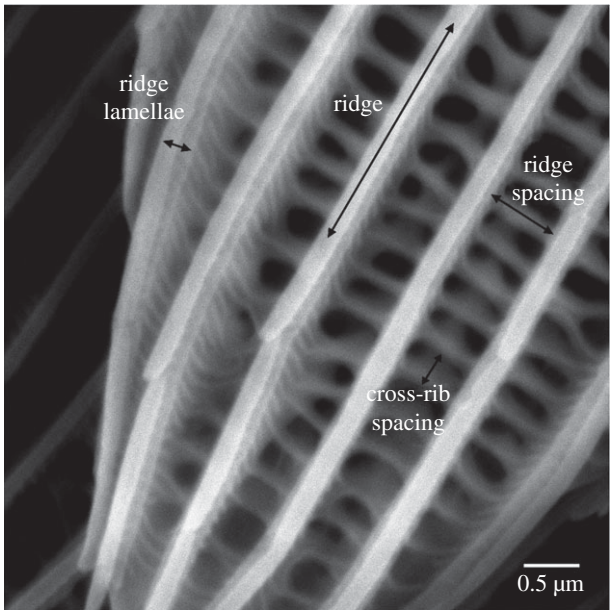

Figure 1. Scanning electron microscope image showing the structures on a *Heliconius* wing scale. Longitudinal ridges, composed of overlapping lamellae, are connected by cross-ribs.

thickness and patterning, producing different visual effects. F-actin filaments are important in the development of wing scale cells and appear to pre-pattern where the ridges will form [6].

The neotropical *Heliconius* butterflies (Nymphalidae) are well known for the diversity in their wing colour patterns and mimicry between species [7]. Many of these colour patterns are formed by chemical pigments, but several species also exhibit structurally produced blue reflectance. *Heliconius* butterflies can produce structural colour by thin film interference using different features on their scales. Longwing *H. doris*, for example, display hindwing colour reflected by their lower lamina; the resulting colour can be blue or green depending on the absence or presence of the yellow pigment 3-OH-kynurenine [8]. Several other species, including *Heliconius erato*, produce iridescent colours, that change in both brightness and wavelength of peak reflectance with angle, using layered lamellae that make up their scale ridges. Density of the ridges, the curvature and layering of the lamellae affect the intensity of the structural colour, with denser ridge spacing producing higher reflectance [9].

Heliconius erato is found across Central and South America and has evolved more than 25 races with a diversity of colour patterns. These aposematic patterns are mimetic with *Heliconius melpomene* and are an example of Müllerian mimicry. Variation in pigment colour patterns has been found to map to a handful of loci that control a diversity of patterns in several distantly related species [10–13]. Despite iridescent colour evolving multiple times in *Heliconius*, the genetics of this trait have not been studied to the same extent as pigment colour patterns, likely due to the difficulty of measuring the trait. Iridescent *H. erato cyrbia* is found on the western slopes of the Andes in Ecuador. *Heliconius erato* races found further north in Panama lack this structural colour, and hybrid zones arise between the iridescent and non-iridescent races, where populations with intermediate levels of iridescence can be found. Previous researchers have noted that levels of iridescence vary in F_2 hybrid crosses and appear to do so in a continuous manner [12,14], but have not attempted to quantify the variation. Continuous variation in the F_2 would suggest that the trait is controlled by multiple loci and therefore not controlled by the 'tool kit' of major effect loci that regulate pigment colour patterns. The genes controlling variation in iridescence may perhaps be those directly controlling the formation of scale structure.

Experimental genetic crosses can be used to estimate the number of genes involved in controlling a trait by investigating the distribution of the phenotype across segregating generations [15]. Traits that are controlled by a single locus of major effect will segregate according to Mendelian ratios, with 50–100% of individuals in the F_2 generation having phenotypes the same as one or other of their parents (depending on dominance of the alleles). The more individuals there are with intermediate phenotypes, the more loci are likely to be involved, as a greater number of allele combinations will be possible. We can also estimate positions of loci in the genome by looking for links to known loci which control other phenotypes and by looking for patterns of sex linkage.

Here, we aim to determine whether iridescence in *H. erato* is a quantitative trait controlled by multiple genes, and if any of these genes are sex-linked or linked to known colour pattern loci, by looking at the segregation of the trait in F_2 crosses between different races. *Heliconius erato demophoon* from Panama is black with red and yellow bands. This race was crossed to *H. erato cyrbia* from Ecuador, which has a similar colour pattern but has an iridescent blue colour instead of being matt black (figure 2). The only major colour pattern differences between these races are the white margin on the hindwing of *H. erato cyrbia* and the yellow bar on the dorsal hindwing of *H. erato demophoon*. Based on previous crosses, these are likely to be controlled by alternative alleles of the *Cr* locus on linkage group 15, which is homologous to three tightly linked loci (*Yb*, *Sb* and *N*) in *H. melpomene* [10] and corresponds to the gene *cortex* [16]. There are also differences in the size and position of the red forewing band between *cyrbia* and *demophoon*, likely controlled by the gene *WntA*, found on chromosome 10 [12,17,18]. We also use small-angle X-ray scattering (SAXS) to quantify ridge spacing in broods. As several aspects of scale morphology are known to vary between the iridescent and non-iridescent races [9], it is possible that apparent continuous variation in the reflectance in the F_2 could be due to independent segregation of these different features, each of which may be controlled by a major effect gene. Therefore, we also test whether ridge spacing shows continuous variation in the F_2 generation.

2. Material and methods

2.1. Crossing experiments

Experimental crosses were performed between geographical races of *H. erato* at the insectary in Mashpi Reserve, Ecuador, over a period of 2 years. *Heliconius erato demophoon* were collected from Gamboa, Panama (9.12° N, 79.67° W) in May 2014, then transported to Mashpi, Ecuador (0.17° N, 78.87° W), where they were kept as stocks. Iridescent *H. erato cyrbia* were collected from the area around Mashpi. *Heliconius erato demophoon* were crossed with *H. e. cyrbia*, and the F_1 generation crossed together, along with the addition of two backcrosses (BC) between the F_1 and *cyrbia* (figure 2). Crosses were reciprocal, so that in roughly half of the first generation crosses the female was the iridescent race and the male non-iridescent, and vice versa. In line with previous studies with intraspecific *Heliconius* hybrids [12,19], races readily

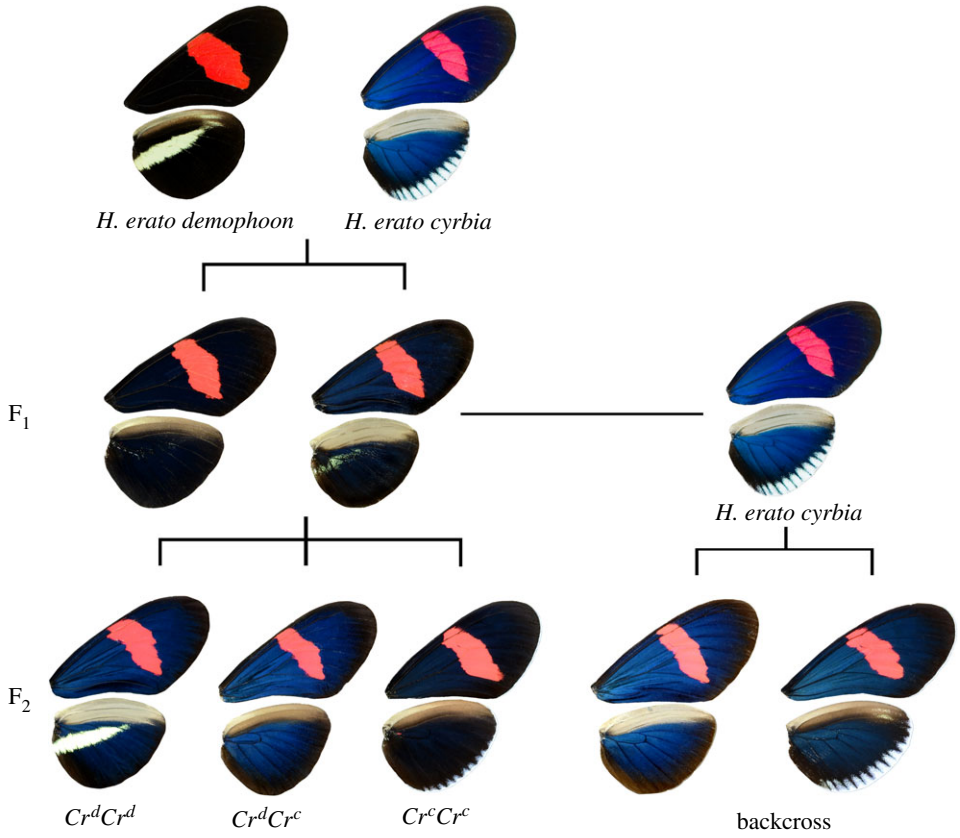

Figure 2. Cross-design and examples of colour pattern variation in *H. erato* F_1, F_2 and backcross generations. Examples of the *Cr* genotypes are shown in the F_2 generation.

Table 1. *Heliconius erato* crosses performed and the number of offspring produced from each. See electronic supplementary material table S2 for details of each cross.

cross type	number of crosses	number of offspring phenotyped for blue values	number of offspring phenotyped for ridge spacing
F_1: *demophoon* ♂ × *cyrbia* ♀	2	37	3
F_1: *cyrbia* ♂ × *demophoon* ♀	3	33	3
F_2: *cyrbia* maternal grandfather	3	100	59
F_2: *demophoon* maternal grandfather	3	14	0
backcross: *cyrbia* ♂ × (*demophoon* ♂ × *cyrbia* ♀)	2	16	0
backcross: *cyrbia* ♀ × (*cyrbia* ♂ × *demophoon* ♀)	1	49	0

hybridized and we did not observe any evidence of hybrid inviability or differing success between the reciprocal crosses. *Passiflora* species were provided as larval food plants and for oviposition, and butterflies were given *Lantana camara* and other locally collected flowers, plus sugar solution (10%) and pollen to feed. The bodies of the parents and offspring were preserved in NaCl saturated 20% dimethyl sulfoxide 0.25 M EDTA solution to preserve the DNA, and the wings stored separately in glassine envelopes. A total of 302 individuals obtained from 14 crosses were used in the analysis (table 1).

2.2. Phenotypic colour analysis

All butterfly wings were photographed flat under standard lighting conditions using a mounted Nikon D7000 DSLR camera with a 40 mm f/2.8 lens set to an aperture of f/10, shutter speed of 1/60 and ISO of 100. Lights were mounted at a fixed angle of 45° to maximize the observed blue reflection from the iridescent wing regions. All photographs also included an X-Rite Colour Checker to help standardize the colour of the images. RAW format images were standardized using the levels tool in Adobe Photoshop CS2 (v. 9.0). Using the colour histogram plugin in ImageJ [20,21], red-green-blue (RGB) values were recorded from two sections of the wings and averaged (figure 3). These areas were chosen because the scales on these sections of the wings close to the body tended to be the least damaged and worn, so a more accurate measurement of the colour could be taken, and the wing venation was used as a marker to allow the same areas to be measured each time.

Blue reflection from the iridescent wing regions was measured as variation in blue-red (BR) colour. This was calculated as $(B - R)/(B + R)$, with -1 being completely red and 1 being completely blue. The level of UV reflectance could not be measured from our photographs. Previous spectral measurements of the wing reflectance show that peak reflectance for *H. erato cyrbia* is just below the visible range at about 360–370 nm, with much of the reflectance being within the human visible range, while *H. erato demophoon* reflects very little but tends to show highest reflectance

Figure 3. RGB values were measured in the hatched areas highlighted on the right wings and averaged for each butterfly. Left wings were used when the right side were too damaged. SAXS measurements were taken along the dotted line shown on the left forewing. (Online version in colour.)

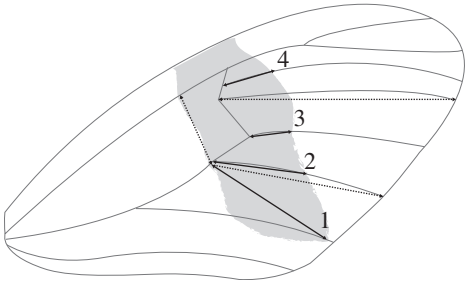

Figure 4. Four measurements of forewing band width were taken (bold arrows) along with three further measurements to standardize wing size (dotted arrows), using wing veins as points of reference.

in the red–infrared range [9]. Therefore, the colour values will allow variation in colour and reflectance to be measured but will not represent butterfly visual systems. Repeatability of the colour measurements was tested using the repeatability equation of Whitlock & Schluter [22] by taking five measurements each on five randomly selected individuals. This estimates the fraction of total variance that is among groups in a random-effects ANOVA. We used the Castle–Wright estimator:

$$n_e = \frac{[\mu(P_1) - \mu(P_2)]^2 - \mathrm{Var}[\mu(P_1)] - \mathrm{Var}[\mu(P_2)]}{8\mathrm{Var}(S)},$$

where $S = \mathrm{Var}(F_2) - \mathrm{Var}(F_1)$, to estimate the effective number of genetic loci (n_e) contributing to variation in the trait [15,23,24]. This is the difference between the mean BR values of the parental races squared, then the subtraction of the two variance terms, which corrects for sampling error of the estimates of the parental means (P_1 and P_2).

The genotype at the *Cr* locus was scored in 286 individuals based on the presence and absence of the white hindwing margin and the dorsal hindwing yellow bar, under the assumption that these pattern elements are controlled by alternative alleles of the *Cr* locus [10,25]. The *demophoon* genotype has the yellow bar present and is scored as Cr^dCr^d, a white margin indicates the *cyrbia* genotype and this is scored as Cr^cCr^c, and the Cr^dCr^c heterozygous genotype has neither of these elements (figure 2). To look for association between variation in the red band and blue colour, we took four measurements of forewing band size in 71 F_2 individuals and three further measurements to adjust for wing size (figure 4), based on methods from Baxter *et al.* [26]. Using ImageJ, band measurements were carried out on the dorsal side of the wing and repeated for both the left and right wings. The average of these two measurements was divided by the average of the three standardizing wing measurements. The three standardizing wing measurements were also used to assess overall size of these individuals.

All statistical analyses were carried out in the R statistical package v. 3.4.2 [27]. Welch's *t*-tests were used for analysis of differences between sexes and reciprocal crosses. ANOVA models were used to compare blue values with *Cr* genotypes. Yellow bar and white margin traits were tested for departures from the expected segregation ratios, based on the above hypothesis of the linkage and Mendelian inheritance, using a χ^2 test. Correlations between BR values and forewing red band measurements, ridge spacing and cross-rib spacing (see below) were tested with the Pearson correlation coefficient.

2.3. Small-angle X-ray scattering data collection

We estimated the size of the spacing between scale ridges and between cross-ribs (figure 1) using SAXS carried out at the ID02 beamline at the European Synchrotron (ESRF), Grenoble, France [28]. The detector was a high-sensitivity FReLon 16 M Kodak CCD with an effective area of 2048 × 2048 pixels (24 µm pixel size). The X-ray wavelength λ was 0.0995 nm (12.45 keV), the beam was collimated to 50 µm × 50 µm and the accessible q-range was from 0.0017 to 0.07 nm^{-1} at 30.7 m sample-to-detector distance. All two-dimensional (2D) images were corrected for dark, spatial distortion, normalized by transmitted flux and masked to account for the beam stop and the edges of the detector. We azimuthally integrated the 2D images to obtain one-dimensional patterns of scattered intensity I as a function of the momentum transfer vector q, where $q = (4\pi \sin\theta)/\lambda$. Here, 2θ is the scattering angle. A typical scattering profile of a *Heliconius* scale is shown in figure 5.

Wings were mounted in a frame that could be rotated to precisely align the samples. We collected between 33 and 113 measurements over 10–20 mm between two of the wing veins on the forewing (figure 3) of 74 *H. erato* individuals: eight *cyrbia*, one *demophoon*, six F_1 (from two crosses in reciprocal directions) and 59 F_2 (all from a single cross). In addition, we measured four *Heliconius erato hydara* individuals to be analysed alongside the *demophoon*. The *H. e. hydara* were also collected in Panama, do not have iridescent colour and differ from *demophoon* only in the lack of yellow hindwing bar. To obtain estimates of the ridge spacing, we fitted the peak positions in the one-dimensional scattered intensity to a composite Lorentzian + linear profile using the lmfit Python module [29]. We then used the centre of each fitted profile to calculate ridge spacing using the expression $d = 2\pi/q$ and averaged these to obtain a single estimate per individual. The average distances between ridges are in good agreement with those previously reported for *H. erato* [9].

3. Results

3.1. Segregation of blue colour

Measurements of blue scores were shown to be repeatable, with 99% of variation due to differences between individuals and 1% due to measurement error ($R^2 = 0.99$, $F_{4,20} = 54159$, $p < 0.001$; electronic supplementary material, table S3). *Heliconius erato demophoon* showed very little blue colour with an average BR value of -0.56 ± 0.08 compared with iridescent *H. erato cyrbia* which had a mean value of 0.97 ± 0.05 (table 2). The mean for the F_2 generation fell midway between the two parental races (figure 6), suggesting additive effects of alleles. The mean of the F_1 was slightly skewed towards *demophoon*, although the median was in a similar position to the F_2 (0.13 and 0.14). The mean BR value of the backcrosses did not fall halfway between that of the F_1 and the

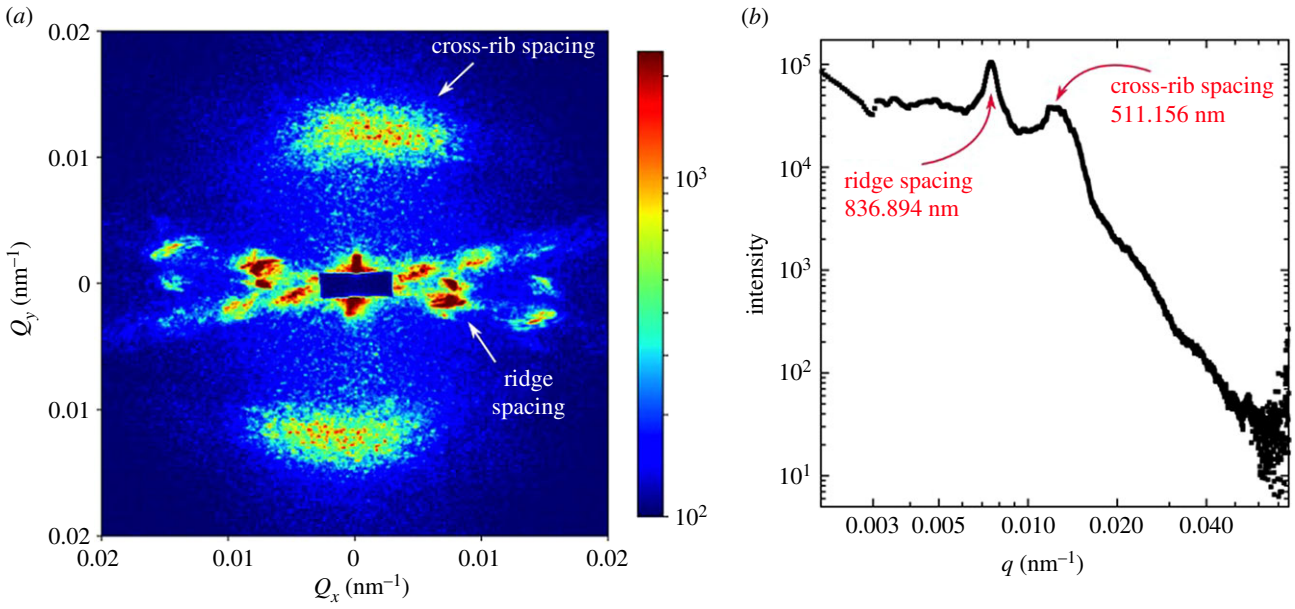

Figure 5. Representative SAXS patterns for a single frame of a male *H. e. cyrbia* parent. (*a*) The 2D pattern reveals approximately perpendicular scattering intensity from scale features. From their orientation, length scales of the scattered intensity and previous interpretations, we infer that they correspond to the spacing between ridges and cross-ribs. (*b*) Full azimuthal integration of the scattered intensity as a function of the magnitude of the momentum transfer vector q. The peaks corresponding to ridge and cross-rib spacing are indicated together with the measurements in real space.

Table 2. Summary statistics for BR values in each generation of *H. erato*.

generation	mean BR value	standard deviation	variance	sample size
demophoon	−0.56	0.08	0.01	12
F_1	0.13	0.23	0.05	60
backcross	0.69	0.28	0.08	65
F_2	0.21	0.30	0.09	114
cyrbia	0.97	0.05	0.00	51

parental race, which they were crossed with, but were skewed towards *cyrbia*, the Ecuadorian race. This suggests that the effects of the alleles are not completely additive, and there may be some dominance of the *cyrbia* alleles or epistatic interactions between loci.

The lack of discrete groups in the F_2 generation suggests that variation in the trait is controlled by more than one locus. Using the Castle–Wright estimator, with mean BR values and variances from only one cross direction to reduce variation due to sex linkage (see subsequent results), we obtained an estimate of 4.6 loci contributing to the trait. While this formula assumes that crosses started with inbred lines, it is generally robust to deviations from the assumptions [30]. However, it likely underestimates the total number of loci as it assumes loci all have equal effects. It is therefore perhaps best interpreted as the likely number of loci with medium to large effects on the phenotype. In addition, the F_1 individual wings that we measured were of varying age and condition, which may have increased the variance and decreased the mean value of blue reflectance seen in these individuals relative to the F_2 individuals, which were all preserved soon after emergence. This could influence the estimation of the number of loci.

3.2. Sex linkage

Sex linkage leads to a difference in the trait between reciprocal crosses in the F_1 generation, which is confined to the heterogametic sex, or a difference between reciprocal crosses in the F_2 generation in the homogametic sex [31]. As in birds, female butterflies are the heterogametic sex; they have ZW sex chromosomes whereas males have ZZ. Differences would occur depending on which parent or grandparent the Z or W is inherited from (figure 7). If the sex difference is present in the parental population, or the pattern is the same in reciprocal crosses, this would indicate a sex-limited trait (i.e. an autosomal trait that is expressed differently between the sexes).

Comparing the F_1 offspring of reciprocal crosses suggested some sex linkage (figure 8 and table 3). Offspring of crosses with a male *cyrbia* parent had significantly higher blue values than those which had a female *cyrbia* parent. Separated by sex, there was no difference between the males from reciprocal F_1 crosses, which had a mean of 0.23 and 0.25, respectively ($t_{11} = -0.19$, $p = 0.85$). The variation was among the female offspring which had means of −0.03 and 0.26 ($t_{44} = -5.55$, $p < 0.001$; table 4). This pattern would be expected if there were one or more loci controlling iridescence on the Z chromosome. In each case, males will be receiving one Z chromosome from an iridescent parent, and the other from a non-iridescent parent. The female offspring, in contrast, will only receive a Z chromosome from their father (figure 7). To confirm that these results were not biased by a particular cross, individual crosses were plotted and the same pattern was found (electronic supplementary material, figure S1). We did not find any difference in blue score between the sexes in pure *H. erato cyrbia* (table 3), demonstrating that the difference between the sexes in the crosses is not due to autosomally mediated sexual dimorphism.

If blue colour was controlled only by genes on the Z chromosome, we would expect that females from crosses with a non-iridescent father would have the same phenotype as *demophoon* females. However, they are significantly bluer

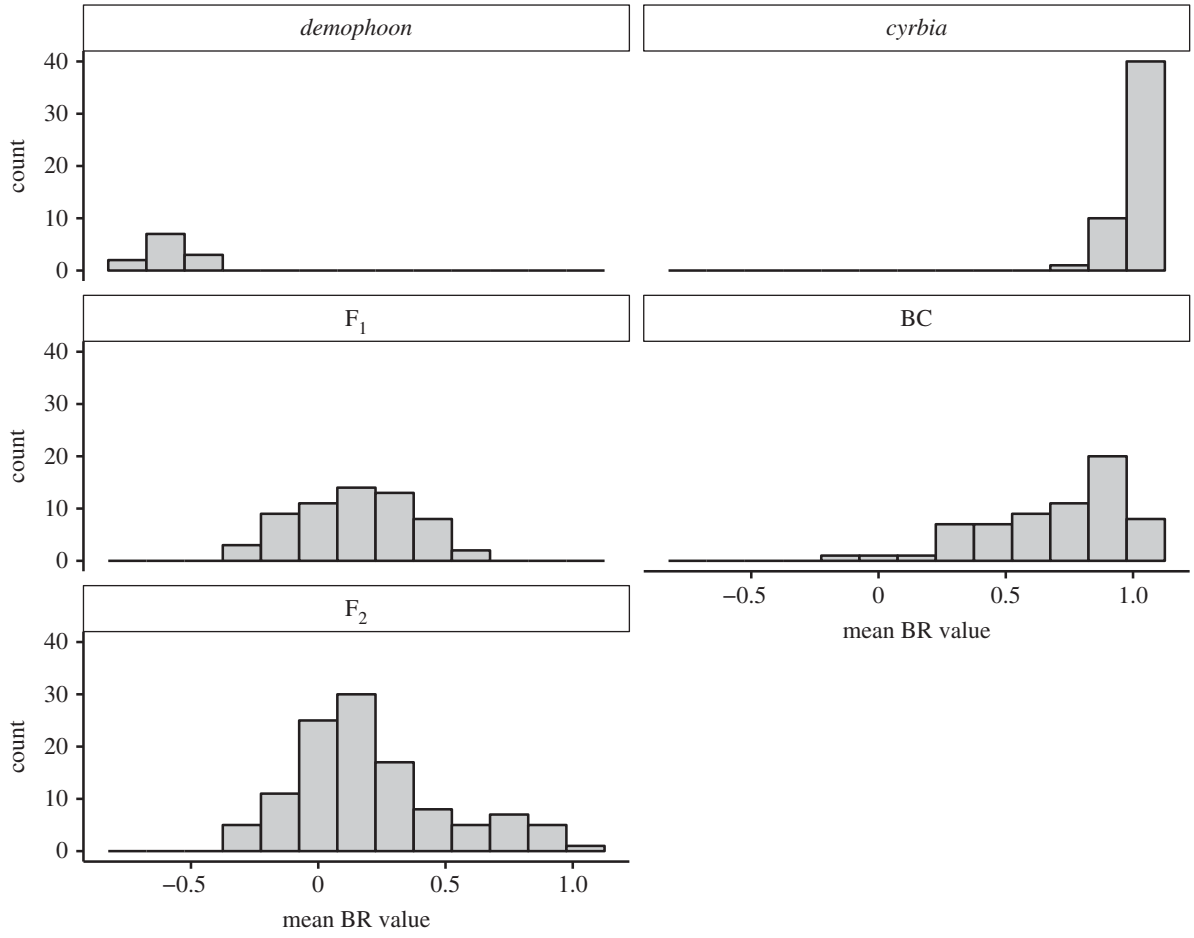

Figure 6. Mean BR values across *H. erato* generations. F_1 and F_2 individuals largely fall between the parental *demophoon* and *cyrbia* races. The backcross generation (BC) are highly skewed towards *cyrbia*, which is the race they were crossed with.

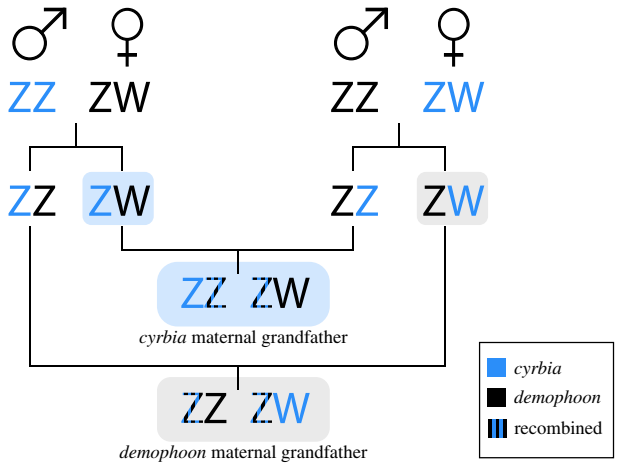

Figure 7. If there are loci of interest on the Z chromosome, F_1 females with an iridescent *cyrbia* father will be bluer than those with a non-iridescent *demophoon* father because they inherit a '*cyrbia*' Z chromosome. In the F_2, males always inherit a complete, non-recombined Z chromosome from their maternal grandfather, so if he is iridescent they will be bluer than offspring from the reciprocal cross.

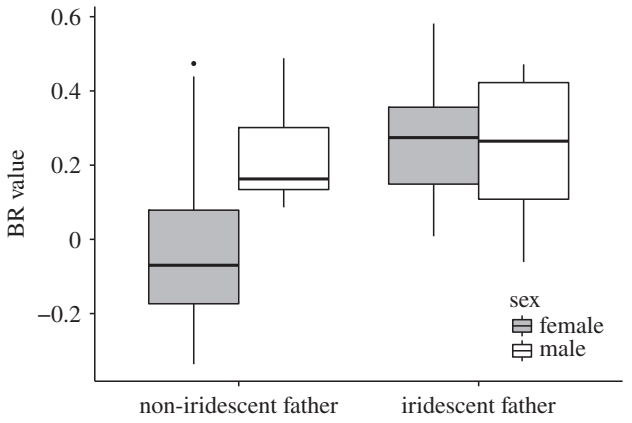

Figure 8. F_1 females with an iridescent *cyrbia* father were significantly bluer than those with a *demophoon* father. There were no differences in males.

than wild *demophoon*, supporting the hypothesis that the colour is controlled by multiple loci on different chromosomes (-0.03 ± 0.2 and -0.56 ± 0.1, $t_{25} = -10.6$, $p < 0.001$).

In the F_2 generation, sex linkage would be shown as males with an iridescent maternal grandfather being more blue than those with an iridescent maternal grandmother. The results point towards this pattern; however, the differences between the male groups are not significant, possibly due to small sample sizes in the first group (figure 9 and table 4). There was little difference in females. Overall, however, offspring with an iridescent maternal grandfather were bluer than those with black maternal grandfather. This is consistent with sex linkage, due to the greater number of '*cyrbia*' Z chromosomes present in the F_2 offspring with an iridescent maternal grandfather (figure 7). Within the offspring with an iridescent maternal grandfather, males were bluer than females, while this was not the case for crosses with a black maternal grandfather, also supporting Z linkage (table 3). In summary, F_1 females were bluer when they had an iridescent father, and

Table 3. Comparison of BR values (±s.d.) between females and males in each *H. erato* generation. Males are bluer than females in crosses with a *demophoon* father or *cyrbia* maternal grandfather (MGF). Males are also bluer in backcrosses with a *cyrbia* MGF. There are no differences in the parental races.

generation	female BR value	female sample size	male BR value	male sample size	*t*-statistic	d.f.	*p*-value
demophoon	−0.56 ± 0.1	6	−0.56 ± 0.1	6	−0.06	9.0	0.955
all F_1	0.10 ± 0.3	46	0.24 ± 0.2	14	−2.37	28.9	0.025
F_1 *cyrbia* father	0.26 ± 0.2	21	0.25 ± 0.2	7	0.17	8.4	0.872
F_1 *demo.* father	−0.03 ± 0.2	25	0.23 ± 0.1	7	−3.80	13.3	0.002
all F_2	0.10 ± 0.3	63	0.33 ± 0.3	51	−4.28	96.4	<0.001
F_2 *cyrbia* MGF	0.12 ± 0.3	53	0.35 ± 0.3	47	4.00	92.1	<0.001
F_2 *demo.* MGF	0.02 ± 0.2	10	0.15 ± 0.4	4	−0.72	3.5	0.512
all BC	0.60 ± 0.3	35	0.79 ± 0.2	30	−2.93	62.9	0.005
BC *cyrbia* MGF	0.58 ± 0.3	24	0.83 ± 0.2	25	−3.86	42.7	<0.001
BC *demo.* MGF	0.65 ± 0.4	11	0.62 ± 0.4	5	0.16	7.6	0.877
cyrbia	0.98 ± 0.2	16	0.97 ± 0.1	35	0.79	48.2	0.431

Table 4. Comparison of BR values for offspring from reciprocal F_1 crosses, which had either an iridescent mother or iridescent father, and for F_2 crosses, which had either an iridescent maternal grandfather or grandmother. Mean values and sample sizes are shown in table 3.

F_1 *cyrbia* or *demophoon* father				F_2 *cyrbia* or *demophoon* maternal grandfather			
	t	d.f.	*p*-value		*t*	d.f.	*p*-value
female	−5.55	43.6	<0.0001	female	−1.64	19.5	0.118
male	−0.19	10.8	0.85	male	−1.06	3.4	0.357
all	−4.67	56.8	<0.0001	all	−2.53	20.2	0.020

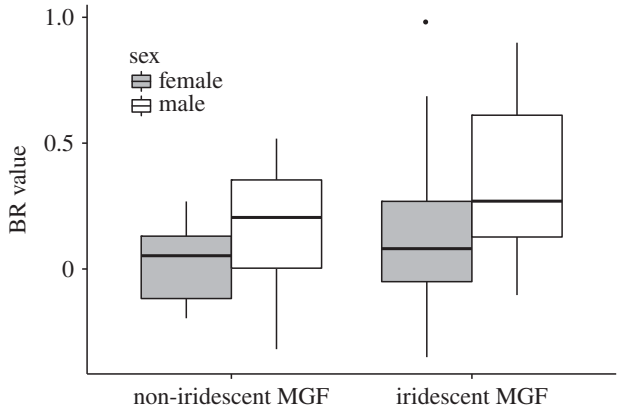

Figure 9. Mean BR values for F_2 males with an iridescent maternal grandfather (MGF) were higher than those with an iridescent maternal grandmother, although not significantly. Females in both groups had similar BR values.

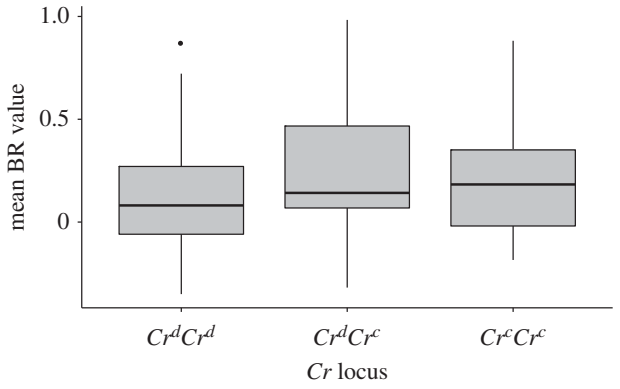

Figure 10. In the F_2 generation, BR values did not differ with the different *Cr* phenotypes. Cr^dCr^d represents the *demophoon* genotype with the yellow bar present on the hindwing, and Cr^cCr^c is the *cyrbia* genotype with the white margin. Cr^dCr^c is heterozygous and has neither of these elements.

males were bluer in the F_2 when they had an iridescent maternal grandfather. There were no differences in BR values between males and females in the parental races, *H. e. demophoon* and *H. e. cyrbia*. These results support the presence of loci controlling iridescence in the Z chromosome.

3.3. Links to other colour pattern loci

In *H. erato*, the *Cr* locus controls the presence of a yellow forewing bar in *demophoon* and a white margin in *cyrbia*. There were three observed phenotypes in the F_2 generation—yellow bar present, white margin present and both absent (figure 2). Consistent with the hypothesis that these two features are controlled by recessive, tightly linked loci or are alternative alleles of the same locus, we did not find any individuals that had both a yellow dorsal bar and a white margin present. The ratio of these traits was also consistent with a 1 : 2 : 1 ratio as expected under the assumption that the individuals lacking both features were heterozygous at this locus ($x^2 = 2.1$, d.f. = 2, $p = 0.35$). There was no significant difference in BR values between individuals with different *Cr* genotypes ($F_{2,107} = 2.05$, $p = 0.133$) (figure 10), suggesting that *cortex* is not one of

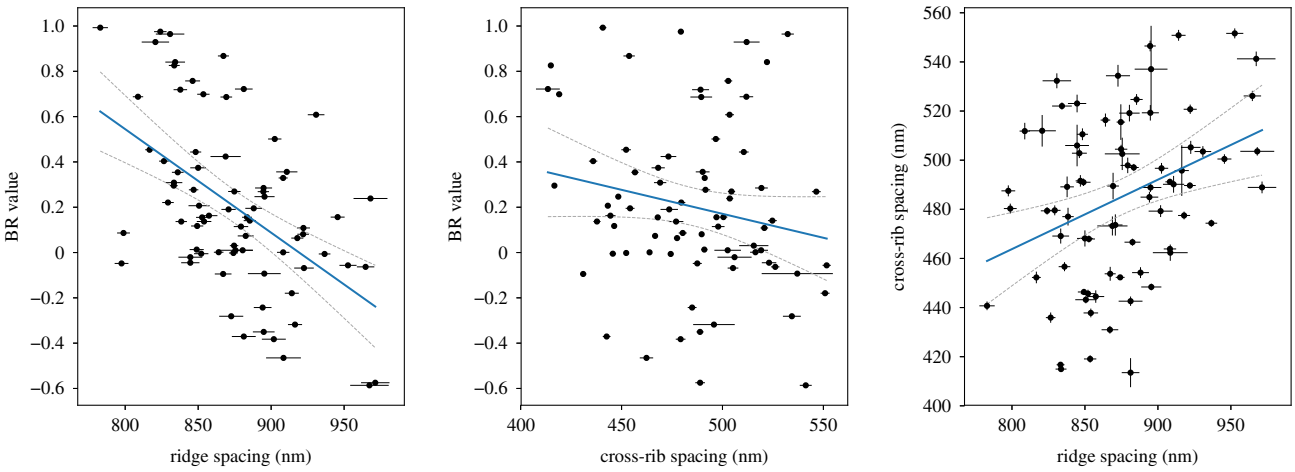

Figure 11. An increase in longitudinal ridge spacing correlated with a decrease in BR values. Blue colour slightly decreased with cross-rib spacing, but ridge spacing and cross-rib spacing were also highly correlated. The cross-hairs show the standard error from the 33 to 133 SAXS point measurements for each individual. Blue lines indicate the fitted linear regression, with the dotted lines showing the 95% confidence interval. (Online version in colour.)

Table 5. There are no significant correlations between the forewing red band measurements and BR colour in the F_2 generation. Measurements are ratios of band measurements to wing size. Degrees of freedom = 69. $N = 71$.

standardized measurement	mean	standard deviation	*t*	*r*	*p*-value
linear 1	0.76	0.08	−1.65	−0.20	0.10
linear 2	0.55	0.06	−1.41	−0.17	0.16
linear 3	0.35	0.05	−1.69	−0.20	0.10
linear 4	0.41	0.05	0.38	0.05	0.71

the genes controlling iridescence, nor are there any major effect loci linked to this region on *Heliconius* chromosome 15. In the F_2, there were also no significant correlations between blue colour and any of the standardized linear measurements used to determine shape of the red forewing band (table 5; electronic supplementary material, figure S2), showing iridescence is unlikely to be linked to *WntA* on chromosome 10.

3.4. Nanostructure variation

As we expected, there was a negative correlation between longitudinal ridge spacing and BR values ($r = -0.52$, $p < 0.001$; figure 11), indicating that blue reflectance increases with increasing density of ridges on the scale. The strength of this correlation shows that ridge spacing is only one factor which is affecting the intensity of iridescence, and that other aspects of scale morphology that determine blue reflectance may segregate somewhat independently in the crosses. BR values also declined with increasing cross-rib spacing, although not significantly ($r = -0.20$, $p = 0.09$; figure 11). Ridge spacing and cross-rib spacing were highly correlated with each other ($r = 0.34$, $p = 0.002$; figure 11) suggesting a genetic correlation between these traits. Therefore, the correlation between cross-rib spacing and BR value is likely due to this association between ridge and cross-rib spacing, as we do not expect the cross-ribs to directly affect colour.

Consistent with previous findings [9], *H. erato cyrbia* had closer ridge spacing than *H. erato demophoon* (table 6). Like the BR values, measurements of ridge spacing in the F_2 generation fell between the parental races (figure 12) and were fairly continuous, consistent with the action of multiple genes.

Table 6. Mean spacing (±s.d.) between longitudinal ridges and between cross-ribs. The narrower ridge spacing in *cyrbia* results in a brighter iridescent colour. The mean values for the F_1 and F_2 generations fell between the values for the parental races.

generation	mean longitudinal ridge spacing (nm)	mean cross-rib spacing (nm)	sample size (male, female)
demophoon/ hydara	926.05 ± 40.1	482.87 ± 37.1	5 (3, 2)
F_1	875.64 ± 57.8	476.66 ± 20.0	6 (4, 2)
F_2	876.25 ± 36.0	484.46 ± 35.0	59 (25, 34)
cyrbia	822.55 ± 30.8	494.82 ± 30.1	8 (5, 3)

Interestingly, ridge spacing in the F_1 generation was highly variable between individuals. This could indicate variation in epistatically acting alleles in the parental populations that segregate in the F_1 generation, or may suggest environmental effects. However, the phenotyped F_1 individuals in this comparison were from two different reciprocal crosses, with apparent differences between these two groups. Therefore, some of the variation that is observed may be due to cross-specific genetic effects and possibly sex linkage, but we have data from too few individuals to fully dissect these effects.

Cross-rib spacing in the F_2 generation appears to extend beyond the range of the parental races (figure 13), again possibly indicating epistatically acting alleles in the parental

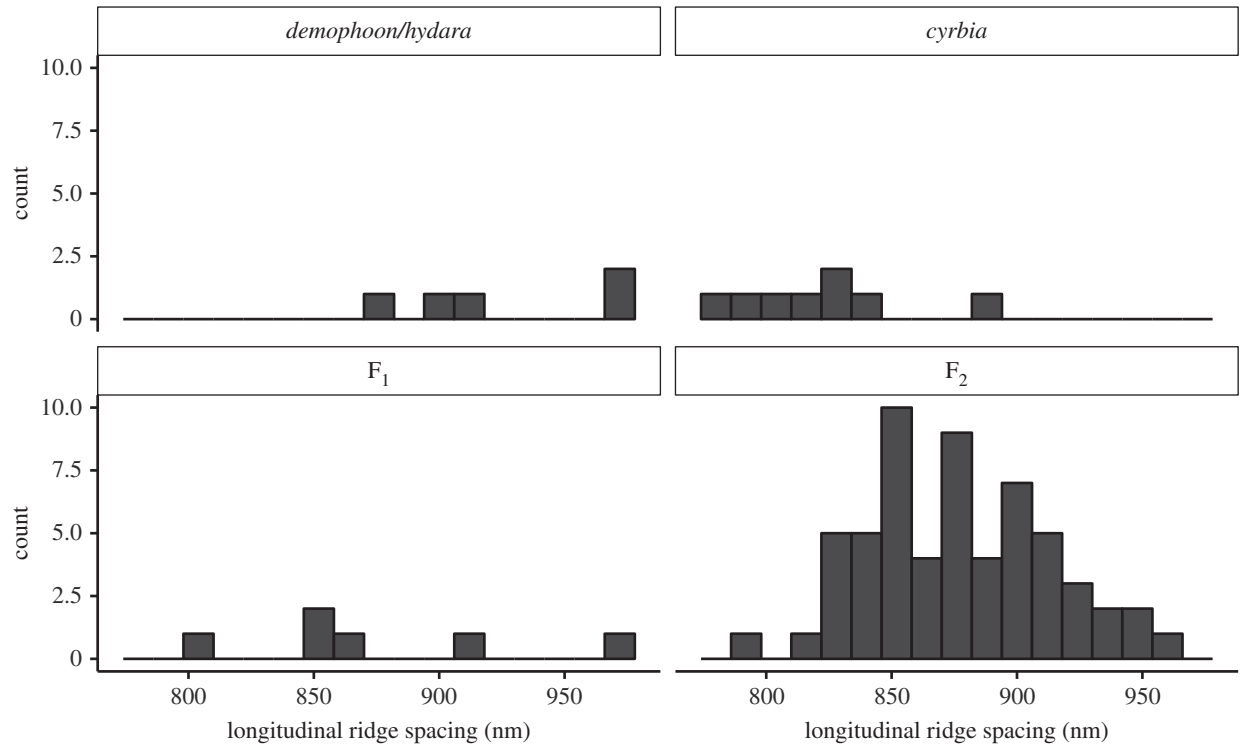

Figure 12. Variation in longitudinal ridge spacing in the F_2 suggests that it is controlled by multiple genes. In the F_1, those with an iridescent father had lower ridge spacing, reflecting the higher BR values seen in this cross.

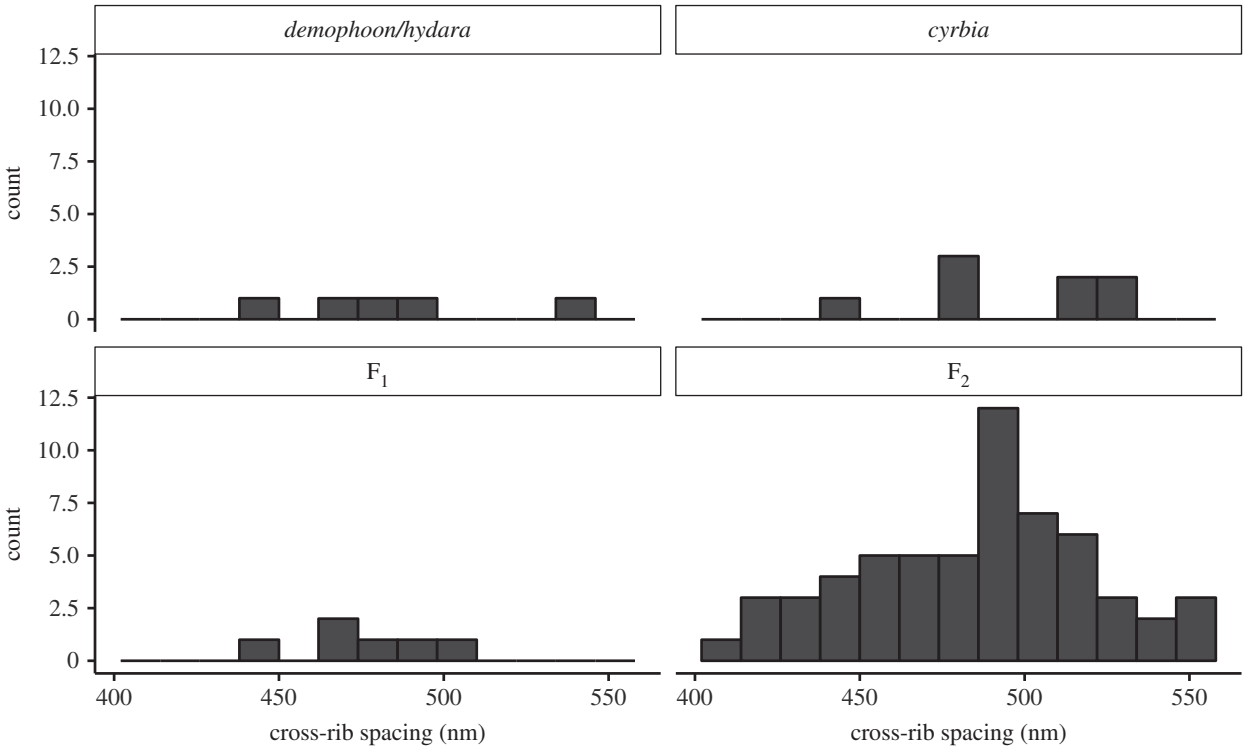

Figure 13. Cross-rib spacing also shows continuous variation in the F_2 generation and extremes extended beyond the values of the few parental individuals which were measured.

populations, although not all parental individuals were measured. Large variation in cross-rib spacing may be expected as it is not predicted to have an effect on colour, so may be under weaker selection. In the F_2 generation, males had narrower longitudinal ridge spacing than females, which was similar to the differences seen in this generation in blue values, and may suggest sex linkage of loci controlling ridge spacing ($t_{57} = 3.80$, $p < 0.001$; figure 14). Cross-rib spacing was also smaller in males ($t_{43} = 4.95$, $p < 0.001$), supporting the idea that ridge spacing and cross-rib spacing may be genetically correlated. However, in this case, we cannot rule out a contribution of autosomally mediated sexual dimorphism because we only have data from one F_2 cross. There was not a significant difference in ridge spacing between sexes in the parental populations (*hydara*/*demophoon* $t_{2.3} = 0.34$, $p = 0.77$; *cyrbia* $t_{4.4} = 0.53$, $p = 0.63$), but this may be due to small sample sizes and the differences were in the same direction as in the F_2, with females having larger

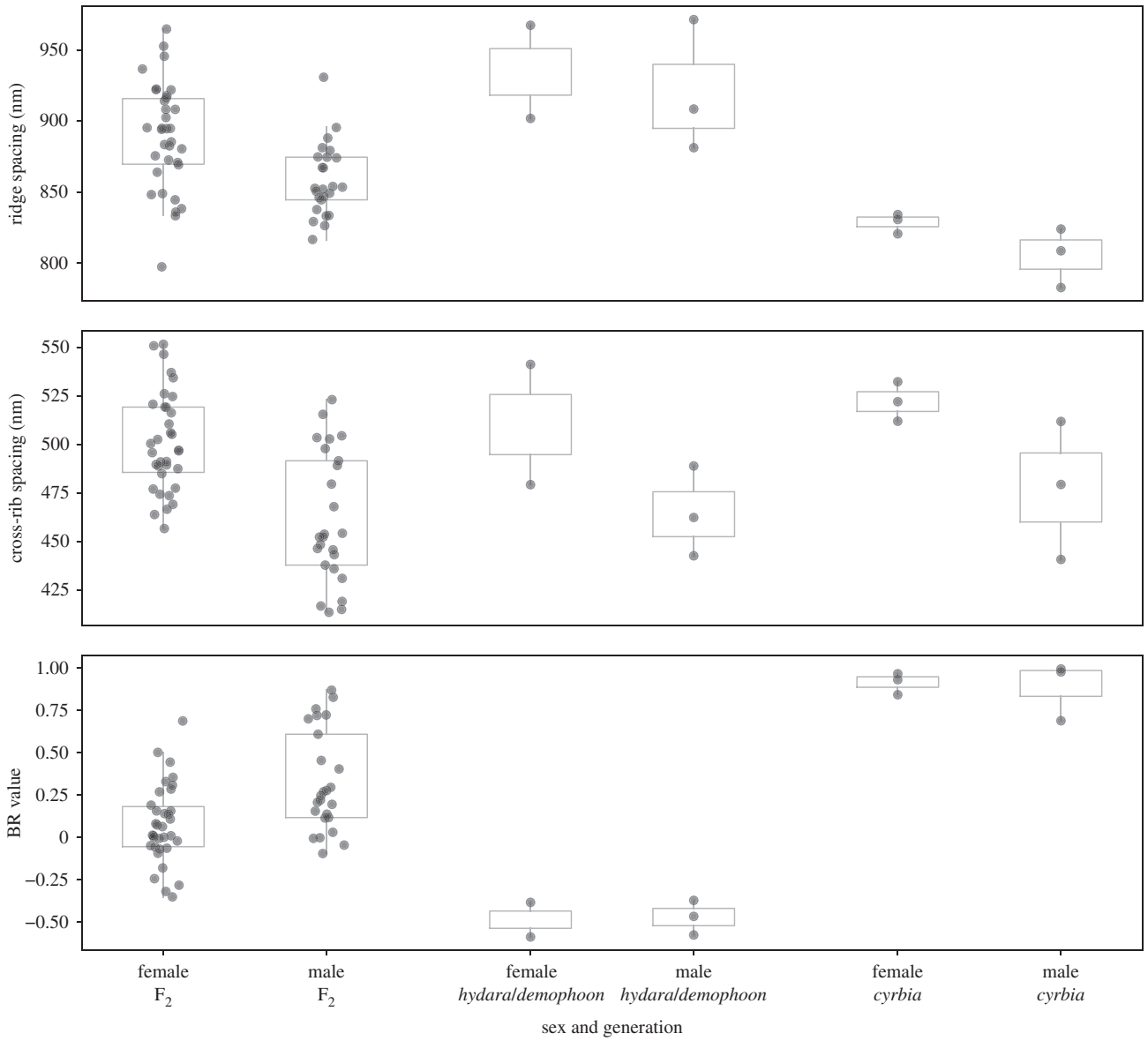

Figure 14. Males have narrower longitudinal ridge spacing than females in the F_2. This difference is less pronounced and not significant in the parental races. Significant differences in cross-rib spacing were seen in *cyrbia* and in the F_2, with males again having narrower spacing. These results are consistent with the finding that males have higher measures of blue colour.

spacing on average (figure 14). There was a significant difference in cross-rib spacing between sexes in *cyrbia* ($t_{5.6} = 3.42$, $p = 0.02$) but not in *hydara/demophoon* ($t_{1.4} = 1.35$, $p = 0.36$). Nevertheless, the differences in ridge spacing seen within the parental races are smaller than those seen in the F_2 generation, supporting a role for sex linkage. Using the wing measurements, there was not a significant difference in wing size between males (11.2 ± 0.5 mm) and females (10.9 ± 0.6 mm) in the F_2 ($t_{68} = -1.82$, $p = 0.07$), and in fact, males tended to be larger, suggesting that the increased ridge and cross-rib spacing in females is not due to overall sexual size dimorphism. Overall, ridge spacing appears to have a very similar genetic architecture to that of the BR colour values, suggesting that it is also controlled by multiple loci.

4. Discussion

Our phenotypic analysis of crosses between iridescent and non-iridescent races shows that iridescence is controlled by multiple loci in *H. erato* with convincing evidence for loci on the Z chromosome. There is an extensive history of using experimental crosses in *Heliconius* to investigate the genes controlling colour and pattern, but although iridescence had been shown to segregate in crosses, the trait has not been investigated due to the difficulty of quantifying the continuous phenotype and measuring the number of different features affecting the colour. We show that standardized photographs and the BR ratio is an effective method of estimating variation in blue iridescent reflectance. As expected, iridescent *H. erato cyrbia* gave the highest blue values, and non-iridescent *H. e. demophoon* the lowest. BR values correlated with longitudinal ridge spacing, which has previously been shown to have an effect on the brightness of the blue iridescent colour [9]. The distribution of blue values in the F_2 generation suggests that variation in the trait is not controlled by a single locus.

The differences in blue values found between sexes in the F_1 reciprocal *erato* crosses suggest that there could be a major effect locus involved in iridescent colour on the Z chromosome. We may expect that genes on the sex chromosomes will control sexually selected traits [32]. Reinhold [33]

calculated that in *Drosophila*, around a third of phenotypic variation in sexually selected traits was caused by X-linked genes, and that X-linked genes only influenced traits classified as under sexual selection. Iridescent structural colours are used as sexual signals in many butterfly species [2,34,35]. Work with *Colias* butterflies has found many wing pattern elements are sex-linked, including melanization, UV reflectance and yellow wing pigmentation [36,37]. These studies found that sex linkage was important in prezygotic isolation and species differentiation. Therefore, sex linkage of iridescence in *Heliconius* may have contributed to the differentiation of this trait between geographical races.

Unlike some Lepidoptera, *Heliconius* do not show complete sex chromosome dosage compensation. Analysis of *H. cydno* and *H. melpomene* gene expression showed a modest dosage effect on the Z chromosome, and overall reduced expression compared to autosomes [38]. Our results are also consistent with a lack of complete dosage compensation, with some evidence for expression of both Z chromosome alleles in males. A lack of dosage compensation could also favour the build-up of sexually selected or sexually antagonistic loci on the Z chromosome, as these will automatically be expressed differently between the sexes.

The three *erato* phenotypes controlled by the *Cr* locus did not show any correlation with iridescent colour values. The gene *cortex*, found in this genomic region, has been shown to underlie these colour pattern differences [16]. There are several reasons why major colour patterning genes could have been hypothesized to also control structural colour variation in *Heliconius*. Knockouts of one of the genes that control colour pattern in *Heliconius*, *optix*, in *Junonia coenia* butterflies resulted in a change in pigmentation, and the gain of structural colour [39], although this was not observed in the same tests with *H. erato*. In addition, linkage between divergently selected loci would be expected under 'divergence hitchhiking', in which genomic regions around key divergently selected loci are protected from recombination during speciation [40]. Hitchhiking regions can be small in natural populations unless recombination is reduced, but in Lepidoptera there is no recombination in the female germline. Furthermore, for highly polygenic traits, we would expect many loci to be distributed throughout the whole genome, so that for any genetic marker there will be some phenotypic association. Individuals with homozygous *Cr* phenotypes, for example, will have inherited an entire chromosome 15 from either an iridescent or non-iridescent grandparent, due to the lack of female recombination. Therefore, any combination of a single major effect locus or multiple smaller effect loci on chromosome 15 would have been seen as a difference in iridescence between individuals with different *Cr* phenotypes. The fact that we find no association with *Cr* suggests that structural colour is not highly polygenic, but controlled by a moderate number of loci, none of which are located on chromosome 15. It is also consistent with it being controlled independently of colour pattern. Similarly, we see no association with variation in forewing red band size, which is largely determined by the gene *WntA*. This region on chromosome 10 controls forewing band shape in multiple races of *H. erato*, as well as other *Heliconius* species [12].

In *Heliconius* pigment colour patterns, a small set of major effect genes have been well studied but a larger set of 'modifier' loci have also been found which adjust colour pattern [12]. It is possible that the iridescence genes have a similar distribution of effect sizes, with a small number of major effect genes, including one on the Z chromosome, and a distribution of other smaller effect genes. This supports the existing evidence of the importance of major effect loci in adaptive change [10–12]. Future work with the co-mimic of *erato*, *Heliconius melpomene*, will allow us to compare the genetic basis of iridescence between the two species. Following the two-step process of Müllerian mimicry described by Turner [41,42], a large effect mutation, such as the one we have found on the Z chromosome, allows an adaptive phenotypic change large enough for the population to resemble those in the mimicry ring and survive, then smaller changes will produce incremental improvements in mimicry.

Longitudinal ridge spacing also appears to have a polygenic architecture. The continuous variation that is observed in blue colour in the F_2 broods does not seem to be due to major effect loci with discrete effects on different aspects of scale structure. Rather it seems that multiple interacting genes are involved in controlling scale morphology. The correlation between ridge and cross-rib spacing suggests that some of these loci produce correlated effects on various aspects of scale morphology. However, the fact that we do not see a perfect correlation between these and blue colour suggests that there is some independent segregation of other aspects of scale morphology that contribute to the colour. Measurements of other aspects of scale morphology, such as ridge curvature and layering, will be needed to confirm this.

5. Conclusion

Crosses are ideal for investigating the genetic basis of colour and pattern as traits will segregate in following generations. Crossing iridescent and non-iridescent *H. erato* has allowed us to quantify variation in the colour and determine that it is sex-linked and controlled by multiple loci.

Data accessibility. SAXS data (doi:10.15131/shef.data.6839315) and accompanying code (doi:10.15131/shef.data.6837905) have been uploaded to an online repository. Colour measurements, repeatability measurements and cross pedigree information can be found as part of the electronic supplementary material.

Authors' contributions. M.N.B. collected the colour data, performed the genetic analysis and wrote the manuscript. J.E.R. analysed the SAXS data under the supervision of A.J.P. A.J.P. coordinated collection of the SAXS data. The crosses were performed by P.A.S., C.M., D.C., M.N.B., N.J.N. and E.V.C. The SAXS data were collected by A.J.P., T.Z., E.V.C., N.J.N. and M.N.B. Wing size and red band measurements were performed by H.E.B. The study was devised and coordinated by N.J.N. All authors read and commented on the manuscript.

Competing interests. We declare we have no competing interests.

Funding. This work was funded by the UK Natural Environment Research Council (NERC) through an Independent Research Fellowship (NE/K008498/1) to N.J.N. M.N.B. and E.V.C. are funded by the NERC doctoral training partnership, ACCE. J.E.R. is funded through the Leverhulme Centre for Advanced Biological Modelling as well as scholarships from Universidad del Rosario and the University of Sheffield.

Acknowledgements. We thank the governments of Ecuador and Panama for permission to collect butterflies. Thanks to Juan López and Gabriela Irazábal for their assistance with the crosses. We are grateful to the European Synchrotron Radiation Facility for provision of X-ray beamtime under proposal LS2720 and to Andrew Dennison for assistance with SAXS data collection.

References

1. Bálint Z, Kertész K, Piszter G, Vértesy Z, Biró LP. 2012 The well-tuned blues: the role of structural colours as optical signals in the species recognition of a local butterfly fauna (Lepidoptera: Lycaenidae: Polyommatinae). *J. R. Soc. Interface* **9**, 1745–1756. (doi:10.1098/rsif.2011.0854)
2. Sweeney A, Jiggins C, Johnsen S. 2003 Insect communication: polarized light as a butterfly mating signal. *Nature* **423**, 31–32. (doi:10.1038/423031a)
3. Hadley NF, Savill A, Schultz TD. 1992 Coloration and its thermal consequences in the New Zealand tiger beetle *Neocicindela perhispida*. *J. Therm. Biol.* **17**, 55–61. (doi:10.1016/0306-4565(92)90020-G)
4. Vukusic P, Sambles JR, Lawrence CR, Wootton RJ. 1999 Quantified interference and diffraction in single *Morpho* butterfly scales. *Proc. R. Soc. B* **266**, 1403–1411. (doi:10.1098/rspb.1999.0794)
5. Winter B, Butz B, Dieker C, Schröder-Turk GE, Mecke K, Spiecker E. 2015 Coexistence of both gyroid chiralities in individual butterfly wing scales of *Callophrys rubi*. *Proc. Natl Acad. Sci. USA* **112**, 12 911–12 916. (doi:10.1073/pnas.1511354112)
6. Dinwiddie A, Null R, Pizzano M, Chuong L, Leigh Krup A, Ee Tan H, Patel NH. 2014 Dynamics of F-actin prefigure the structure of butterfly wing scales. *Dev. Biol.* **392**, 404–418. (doi:10.1016/j.ydbio.2014.06.005)
7. Merrill RM *et al.* 2015 The diversification of *Heliconius* butterflies: what have we learned in 150 years? *J. Evol. Biol.* **28**, 1417–1438. (doi:10.1111/jeb.12672)
8. Wilts BD, Vey AJM, Briscoe AD, Stavenga DG. 2017 Longwing (*Heliconius*) butterflies combine a restricted set of pigmentary and structural coloration mechanisms. *BMC Evol. Biol.* **17**, 226. (doi:10.1186/s12862-017-1073-1)
9. Parnell AJ *et al*. 2018 Wing scale ultrastructure underlying convergent and divergent iridescent colours in mimetic *Heliconius* butterflies. *J. R. Soc. Interface* **15**, 20170948. (doi:10.1098/rsif.2017.0948)
10. Joron M *et al*. 2006 A conserved supergene locus controls colour pattern diversity in *Heliconius* butterflies. *PLoS Biol.* **4**, 1831–1840. (doi:10.1371/journal.pbio.0040303)
11. Baxter SW, Papa R, Chamberlain N, Humphray SJ, Joron M, Morrison C, ffrench-Constant RH, McMillan WO, Jiggins CD. 2008 Convergent evolution in the genetic basis of Mullerian mimicry in *Heliconius* butterflies. *Genetics* **180**, 1567–1577. (doi:10.1534/genetics.107.082982)
12. Papa R, Kapan DD, Counterman BA, Maldonado K, Lindstrom DP, Reed RD, Nijhout HF, Hrbek T, McMillan WO. 2013 Multi-allelic major effect genes interact with minor effect QTLs to control adaptive color pattern variation in *Heliconius erato*. *PLoS ONE* **8**, e57033. (doi:10.1371/journal.pone.0057033)
13. Nadeau NJ. 2016 Genes controlling mimetic colour pattern variation in butterflies. *Curr. Opin. Insect Sci.* **17**, 24–31. (doi:10.1016/j.cois.2016.05.013)
14. Emsley M. 1965 The geographical distribution of the color-pattern components of *Heliconius erato* and *Heliconius melpomene* with genetical evidence for the systematic relationship between the two species. *Zoologica* **49**, 245–286.
15. Lynch M, Walsh B. 1998 Analysis of line crosses. In *Genetics and analysis of quantitative traits*, pp. 205–250. Sunderland, MA: Sinauer Associates.
16. Nadeau NJ *et al*. 2016 The gene *cortex* controls mimicry and crypsis in butterflies and moths. *Nature* **534**, 106–110. (doi:10.1038/nature17961)
17. Martin A *et al*. 2012 Diversification of complex butterfly wing patterns by repeated regulatory evolution of a *Wnt* ligand. *Proc. Natl Acad. Sci. USA* **109**, 12 632–12 637. (doi:10.1073/pnas.1204800109)
18. Mazo-Vargas A *et al*. 2017 Macroevolutionary shifts of *WntA* function potentiate butterfly wing-pattern diversity. *Proc. Natl Acad. Sci. USA* **114**, 10 701–10 706. (doi:10.1073/pnas.1708149114)
19. Mallet J. 1989 The genetics of warning colour in Peruvian hybrid zones of *Heliconius erato* and *H. melpomene*. *Proc. R. Soc. B* **236**, 163–185. (doi:10.1098/rspb.1989.0019)
20. Abramoff, M.D., Magalhaes PJ, Ram SJ. 2004 Image processing with ImageJ. *Biophotonics Int.* **11**, 36–42.
21. Comeault AA, Carvalho CF, Dennis S, Soria-Carrasco V, Nosil P. 2016 Color phenotypes are under similar genetic control in two distantly related species of *Timema* stick insect. *Evolution* **70**, 1283–1296. (doi:10.1111/evo.12931)
22. Whitlock MC. 2007 *The analysis of biological data*, 1st edn. Greenwood Village, CO: Roberts & Company Publishers.
23. Cockerham CC. 1986 Modifications in estimating the number of genes for a quantitative character. *Genetics* **114**, 659–664.
24. Otto SP, Jones CD. 2000 Detecting the undetected: estimating the total number of loci inderlying a quantitative trait. *Genetics* **156**, 2093–2107. (doi:10.1007/s001220050781)
25. Mallet J. 1986 Hybrid zones of *Heliconius* butterflies in Panama and the stability and movement of warning colour dines. *Heredity* **56**, 191–202. (doi:10.1038/hdy.1986.31)
26. Baxter S, Johnston S, Jiggins C. 2009 Butterfly speciation and the distribution of gene effect sizes fixed during adaptation. *Heredity* **102**, 57–65. (doi:10.1038/hdy.2008.109)
27. R Core Team. 2018 *R: a language and environment for statistical computing*. Vienna, Austria: Foundation for Statistical Computing. See https://www.r-project.org.
28. Van Vaerenbergh P, Lonardon J, Sztucki M, Boesecke P, Gorini J, Claustre L, Sever F, Morse J, Narayanan T. 2016 An upgrade beamline for combined wide, small and ultra small-angle x-ray scattering at the ESRF. *AIP Conf. Proc.* **1741**, 030034. (doi:10.1063/1.4952857)
29. Newville M, Stensitzki T, Allen DB, Ingargiola A. 2014 LMFIT: non-linear least-square minimization and curve-fitting for Python. *Zenodo*. (doi:10.5281/zenodo.11813)
30. Lande R. 1981 The minimum number of genes contributing to quantitative variation between and within populations. *Genetics* **99**, 541–553.
31. Mather K, Jinks JL. 1982 *Biometrical genetics*, 3rd edn. Cambridge, UK: Cambridge University Press.
32. Fairbairn DJ, Roff DA. 2006 The quantitative genetics of sexual dimorphism: assessing the importance of sex-linkage. *Heredity* **97**, 319–328. (doi:10.1038/sj.hdy.6800895)
33. Reinhold K. 1998 Sex linkage among genes controlling sexually selected traits. *Behav. Ecol. Sociobiol.* **44**, 1–7. (doi:10.1007/s002650050508)
34. Kemp DJ. 2007 Female butterflies prefer males bearing bright iridescent ornamentation. *Proc. R. Soc. B* **274**, 1043–1047. (doi:10.1098/rspb.2006.0043)
35. Rajyaguru PK, Pegram KV, Kingston ACN, Rutowski RL. 2013 Male wing color properties predict the size of nuptial gifts given during mating in the Pipevine Swallowtail butterfly (*Battus philenor*). *Naturwissenschaften* **100**, 507–513. (doi:10.1007/s00114-013-1046-1)
36. Silberglied RE. 1979 Communication in the ultraviolet. *Annu. Rev. Ecol. Syst.* **10**, 373–398. (doi:10.1146/annurev.es.10.110179.002105)
37. Ellers J, Boggs CL. 2002 The evolution of wing color in *Colias* butterflies: heritability, sex linkage, and population divergence. *Evolution* **56**, 836–840. (doi:10.1111/j.0014-3820.2002.tb01394.x)
38. Walters JR, Hardcastle TJ, Jiggins CD. 2015 Sex chromosome dosage compensation in *Heliconius* butterflies: global yet still incomplete? *Genome Biol. Evol.* **7**, 2545–2559. (doi:10.1093/gbe/evv156)
39. Zhang L, Mazo-Vargas A, Reed RD. 2017 Single master regulatory gene coordinates the evolution and development of butterfly color and iridescence. *Proc. Natl Acad. Sci. USA* **114**, 10 707–10 712. (doi:10.1073/pnas.1709058114)
40. Via S, West J. 2008 The genetic mosaic suggests a new role for hitchhiking in ecological speciation. *Mol. Ecol.* **17**, 4334–4345. (doi:10.1111/j.1365-294X.2008.03921.x)
41. Turner J. 1977 Butterfly mimicry: the genetical evolution of an adaptation. *Evol. Biol.* **10**, 163–206.
42. Turner JRJ. 1981 Adaptation and evolution in *Heliconius*: a defense of NeoDarwinism. *Annu. Rev. Ecol. Syst.* **12**, 99–121. (doi:10.1146/annurev.es.12.110181.000531)